BONDING AND DEBONDING MECHANISM OF PRESSURE SENSITIVE ADHESIVES

A thesis submitted for the degree of
Doctor of Philosophy

By

SAMUEL AKOGYERAM

Department of Engineering and Design,
Brunel University,
Uxbridge, Middlesex.

June 2010

Brunel University, Uxbridge, Department of Engineering and Design; June 2010.

BONDING AND DEBONDING MECHANISM OF PRESSURE SENSITIVE ADHESIVES

Samuel AKOGYERAM

ABSTRACT

Pressure-sensitive adhesives (PSAs) are complex macromolecular-based blend formulations that, in dry form will adhere permanently to diverse surfaces with the application of mere finger pressure. This thesis addresses the bonding and debonding mechanisms of coated films of different commercially available PSAs by systemically investigating the film characteristics on multiple levels. The methods implemented involve a novel procedure in investigating viscoelastic properties with Dynamic Mechanical Analysis, film surface chemistry with Time-of-flight Secondary Ion Mass Spectrometry and film morphology, modulus and bonding characteristics with Atomic Force Microscope. The theoretical aspect invoked rubber elasticity, viscoelasticity and thermodynamic concepts in representation of film morphology with corresponding adhesion nature.

The results indicate that the bonding and debonding behaviour of PSA films are of a viscoelastic nature, dictated mainly by two fundamental morphological elements. These elements are; (1) the formation of phase-separated self-assembly of polystyrene-rich-copolymer nano-domains within the adhesive matrix and (2) the inter-linking of the nano-domains by elastically active elastomer segments into a physical crosslinked network system that is highly efficient in dissipating large strain energy. These morphological factors are manifested through a profound contribution to the peel strength of the adhesive films when either coated at high temperatures or annealed. Increasing the content of the polystyrene endblock-tackifier in the adhesive blend formulation increased the PSA's performance sensitivity to the film coating temperature. Meanwhile increasing the *cis*-C=C bond concentration in the formulation reduced the film's performance sensitivity to coating temperature, as polydienes are premised to promote the entropy-elasticity of the film matrix by contributing to the nano-domain interconnections. This thesis generates many qualitative similarities, despite the significantly different adhesive blends investigated and hopefully the results reported here are more universal than one might expect.

Table of Contents

Chapter 3

Materials and characterisation of coated hot-melt PSA films

71

Chapter 4

Classical investigation of the mechanical properties of PSA and the peel strength to non-woven fabrics

112

Chapter 5

Thermal Phase Transition and Viscoelastic Behaviour of Styrene-based hot-melt Pressure Sensitive Adhesive Films

125

List of Tables

List of Figures

Acknowledgements

First and foremost I would like to extend my overwhelming gratitude to my supervisor, Dr Wenhui Song, for your continuous guidance, enlightening suggestions, support and trust throughout the over three year of my research studies.

I am highly thankful to my second supervisor Dr Wei Kong of Henkel, for the support, the opportunity, the encouragement, the invaluable comments, the supply of samples and some experimental results, which helped in making my studies possible. My profound gratitude to Andy Swain and Corbett Wallace, of Henkel, for the opportunity, the enlightening comments, and encouragement throughout my studies.

I will forever be grateful to Dr Marco Wenger, Dr David Scurr of School of Pharmacy, Nottingham University and Dr Wei Wang, for the supervision and providing experimental facilities. My gratitude to Dr Benjamin Jones and Dr Allen, of ETC, Brunel University, for the training and support. My special acknowledgment is directed to the Wolfson Centre, Brunel University, for the support, and the accommodation with my office. I am profoundly indebted to Abdul Ghani and Dr Ansgar Rose, for your guidance and assistance with some experimental work.

To my family, I offer my reserved gratitude for your love and support throughout my studies.

Finally my concluding gratitude to the EPSRC for the bulk of the funding, and Henkel for the part funding, offered for my PhD studies.

SA, June, 2010

Chapter 1

1 Introduction

1.1 General Introduction

Everybody has perhaps during their lifetime experienced the stickiness of some materials by the touch of a finger. This is simply adhesion, and is caused by the mutual intermolecular force attractions between ones finger and the material in question. Adhesion is a surface physico-chemical phenomenon measured by the nature of the bonded adhesive joint. The word "adhesive" is a general term assigned to any material used to bond two surfaces together, and adherends are the materials being adhered together[1]. Since ancient times, humans have used naturally occurring adhesives such as pinesap and tar for various construction/domestic purposes. In the past century, as the number of manufacturing applications has blossomed, the need for adhesives to fit diverse applications has followed suit. Accordingly, adhesives have been designed for nearly every imaginable application. We rely on adhesives to seal our letters, catch flies, and partly to keep our mobile phones from falling apart.

The mechanisms of adhesion are still not fully understood and many theories can be found in the current literature. Often, the advocates of each theory offer their hypothesis as a comprehensive explanation of all adhesion phenomena and exclude other alternative explanations. Much of this confusion undoubtedly arises because the test methods commonly employed to measure the strength of adhesive joints are not well suited for comprehensive theoretical analysis, as they fail to account for indeterminate contributions from viscoelastic energy losses in the adhesive and susbtrate that inevitably influences the magnitude of the adhesion force. Nevertheless the four main mechanisims of adhesion

which have been proposed are (1) mechanical interlocking, (2) diffusion theory, (3) electrostatic theory, and (4) adsorption theory.

Mechanical interlocking[2,3] is enforced on rough surfaces where the adhesive fills the surface pores of the adherend and is partially blocked from flowing by the adherend due to the surface roughness. This is best exemplified by anyone who has amended a puncture on a bicycle hose before. The region of the puncture is usually scratched with a sand paper to roughen up the area before applying the adhesive to ensure a strong and permanent bond as interlocking is exerted.

Diffusion theory[4,5] proposes that the intrinsic adhesion of high polymers to themsleves (autohesion), and to each other, is due to mutual diffusion of polymer molecules across the interface and requires that the polymer chains are suffieciently and mutually soluble with each other. For example if two solutes are compatible with each other, they will form a homogeneous solution when mixed together. Diffusive bonding is therefore exceptionally strong bonding. In situations where an adhesive is not compatible with an adherend, a thin layer of a block copolymer which is compatible with both materials could first be coated to the substrates before bonding. A reported work demonstrated this when polystyrene (PS) was adhered to polyisoprene (PI), by the application of a thin layer of a PS-PI block copolymer at the interface of the two incompatible materials[6].

Electrostatic theory depicts surfaces forces that are strong and occur due to the attraction of a negatively charged adhesive surface which is brought into contact with a positively charged adherend and vice versa. Adhesion by electrostatic forces was confirmed by Derjaguin, who postulated that all adhesion mechanisms have relation to electrostatic forces[6,7].

Adsorption theory of adhesion is the most generally accepted theory and has been discussed in details by Kemball[8], Staverman[9] and Wake[10]. This theory stipulates that, provided sufficiently intimate intermolecular contact is established at the interface, the materials will adhere because of the surfaces forces acting between the atoms of the two bonding surfaces; the most common of such forces being Van der Waals forces (Figure 1.1). Van der Waals dispersion forces or London forces[11,12] occur between any two molecules in the close vicinity of each other, due to fluctuating temporary dipoles created because of a delocalization of the electron clouds. Van der Waals force is not an explicitly

strong attraction force. Dipole-dipole forces emerge when two molecules with permanent dipoles come close to each other. A strong intermolecular force is hydrogen bonding which occurs between hydrogen and either one of the atoms with a high affinity for electrons, i. e. nitrogen, oxygen or fluorine[13].

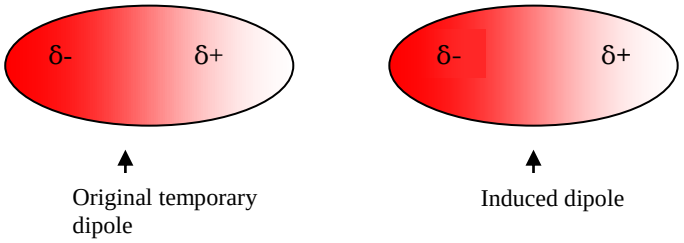

Figure 1.1: The original temporary dipole of the electron cloud to the left induces temporary dipole with opposite charge to the approaching molecule to the right, generating Van der Waals attractive force between the two atoms[11]

For the forces discussed above to be highly effective during adhesion, there should be good wettability between the adhesive and adherend. This can only be achieved if the surface energy of the adhesive is equal to or lower than the surface energy of the adherend. Surface energy is measured with contact angle technique. Flame, plasma, primers and corona discharge pre-treatments of substrate surfaces are frequently implemented in the adhesion industry, to enhance wettability which consecutively leads to good adhesion[14].

1.2 Pressure-sensitive adhesives

Today there are many types of adhesives, and the categorization is based on the fact that some adhesives require a chemical reaction, activation of UV light, heat or a solvent to generate adhesion[15,16]. This research focuses on the category of removable adhesives termed as hot-melt pressure sensitive adhesives (HMPSA), which for simplicity will be termed as pressure-sensitive adhesives (PSAs). PSAs are a version of hot-melt adhesives which adhere to most surfaces with very slight pressure. They are defined by the Pressure Sensitive Tape Council[17] as adhesives that in dry form are aggressively and permanently tacky at room temperature and will firmly adhere to a variety of dissimilar surfaces upon mere contact without the need of more than finger or hand pressure, thereby the name. PSAs are available in solvent and latex or water based forms. Some of the most common types of PSA systems include acrylic and methacrylate adhesives, styrene copolymers (SIS / SBS) and silicones[18].

The large scale application of PSAs dates back to the period during 1920-1930[19]. They were manufactured as tapes and plasters, and mainly used for medical, construction and domestic purposes. Further areas of application comprise office and fabric art tapes, packaging and surface protection materials, automotive and building products, corrosion protection tapes, etc. PSAs' universal utilization is indisputably due to their permanent tackiness, free from toxic solvents, the ease at which they bond to substrates and are removed from the substrates, without leaving any residues.

Some indispensable demands that PSAs need to meet are that they should be resistant to creep but yet have adequately low viscosity in order to flow under application processing. They should also display an elastic property after application in order to ensure long-term durability, and possess sufficient cohesiveness to be able to be peeled away from surfaces without leaving residues. For PSAs to undergo strong adhesive bonds, they should have high macromolecular mobility to ensure diffusion either across interfaces or along it[20]. For adhesives to have good creep resistance, they should have a large average molecular weight between entanglements, M_e[21,22,23] (molecular segments between entangled units in the elastomer phase). Crosby and Shull[24] have reported that for an adhesive to show outstanding bonding properties, an optimal M_e value (inversely proportional to the rubbery plateau shear elastic modulus G') needs to be reached.

Up to date, the polymer scientist has not been able to identify one polymer fulfilling these contradictory criteria. In an attempt to combat the challenge, research has taken a different path, namely the modification of adhesive products by introducing block copolymers comprised of polymers with the desired properties. Other typically used constituents in PSA blends are low molecular weight tackifying resins, mineral oil and antioxidants[1]. Linear styrene-rubber-styrene copolymers, with the rubber being isoprene, butadiene, ethylene/propylene or ethylene/butylene, are the most widely used block copolymers. This class of PSAs have unique properties which are related to their molecular superstructure[25,26].

PSAs are sophisticated blend systems and currently, there is no simple relationship between the properties of the constituents and the product performance. Michiharu et al[27] explained in their study of acrylic based PSA where adhesion is improved by the formation of micro-domain structure imparting strong hydrogen bonds to substrates. Zosel[28] used for

the first time in-situ optical observations during the debonding of a metal disk probe with adhesive deposited on the metal surface in a probe tack test, and demonstrated that good adhesives are able to form bridging fibrils between the probe and the substrate. More of the understanding of the PSA behaviour is presented in Chapter 2.

PSA is still widely used today and one of the areas of interest for this project is its application to hygienic products such as diapers and feminine utilities. During manufacturing of such products, the blended bulk adhesive is heated at a specified temperature of preference to acquire a low viscosity, and the molten adhesive is typically slot-coated directly onto a non-bonding paper stock substrate at room temperature and then covered with a release liner. Alternatively, the adhesive may be transfer-coated by first applying the adhesive to the release liner and subsequently contacting the adhesive to the substrate layer, sandwiching the hot melt PSA between the substrate and the release paper[29]. Film processing by dissolving the adhesive in a suitable solvent[30] and allowing the solvent to dry off before application does occur but the hot-melt processing is more environmentally friendly and a preferred choice in the industry. The adhesive manufacturing process in presented in Chapter 3.

The challenge currently facing the industry is the impact of the film coating temperature which seems to govern the performance of the thin adhesive film. This temperature has proved to generate adhesive films with superior peel strength if the coating is performed typically beyond 150^{o}C, as compared to poor bonding ability if the coating is performed typically below 150^{o}C. This generates high film manufacturing costs, as well as the detrimental impact on substrate materials such as shrinkage. Therefore the commercial importance of PSAs underlies the quest for a better fundamental understanding of these materials on the macro- to the molecular level. Such an understanding will enable the predictions of adhesive performance which will consequently lead to the design of more cost-effective and yet better PSAs.

On a practical point of view the findings in this thesis work may prove significant for the industry when applying the results to technical multi-blend systems, where the quality of the blend processing and application are influenced by the nature of the product. Such nature can be the product morphology down to the nanoscale range, as is the situation in adhesive technology and other thermoplastic product engineering. The understanding of the relationship between the film molecular architecture and property, to the adhesion

performance, should help in designing and optimising adhesive products suitable for a wide variety of substrates.

1.3 Thesis Structure

1.3.1 Aims of the Thesis

Although the research and development of the hot-melt PSAs has been well-developed, the demands for easy-processing and high-performance adhesives are still a driver for future PSAs. Meanwhile the methodology of formulation and characterisation used in this discipline and industry is still traditional and partially empirical, and it fails to explain some of the problems and phenomena often occurred in the product development and industrial processing, as mentioned above.

The results gained in this thesis will contribute to new fundamental knowledge as well as to new PSA product development and process. The main areas of the research therefore include:

- Characterization and analysis of chemical and physical properties at the surfaces of PSAs on multiple levels. The analysis will focus on surface morphology and adhesion properties on the macro- to the nanometre scale.
- Effect of factors at the coating manufacturing process to the adhesive film's bonding and debonding characteristics.
- The interfacial characterisation and analysis of adhesion and debonding.
- Provide an understanding of the adhesion mechanism between pressure sensitive adhesive film and the soft non-woven fabrics used for hygiene product applications

1.3.2 Outline of the Thesis

Chapter 1. Introduction to adhesion, PSA, and outline of thesis.

Chapter 2. Includes review on thermodynamics of polymer mixing. Emphasis is directed towards block copolymers that underpin the property of the PSA, and tackifiers. Literature

review on the principles of PSAs is presented, with the current understanding of PSAs and the roles of the blend constituents.

Chapter 3. Presents the materials and methods used in this research work.

Chapter 4. Establishes the problem facing the adhesive industry, through the investigation of the mechanical properties of PSA bulk samples annealed at temperatures typically implemented at film manufacturing process. The investigation of the adhesive peel strength with some non-woven fabrics is also presented.

Chapter 5. Exploration of the dynamic viscoelastic behaviour of different PSA films with discernible film processing thermal histories. *This chapter is in preparation for publication.*

Chapter 6. Demonstates the hierarchal adhesive film structure, from the micro- to nanoscale level, including the chemical nature of the near-surface of coated and annealed films. *This chapter is in preparation for publication.*

Chapter 7. Local adhesion properties on the nano-scale level are discussed here, together with measurement of film surface elastic modulus. *This chapter is in preparation for publication.*

Chapter 8. Gives concluding remarks and suggestions for future studies.

Chapter 2

2 Polymers, Block copolymer blends and pressure sensitive adhesive

2.1 Introduction

This chapter discusses hierarchical thermodynamics of polymer mixing. Parameters such entropy and enthalpy contributions to the Gibbs free energy of mixing are presented. Topics like polymer phase separation, structure and viscoelasticity are also discussed. The behaviour of block copolymers and tackifiers are especially highlighted since they serve as the fulcrum of the adhesive formulations utilized in the research work. Furthermore literature review on the principles of hot melt PSAs, and the current understanding of the end-use performance are introduced.

2.2 Polymers and copolymers

2.2.1 Polymers

A polymer is a substance made up of recurring structural units termed monomers. Prior to the early 1920's, chemists doubted the existence of molecules having molecular weights greater than a few thousand[31,32,33]. This view was changed by Hermann Staudinger, who received the Nobel Prize in Chemistry in 1953. Staudinger proposed that polymers were made up of macromolecules composed of 10,000 or more atoms, contradicting the previous rationalization that they were colloidal aggregates of small molecules with quite non-specific chemical structures[32-34]. The mass of polymers are generally defined by two experimentally determined values[34], which are the number average molecular weight $M_{n,}$ according to

$$M_n = \sum n_i M_i \quad 2.1$$

Where n_i is the mole fraction of chains with molecular weight M_i, and the weight average molecular weight M_w, according to

$$M_w = \sum w_i M_i \quad 2.2$$

Where w_i (= $n_i M_i / M_n$) is the weight fraction of chains with molecular weights M_i. Since the larger molecules in a sample weigh more than the smaller molecules, the weight average M_w is skewed to higher values, and is always greater than M_n. As the weight dispersion of molecules in a polymer sample narrows, M_w approaches M_n, and in unlikely cases whereby the polymer molecules have identical weights equivalent to a pure monodispersed sample, the ratio M_w/M_n which defines the polydispersity becomes unity[35].

The knowledge of definite chemical structures for polymers has had far reaching practical applications, because it has led to an understanding of how and why the physical and chemical properties of polymers change with the nature of the monomers from which they are synthesized. This means that to a very considerable degree, the properties of a polymer can be tailored to particular practical applications[32-34].

In a homopolymer sample, if there exists a high degree of order between the chain segments, the segments can undergo intermolecular bonding typically via Van der Waals forces, to generate crystallites. Factors that influence the degree of crystallinity are[35]: (1) chain length, (2) chain branching, (3) molecular structure (tacticity) and (4) Interchain bonding (crosslinking). If the polymer segments lack any degree of order and are essentially randomly placed with respect to each other, they form what is known as an amorphous polymer[32-35]. Semi-crystalline polymers often occur when the polymeric material exhibits both crystallite and amorphous regions, as illustrated in Figure 2.1.

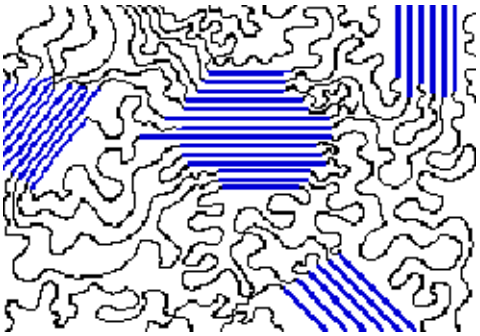

Figure 2.1: An illustration depicting a polymer with ordered or crystalline-like regions mixed together with disordered or amorphous regions[35].

In terms of general properties, polymers are usually classified according to their chain architectures. The structural characteristics that are the most important in determining the properties of polymers are (1) the degree of rigidity of the polymer molecules, (2) molecular weight, (3) the electrostatic and Van der Waals attractive forces between the chains, (4) the degree to which the chains tend to form crystalline domains, (5) the degree of cross-linking between the chains and (6) chain branching with side configuration (tacticity)[34,35]. Because of the diversity of function and structure found in the field of polymers, they are commonly placed under convenient headings as shown in Figure 2.2. The Classification (Fig. 2.2) based on the physical and chemical properties of synthetic polymers typically assigns them to two major categories known as **thermoplastic and thermosetting** polymers.

Thermoplastic polymers are made of linear (1D) or branched, dentritic (2D) chains in an amorphous or semi-crystalline hard phase in most cases at room temperature, but on heating they become soft, more or less fluid and can be molded. Their properties are thermoreversible. **Thermoplastic adhesive** is applied in its molten form, and will adhere to a surface when cooled to temperatures below its melting point[31]. Some of the thermoplastic adhesives are sensitive to UV rays, have poor heat, chemical, and creep resistance. However innovations in the area by tailoring special combinations of copolymers, can remove some of the limitations. Some common thermoplastic adhesives are polyvinyl acetate (PVA), polyvinyl alcohol (PVA), polyacrylates, polyamides, ethylene vinyl acetate (EVA) copolymers, and styrene-rubber copolymers[36].

Thermosetting polymers are made of 3D network chains which can be moulded at room temperature or above, but when heated more strongly become permanently hard and

infusible[32-34]. **Thermosetting adhesives** adhere to a surface by chemical curing or by the application of heat[31]. They set as a result of the build up of molecular chains to produce a rigid crosslinked structure. They have good creep resistance, higher modulus, and higher temperature resistance than thermoplastics and elastomers. Commonly used thermo-setters include epoxy resins and polyurethanes that are heat resistant once cured.

From the application viewpoint, polymers can either be plastics, rubbers (elastomers), adhesives or paints. These can still be either thermoplastics or thermo-setters depending on their characteristics. A plastic is not well defined and is an organic high polymer capable of changing its shape on the application of a force and retaining this shape on removable of the force, i.e. a material in which a stress produces a non-reversible strain[32-36].

An elastomer is a polymer that exhibits rubber properties, i.e. a material that can be stretched to several times its original length without breaking and which, upon release of the stress, immediately returns to its original length. Rubbers are almost elastic materials, i.e. their deformation is instantaneous and they almost show no creep[37]. The fundamental requirements of any potential elastomer are that the polymer is amorphous with a low cohesive energy, and that it is used at temperatures above glass transition. Such a polymer is characterised by a low modulus (about 10^5 Nm^{-2})[34] and, for useful elastomers, by large reversible extensions. This reversibility characteristic requires a polymer in which there is a highly localized mobility of segments, but a low overall movement of chains relative to one another. The first requirement is satisfied by flexible chains, with low cohesive energy, which are not inclined to crystallize (although the development of some crystalline order on stretching is advantageous). The second requirement, prevention of chain slippage, is overcome by cross-linking the chains to form a three-dimensional network. Crosslinking provides anchoring points for the chains and these anchor points restrain excessive movement and maintain the position of the chain in the network[34,35,37].

The unique characteristics of rubber was discovered in 1805 by John Gough, whose work was based on studies of natural rubber (polyisoprene), obtained in the form of latex from the tree *Hevea Braziliensis*[38]. Later development of rubber technology has involved peroxide crosslinking and thermoplastic elastomers. The former is achieved through covalent bonds (chemical crosslinks), and the latter consists of block-copolymers with hard (physical crosslinks) and flexible segments. The crosslink domains (physical crosslinks) can either be in glassy amorphous or semi-crystalline states[38]. These materials can be

processed by conventional thermoplastic processing methods at temperatures above the glass transition temperature or above the crystal melting point of the hard segments. More about elastomers is presented in Section 2.5.1.

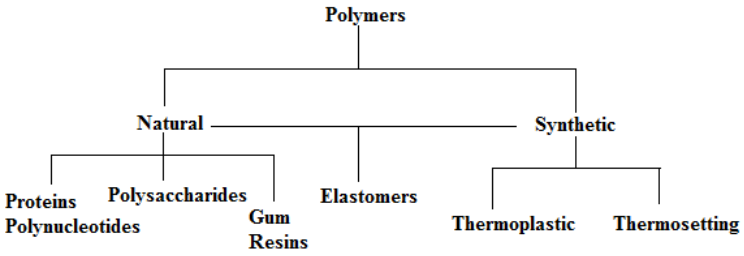

Figure 2.2: Classification of polymers[34]

2.2.2 Copolymers

The molecular structure achieved by covalently bonding different incompatible monomers with anionic polymerisation has allowed the formation of AB and ABA, diblock and triblock copolymers, respectively[33-35,39]. It is useful to distinguish the several ways in which different monomeric units might be incorporated in a polymeric molecule into a copolymer. The following examples refer to a two component system, in which one monomer is designated A, and the other B[33-35,39].

- **Statistical Copolymers** – Also called random copolymers, where monomer units are distributed randomly: ~AABABAAABBBABB~
- **Alternating Copolymers** – Here monomer units are distributed with nearly equimolar amounts of each in the chain:~ABABABABABABABA~
- **Block Copolymers** – A long sequence or block of one monomer is joined to a block of the other monomer (Fig. 2.3): ~AAAAAAA-BBBBBBB-AAAAA-BBBB
- **Graft Copolymers**: As the name suggests, side chain of a given monomer is attached to the main chain of the second monomer: ~AAAAA(BBBBB~)AAAAA(BBB~)AA~

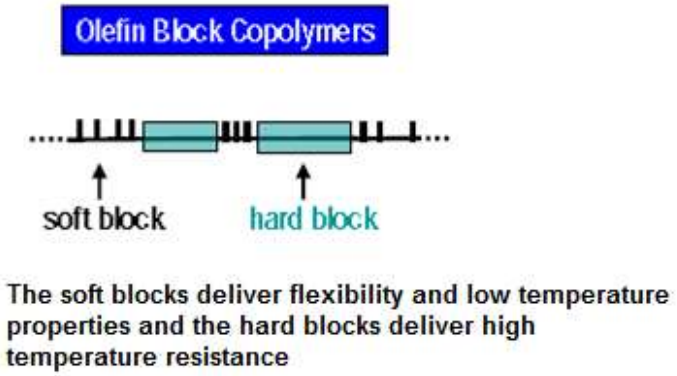

Figure 2.3: Microstructure of olefin block copolymer typically used for pressure-sensitive adhesive application[40]

Block copolymers are lauded as a breakthrough in PSA technology due to a unique block structure that delivers novel combinations of end-use properties and processability with cost-effective product manufacturing. The choice and function of some block copolymers for PSA application relate to the unique rheological characteristics, indicative of a low softening point and low molten viscosity in combination to high cohesive strength[1,41]. Thermoplastic block copolymers[40,41] (Fig. 2.3) constitute the most frequently used category of polymers, of which poly(styrene-*b*-butadiene-*b*-styrene) (SBS) and poly(styrene-*b*-isoprene-*b*-styrene) (SIS) are commonly preferred.

2.3 Polymer mixing and phase separation

2.3.1 Entropy of mixing

In the blending of polymers or copolymers applied to the adhesive industry, compatibility is a key parameter for mixing of the formulation components. Many polymers having high molecular mass are immiscible[42]. To understand the behaviour of polymer blends and polymers in solution more fully, knowledge of the enthalpic and entropic contributions to the Gibbs free energy of mixing ΔG^M is required. The state of miscibility of any mixture is given by the Gibbs free energy of mixing[38,42,43] as,

$$\Delta G^M = \Delta H^M - T\Delta S^M \qquad 2.3$$

Where ΔH^M and ΔS^M are the enthalpy and entropy of mixing, respectively, and T is the absolute temperature. According to the Second Law of Thermodynamics two components will only mix if the free energy of mixing is negative[38,42,43]:

$$\Delta G^M < 0 \tag{2.4}$$

Based on the thermodynamic theory of molecular mixing the following effects contribute to the Gibbs free energy of mixing: the combinatorial entropy of mixing, the intermolecular interaction and the free volume effect arising from the different free volumes of any two components[38,42,43]. For combinatorial entropy of mixing, an equation begins with the Boltzmann relationship as[38,42,43].

$$\Delta S^M = k \ln \Omega \tag{2.5}$$

Where k is the Boltzmann constant, and Ω represent the summation of combinations of arranging of N molecules of component (A) (N_A) and N molecules of component (B) (N_B) into a regular lattice of N ($N=N_A + N_B$) cells[42,43],

$$\Omega = \frac{N!}{N_A!\, N_B!} \tag{2.6}$$

And application of Stirling's approximation yields[38]:

$$\ln N! = N \ln N - N \tag{2.7}$$

Substitution of Eq. 2.7 into Eq. 2.6 and then Eq. 2.5 yields[38]:

$$\Delta S^M = k(N \ln N - N_A \ln N_A - N_B \ln N_B) = -k(N_A \ln x_A + N_B \ln x_B) \tag{2.8}$$

Where $x_A = N_A/N$ and $x_B = N_B/N$. This expression is derived assuming that[43,44] (a) the volume change on mixing $\Delta V^M = 0$, (b) the molecules in the mixture are all of equal sizes, (c) all possible arrangements have the same energy, $\Delta H^M = 0$, and (d) the motion of the components about their equilibrium positions remains unchanged on mixing. Thus the free energy of mixing ΔG^M is

$$\Delta G^M = -T\Delta S^M = -kT(N_A \ln x_A + N_B \ln x_B) \qquad 2.9$$

This shows that mixing in ideal systems is an entropically driven, spontaneous process. Nevertheless, it was recognised that, for a mixture of solvent and polymer the above expression did not agree with experimental observations, as deviations from the assumptions (a) to (d) occur[43-44]. Due to the disagreement between the experimental evidence acquired with vapour pressure measurements[44] and the theory, the value of the mole fraction (x_i) was therefore replaced with volume fraction, ϕ_i, to yield a more realistic agreement[42-44].

Flory[45] and Huggins[46] considered that the formation of a polymer solution depends on (a) the transfer of the polymer chain from the pure, solid state where it is restricted to only one of many conformations, into a state of disorder which has the necessary freedom to allow the chain to be randomly placed on a lattice, and (b) on passing into the liquid solution the chain achieves relative freedom and can now change rapidly among a multitude of possible equi-energetic conformations, dictated partly by the chain flexibility and partly by the interactions with the solvent. For polymer blends, the assumption made is that, the lattice consists of N cells with a volume of V. Each polymer molecule occupies volumes V_A and V_B, respectively. The molecular volume, V_i, is equal to the product of V_{mer} and the number of *mer* units. For solvents, the number of *mer* is 1. The volume fractions ϕ_A and ϕ_B are represented by the relations[38,42-44]:

$$\phi_A = \frac{V_A N_A}{V_A N_A + V_B N_B}; \quad \phi_B = \frac{V_B N_B}{V_A N_A + V_B N_B} \quad and\ V = V_A N_A + V_B N_B \qquad 2.10$$

In accordance with the assumptions for placement of polymers in the lattice, substitution of Eq. 2.10 into Eq. 2.8 generates[38]:

$$\Delta S^M = -k(N_A \ln \phi_A + N_B \ln \phi_B) = -kV\left(\frac{\phi_A}{V_A}\ln \phi_A + \frac{\phi_B}{V_B}\ln \phi_B\right) \qquad 2.11$$

for molecular volume or molar volume, respectively. As V_i can conveniently be expressed as a function of a reference volume V_o such that $V_i = N_i V_o$ and assuming that, without introducing significant error, N can be equated with the degree of polymerization for the polymer then[38,42-44]:

$$\Delta S^M = -\frac{RV}{V_o}\left(\frac{\phi_A}{N_A}\ln\phi_A + \frac{\phi_B}{N_B}\ln\phi_B\right) \qquad 2.12$$

The change from mole fraction to volume fraction for x_A and x_B is only valid if it is assumed that this ratio is expressed as the number of cells occupied by segments of A (or B) over the total number of cells in the lattice. If the volume fraction form is retained, then for a simple liquid-liquid mixture, $N_A = N_B$, but for a solution of solvent molecule (A) and polymer (B) solution, $N_B >> 1$ and the last term in Eq. 2.12 will be smaller than equivalent term calculated for small molecules[38,42-44]. Consequently the combinatorial entropy to the mixing process in a polymer solution is not as large as that for solutions of small molecules when calculated in terms of volume fractions and expressed as per mole of sites. The one basic problem with the Flory-Huggins approach is the selection of the *mer* units such that the *mer* units of the different polymers occupy a similar volume[42]. Though this theoretical approach is not ideal, it nevertheless allows for at least a qualitative assessment of the thermodynamics of polymer blends[42-46]. An illustration in Figure 2.4 demonstrates lattice arrangements for, solvent-solvent >> solvent-polymer >> polymer-polymer[42].

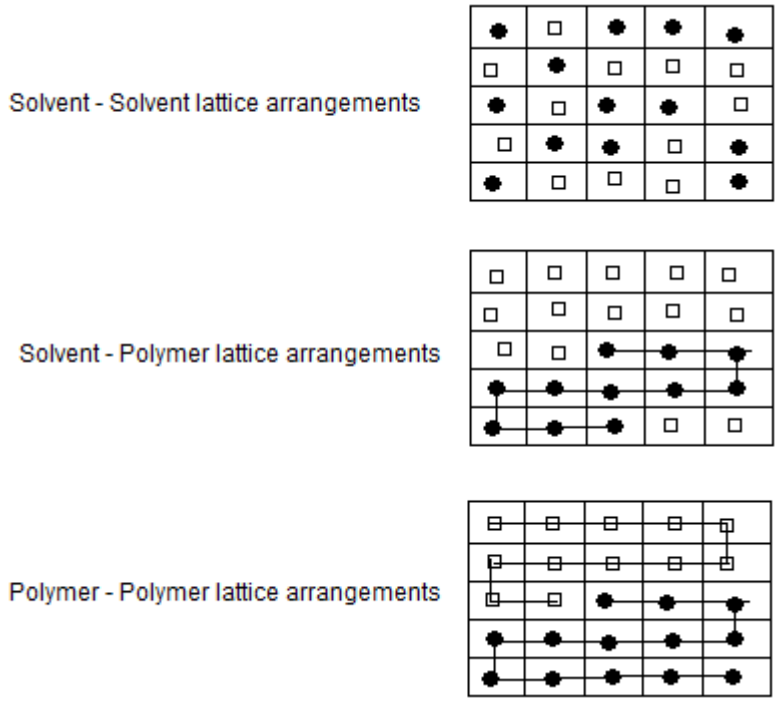

Figure 2.4: Schematic of solvent-solvent, solvent-polymer and polymer-polymer arrangements in a lattice of N cells, a visual illustration of combinatorial entropy[42].

2.3.2 Enthalpy of mixing

In addition to the entropy effect, an enthalpy change can also be expected with molecular mixing. Applying the regular lattice model, the enthalpy can be represented by a quasi-chemical process where three molecular interactions can be considered and related as[33,42-44]:

$$w_{AB} = \frac{1}{2}(\varepsilon_{AA} + \varepsilon_{BB}) - \varepsilon_{AB} \qquad 2.13$$

Where ε_{ij} is the energy of contacts between components i and j and w_{AB} is the exchange energy of interacting segments. Assuming the mixture is incompressible, every site of the lattice must be occupied either by an A component or by a B component, so $\phi_A + \phi_B = 1$. The heat of mixing is then related to the w_{AB} by the expression:

$$\Delta H^M = z w_{AB} \phi_A \phi_B \qquad 2.14$$

Where z is a coordination number, i.e. the number of nearest neighbours for a lattice site where each one is occupied either by one polymer chain segment or a solvent molecule. To eliminate z a dimensionless parameter commonly termed the Flory-Huggins interaction parameter, χ_{AB}, is employed and defined as[38,42-46],

$$\chi_{AB} = \frac{zw_{AB}}{kT} \quad 2.15$$

Leading to

$$\Delta H^M = \chi_{AB}\phi_A\phi_B kT \quad 2.16$$

In words, χ is the energy change, in units of kT, when for instance a segment of A is taken from an environment of pure A and swapped with a segment of B in an environment of pure B[38,42-46]. If χ is positive for components in a mixed state, the state will exhibit energy and therefore such a mixture is energetically unfavourable and will be prone to phase separation, though sometimes entropic factors may outweigh the enthalpic factors. Conversely a negative χ means that mixing is energetically favourable[38,42-46]. Having calculated the entropy and enthalpy contributions to mixing, these can now be combined to give the expression for the free energy of mixing, $\Delta G^M = \Delta H^M - T\Delta S^M$ as:

$$\Delta G^M = kT\left(\frac{\phi_A}{N_A}\ln\phi_A + \frac{\phi_B}{N_B}\ln\phi_B + \chi\phi_A\phi_B\right) \quad 2.17$$

It has already been stated how for instance a mixture of polymers generating a negative χ will be thermodynamically favourable and the polymers will mix fully. This is often due to specific interactions such as a hydrogen bond formation between the different polymer segments. In the absence of a specific interaction, segments interact via the Van der Waals force[45], and this always leads to a positive χ value. Van der Waals interaction energies are essentially proportional to the product of the polarisabilities of the interacting species, which always results in positive χ value. So it can be said that, in the absence of a specific interaction, for a high enough relative molecular mass, polymers are always immiscible[42-46].

Based on the simple Flory-Huggins concept, χ is entirely of energetic, rather than entropic origin, and it is inversely proportional to temperature (Eq. 2.15). This then insinuates that phase separation takes place in polymer mixtures as one lowers the temperature. This usually occurs at a critical temperature[38,42-444], the so-called 'upper critical solution

temperature' (UCST), as illustrated in Figure 2.5. In fact it is observed in many polymer mixtures that phases separate as the temperature is raised, and these systems exhibit the so-called 'lower critical solution temperature (LCST) at the critical temperature where phase separation occurs (Fig. 2.5). This means that the interaction parameter must have different temperature dependency and from this, it follows that the parameter is not entirely energetic in nature[43,47]. It must therefore contain an entropic component, a so-called non-combinatorial entropy of mixing, which arises from local packing constraints at the level of the polymer segments. Moreover, when χ is measured by scattering techniques, it is often found that the value χ depends quite strongly on composition[47].

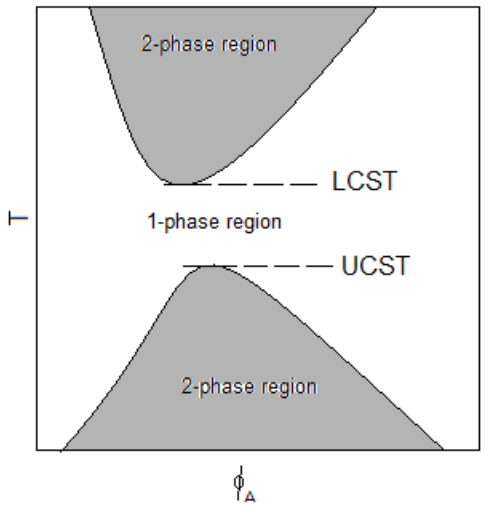

Figure 2.5: Schematic diagram of the two types of phase boundaries commonly encountered in polymer solutions. The two-phase regions characterised by the upper critical solution temperature (bottom shaded region), and the lower critical solution temperature (upper shaded region), with a single phase region, lying between the two[34].

Thus there is strong experimental evidence that Flory-Huggins theory is inadequate as a quantitative description of mixing thermodynamics in polymer mixtures. From a theoretical point of view it can be seen that errors arise due to four potential sources,

1. Implicit in the Flory-Huggins theory is the assumption of unperturbed chain statistics. This is not expected because a polymer chain in a solvent collapses as conditions are changed to bring about phase separation between the polymer and the solvent[48]. One would expect a polymer chain in a mixture to do the same as conditions for phase separation were approached[49].

2. Neglect of fluctuations. Flory-Huggins theory is a mean field theory and so neglects large composition fluctuations that occur close to the critical point. This will result in the failure of the theory close to the critical point, but for polymers it is expected that this region of failure is rather small because screening effects observed in systems of high relative molecular mass reduce the significance of these fluctuations[50].
3. The assumption that no change of volume takes place upon mixing, that there is no extra free space created when two polymers are mixed has been found experimentally to be inaccurate[34]. The reason is that if two species have a strongly unfavourable interaction, then, if mixed it will be energetically favourable for the system to lower its density slightly, thereby reducing the number of unfavourable contact and gaining some extra translational entropy associated with the 'free space'.
4. Finally, the local structure of monomers may lead to difficulties in packing, which will lead to restrictions of configurations available and thus to changes in the entropy of mixing. This is most important for pairs of polymers with very different local stiffnesses or with monomers with bulky side groups. A huge amount of effort has been done into making a more refined theory of polymer mixtures. Although many of the resulting methods have had their successes[51,52], it is probably fair to state that no single improved method has achieved universal applicability.

Despite all its shortcomings, Flory-Huggins theory provides the universal framework for considering polymer blend problems. This is partly because if one allows χ to vary with both composition and temperature in an empirical way, one is using Flory-Huggins less as a theory and more as a convenient parameterisation of the free energy. In multi component blend systems comprising for instance of homopolymers and copolymers, phase behaviour can be very complex[53], and different approaches are then required. Even simple ternary blends which only contain chemically homogeneous polymers have complicated phase-separation kinetics with complicated interfaces[54].

2.3.3 Phase separation

The Flory-Huggins theory on the free energy of mixing has clarified why it is difficult to form homogeneous mixtures of two polymers. The combinatorial entropy of mixing of two polymers is less than that of low molecular mass components. This is because the disorder

refers to the segments of the polymer, and therefore for polymer blends, due to the high molecular masses of the polymers, the term ΔS^M is virtually zero, and the entropic stabilization can be neglected[34,42,44]. Homopolymers are only miscible if there are favourable specific interactions between them leading to a negative contribution to the Gibbs free energy of mixing. Therefore $\Delta G < 0$ required for mutual miscibility of polymers can only result from other effects related to interactions between the components other than the contribution from the combinatorial entropy. The miscibility behaviour of mixtures of components may be characterised by the Hildebrand solubility parameter, δ, of each component, where a general rule of thumb is miscibility occurs if $\delta_A \sim \delta_B$[55]. According to Hildebrand[56] the solubility parameter δ is defined as the square root of the cohesive energy density as:

$$\delta = (\frac{E}{V})^{1/2} \qquad 2.18$$

Where V is the molar volume of pure solvent, and E is the molar energy of vaporization. The numerical value of the solubility parameter in the unit[57] $MPa^{1/2}$ is 2.0455 times larger than that in $(cal/cm^3)^{1/2}$. Based on solubility, Hildebrand then proposed[30-32] the heat of mixing of two non-polar components as:

$$\Delta H^M = (\delta_A - \delta_B)^2 \phi_A \phi_B V^M \qquad 2.19$$

Where ϕ_A and ϕ_B are the volume fractions of solvent and polymer, respectively, and V^M is the volume of the mixture. Equation 2.19 was found not to be correct since positive heats of mixing are only allowed and solubility parameters can be used to predict both positive and negative heats of mixing. Patterson et al[58] modified the Hildebrand Equation and proposed a non-combinatorial free energy of solution $\Delta G^M_{noncomb}$ as :

$$\Delta G^M_{noncomb.} = (\delta_A - \delta_B)^2 \phi_A \phi_B V^M \qquad 2.20$$

The non-combinatorial free energy of solution, $\Delta G^M_{noncomb,}$ includes all free energy effects other than the combinatorial entropy of solution that results by simply mixing the components. However this approach is limited when applied to polymers with high levels of secondary bonding, and it is often more advantageous to implement Hansen's concept[58] of a three-dimensional solubility parameter which includes contributions of hydrogen bonding, permanent dipole interactions and dispersion forces according to

$$\delta^2 = \delta_d^2 + \delta_p^2 + \delta_h^2 \qquad 2.21$$

Where δ_d, δ_p, and δ_h are the dispersion, electrostatic, and hydrogen bond components of δ, respectively. For molecules whose heats of vaporization can be measured, or calculated[35], one can easily determine the value of δ. The Hansen solubility is determined empirically based on multiple experimental solubility observations. However, for polymers the Hansen parameters are assigned to the parameters of the solvent causing the maximum swelling in a series of polymer swelling experiments[34], as especially crosslinked polymers do not dissolve but swell. Thus, the two quantities represented by Eq. 2.18 (Hildebrand) and Eq. 2.21 (Hansen) are expected to be similar but not always identical, because Hildebrand parameters are not always determined from heats of vaporization, particularly for substances with high boiling points. For polymers, a variety of other experimental methods are also employed[59] leading to a wide variety of experimentally reported values. Values of the solubility parameter can also be calculated from knowledge of the chemical structure of any compound, polymer or otherwise, given in tables by Small[60] and Hoy[61]. Use is made of the group molar attraction constants, G, for each group according to[61,62],

$$\delta = \frac{\rho \sum G}{M} \qquad 2.22$$

Where ρ is the density and M is the molecular weight. For a polymer M is the *mer* molecular weight. The use of solubility concept has been extended to predict the heat of mixing for polymer (A)-polymer (B) mixtures through the interaction parameter χ as[42-44,56-62].

$$\chi_{AB} = \frac{V_o}{RT}(\delta_A - \delta_B)^2 \qquad 2.23$$

Where V_o is a reference volume[44] normally assumed at a value of 100 $cm^{-3}.mol^{-1}$. A practical aspect of this is that, $(\delta_A - \delta_B)^2$ will always be zero or positive, leading to positive values for ΔH^M, thus immiscibility in the limit of very high molecular weight polymers, as stated earlier. With lower molecular weight and values of $(\delta_A - \delta_B)^2$ equal or very close to zero, miscibility can be achieved through small contribution of the combinatorial entropy[44]. Table 2.1 presents reported values of solubility parameters for some selected materials determined at 25°C. Recently Chee et al[62], proposed a relationship of temperature dependence on the solubility parameter for polymeric materials according to,

$$\delta = \delta_g + m_i(T - T_g) \quad 2.24$$

Where δ_g is the δ at the glass transition temperature (T_g)., and m_i is an empirical constant with the subscript 'i' = s, l designating the polymers below and above T_g respectively.

Table 2.1: Solubility parameters of some selected materials at 25°C.

Material	Solubility parameter δ $(cal/cm^3)^{1/2}$	Reference
Acetone	9.9	64
Benzene	9.2	64
Water	23.4	64
N-dodecane (paraffin)	7.8	63
Polyethylene	7.9	64
Polyisoprene	7.9.	64
Polybutadiene	8.4	64
Polystyrene	9.10	64

2.4 Block copolymer self-assembling and mesophase

Scientific interest in the fabrication of ordered nanostructures of block copolymers has attracted huge attention over the last decade. There has been considerable progress in the development of synthetic strategies for preparing block copolymers of various nano-structured architectures, solubilities, and functionalities[65,66]. Such architecture comprises diblock, triblock and multi-block copolymers arranged into different morphological shapes. The preparation of well-defined block copolymers requires a chain-growth polymerization mechanism than can be conducted in the absence of undesired transfer and termination steps. The anionic polymerization of styrene and isoprene was the first successful demonstration of this approach using AB diblock copolymers, i.e. poly(styrene-block-isoprene) (PS-b-PI)[67]. Subsequently a number of different routes to block copolymer synthesis have been reported, e.g., group transfer polymerization[68], cationic polymerization[69], combined anionic and photo polymerization[70], and direct anionic polymerization[71].

The unique properties of block copolymer materials rely crucially on the mesoscopic self-assembly of these materials in the molten and solid states. Such self-assembly spatially produces periodic structural patterns that can exhibit considerable complexity. These patterns are commonly referred to as microphases, mesophases, or nanophases, depending on the length of the block copolymer system[72]. Mesophases are intermediate phases between rigid, fully ordered crystals and the mobile melt[73]. The basic reason behind the self-assembling is clear. The monomers comprising the different blocks prefer energetically to be surrounded by monomers of the same kind and to avoid contact with monomers of other species[72,74,75,76,77].

At sufficiently low temperatures, known as the strong segregation limit (SSL)[65,74-77], the block polymers will arrange themselves so as to minimize contact between the different species of monomers. Were the blocks not chemically bonded to one another, they would undergo phase separation as two separated phases (Fig. 2.5). Because they are covalently bonded, they cannot separate but must arrange themselves in an ordered manner. In the simplest case of an AB diblock copolymer, there is only the issue of compatibility between dissimilar A and B blocks. Unlike binary mixtures of low-molecular-weight fluids, the entropy of mixing per unit volume of dissimilar polymers is small, as explained earlier. Thus, even minor chemical or structural differences between A and B is sufficient to produce excess free energy contributions that are usually unfavourable for mixing[65,74-77].

In the solid state of the phase segregated structures, microscopic statistical theories on phase equilibria[75,78,79,80] swelling equilibria[81], and the illustrations of models for small angle X-ray scattering (SAXS)[82],[83] profiles of block copolymers have been subsequently studied. From the experimental results of SAXS, neutron scattering[84], and transmission electron microscopy (TEM) of ultra-sectioned samples[85], and within mean-field theory[74-76,81-85], two parameters, χN, and f, have been found to control the order and disorder in block copolymers melts[86]. The parameters are ,χ, which has already been presented, the N = N_A + N_B is the total degree of polymerization, and the volume fraction of for instance the (A) component $f_{A.}$ Recently fluctuation effects have been found to contribute a third parameter to the self-assembly as[82], $\bar{N} = a^6 v^{-6} N$, where $a = R_g(N/6)^{-1/2}$ and R_g is the Gaussian coil radius of gyration and v is the segment volume. Conformational asymmetry leads to a fourth parameter[82], $\epsilon = \beta_A^2/\beta_B^2$ where $\beta^2 = a^2/6v$. The analyses and observations of microphase separation in polystyrene-polyisoprene (PS-PI) diblock copolymer have been systematically demonstrated as shown in the illustration in Figure

2.6, presenting microstructures from body-centred-cubic (BCC) spherical, hexagonal (hex) cylinders, complex bicontinuous gyroid (gyr) discovered recently between lam and hex near the ODT, and lamellae (lam), in the order of increasing f_A of polystyrene[73,85-87].

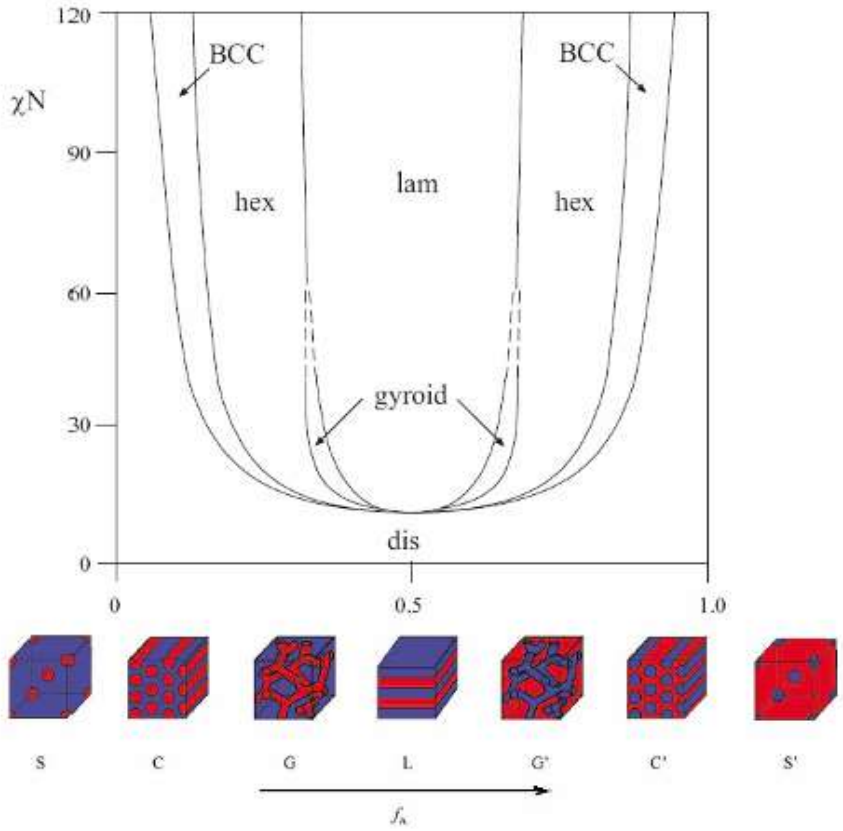

Figure 2.6: Strong segregation limit (SSL) equilibrium morphologies for $(A\text{-}B)_n$ type block copolymers. The order-disorder transition compositions shown apply to polystyrene-polyisoprene diblock copolymers where f_A corresponds to the polystyrene volume fraction[87].

At sufficiently high temperatures, of course, the system is disordered due to dominance of entropy considerations, but will order when the temperature is reduced sufficiently. The transition temperature is, to a good approximation, determined by the product χN[74-77]. Thus $\chi^* N$ = constant determines the transition temperature T^*. Note that the transition temperature is proportional to the length of blocks, because longer blocks have much smaller entropy per monomer, making it easier for the system to order.

Over the last decade, together with the complex bicontinuous gyroid phase[88], two new ordered microstructures have been discovered for the PS-PI systems. These are the hexagonally perforated layers (HPLs)[89], and the hexagonally modulated lamellae[88], as

shown in Figure 2.7. It is reported that the occurrence of these new morphologies is controlled by the overall molecular weight (i.e. N or $\overline{N}$), in addition to the classical parameters χN, and *f*, suggesting a new type of non-universality for block copolymer self-assembling[74-82].

The extent of segregation for diblock copolymers can be summarised based on the χN, and *f*, into three major regimes as: weak segregation limit (WSL) where χN ~ 10, intermediate segregation limit (ISL) with χN ~ 10 – 100, and SSL with χN > 100. Details of the other limits are found elsewhere[72].

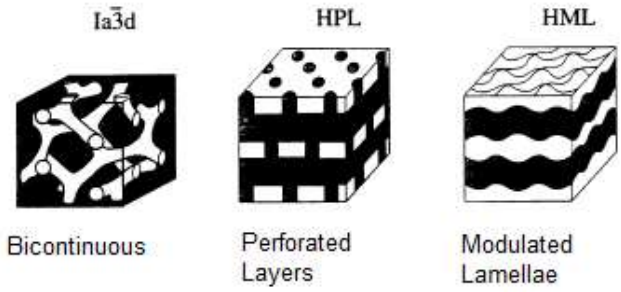

Figure 2.7: The additional microstructures of diblock copolymer self-assembly to the classical ones[72].

2.4.1 Block copolymer self-assembly in solution

Block copolymers consisting of chemically distinct homopolymers that are covalently bonded in an AB or ABA sequences, are capable of spontaneously self-organising into a variety of classical nanoscale morphologies such as lamellae, cylinders, spheres, gyroid, etc., alone as explained above, or in the presence of a solvent, homopolymer or another copolymer[90,91]. Addition of an organic solvent to a microphase-separated AB diblock[92] or ABA triblock[93,94] copolymer provides a straightforward route by which to controllably modify copolymer morphologies and accompanying properties. The presence of solvent affects segmental interactions and may alter interfacial curvature, thereby influencing morphological development, especially if the solvent is preferentially compatible with one block of the copolymer[95].

The possible utility of adding small amounts of block copolymers in adhesive blends as impact modifier is widely recognised by the adhesive industry. Efficient utilization of the copolymers calls for a better understanding of the thermodynamics governing the miscibility behaviour and adhesive film morphology as a result. Both theoretical concepts[74,96,97] and experimental observations[82,98,99,100,101,102,103] have shown that when di- or triblock copolymers are used in a solvent-selective blend system, the block polymer compatible with the solvent will form an equilibrium continuous phase with the solvent and the incompatible block polymer will assemble into independent microphase separated domains. Efforts have been done in an attempt to explain how, when, and to what extent phase separation occurs in an incompatible copolymer[74,96-103]. Many of the explanations ultimately rest in the realm of thermodynamics, and in particular with arguments based upon issues of solubility. In systems for instance, with adhesive blend formulations where the triblocks are covalently attached, they are restricted with regard to the scale over which they may phase separate.

In small amounts, both diblock and triblock copolymers form micelles with selective solvents, however triblock copolymers can adopt more topologies[90-99]. In reported studies by Kossauth et al[104]., and others[105], about styrene-ethylene/butylene-styrene (SEBS) gel systems, they found that the polystyrene (PS) formed different phase-separated glassy domains from spherical-to-hexagonal-to-lamellae structures within the continuous phase of oil and elastomers. The PS was incompatible with the continuous phase and therefore undertook the different energetically favourable distinguished structures as its content in the gel was increased. Balsara et al[102]., schematically showed the possible structures formed by diblock and triblock copolymers in a selective solvent, as displayed in Figure 2.8. Figure 2.8(a) reveals the case of diblock (AB) and triblock (BAB) copolymers where solvent is selective to the endblocks. The micelle core is made up of A block surrounded by a corona of solvated B blocks with one end "tethered" to the core-corona interface, while the other end is free. Preferential dissolution of midblock in BAB triblock is shown in Figure 2.8b-d. Figure 2.8(b) shows flower-like micelles due to the formation of loop by solvated midblocks, which causes an additional entropy penalty. If this penalty is too large, endblocks extend into the solution as free ends, Fig. 2.8(c). This entropic penalty is also overcome by formation of branched structures of the triblock copolymers (BAB) where endblocks (B blocks) connect to different cores, as illustrated in Fig. 2.8d.

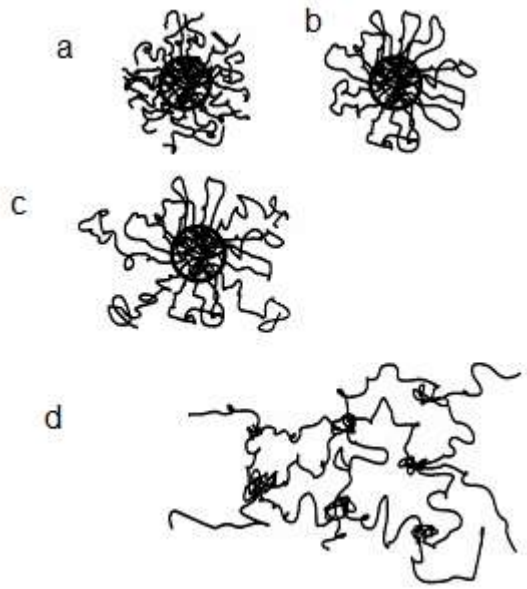

Figure 2.8: Possible micelles and aggregates formed by diblock and triblock copolymers in selective solvents. (a) Solvent is selective towards endblock or B block in case of AB and BAB block copolymers. (b) For high loop/bridge ratio, flower-like micelles in case of BAB triblock copolymer where solvent is selective towards A block. (c) A block selective BAB triblock with some free B block extending into solution. (d) A block selective BAB triblocks, branched structure formed where strands of B blocks extending into the core of different micelles[102].

In semidilute and concentrated solutions, the microdomain formation of diblock and triblock copolymers are different. In the case of diblock (AB) copolymers, molecules are coupled through the entanglement of solvated B blocks in the corona of the close-packed microlattice[106,107,108]. In the case of the triblock copolymers at high copolymer dilution, the midblock adopts conformations such as loops (both endblocks resides in the same micelle), bridges (each endblock resides in different micelle), and dangling ends where a fraction of the endblocks choose to reside in the matrix and remain unassociated with a micelle, as clearly illustrated in Figure 2.9. In these systems gelation could occur by bridging of the micelles[109,110], along with entanglements[94], which results in a 3-D network formation, the so-called physical gel[99]. Bridged midblocks are responsible for the formation of the 3-D network that binds the solvent and creates the physical gel, that is stabilized by the micelles of the glassy or semcrystalline copolymer enblocks. Gels represent a state of matter between solid and liquid exhibiting a solid-like behaviour when one of the components in solution forms a 3-D network[105]. Previous studies[111,112] on SEBS copolymer/oil blends

have shown that the oil is completely bound within the midblock network at oil mass fractions of up to 0.90.

Thermoplastic elastomer triblock or multiblock copolymers with rubbery midblock and glass/semicrystalline endblocks, in the presence of midblock selective solvent are designated as thermoplastic gels (TPEGs)[105,113]. Properties of TPEGs are greatly influenced by chemical nature of both the midblock and the endblock polymer. TPEGs are also physical gels. Physical gels are formed by intermolecular forces such as hydrogen bonds, Van der Waals forces, electrostatic forces, or other molecular interactions that favour association between certain points on different polymeric chains. These gels are also termed thermoreversible gels because the interactions taking place between connected domains are of the order of kT (k, Boltzman constant and T, absolute temperature). Hence, the network can collapse upon heating and reform upon cooling[114]. If the solvents molecules are organic, the formed physical gel is known as an "organo gel"[115].

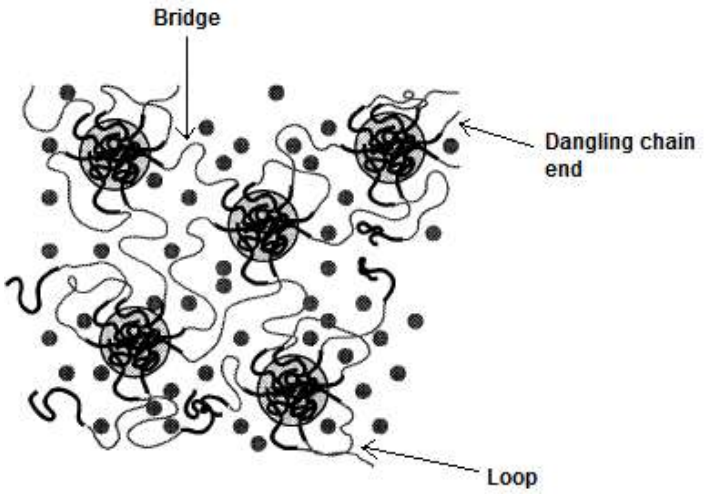

Figure 2.9: Possible micellar chain topologies for SEBS gel system[105,113]. The glassy PS micelles stabilize the gel by serving as physical crosslinks for the EB matrix containing solubilised oil.

2.4.1.1 Diblock versus triblock

An AB diblock in a micelle can only be found in a dangling topology in which the A block is in the micellar core, whereas an ABA triblock chain can form a loop, bridge or dangeling end[102]. The ability of self-associating triblock chains to bridge two insoluble domains is one main feature distinguishing them from self-associating diblock chains[116,117].

This distinction leads to a very important qualitative difference in the phase behaviour of the two systems; namely, that ABA triblock chains can form a network structure[100]. This qualitative difference also leads to different viscoelastic behaviour for the two systems. At low concentrations, diblock copolymer solutions behave like fluid suspensions of soft particles. The viscoelastic behaviour exhibited by diblocks, at high concentrations, is dominated by extensive entanglements of the B blocks in the corona of the close-packed micelles[118,119,120]. This structure has also been observed for the equivalent system of BAB triblock copolymer[121,122]. In an ABA triblock system, on the other hand, gelation could occur by bridging of the micelles in addition to entangelemnets[94]. Not only would a triblock copolymer gel have a higher elastic modulus but also a larger average lifetime (broader plateau modulus region). Furthermore, at zero or very low shear rate, a diblock "gel" would behave like a fluid because of gradual disentanglement of the polymer chains whereas the ABA triblock gel would have a finite elastic response[105-113].

In a study by Gilbert et al[123], they analyzed the individual behaviour of a styrene-isoprene-styrene (SIS) triblock and styrene-isoprene (SI) diblock copolymers of a PSA blend system. With dynamic rotational rheology measurements, they observed an onset of flow region (storage modulus $\rightarrow$ 0) for the SI diblock between 10^2 to 10^{-2} rad/s at room temperature but a frequency independent storage modulus (G') for the SIS triblock copolymer. The observation for the SIS copolymer was attributed to a viscoelastic solid-like behaviour due to the organisation of a physical network of polyisoprene trapped between glassy polystyrene nodules in the triblock network. The lack of physical network system within the SI diblock enabled the polymer chains to disentangle, align and to slip pass each other at the low frequency measurement condition. The sample then displayed behaviour as indicative of flow. However for the SIS sample, the entrapment of the elastomer segments between the styrene sequences hindered their relaxation significantly at room temperature. In terms of adhesive behaviour, this observation is significant because no creep (flow) should occur at long times, and the formulations must exhibit a rubbery-like behaviour at room temperature, once cooled[124]. The rubbery plateau (frequency independent G') region for the SI diblock was reported to be between 10^3 to 10^6 rad/s at room temperature, in the work by Gilbert et al[123].

Although there are several contrasting features between the association behaviour of diblock and triblock systems, the driving force for assembling is the same and that is the

reduction of the enthalpic contribution[110]. Table 2.2 shows comparision between diblock and triblock gels.

Table 2.2: Diblock versus triblock copolymer gel systems

Property	Diblock copolymer (AB) gel	Triblock copolymer (ABA) gel	Reference
Topology	Dangling ends	Bridges, loops, and Dangling ends	125
Gelation	Gelation occurs by Extensive Entanglement of the coronial chains	Gelation occur by bridging and entanglement	125
Aggregation number	For same M_w, higher aggregation number	Lower than diblock at same M_w	125
Elastic modulus	Lower than triblock copolymer gel	Higher than diblock copolymer gel	125
Rheological response at very low shear strain rate ($T < T_g^{core}$)	Behaves as fluid	Behaves as elastic solid	125

Over the past decade, numerous experimental studies have aimed to establish fundamental relationships between morphological and property development in styrenic triblock copolymer gels. Both commercial[126] and synthesised[127,128] styrenic based copolymers have been used for studying the effect of molecular weight, copolymer compositions, and process parameters such as temperature and shear on the properties of theses gels. Bordeianu and co-workers[129,130,131] established the relationship between the mechanical properties of styrene-butadiene-styrene (SBS) diluted with two different types of mineral oils. They found that oil with more aromatic hydrocarbons exhibited larger stress values at any given elongation and oil level. Watanabe et al.[132]., developed a transition map which classified the temperature response of SBS, diluted with n-tetradecane. They found that the rubbery-to-plastic transition temperature (48-53^oC) did not show pronounced dependency on the SBS concentration. However the plastic-to-viscous transition (103-119^oC) showed a strong concentration dependency.

Linear viscoelastic response of styrene-isoprene-styrene (SIS) copolymers dissolved in polyisoprene selective n-tetratdecane (C14) was studied by Sato at al[133]. They found that SIS/C14 exhibited a composition fluctuation in the vicinity of the order-disorder transition temperature (T_{ODT}). The stress relaxation response of SEBS TPEGs was determined under compressive deformation by Quintana et al.,[128]. They found large relaxation rates for the SEBS gels which was indicative of high mobility of the physical networks over the time of the measurement. They believed that a dynamic equilibrium existed in the SEBS gels where some junctions were broken and new ones were formed continuously. They also showed that the relaxation rates were relatively independent of the copolymer concentration. Spontak et al[134,135] have studied in details a class of styrenic TPEGs with TEM to reveal the microstructure. They found that the shape and size of the styrenic micelles are not strongly dependent on either the wt-% copolymer or processing history (quenching vs. slow cooling). They observed that as the copolymer fraction increased, the inter-domain distance (D) and linear viscoelastic strain (γ_{LVE}) decreased (Fig. 2.10). However, time to rupture, dynamic tensile and shear storage moduli, and order-disorder temperature (ODT) increased[134]. In addition they reported that the γ_{LVE} decreased with increase in both temperature and copolymer fraction[134]. They found a power law relationship between the storage modulus, and copolymer concentration (C in g/cm^3) for SEBS/oil blends and concluded that the measured modulus was a contribution of entangled midblock loops and dangling ends, along with bridged midblocks.

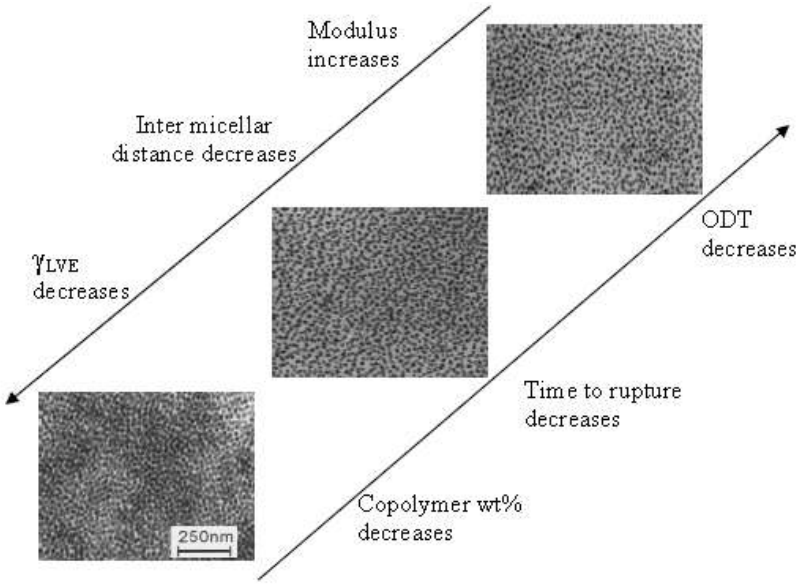

Figure 2.10: TEM micrograph of SEBS TPEG with 30, 20, 10 weight percent (wt-%) copolymer quenched from 180^{o}C to 0^{o}C[134].

King et al.[136] monitored the change in the time dependent oil content upon swelling of SIS and SEBS triblocks. Due to the greater chemical similarity of EB than I with mineral oil, they found that maximum oil uptake in the SEBS/oil and SIS/oil blends was 154% and 34% mass increase, respectively.

The alteration of the mechanical properties of TPEGs by the addition of either an endblock compatible homopolymer, to swell the micellar core[137,138], or by the addition of a diblock copolymer[139], to alter the extent at which midblock connects neighbouring micelles are also mentioned in the literature. Register and co-workers[140] have obsevered that the addition of SI diblock to SIS triblock copolymer system eliminated the macrophase separation and produced optically clear gels of very low modulus. They found that an increment in the modulus as the diblock was added at a constant triblock content was due to entanglements by the diblocks and reduction in the intermicellar spacing. A similar observation was made by Spontak et al.[134], in the storage modulus upon the addition of SI diblock in SIS triblock, in the presence of mineral oil. They explained the results based on tail-induced volume exclusion, assigned to the presence of diblock molecules, within the micellar coronas that improved the network development by increasing the population of bridged midblock (I).

2.5 Viscoelasticity of PSAs

When a PSA is applied to a substrate, the adhesive is expected to spontaneously spread on the surface with little or no applied pressure, i.e. easy wettability. However, when peeled or a weight is hung from the sample, it is expected to resist the applied force, i.e. display solid-like property[141]. This contradictory behaviour is available from viscoelastic materials. Since block copolymers provide the underlying bases of PSA formulations, it is then believed that the viscoelastic behaviours of the products are consequently governed by that of the copolymers[141]. The viscoelastic property of polymers or PSAs is typically determined by dynamic mechanical measurements (DMA), which will be further presented in Chapter 3. Based on the mechanical models by Maxwell[142,143], and Kelvin-Voigt[142,143], Hata et al[144] described that the deformation of PSAs during a peel test can be approximated as a uniaxial extension of independent adhesive strands.

When subjected to a uniaxial stress, σ, an ideal elastic material will deform proportionally to the applied stress and and return completely to its original dimensions by removal of the stress. Such material is said to obey Hooke's law, and at small applied shear stress, the corresponding strain, ϵ, which is lineraly proportional to the stress is[34,142,143].

$$\sigma = G\varepsilon \tag{2.25}$$

Where E which is the tensile modulus or Young's modulus in a stress-strain measurement is equal to the slope of the initial curves of the measurement, as illustrated in Figure 2.11. The application of a shear stress to a viscous liquid on the other hand, is relieved by viscous flow, amd for small values of σ_s can be described by Newton's law[34,142,143].

$$\sigma_s = \eta \frac{d\varepsilon_s}{dt} \tag{2.26}$$

Where η and $\frac{d\varepsilon_s}{dt}$ are the viscosity and applied shear rate, respectively. Because of their chain-like structure, polymers are not perfectly elastic bodies and deformation is accompanied by a complex series of long and short co-operative molecular rearrangements[34,142,143]. Consequently their mechanical behaviour is dominated by viscoelastic phenomena. Maxwell's model[142,143] assumes that the ideal viscoelastic strain response of a polymer to a small applied stress can be described by both Hook and Newton's laws. The two units are connected in series as shown in Figure 2.12, and the total deformation is additive of the elastic and viscous components,

$$\varepsilon_{tot} = \varepsilon_{el.} + \varepsilon_{vis.} \tag{2.27}$$

Leading to

$$\frac{d\varepsilon}{dt} = \frac{1}{G}\frac{d\sigma}{dt} + \frac{\sigma}{\eta} \tag{2.28}$$

The Kelvin-Voigt model[142,143] is constructed from the ideal elements by placing a spring and a dashpot in parallel. Any applied stress is now shared between the elements and each is subjected to the same deformation. The corresponding relationship for the constitutive relation is expressed as a linear first-order differential equation as;

$$\sigma(t) = E\varepsilon(t) + \eta\frac{d\varepsilon(t)}{dt} \qquad 2.29$$

In reality the viscoelastic behaviour of most polymers cannot be described very well by only the Maxwell or Kelvin-Voigt models based on only the two parameters. Generally more complicated models with larger numbers of the constitutive relationships are used to approximate more closely the behaviour of real polymers[142,143].

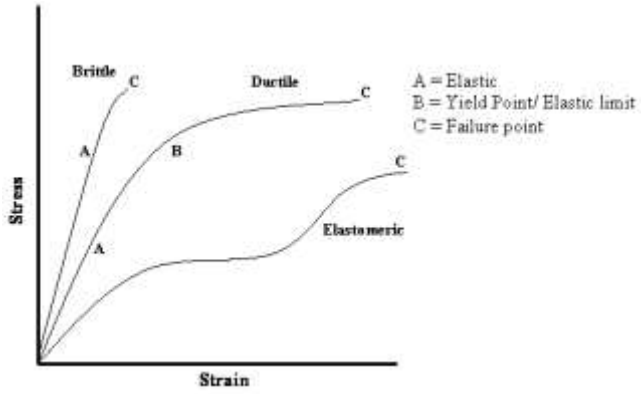

Figure 2.11: Stress-strain curves for brittle, ductile and elastomeric material[142,143].

In a stress-strain experiment, at the early low strain portion of the curve, most materials obey Hooke's law to a resonable approximation (Fig. 2.11). As the strain is increased, many materials eventually deviate from linear proportionality, the point of departure being the proportional limit. This nonlinearlity is usually associated with "stress-induced" plastic flow in the specimen[145,146]. Here the material is undergoing an internal molecular rearrangement, in which atoms are being moved to new equilibrium positions. Brittle materials lack this phenomenon since they exhibit internal microstructures that block dislocation motion[142,143]. They typically exhibit linear behaviour over full range of strain, and eventually fracture without appreciable plastic flow (Fig. 2.11). Ductile materials will continue to plastically deform above the proportional limit, with ever increasing stress, a mechanism termed strain hardening, until they eventually fracture. Their microstructural rearrangement associated with plastic flow is usually not reversed when the stress is removed, so thier proportional limit is often the same as or close to the material's elastic limit.

Elastomers strain significanlty under small stress due to the relatively high mobility of their molecular segments, which enable them to reconfigure themselves to distribute an applied stress[37,43,135]. The entropy of the chains is more favourable in the relaxed state than in the stretched state. The covalent cross-linkages ensure that the elastomer will return to

its original configuration when the stress is removed. As a result of this extreme flexibility, elastomers can reversibly extend from 5-700%, depending on the specific material[37]. Without the cross-linkages the strain of elastomers under an applied stress would result in a permanent deformation[37]. Each material's toughness is defined as the area umderneath the various curves from the strain=0, to the strain value at failure point C, and it is equivalent to the energy each sample can absorb before it breaks (Fig. 2.11).

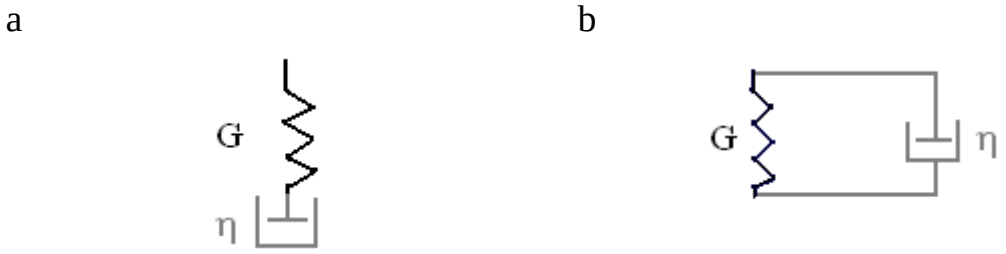

Figure 2.12: Mechanical models of. a) Maxwell and , b) Kelvin-Voigt[143,144].

2.5.1 Elasticity of polymer network systems

The molecular mechanism that underlines rubber elasticity remains one of the most unsolved problems in polymer physics. Numerous attempts to develop a molecular description of polymer networks in the last half century have been only partially successful and have left the field with a dozen competing and often conflicting models[137]. What causes such ambiguity in understanding the molecular dynamics is the unusual properties inherent to the chain-like structure of rubbers[145,146]. For example a polymer material in rubber-like state will exhibit a mechanical behaviour, which at first glance, might appear Hookean, in that extension is close to 100% recoverable[142-145]. However the force extension curve, as illustrated in Figure 2.11 does not approximate to what is expected from Hookean behaviour, except in the regions of small strains. The most obvious and also the most important physical characteristics of the rubber-like state is the high degree of deformability exhibited under the action of comparatively small stress. The maximum extensibility normally falls within the range 500 – 1000 %[34]. These properties, i.e. high extensibility and low modulus, are to be contrasted with the properties of typical hard solid (e.g steel), for which the value of Young's modulus is 2.0×10^5 N mm^{-2} and the corresponding maximum elastic (i.e. reversible) extensibility about 1.0 percent or less[34].

In rubbers, the necessary cross-linkages between the chains are normally introduced by a chemical process called vulcanization, which was originally discovered by Charles Goodyear in 1839[147]. The chemical reaction involves the formation of interchain links, composed of two, three, or four sulphur atoms, between sites of unsaturation on adjacent chains. Such crosslinks are known as chemical crosslinks (Fig. 2.13a)[148]. In systems involving copolymers of glassy polystyrene domains and elastomer chains, the crosslinks are formed by glassy polystyrene regions interconnecting elastomer chains. This is a thermo-reversible physical crosslink (Fig.2.13b).

a b

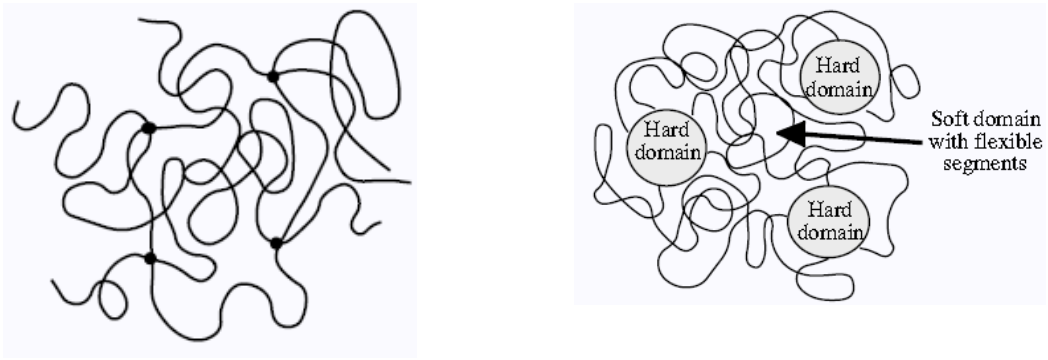

Figure 2.13: Illustrations depicting, (a) chemical Crosslinked rubber via covalent bonds and, (b) structure of thermoplastic rubber with glassy hard crosslinks[37]

Despite the complexity of the deformation curve for a rubber, the curve can be well described with a simple model based on the random arrangement of segmental units in a polymer chain. A hint at the relationship between the entropy of a polymer chain and the mechanical properties is seen when a stressed rubber is subjected to changes in temperature[149,150]. A rubber band stretched by a fixed load will shorten with increasing temperature, reflecting a net thermal contraction rather than expansion. This unique rubber property was examined further through relationships between force, length, and temperature on one hand and thermodynamic quantities, internal energy and entropy, on the other[147]. In discussing the equilibrium of a system which is subjected to reversible changes (e.g. elastic deformations), the reversible adiabatic extension of an ideal elastomer is considered first by the Helmholtz function for a system according to[143,145-150],

$$A = U - TS \qquad 2.30$$

Where A is the Helmhotz free energy and U is the internal energy. If the applied force is *f*, and l^o and l are the lengths of the sample in the un-extended and extended states, then differentiation of Eq. 2.30 with respect to l, at constant temperature gives,

$$(\frac{\partial A}{\partial l})_T = (\frac{\partial U}{\partial l})_T - T(\frac{\partial S}{\partial l})_T \qquad 2.31$$

The work done on the system during a reversible extension of the sample by an amount d*l* of an applied force *f*, is given by dA = *f* d*l* and so,

$$f = (\frac{\partial U}{\partial l})_T - T(\frac{\partial S}{\partial l})_T = f_v + f_s \qquad 2.32$$

The force is constitutive of two contributions; the energy f_v and entropy f_s. For an ideal elastomer the contribution of f_v to the total force is negligible because there is no energy change during extension and[145-150],

$$f = -T(\frac{\partial S}{\partial l})_T \qquad 2.33$$

This is the expression for an entropy spring and shows that the strain in a stretched elastomer is caused by a reduction in conformational entropy of the chains under stress. This is the fundamental reason why extended rubbers tend to retract spontaneously when the load is removed. It depends on the fact that the number of possible ways a polymer coil can exist in a compact form is overwhelmingly greater than the number of available arrangements of the chain segments in an extended ordered form. In reality the behaviour of most elastomers and polymer networks are far from ideal, and a significant contribution from f_v is found. This is because an elastomer is a three dimensional network system[37, 147,149,150], and when subjected to stress, there is a volume change and though this is small, it contributes significantly to the internal energy

A number of models have been developed to describe the relaxation properties of crosslinked polymer networks. The phantom model assumes that the cross-linkers are completely free to move in space. At the opposite extreme, the affine model assumes that the cross –linkers are confined to fixed locations and move affinely under deformation. For real networks, the fluctuations of the cross-linker junctions are partially suppressed by entanglements of the strands which are described by the constrained model. When the

strands between two neighbouring cross-linkers are longer than critical chain length, interchain entanglements may significantly affect the motion of the cross-linkers and the modulus. One of the most successful theories for the treating of the interchain entanglement is the reptation model initially proposed by de Gennes, Doi and Edwards[151]. The theory of reptation confines the motion of a polymer chain within a tube formed by neighbouring polymer chains, and the chains diffusion coefficient is proportional to the inverse of the molecular weight. The diffusion behaviour of unentangled systems can be described by the Rouse model, in which the polymer chains are modelled as a series of beads joined by rings. The diffusion coefficient is proportional to the inverse of the molecular weight. Details of the concepts and theories explaining the deformations of polymer network systems are extensively presented in the literature[147-151,152,153].

The quantitative description of the viscoelastic behaviour of multiphase thermoplastic block copolymer systems such as the PSAs is complicated by effects arising from incomplete phase separation and impacts from network structure due to physical crosslinks of hard domains and trapped entanglements of elastomer chains[154]. Roos and Creton have nevertheless proposed a model to explain the elastic behaviour of PSAs based on thermoplastic styrenic triblock copolymers[155]. Their model was developed from the more commonly affine and phantom rubber elasticity models considered that microphase separated polystyrene (PS) hard domains and soft elastomers + resin/oil matrix could be assimilated to a loosely crosslinked rubber where the PS domains were the crosslink points and the elastomers provided the entropic springs between them. The elastic modulus G' was represented by a reduced stress according to[155],

$$\sigma_R = G_c + \frac{G_e}{(0.74\lambda + 0.61\lambda^{-\frac{1}{2}} - 0.35)} \qquad 2.34$$

Where G_c represented the contribution from the fixed crosslinks, i.e., the crosslinks formed by the PS domains connected by the elastomer blocks. G_e represented the entanglement parts made up of the elastomers/resin units. Lambda λ, represented the extension ratio l/lo. According to the relationship, the elastic modulus G' observed at small strain oscillatory measurement, would be dominated by the entanglement domains G_e. At large strain (large λ), investigated with a tensile test, they found that the non-linear elastic modulus of the system was strongly controlled by G_c, i.e. the modulus of the PS domains.

2.6 Pressure-sensitive adhesives

2.6.1 Principles of development of PSAs

It is known in the adhesive industry that the base polymer and the formulation additive influence the peel of the finished product[1,19]. Hence the science and technology are based on this dependency. As known from formulation praxis, various base elastomers or visco-elastomers provide different peel resistance. Such demand requires blending of components with different properties. Diblocks and triblocks are synthesized separately and then volumetrically combined[156]. The diblocks reduces the rubbery plateau modulus and results in softening at a lower temperature[157]. When only triblock copolymers are used as base in a PSA formulation, the product will exhibit higher shear resistance, higher viscosity and a better high temperature performance[157]. The diblock/triblock content strongly affects the adhesion-cohesion balance of the formulation. In earlier work, the increase of SI/SIS ratio was found to improve the tack and peel but reduced the shear adhesion failure temperature (SAFT) of a formulation[158]. There are similarities in the role of a tackifier and that of diblocks in styrenic rubber based adhesive formulation. Principally it is possible to design a formulation on pure triblock and tackifier where the softening role of the diblock is played by the resins and a major incentive to the choice is the generally lower cost of the resins as compared to the diblocks[157,159].

Because of their unique domain structures, styrenic block copolymers (SBCs) typically used for PSAs exhibit high viscosities that are very sensitive to shear rate. During blending and application the viscosity of the SBC must be lowered by decreasing the strength of the polystyrene endblock domains[153]. In solution application this is done by dissolving the endblocks in a solvent. In hot melt applications this is accomplished by heating the polymer to a temperature substantially above the T_g of the polystyrene (PS) endblocks[160,161]. Normally, styrene-isoprene-styrene (SIS) polymers will give formulations having the lowest viscosity. However, styrene-ethylene/butylene-styrene (SEBS) and styrene-ethylene/propylene-styrene (SEPS) based adhesives can be processed at higher temperatures than the SIS and styrene-butadiene-styrene (SBS) based adhesives with less concern about polymer degradation. Thus, processing SEBS or SEPS based adhesives can be made easier by working at a higher temperature[162,163].

2.6.1.1 Role of Styrene

The styrene content is a very important polymer design parameter and greatly influences the relaxation of the rubbery matrix of the PSA[164]. The effect of the styrene content on the storage modulus of pure SIS is shown in Figure 2.14, as reported by Sims[164]. In viscoelastic terms, increasing the styrene content increases the elastic response. The storage modulus G' increases significantly as the styrene content increases from 18% to 44%. The increase in G' values shown (Fig. 2.14) with increasing styrene level is not linear because the styrene domains are going through morphological changes from spheres to rods to lamellae configuration (Fig. 2.7), which also leads to an increase in the polymer hardness[165,166]. The best SBC lattices usable for PSA include no more than 25-35% styrene with the formulation T_g between -60°C to 35°C[167]. An increase of the polystyrene content in PSAs is not possible because of the increase of the plateau modulus[19,167]

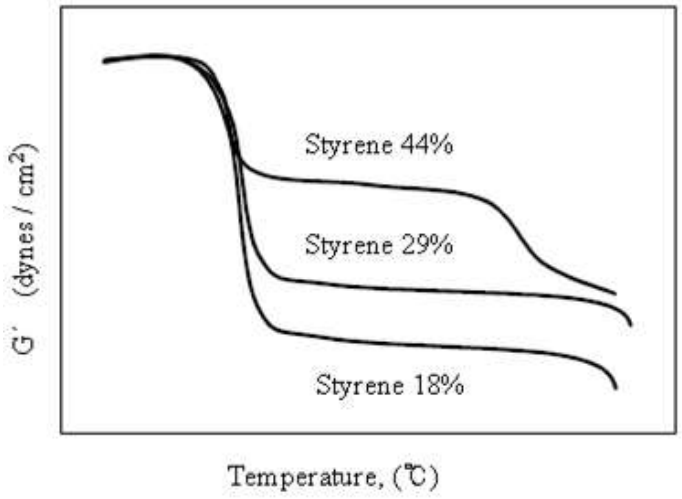

Figure 2.14: Effect of the styrene wt-% on the modulus of SIS[164].

2.6.1.2 Role of Tackifiers

Tack is defined as an adhesive's ability to form a physical bond with a substrate, under application of a very light pressure[15]. In order to obtain the required tack property, adhesives must have a relatively low moduli and short relaxation times to relieve internal stresses. Hence low molecular weight middle block compatible resins/tackifiers are added to PSA blends to increase the flow properties and surface wettability[15]. A good compounding tackifier must also have a high T_g to increase the T_g of the blend. Unlike peel

adhesion and shear resistance, the concept of tack is difficult to define. According to Johnston[168], tack has been assigned diverse names such as wet grab, quick stick, initial adhesion, finger tack, thumb tack, quick adhesion, and wettability by the PSA industry. Tack is defined by Zosel[169] as the ability of an adhesive to form a bond of measurable strength to another material under conditions of low contact pressure and short contact time. The American Society for Testing and Materials (ASTM)[170] defines tack as "the force required to separate an adherend and an adhesive at the interface shortly after they have been brought rapidly into contact under light load of short duration". However, it is not clear how long a time is considered as a short duration and also the amount of load defined as slight or light.

Nevertheless tack is not merely a material property of the adhesive, but also depends on a wide range of factors. These factors are the nature of the adherend, adhesive processing condition, contact load, dwell time, temperature of application, air humidity and the adhesive flow characteristics[171]. Due to the interaction of these variables, it is hard to describe tack by a unified theory. Creton and Leibler[172] attempted to better understand the dependence of tack on the pressure and contact time during a tack test, and to quantitatively relate the results to the molecular structure of the adhesive and the roughness of the substrate. Zosel[173] presented experimental studies of the influence of the contact formation on the adhesive or interfacial fracture energy and tack of polymer. The easiest test method of measuring tack is touching the finger lightly for a short time to a PSA and then quickly withdrawing it. Numerous standard tack tests have been developed for PSAs by different organisations and comprised by Johnston[168].

The tackifiers typically consist of short chain polymers of molecular mass between 300 and 3000 g/mol, with a softening temperature between 60^{o}C and 115^{o}C, depending on the desired nature to the final adhesive compound[174,175,176,177]. Due to the two-phase nature of styrenic elastomer block copolymers, the choice of the resin type is very important because the main properties depend on the compatibility of the resin with either the elastomeric or styrenic phase of the copolymers. For example the tackification of the styrenic aromatic domains affects the cohesion, creep and heat resistance[178,179]. The tackification of the middle block (midblock) influences the modulus, elongation and tack of the adhesives[177,179]. The midblock-associating tackifiers mix with the elastomeric domains by diluting the entanglement network and lowering the rubbery plateau modulus[123,169]. This action also creates an increase of the molecular weight between entanglement (M_e)[169]. A

lowered modulus always promotes bond formation (creep compliance), and the entanglement dilution makes the adhesive dissipate energy during deformation which causes moderately high peel force[180,181]. Generally a mixture of tackifiers with different rheological properties is added in an attempt to optimise the performance of the PSA, as depicted in the illustration by Hansen et al[182] in Figure 2.15.

Aliphatic, aliphatic/low aromatic and cycloaliphatic petroleum resins, rosin esters, and polyterpenes having low solubility parameters particularly, are strongly midblock associating resins. Such resins can show desirably lower melt viscosities and produce softer adhesives but tend to reduce cohesive strength at elevated temperature performance due to some softening of the endblocks[183,184]. The molecular weight distribution of the resin also play a decisive role in tackification and the narrower it is, the more compatible it is with the base polymer[183].

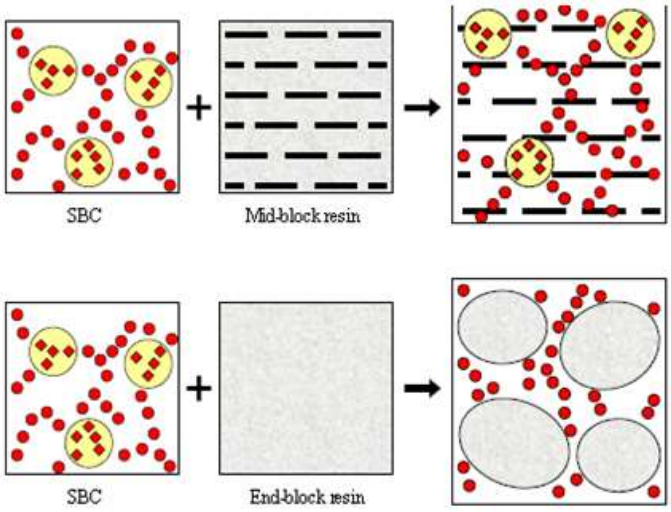

Figure 2.15: Effect of midblock and endblock tackifiers of styrene based copolymer phases[182].

Mixing of tackifiers and base copolymers depends on the mutual compatibility of the components of the blend (See Section 2.3.3). Common tackification of the base copolymers and the low molecular weight resins obeys the thermodynamic laws. The components of the blend can be mixed if the ΔG^M is negative, as elucidated in the earlier sections The tackifying effect of resins is generated if the solubility range of the base copolymer is equivalent/or equal to that of the resins. The choice of resins suitable for a certain blend formulation is made by the adhesive industry[1,19] by following a chart supplied by the resin manufacturer as that given by Exxon[184], presented in Figure 2.16.

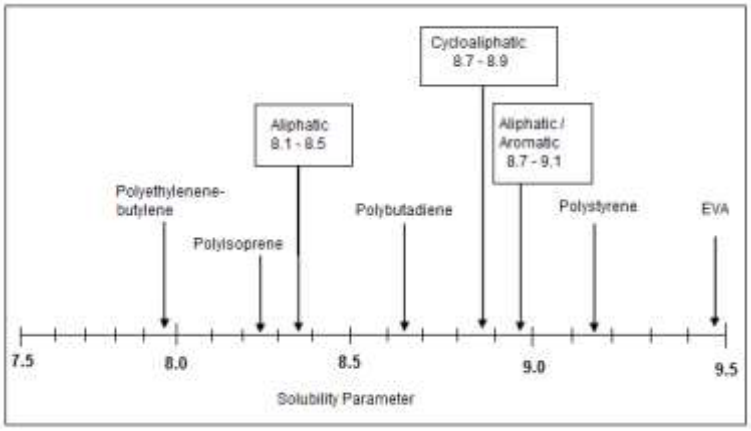

Figure 2.16: Type of resin and polymer solubility regions[184].

It has been observed experimentally that the tackifying effect prediction made by the PSA industry in regards to the mutual solubility parameters is not that straightforward. De Walt et al[185], investigated the complex behaviour of the solubility parameter, δ, in studies about blends of natural rubber (NR) and styrene butadiene rubber (SBR), with hydrocarbon and polyterpene resins based on α- and β-pinene. With the three dimensional presentation of δ (Section 2.3.3), they found that the δ ranges of the NR and the hydrocarbon resin were very different and this insinuated no tackifying effect by the resin. However their experiment generated a very high tack of the NR/hydrocarbon resin system. Similar trend was observed for the SBR/hydrocarbon resin system. Han et al[186]., reported in their studies about the viscoelastic property of SIS and endblock-associating alpha-methyl styrene (AMS) mixtures that, low M_w AMS associated more with the polyisoprene (PI) phase than with the polystyrene (PS) domains. As the M_w of AMS was increased, the resin partitioned more in the PS phase. Their observation was attributed to segregation effect whereby with the increase in the AMS blocks, the resin became less compatible with the PI phase. Lim et al[187]., found in their studies about the viscoelastic properties of SIS-based PSA with midblock-associating tackifiers that, though the resin was more compatible with the PI phase, it also associated with the PS domains, by shifting the T_g of the latter to lower temperatures. Kim and Ryu[188,189] have performed various studies on how the compatibility of aromatic resins shifted towards the different domains in an SIS and SBS systems, respectively. They reported that the shift towards each separated phase depended on the degree of hydrogenation of the cyclic resins which altered the δ of the resin. Therefore it was concluded that it is not possible to elucidate the effect of the tackifying resin based on the solubility parameter only.

The compatibility between resins and the base copolymers can also be examined with viscoelastic measurements by observing the glass transition (T_g) of the blend system. The position of the T_g is an index of the molecular mobility and pressure sensitivity. The T_g of compatible blends depends on the polymers and on their respective molecular weights. Several theoretical and empirical equations have been developed to describe the T_g dependence of polymer/polymer blends. One of these is the Fox equation[19,161]. According to the equation the T_g of a polymeric blend is related to the T_g of the pure components as:

$$\frac{1}{T_g} = \sum \left(\frac{w_i}{T_{gi}} \right) \qquad 2.35$$

Where w_i and T_{gi} are the weight fraction and the glass transition of each component, i, of the mixture. This equation assumes miscibility at random level. A compatible tackifier with endblock will affect the T_g of polystyrene by shifting it to lower, or higher temperature, depending on the T_g of the resin. The Fox equation is a quick way to investigate if the final T_g will fall between the T_gs of the two compatible components. The information obtained with the Fox Equation can be found in the phase transition observation from a viscoelastic test with dynamic mechanical analysis (DMA)[19] (Fig. 2.17).

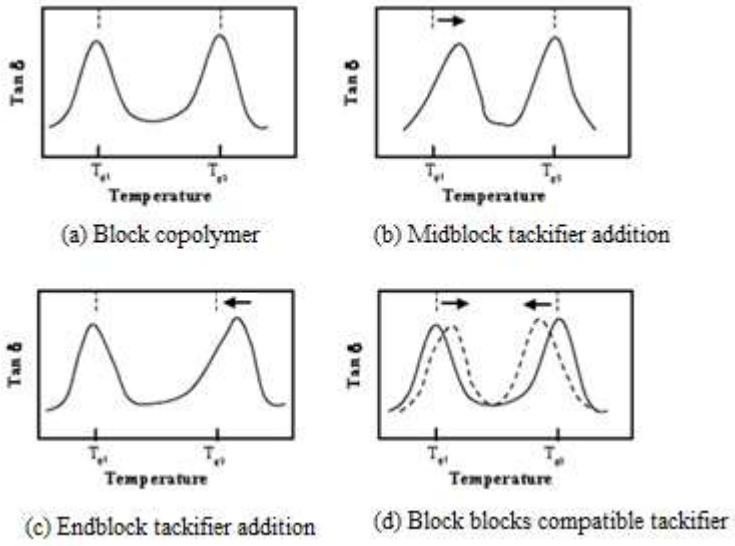

Figure 2.17: Block copolymer tackifier compatibility[19] depicting (a) phase transition of the pure base copolymer, (b) phase transition of midblock compatible resin and base copolymer where the midblock T_g is shifted to higher temperature. In (c) endblock compatible tackifier with low T_g, shifts the endblock base copolymer T_g to lower temperature and in (d) each copolymer T_g is altered as both phases are compatible with the resin.

2.6.2 Role of mineral oil

Mineral oil is a plasticizer, and plasticizers are essential in the compounding of the hot melt PSAs in order to achieve desirably low viscosities. The main effect of oil addition is to create a significant decrease in the melt viscosity and the formation of softer compounds with improved tack[190]. However it also reduces adhesion and resistance to heat and deformation. Naphthenic-paraffinic oils with a low aromatic content are preferred in HMPSA formulations[191], while aromatic oils are not used because their interaction with the polystyrene domains causes a drastic reduction in product strength[192].

2.6.3 Current understanding about structure of PSA and theory

A lot of research and industrial studies about the properties of hot-melt PSAs have been confined to the macroscopic scale and/or the behaviour of the bulk adhesive. Many studies have discussed how tailoring different blocks and resins will be suitable for diverse applications. The bonding and debonding characteristics of PSAs have been reported to depend on many factors, and earlier reports discuss how changing factors such as chemical composition, molecular weight, or molecular structure of the base polymers alter the adhesion properties entirely[193,194]. Surface properties[195], including morphology[196] also play a very important role in the strength of an adhesive bond. It has been reported that surface roughness enhances adhesion between adhesives and adherends[197]. However if the tortuousness is due to cracks or cavities, these areas deteriorate the bond strength since accumulated forces at the edges of the defected regions initiate propagation of the cavities, eventually leading to failure of the bonded joints.

The effect of a flexible substrate on the bonding ability of PSAs has been examined by A.J. Steven-Fountain et al[198]. The wettability and tackiness of a PSA system based on natural rubber and pentaerythritol ester of hydrogenated rosin have been reported in a study by Kinnosuke et al[199]. Shankaragouda et al[200] conducted a study about the impact of the viscoelasticity of adhesives on adhesively bonded lap joints. They examined how different factors affect the adhesive bond strength and found that the boundary conditions have a profound impact on the stress distribution at the bonded interface. The impact of melt versus solvent coating on the structure and properties of block copolymer based PSAs have been investigated by O'Connor et al[201]. Ick Kyung Sung et al have investigated the mechanical properties of pressure-sensitive adhesive (PSA) by examining the compatibility of various tackifiers with either polystyrene or polybutadiene in an SBS based PSA[202]. Sherriff et al have reported how the addition of a tackifying resin to an elastomer shifted the onset of the transition zone to a lower frequency and also reduced the plateau modulus[203,204]. Class and Chu have studied the viscoelastic properties of rubber-resin blends based on resin structure, resin molecular weight, and resin concentration[205]. In 1966 Dalquist proposed[206] the correlation between the viscoelastic property and performance of a PSA. He stated that in order for a PSA to wet a substrate properly during the short time of the contact charcteristics of a tack test, the one-second creep compliance at the use

temperature must be greater than 10^{-7} cm^2/dyne which is equivalent to a dynamic storage modulus (G') below 0.1 MPa at a frequency of 1 Hz in a DMA test[207].

An important usage property of commercial PSAs is the ability to debond from the substrate without leaving much residual adhesive[208], that is, it should exhibit interfacial failure. In the work on viscoelastic properties of PSAs by Creton et al.[208], they reported that the performance of PSAs which was based on tack, peel strength and shear depended on the viscoelastic response of the bulk adhesive, as well as the surface energies of the adhesive and adherend. Chang et al[209], have reported that the glass transition temperature and dynamic storage modulus (G') at the application temperature are the most important parameters for PSA performance.

High tack or peel strength generated by the adhesive's ability to dissipate a large amount of energy during debonding has been reported to occur by the formation and growth of fibrils during the bond separation[23]. Fibrillation was first observed in peel tests by Kaelble et al.,[210]. Creton and Lakrout[208] showed that the debonding process of PSAs generally proceeds in the following manner:

1. Homogenous deformation of the film in tension.
2. Nucleation of cavities at the interface between the film and probe (the number and location of these cavities are related to the presence of air pockets trapped at the interface between film and probe)
3. Simultaneous expansion of these cavities as interfacial cracks
4. Growth of the cavities in the direction normal to the plane of the film and formation of a fibrillar structure.
5. Fracture of the fibrils by creep or debonding of the foot of the fibril from the test probe.

The formation of the cavities has been observed to occur in rubbery elastic medium and suggested to be controlled by the elastic modulus of the adhesive. The cavity nucleation sites can be imparted by air pockets trapped at the adhesion interfacial layer. The nucleated cavities will then propagate and result in the formation of fibrils as the debonding process continued. Fibrils will not be formed if the cavities coalesce due to diffusion and molecular mobility processes[209]. In Crosby et al[211], they categorized various deformation and failure modes of adhesively bonded elastic layers. It was stated that three main deformation modes

can be used to categorize the early stages of the debonding processes of a compliant layer from a rigid substrate:

- Edge crack propagation
- Internal crack propagation
- Cavitation

In addition to these three main classes of deformation, the following two subclasses, related to the shape of the edge of the complaint layer, can also be defined:

- Edge crack fingering
- Bulk fingering

They considered the two classes, which are the interfacial deformation modes (edge crack propagation, edge crack fingering, and the internal crack propagation) and the bulk deformation modes (cavitation and fingering). The former are governed by the energy release rate describing the driving force for crack propagation, whereas the latter are governed by the stress within the layer. Williams et al.,[212], have reported that the debonding criterion depends on the maximum pressure applied to the adhesive, and also in one case on the time of contact.

S A. Zosel[23] adopted fracture mechanics to analyze a probe tack test, where a cylindrical probe of stainless-steel with diameters of 2-4 mm was brought into contact with PSA surfaces under well-defined conditions of contact, force and time, and subsequently separated with defined rate of separations. Plots showing the debonding processes observed by Zosel are presented in Figure 2.18. The curve in Fig. 2.18a shows a homogenous deformation of an adhesive debonding where a sharp stress maximum at comparatively low adhesive strain is observed. Zosel reported that the debonding curve exhibited a similar shape to the stress-strain plots of brittle polymeric materials in the usual tensile tests (Fig. 2.11). This behaviour was observed for the adhesives with low tack and debonded without fibril formation. The stress-strain plot shown in Fig 2.18b with a stress maximum and the pronounced shoulder with large strain at break was observed for adhesives with high tack properties and debonded through fibril formation[23].

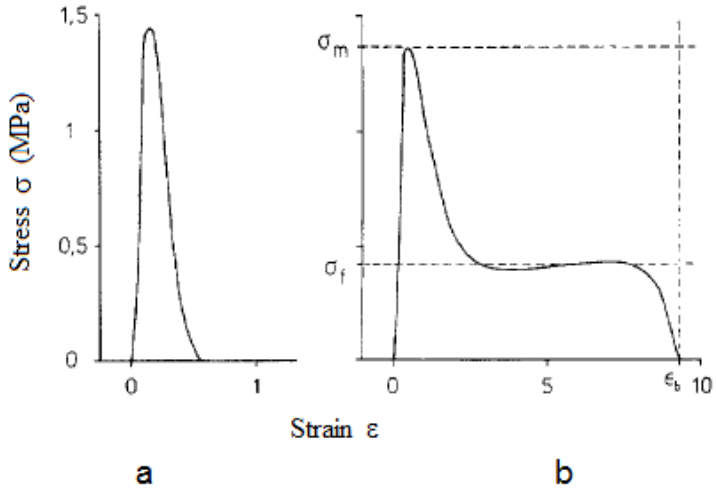

Figure 2.18: Stress-strain diagrams[23] of the debonding process for (a) homogenous deformation, and (b) fibrilation deformation.

Zosel confirmed the observation of the adhesives with high tack by means of high speed photography, that showed the adhesives deformed by the growth of fibrils and debonded from the probe surface by interfacial (fibril) fracture. The stress versus strain in Fig 2.18b offered a way to characterise the formation and growth of fibrils more quantitatively than by simple visual inspection. Three quantities are deduced from his studies[23]: (1) the apparent maximum stress σ_m, which is regarded as the critical stress for cavitation and fibril formation, (2) the height of the plateau or shoulder σ_f, which is the stress required to deform fibrils, and (3) the strain at fracture, i.e., the maximum elongation of fibrils ε_b. The nucleation of cavities under the influence of the tensile stress at the beginning of the debonding process and their growth is supposed to be the origin of fibrilation.

Additionally, the M_e has been found to play a very important role on the debonding stage in a PSA, by influencing the ability for the adhesive fibrilation, the type of rupture, and consequently the debonding energy[213]. In adhesive failure studies by Crosby et al.,[24,214] they observed with adhesives of low M_e polymers that failure was caused by crack propagation while blends of high M_e polymers failed by cavitation and the formation of fibrils. The transition was understood to be purely mechanical. The critical stress, σ_c, for cavitation in the bulk to occur is said to be proportional to the elastic modulus E' of the polymer at a testing frequency[24,214]. Therefore when E' decreases, the critical stress for

cavitation decreases, and becomes eventually smaller than a critical energy release rate G_c at the interface[215].

Tack has been reported to be predominantly related to the mechanical behaviour in the plateau range[15,216]. Therefore E' is equivalent to the plateau shear modulus, G', obtained during linear viscoelastic measurement under shear strain, as reported by Zosel[23]. The G' is inversely proportional to M_e [23,216,217]. Hence, for low M_e, the initial debonding is by crack propagation and cannot evolve towards a fibrillar structure while for high M_e, the debonding occurs through cavitation and fibrilation, and a larger amount of energy is dissipated in the process[23,24,218]. Similar observations and cavitation in rubber-like polymers have been treated by Gent and co-workers[218,219]. They reported that adhesives based on polymers with M_e about 1.5 x 10^4 g/mol showed fibrilation during debonding, whilst materials with M_e below this limit debonded by homogeneous deformation[218,219]. It is obvious therefore that high a M_e is favourable for cavitation, and polymers with high M_e need a lower critical stress for fibrilisation than those with a low M_e.

The tack of an adhesive has been reported to decrease with the degree of chemical crosslinking of the base polymer[220]. In the study it was found that the adhesive deformed by homogeneous deformation and not by fibrilation, when the polymer was crosslinked to such a degree that the strand length in the network becomes comparable to M_e. The degree of physical crosslinking of the copolymers used for PSAs has proved to have a positive influence on the bond failure mechanism. In a shear failure study, it was detected that the bonding of the lightly crosslinked adhesive failed by creep at the interface due to the adhesives fluid-like behaviour. The higher crosslinked adhesive exhibited more of an elastic behaviour and the nature of the failure was assigned to interfacial slippage[221].

On the basis of temperature some authors[222] have reported that the adhesion of PSAs strongly depends on the temperature of application and attains a tack maximum between 50^{o}C and 70^{o}C above the T_g of the adhesive blend. Hardly any work has been reported about adhesion on a micro- or nanoscale contact surface. With the information put forward in literature, it seems that the formation of fibrils is the most crucial factor influencing the peel strength and the tack of pressure-sensitive adhesives.

Chapter 3

3 Materials and characterisation of coated hot-melt PSA films

3.1 Materials

3.1.1 The PSAs

3.1.1.1 The triblock copolymers

The three different adhesive products used in this research work are commercially available PSA formulations supplied by Henkel, Slough, England. Their product names are DF645, 7M8 and DFC600. The base triblock copolymers of the DF645 blend are 1,4-*cis* styrene-*b*-isoprene-*b*-styrene (SIS), commonly known as Vector 4114 (*from Dexco Polymers LP, ExxonMobil Chemical Company or as Kraton D-1164 from Kraton polymers)* and styrene-*b*-ethylenebutylene-*b*-styrene (SEBS), known as Kraton G 1650 (*from Shell and Kraton Polymers*). Both triblock copolymers are linear and substantially pure. A study about the different microphase network structures that SIS undergoes and the impact on the copolymer's rheological property has been reported[223]. In recent years others copolymers with similar properties as SIS are being considered for PSA application since the double bonds of the polyisoprene units are susceptible to temperature degradation as well as exhibiting poor weather resistance properties[224].

The plasticizing oil is added to the PSA formulation to enable easy processibility such as blending and coating. The problem that emerges with this action is during the end–use application, e.g in the usage of diapers, low molecular weight additives exude into the oil when the body heat increases, making the underwear dirty. One of the reasons why SEBS is added to the formulation is its capability of engulfing large amounts of oil into the elastomeric polymer structure, enabling less oil to exude into the fabric[225,226]. Other advantages with SEBS are the resistance to degradation due to the polymer backbone

saturation and the highly entangled ethylene-butylene units giving the copolymer a very high modulus[166].

The characterisation data of the copolymers are given in Table 3.1. The 7M8 blend formulation is similar to the DF645 blend, but with higher styrene content. In the DFC600 blend, the SEBS is substituted with Styrene-butadiene-styrene (SBS). The SBS is commercially known as Kraton G 1101, from Shell[202] (Table 3.1). The chemical structures of the triblock copolymers are illustrated in Figure 3.1.

Table 3.1: Block copolymer characterisation data

Trade name	Type	Styrene content (wt-%)[a]	Diblock content (wt-%)[a]	M_w[a] (g.mol^{-1})	M_n[a] (g.mol^{-1})	Mid-block[a] T_g °C	End-block[a] T_g °C	Manufacturer
Vector 4111	Linear SIS	40 %	< 1%	114,000	108,000	-60 -58[b]	98[b]	ExxonMobil Chemical Co.
Kraton G 1650	Linear SEBS	30 %	< 1 %	100,000	91,000	-55 -37[b]	98[b]	Shell, Belgium
Kraton G 1101	Linear SBS	30 %	< 1%	153,000	132,000	-88	98	Shell, Belgium

[a]: Data supplied by manufacturer

[b]:Determined by DMA

3.1.1.2 The tackifying resins

Two types of tackifying resins (Midblock and Endblock) are used in these blend formulations. The midblock tackifiers which are added to be compatible with the midblock rubbery phase of the copolymers (hence the name*)* are aliphatic derivatives of hydrogenated dicyclopentadiene (HDCPD). Other examples of commercially available midblock resins include Escorez 5400 and 5600 from *ExxonMobil Chemical*, Sylvares ZT105LT from *Arizona Chemical* and Eastotac H-1000W from *Eastman Chemical Co*. The endblock resins added to be compatible with the polystyrene endblocks of the copolymers are alpha-methyl styrene (AMS) and rosin esters[227].

3.1.1.3 Blending oil

Mineral oil such as paraffin or naphthalene is typically used in the PSA blend formulation. Paraffinic with the product name ParaLux 6001 or Chevron-Phillips, and napthenic Calsol 5550, from Calumet[41] are used. As is known in the art, various other components can be added to modify the tack, colour, odour, etc., of the hot-melt adhesive. Antioxidants and other stabilizing ingredients are also typically included to protect the formulation from heat and light induced degradation[1,19,161].

a

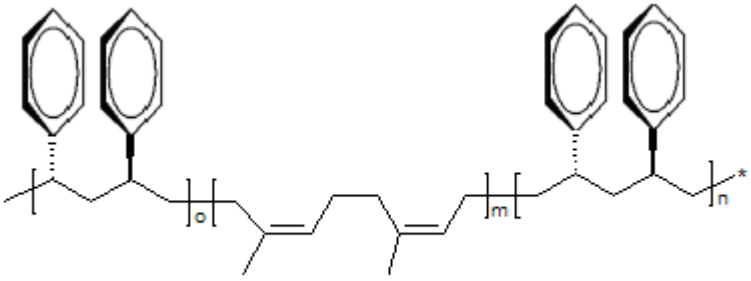

PS-block-poly(1,4-cis isoprene)-block-PS

b

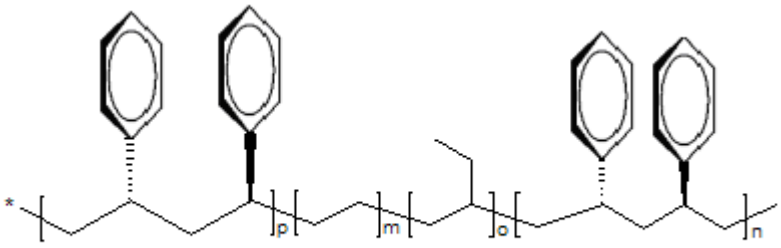

PS-block-poly(ethylenebutylene)-block-PS

c

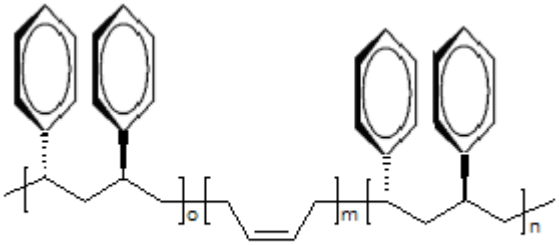

PS-block-poly(1,4-cis butadiene)-block-PS

Figure 3.1: The polymer structures of the base triblock copolymers of the PSA blends are (a) SIS, (b) SEBS and (c) SBS[31]

3.1.1.4 The formulation process

The blend composition of each adhesive is summarised in Table 3.2. The adhesive formulations were prepared by Henkel in a Z-blade mixer at about 160^{o}C – 170^{o}C by blending the copolymers and the tackifying resins in paraffin oil for several hours. An antioxidant, Irganox 1010 is used as thermal stabilizer. The molten blends were then

allowed to cool naturally to room temperature in the mixer chamber, which was a slow process lasting for several hours. After cooling, the bulk blends were cut and packaged in plastic sachets of 1 kg each, sealed, and stored in a temporized environment between 20 to 40^{o}C, until needed for coating. The shelf life of the adhesives blend is a minimum of one year, recommended by Henkel.

Table 3.2: The subcomponents of the various PSA formulations with their total weight percentages (wt-%).

Formulation	Copolymers	Resins	Mineral oil
DF645	SIS V 4114 (wt-% = 12 %) SEBS G 1650 (wt-% = 4 %) Total wt-% PS = 6%	Midblock tackifier, HDCPD (wt-% = 56 %) Endblock tackifier, AMS (wt-% = 8%)	Paraffin (wt-% = 20%)
7M8 (More PS)	SIS and SEBS Higher M_w PS	HDCPD (wt-% < 56%) AMS content (wt-% = 16%) with higher M_w.	Paraffin (wt-% = 20%)
DFC600 (more C=C)	SBS G 1101 (wt-%) > SIS V4114 (wt-%) SBS (M_w) > SIS (M_w)	HDCPD (wt-% = 56 %) AMS (wt-% = 8%)	Paraffin (wt-% = 20%)

During the coating process, the bulk adhesive was heated at the coating temperature of choice. The hot melt adhesive was then slot-coated onto a silicon release paper at room temperature, seen in the diagram in Figure 3.3. The cooled film was subsequently transfer-coated onto a polyethylene film (PE-film) and another silicon paper was adhered on the adhesive surface to protect it from contamination. The coated film was then ready to be used.

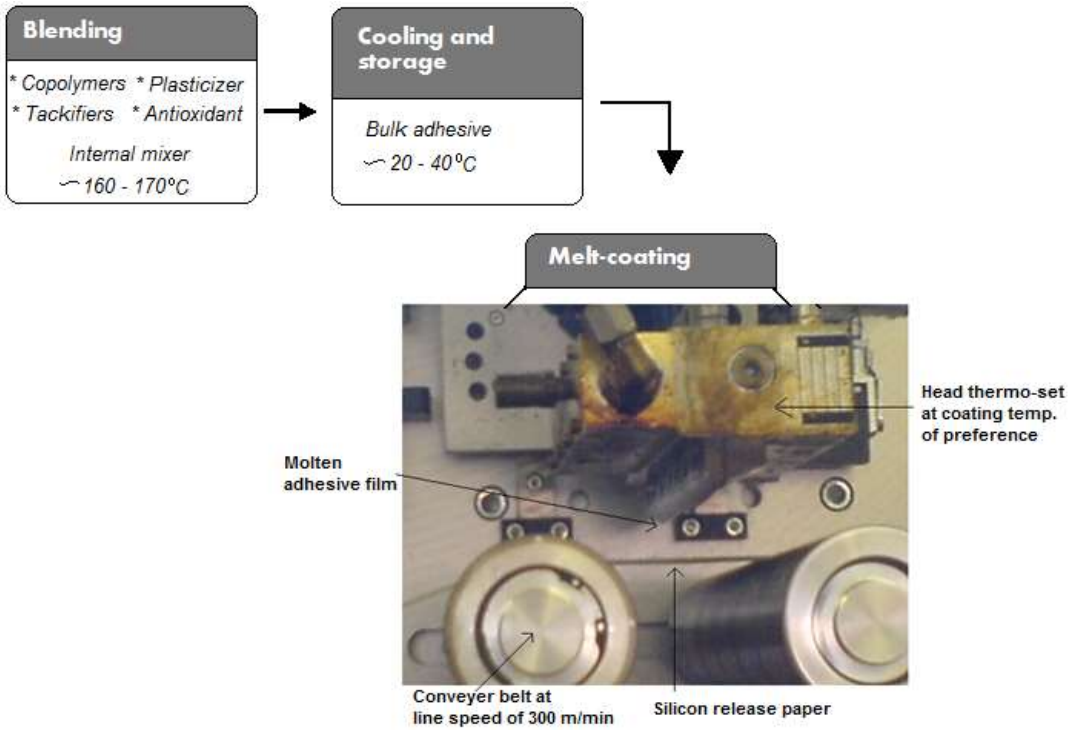

Figure 3.2: A sketch describing the adhesive film manufacturing process.

3.1.2 The non-woven fabrics

3.1.2.1 Cotton fabric

Cotton is a natural fibre grown from the *Gossypium* plant[228]. It is a biological polymer made up of cellulose, small quantities of hemicelluloses, pectins, and proteins that provide excellent wearability and aesthetics. The cottons fibres are tortuous and can grow up to 6 cm in length.

3.1.2.2 Nylon

Nylons belong to the polyamide family[229]., i.e. polymers with amide groups, -CONH- in their main repeating chain. They are denoted with indexes and normally synthesized from diamines and diacids, with a chemical formula as shown in Figure 3.4.

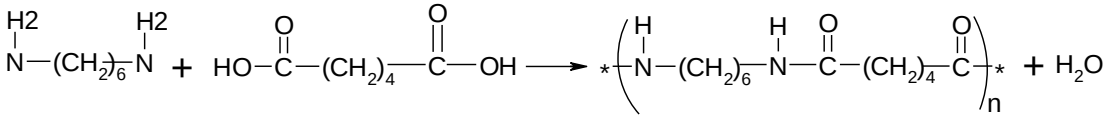

Figure 3.3: Nylon (6/6) is formed by the reaction between hexamethylene diamines and adipic acid under elimination of water. The first 6 in the index represents the carbon atoms in the diamines and the latter, represents the carbon atoms in the diacid[229].

3.1.2.3 Microfibre

A development of synthetic fibres in recent years has been the technology to extrude extremely fine filaments, namely microfibres[230] (less than 1.0 denier per filament) while maintaining all of the strength, uniformity and processing characteristics expected by textile manufacturers and consumers (to provide a measure for comparison, microfibers are half the diameter of a fine silk, one-third the diameter of cotton, one-quarter the diameter of fine wool). Microfibre is by far the best thing that has happened to the garment industry. It is tough, resilient, and many times thinner than other synthetics. Microfibre is a blend of polyester; a polymer consisting of ester repeating units in the main chain (Fig. 3.5), and nylon, commonly manufactured in the blend ratio of polyester/nylon of 80/20, 75/25 or 70/30.

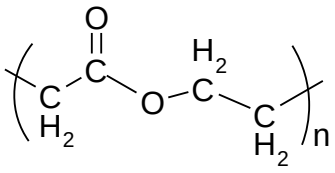

Figure 3.4: A polymer repeating unit of polyester[229].

There is an increase in use of new fabrics based on microfibres since they can bring their outstanding performance to a wide variety of end users[231]. Since the small filaments pack closely together, as a result, the surfaces of the microfibre fabrics offer greater fibre surfaces than other synthetic fabrics. Hence the properties are different from that of conventional fabrics. Microfibres can be used alone or blended with conventional man-made fibres as well as with natural fibres such as cotton, wool, and silk.

3.2 Characterisation

3.2.1 Dynamic mechanical analysis

During a DMA measurement an oscillatory (sinusoidal) stress is applied to the specimen and the strain response (the displacement of the specimen) is recorded[232]. If the sample is an ideal linearly elastic, it will deform instantaneously when the stress is applied and just as quickly return to its original shape after removal of the stress. The material stores all the energy it was subjected to, and uses it to recover its original shape after the stress removal. The strain response measured from elastic material will be in phase with the oscillatory stress applied, since no energy is converted into heat during the cycle. Therefore there will be no phase lag between applied stress and strain response. If the sample is totally viscous, it will strain permanently with time when the stress is applied. It will entirely dissipate all the energy it was subjected to, in the form of heat and the response strain measured will be a lag which is 90^o out of phase with the applied oscillatory stress. A viscoelastic material possesses the properties of both an elastic and viscous material. Hence if a sinusoidal stress is applied to a linear viscoelastic polymer, the strain response will also be sinusoidal, but will be out of phase to the applied stress with an angle δ (Fig. 3.6a), as an indication of some energy dissipation or damping in the material[34,232]. In dynamic measurement the stress is referred to as a complex stress σ^*, and divided into two components according to,

$$\sigma^* = \sigma' + \sigma'' \qquad 3.1$$

Where σ' is an elastic stress in phase with the strain and is also $\sigma' = \sigma^* \cos \delta$. A viscous stress σ'' in phase with the strain rate can also be written as $\sigma'' = \sigma^* \sin \delta$. The materials overall resistance to the deformation can be represented as a vector (Fig. 3.6b),

$$E^* = \sigma^* / \varepsilon = E' + iE'' \qquad 3.2$$

Where ε is the strain. E' is known as the elastic (storage) modulus and a measure of the materials ability to store energy or the elasticity of the material. E' is obtained via the elastic stress divided by the strain according to,

$$E' = \sigma'/\varepsilon = \sigma^*/ \varepsilon \cos \delta \qquad 3.3$$

The viscous part of the material in phase with the strain rate is a measure of the materials ability to dissipate energy (energy loss in the form of heat per cycle strain applied), and measured by the viscous (loss) modulus E'' as,

$$E'' = \sigma''/ \varepsilon = \sigma^*/ \varepsilon \sin \delta \qquad 3.4$$

The tangent of the phase angle (Fig. 3.4b) is the ratio of the loss modulus to the storage modulus according to,

$$\text{Tan } \delta = E''/E' \qquad 3.5$$

This parameter is very useful and provides information about, for instance, the energy loss of the material's response to temperature and frequency, especially a sharp change of the energy loss related to the movement of molecular chains, chain segments and chemical groups occurring within a material during the DMA test. Therefore, tan δ is useful to determine relevant phase transitions and other secondary transitions.

a

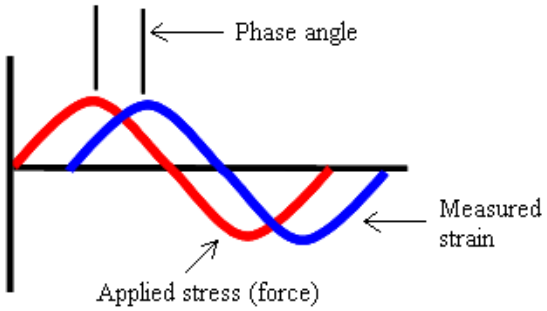

b

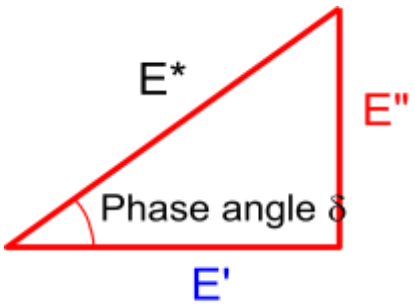

Figure 3.5: (a) An applied strain and delayed response stress with lag δ, and (b), complex modulus given as the hypotenuse, with E' which reflects the in-phase component and E'' which reflects the out-of-phase component with the applied strain[232].

The DMA equipment employed for the research studies was Q800 from TA instruments, integrated with a cooling system based on liquid nitrogen and a computer for measurement operation. An illustration of the equipment by TA, and the single cantilever clamp employed for all the measurements are found in Figure 3.7.

a

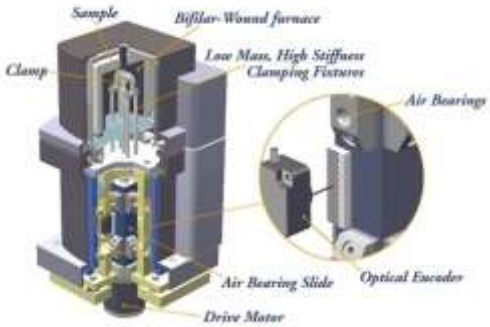

b

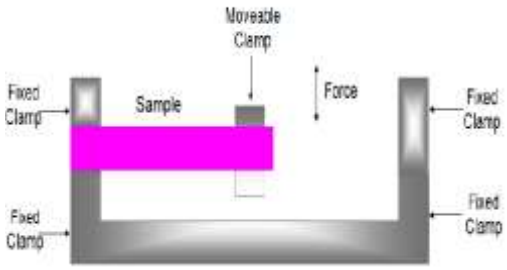

Figure 3.6: (a) The Q800 DMA equipment used for the viscoelastic tests and, (b) an illustration of clamped sample in single cantilever mode[232].

3.2.1.1 Thermorheological spectrum typical for linear amorphous polymers

Generally in thermorheological analysis, transitions observed in the study of a polymer material are associated with different localized or medium-to long-range cooperative motions of molecular segments. These molecular motions are referred to as relaxations. Different types of relaxations as a result of diverse molecular mobility in the form of side group rotation, or a crank-shaft mechanism involving polymer –(CH_2)- units have been reported in the literature[233,234]. The polymer segmental relaxation of interest in this study is the glass transition (T_g), which can simply be defined as the temperature at which co-operative main chain segments in amorphous polymers begin to coordinate large scale motion[235,236]. Since the T_g involves segmental mobility, it is therefore a kinetic transition and any factor that influences the nature of moving chain segments will affect T_g. Such factors are typically chain stiffness or steric hindrance by bulky side groups, molar mass, branching and crosslinking, and those that influence the free volume available for segmental movement[34].

In Figure 3.8, a typical dynamic viscoelastic spectrum depicting the different physical states of a linear amorphous polymer at different temperatures is illustrated. In the Glassy region at low temperatures, the thermal energy supplied to the material is insufficient to allow chain segments to move co-operatively, and the chains are therefore frozen in their disorganised state. Any sort of transitions (γ and β relaxations) observed in this region is caused by local main-chain movement such as independent –(CH_2)- units motion or side group rotation, as mentioned above[145,233,234]. The polymer material will have the characteristic property of glass which is prone to brittle fracture if subjected to large stresses. However, if subjected to small stresses the material will respond like an elastic solid, thereby displaying high E'or G'. As the temperature is increased, the chain segments will eventually gain sufficient thermal energy to co-ordinate large scale movement and a transition region is observed where G' drops significantly and a peak in E'' or G'' is observed. The midpoint of this region is the T_g. The maximum appears in the loss modulus because as stated above, the E'' is a measure of the materials damping ability, and the peak is an indication that the materials is passing from low-damping glassy state, through the high-damping transition region, to the lower-damping rubber-like state[34].

In the rubbery region, the polymer chains have gained enough thermal energy to assume any of the immense number of equi-energetic conformations available, without significant chain untangling taking place. In this state, the material exhibits several properties of rubber[37,145], such as the ability to stretch and retract rapidly if subjected to stress under short times, and several other unique properties which can be attributed to the chain-like structure. In asymmetric copolymer based adhesive systems, it is known that the rubbery plateau modulus G_N^o of the blend scales linearly with the reciprocal of the molecular weight between entanglements (M_e), according to the rubber elasticity equation[123,202],

$$G_N^o = \frac{\rho RT}{M_e} \qquad 3.6$$

Where ρ is the density, R is the gas constant and T is the temperature. As the temperature is raised further, the polymer material moves into the so-called terminal region. Here the chains have gained adequate thermal energy for significant chain disentanglement to occur and a flow-like behaviour is observed as polymer chains slip past each other. For asymmetric block copolymers, different shapes of the terminal region curve manifest the rheological responses of the different phase separated morphological chain organisations [104,223].

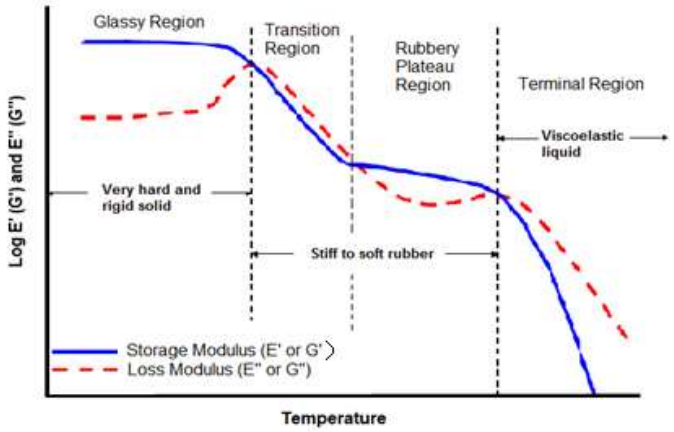

Figure 3.7: Viscoelastic spectrum for a typical amorphous polymer displaying the storage and loss modulus as function of temperature[234].

3.2.2 Rotational Rheometer

Rheology is the science that deals with the flow of fluids and deformation of solids to an external applied force in terms of the material's elasticity and viscosity[145,237]. In polymer based materials, the structure-rheology relationship is a key to the development of polymer

products with the correct rheology for processing. The rheology of a polymer melt is very sensitive to small changes of the polymer structure. The important structure parameters defining the rheology of a polymer melt is molecular weight, molecular weight distribution and chain branching[238], and such information can be obtained with the Rotational Rheometer. Just as the DMA, the Rotational Rheometer is a mechanical spectrometer capable of subjecting a sample to a dynamic (sinusoidal) or steady (linear) shear strain (deformation), and the resultant torque expended by the sample in response to the shear rate is measured. The Rotational Rheometer is however mainly used to perform viscosity measurements and the material properties obtained can be[239]:

- Dynamic shear flow behaviour (G', G'', tan delta or tan δ and the dynamic viscosity, η_d) as a function of frequency (time) and temperature.
- Steady shear flow behaviour (shear viscosity and shear stress) as a function of shear rate
- Molecular architecture (molecular weight, molecular weight distribution, branching) using frequency sweeps and creep/recovery tests (zero shear viscosity).
- Influence of long chain branching on linear viscoelastic properties (zero shear viscosity, steady state recoverable compliance).

The storage shear modulus G', loss shear modulus G'' and tan δ are obtained according to the following relationships[241]:

$$n_d = \frac{G_d}{\omega} \qquad where\ G_d = dynamic\ shear\ modulus \tag{3.7}$$

$$\omega = angular\ frequency = 2\pi f$$

$$n_d = dynamic\ viscosity$$

$$\delta = phase\ lag$$

$$G'' = G_d \cdot \cos\delta \tag{3.8}$$

$$G' = G_d \cdot \sin\delta \tag{3.9}$$

$$Tan\ \delta = \frac{G''}{G'} \tag{3.10}$$

The rotational rheometer used to measure the G' and G'', as function of frequency (time) for the adhesive samples was the ARES (Advanced Rheometrics Expansion System) (Fig. 3.9) from TA instruments.

Figure 3.8: ARES integrated with a computer used for the shear modulus measurements.

3.2.3 Peel test

The strength of an adhesive bond can be investigated with a variety of methods and one of the most frequently applied is the peel test method[1,240]. This test is easily performed and the results are obtained with no time delay. A peel test is basically about peeling apart a two-bonded specimen and measuring the peel force applied. The peel force is actually a sum of different forces combined. These include the force it takes to bend the test materials, elongate soft materials like polymer films and fabrics, and breaking the molecular bonds between the adhesives and the substrates[241].

Different types of peel test methods can be chosen depending on the information of interest. Some commonly used ones are illustrated in Figure 3.10. These methods have specific standard test geometries and are issued by the American Society for Testing (ASTM)[242]. The 90^{o} peel test with standard number BS 5350 is implemented when assessing the performance of flexible-to- rigid joints but can also be used for rigid-to-rigid joints. 180^{o} degree peel test has the standard number ASTM D 903-49 and it is best for testing flexible-to-rigid joints, whilst the T-peel test with the standard number ASTM D 1876 has more of a general application, for both rigid and flexible substrates. Other standard peel test methods not included in the Figure comprise of the single lap joint (ASTM D 905-49) mainly used for wooden substrates, the climbing drum peel test (ASTM 429-73) for rubber-to-metal bonding[243], etc.

Quite a few non conventional peel test methods are also available for testing soft substrates and these include Circular Platen for Adhesives Testing (GF-8) for determining the adhesive property of sealants[244] and the SER peel method for measuring adhesive properties as PSA, gels and pastes[245].

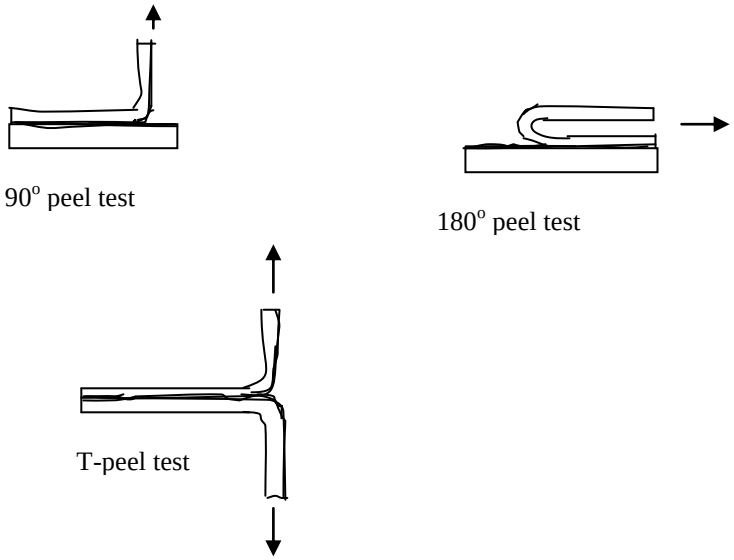

Figure 3.9: Different types of peel tests with arrows indicating directions of peel force applied[244].

In this research 180° T-peel test was conducted with an Instron series IX Automated Materials tester version 8.27.00, according to the American Standard Test Method (ASTM 1876-72). The method was adapted for use with fabric substrates[246], in a thermostated room with a temperature around 21°C and relative humidity of about 31%. The typical experimental set-up is shown in Figure 3.11. The peel strengths of the PSA bonded to cotton, nylon and microfibre fabrics were investigated.

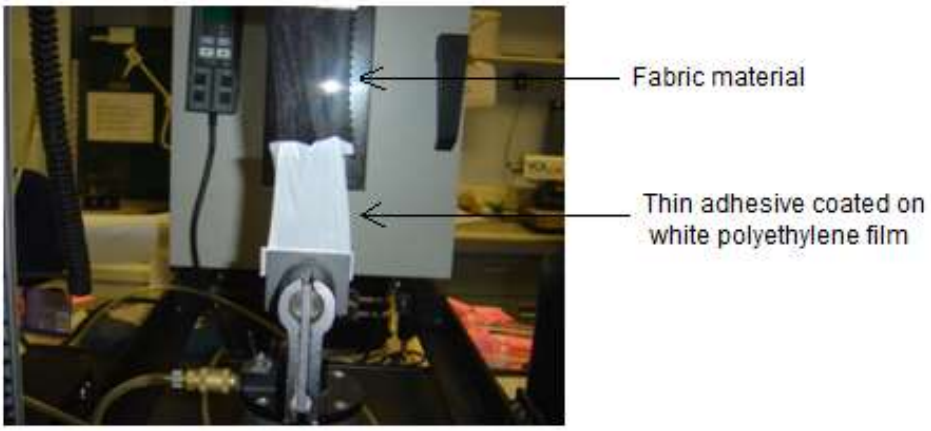

Figure 3.10: An adhesion peel-test being performed showing nylon fabric (black) peeled from a thin transparent adhesive film coating on a PE-film substrate (white).

3.2.4 Scanning electron microscope

The Scanning Electron Microscope (SEM) is an electron microscope that images a sample surface by scanning it with high-energy beam of electrons in a raster scan pattern[247]. The first SEM image was acquired by Max Knoll in 1935 but further pioneering work on the physical principles of the SEM and beam interactions was performed by Manfred Von Ardenne in 1937[248]. In SEM imaging, by scanning an electron probe across a specimen, images of high resolution are produced, which means that closely spaced features can be examined at a high magnification. An electron beam which is generated from an electron gun hits the imaging sample and produces secondary electrons from the sample. These electrons are collected by a secondary detector or a backscatter detector, converted to a voltage and amplified. The amplified voltage is applied to the grid of a Cathode-ray tube (CRT) and causes the intensity of the spot of light to change. The image consists of thousands of spots of varying intensity on the face of a CRT that correspond to the topography of the sample[247].

For SEM, a specimen is normally required to be completely dry, since the specimen chamber is at high vacuum. All samples must also be of an appropriate size to fit in the specimen chamber and are generally mounted rigidly on a specimen holder called a specimen stub. For conventional imaging, specimens must be electrically grounded to prevent accumulation of electrostatic charge at the surface. Metal objects require little special preparation for SEM except for cleaning and mounting on a specimen stub. Non-

conductive specimens tend to charge when scanned by the electron beam, and especially in secondary electron imaging mode, and this causes scanning faults and other image artifacts[249]. They are therefore usually coated with ultrathin coating of electrically-conducting material, commonly gold, deposited on the sample either by low vacuum sputter coating or by high vacuum evaporation. Preparation of sample requirements are[249]:

1. Elimination of water, solvents, or other materials that could vaporize while in vacuum. A vacuum is necessary before samples are coated because gas molecules could get in the way of the coat and this will lead to uneven coating, or no coating at all.
2. Non-metallic samples, such as ceramics, should be coated so they are electrically conductive. Metallic samples can be placed directly into the SEM.

The SEM instrument used in this work was ZEISS SUPRA 35VP from Gemini (Fig. 3.12), and the detector was VPSE (vapour pressure mode) used for non-conductive specimen. The voltage supplier was EHT target 9.93 KV. To make the samples conductive and improve imaging, the samples were coated with thin layer of gold in a sputter coater for approximately 15 sec before the SEM characterisation.

The SEM instrument used was ZEISS SUPRA 35VP from Gemini, and the detector was a VPSE (vapour pressure mode) used for non-conductive specimen. The voltage supplier was EHT target 9.93 KV. In an attempt to improve the imaging, the samples were made conductive by the treatment of a thin layer of gold coating in a sputter coater for approximately 15 sec before the SEM characterisation.

Figure 3.11: Gemini SEM with integrated computer system.

3.2.5 Atomic force microscope

The development of the atomic force microscope (AFM) in 1986 by Binnig et al[249] was a modification of the scanning tunnelling microscope (STM) already introduced back in 1981. The original principle was based on an electronic current, known as the tunnelling current, used to control a probe tip to track the surface of a sample. This tunnelling current was produced in response to a bias voltage applied between the tip and a conducting sample, and was sensitive to the tip-sample separation distance. During operation, maintaining a constant tunnelling current through the use of a feedback loop generally gave a constant separation of the tip above the sample surface. The feedback signal itself was indicative of topography of the sample. Since a tunnelling current was used, the technique required the sample to be conductive. While being a significant advance in surface imaging, this requirement limited the AFMs application. The obstacle was overcome by attaching the probe tip to a cantilever held against the sample surface by a very low force via a piezoelectric actuator.

The AFM technique is now finding increasing use in academic and industrial research due to the broad spectrum of a material's information that can be obtained down to the atomic level[250]. In addition to examining material surface topography and nanostructure, one can employ AFM for investigation of mechanical[251], viscoelasticity[252], and chemical properties[253]. These properties can be examined at micron and submicron scales that are much less accessible by other methods.

The basic objective of the operation of the AFM is to measure the forces (at atomic level) between the sharp probing tip attached to the cantilever and a sample surface[249,250,254,255]. Images are taken by scanning the sample relative to the probing tip or vice versa, and measuring the deflection of the cantilever as function of lateral position. The contributions to the total force between the probe tip and a sample are[256,257]:

$$F_{total=}F_{chem} + F_{vdw} + F_{electr} + F_{magn} \qquad 3.11$$

Where F_{chem} is the short-range chemical force, F_{vdw}, the Van der Waals interaction force, F_{eletr} the electrostatic force and F_{magn} the magnetic force. The typical characteristics of the forces as a function of the tip-sample distance are defined by the Lennard-Jones curve[258] in Figure 3.13. The repulsive part at small distances is due to the overlap of electron clouds

from the tip and sample surface atoms. Repulsive and attractive forces at small distances r, can be described by a Lennard-Jones potential:

$$U_{chem} = 4\varepsilon[(\frac{\sigma_o}{r})^{12} - \left(\frac{\sigma_o}{r}\right)^{6}] \quad 3.12$$

Where σ_o denotes the distance where the potential is zero. Below this distance the forces are repulsive. The Van der Waals force, $F_{vdw,}$ is an attractive electrostatic force between permanent and temporary dipoles. Permanent dipoles are molecules which exhibit a permanent polarity, whereas temporary dipoles are uncharged molecules with constantly changing charge distribution. Since the range of the Van der Waals forces is limited, the interaction between the tip and sample surface can well be approximated by a sphere in front of an infinitely flat surface[257,259],

$$F_{adw} = \frac{HR}{6d^2} \quad 3.13$$

Where H is the Hamaker constant, R is the tip radius and d is the tip-sample distance. The magnetic forces are only relevant for magnetic tips and samples. The electrostatic forces arise as a result of the tip and sample forming a capacitor.

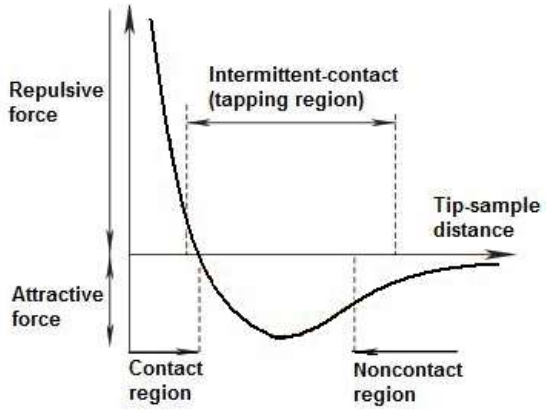

Figure 3.12: A shematic illustration depicting forces governing tip-sample interaction as function of distance between sample surface and probing tip[257,258]

3.2.5.1.1 The AFM set-up

The instrument set-up[260,261] (Figure 3.14a) typically consists of;

- The cantilever having the probe tip at one end.
- The piezoelectric actuator (oscillator) (Fig. 3.14b) to periodically oscillate the cantilever in Z direction.

- A sensor that detects the bending of the cantilever resulting from the interaction force between the probe tip and the sample.
- Measuring electronics that generate force and force gradient information from sensor and drive oscillation of the cantilever.
- A controller that drives the motion of the sample or the probe in accordance with the difference between set point and measured force gradient.
- XYZ stages that move either the tip or the sample in z direction and scan at least one of them in x, y directions.

The cantilever tip is generally made of silicon or silicon nitride and comes in various shapes with the pyramidal shaped frequently used[260]. The cantilever is made of the same material as the tip, but its shape is usually triangular ("V" shaped) or long and rectangular (an "I" beam). These are roughly 100 microns long and only a few microns thick. The geometry makes them very flexible but strong enough to securely hold the tips on their end (Fig. 3.14b).

There are two ways of how the AFM scanning set-up is designed. In one case the sample under investigation is place on the piezoelectric scanner which is made up of crystals that create voltage if pressure is applied, or in reverse can create a pressure by expanding or contracting if a voltage is applied. Using the contraction and retraction of the crystal, the configuration in a scanner allows for the controlled movement on the order of a fraction of a nanometer. Alternatively the tip is placed on the piezo scanner and brought in contact over the sample. This is far better configuration if the sample is large or immersed in a liquid[261].

a b

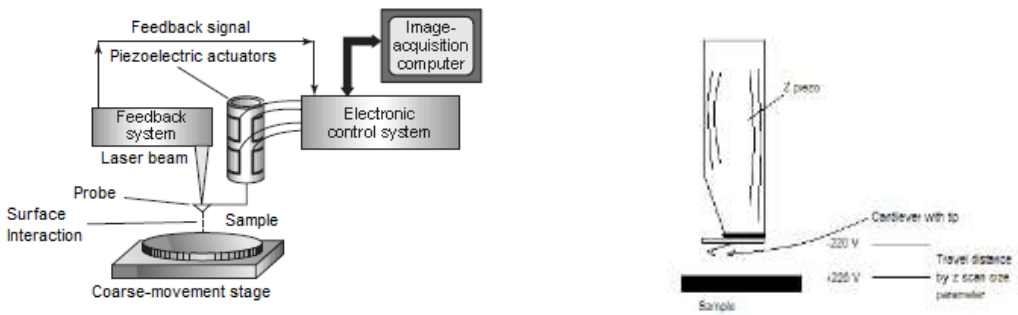

Figure 3.13: A typical AFM instrument setup, (a) with its main components, and (b) the piezo actuator with cantilever and tip[260].

3.2.5.2 Modes of imaging

The primary modes of operation are static or contact mode CM, and dynamic mode. Because the measurement of a static signal is prone to noise and drift, low stiffness cantilevers are used to boost the deflection signal[255,261]. In the **Contact mode** (CM), the probe is maintained in continuous contact with the sample in the region where the inter-atomic repulsive force is very strong (Fig. 3.14). This is accomplished by a feedback system which moves either the sample or the probe relatively perpendicularly to the surface of the specimen in response to the deflection of the cantilever probe assembly as it is scanned across the sample surface. In this way, the data associated with each point are stored and used to construct an image of the sample corresponding to the sample characteristic being measured, e.g., surface topography. The limitation of contact mode is its strong lateral and compressive force generated as the tip is scanned across a sample surface[255,260,261]. While allowing probing of non-conductive samples, there existed the potential to damage the surface and/or tip while dragging the tip across the material. The limitation was of particular concern when polymers and biological systems were being investigated.

The potential for sample damage was overcome by the development of the **Tapping mode** AFM (TM-AFM) by Eling et al[260]. TM-AFM[255,260,261], also known as the intermittent and tends to be more applicable to general imaging in air, particularly for soft samples, as the resolution is similar to the contact mode while the forces applied to the sample are lower and less damaging[255,261]. In fact, the only real disadvantage of the TM compared to the contact mode is that the scan speeds are slightly slower and the AFM operation is a bit more complex, but these disadvantages tend to be outweighed by the advantages. In TM, the cantilever oscillates close to its first bending mode resonance frequency, with large oscillation amplitudes, often in the range of 20 to 200 nm, and the tip makes contact with the sample for a short duration in each oscillation cycle. The oscillation of the cantilever can be approximated by the equation of motion for a damped harmonic oscillator with forced oscillation[257],

$$m\ddot{z} + \frac{m\omega_0}{Q}\dot{z} + k\,z = F_o\cos(\omega t) + F_{total} \qquad 3.14$$

Where z defines the tip-sample distance, Q and ω_0 are the quality factor and resonance frequency of the cantilever respectively, and defines the damping of the oscillation; k is the

spring constant of the cantilever and $F_o \cos(\omega t)$ represents the excitation of the oscillation through the piezoelectric element. The oscillation amplitude, phase and resonance frequency are modified by the tip-sample interaction forces. The changes in oscillation with respect to the external reference oscillation provide information about the sample's characteristics.

During scanning, the amplitude at the operating frequency is maintained at a constant level, called the set-point amplitude A_{sp}, by adjusting the relative position of the tip with respect to the sample. Similar to CM, the data associated with each point change are collected, stored and used to characterise the sample. The images acquired simultaneously with TM-AFM can be of two different types: In one type, the image is a record of the changes of the piezo actuator height necessary to maintain a fixed oscillation amplitude through a feedback loop (the height image). In the other type, the images record changes of the oscillator phase delay relative to the excitation signal[262] (Figure 3.16). This image often provides significantly more contrast than the height image and has revealed in many cases a high sensitivity to the material's surface properties, such as the mechanical, viscoelasticity and the chemical nature[251-253]. A number of studies have shown the possibility to extract useful information from TM images of soft samples, especially with samples showing a particular contrast on small scale, like blends of hard and soft materials or copolymers[252,263,264]. TM is the most popular operating mode since it virtually eliminates the lateral force and allows more delicate samples to be imaged. However, the tapping force can still be excessive for some soft samples. As a result, its resolution for a soft sample is far worse than for a hard sample.

Two types of operating in tapping mode are possible: Either the oscillating amplitude is fixed and the output signal is the resonance frequency (this is called the noncontact resonance force mode) or the oscillation frequency is fixed and the variation of the amplitude and phase are recorded (amplitude modulation)[257]. In *frequency modulation*, changes in the oscillation frequency provide information about tip-sample interactions. The frequency can be measured with very high sensitivity and thus the frequency modulation mode allows for use of very stiff cantilevers. Stiff cantilevers provide stability very close to the surface, and as a result, this was the first AFM to provide true atomic resolution in ultra-high vacuum conditions[265].

In *amplitude modulation*, changes in the oscillation amplitude or phase provide the feedback signal for imaging (Fig. 3.15). These can be used to discriminate between different types of materials on a sample surface, as explained above. Amplitude modulation typically operates at or close to the resonant frequency of the probe cantilever[254,260]. This technique was employed for the AFM studies and is widely used in TM-AFM because of the low interaction force and the ability to operate in an ambient environment. However the technique has limitations. First, the relation between the amplitude and interaction force, whether operated on- or off-resonance modulation, is not linear[254,255]. It is difficult to relate the amplitude directly to the interaction force. Second, the amplitude, if operated on resonance, is susceptible to ambient damping in addition to tip-sample interaction force. For example, the damping between the cantilever and the sample affects the amplitude. As the probe approaches the surface of the sample, the amplitude decreases before the tip enters effective atomic force region due to the increase in damping. As a result, it is difficult to predict the interaction force by presetting the amplitude. If the pre-set value is too high, the tip may not track the surface. If too low, the interaction force may be too excessive, that could damage a sample. It requires considerable training and experience for an operator to operate it properly. Third, it is hard to operate the on-resonance modulation in a liquid. Since the damping is strong, the resonant peak of the cantilever is often difficult to distinguish from unrelated peaks from mechanical structures, making identification of resonant frequency difficult[255,260].

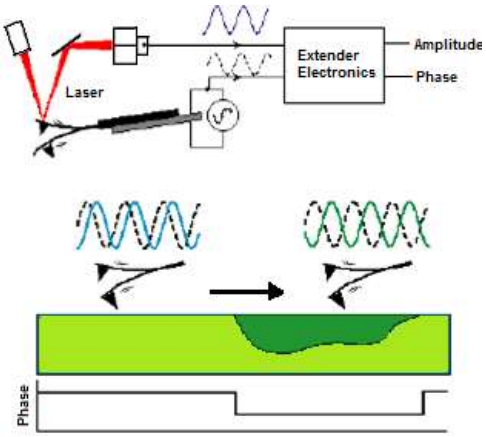

Figure 3.14: Illustration of phase imaging where the Extender Electronics Module measures the phase lag of the cantilever oscillation (solid wave) relative to piezo drive (dashed wave). The amplitude signal is used simultaneously for the TM feedback mechanism. Spatial variations in sample properties cause shifts in the cantilever phase (bottom) which are mapped to produce the phase images shown here[262].

The final mode of AFM operation is known as the **Non-contact mode,** where the tip is scanned above the surface of a sample at such a distance that is no longer in the repulsive regime of the inter-molecular force curve (Fig. 3.13), and the weak Van der Waals attractive force between tip and sample is sensed for feedback control. This mode is very difficult to operate in ambient conditions since the thin layer of water contamination that exists on the surface of most materials will invariably form a small capillary bridge between the tip and the sample and cause the tip to jump-to-contact, becoming a contact mode operation. Amplitude modulation can also be operated in the non-contact mode[266].

3.2.5.3 Advantages and disadvantages

In the respect of surface imaging the AFM has several advantages over the scanning electron microscope (SEM). Unlike the SEM which provides a two-dimensional projection or a two dimensional image of a sample, the AFM provides a true three-dimensional surface profile. Additionally, samples viewed by AFM do not require any special treatments (such as metal or carbon coatings) that would irreversibly change or damage the sample, and it is therefore very suitable for studying an adhesive specimen where imaging of the pristine surface is essential. While an electron microscope needs an expensive vacuum environment for proper operation, most AFM modes can work perfectly well in ambient air or even a liquid environment. This makes it possible to study biological macromolecules[267] and even living organisms[268]. In principle, AFM can provide higher resolution than the SEM.

A disadvantage of AFM compared with the SEM is the image size. The SEM can image an area on the order of millimetres with depth of field on the order of millimetres. The AFM can only image a maximum height on the order of micrometers and maximum scan of about 150 by 150 micrometers[256]. Another inconvenience is that at high resolution, the quality of an image is limited by the radius of curvature of the probe tip, and an incorrect choice of tip for required resolution can lead to image artifacts. The AFM cannot scan images as fast as an SEM, requiring several minutes for a typical scan, while an SEM is capable of scanning at near real-time (although at relatively low quality) after the chamber is evacuated. The relatively slow rate of scanning during AFM imaging often leads to thermal drift in the image[269,270]. To eliminate image distortions induced by thermo drift, several methods are proposed[269,270]. Table 3.2 provides a comparison between optical

microscopy, SEM and scanning probe microscopy (SPM) (AFM belongs in this category), and it is readily seen that SPM provides considerable investigative advantages that optical microscopy and SEM cannot provide[271].

Table 3.3: Characteristics of common techniques for imaging and measuring surface morphology[271]

	Optical microscope	SEM	SPM
Sample operating environment	Ambient, Liquid, Vacuum	Vacuum	Ambient, Liquid, vacuum
Depth of field	Small	Large	Medium
Depth of focus	Medium	Small	Small
Resolution: x,y	1.0 μm	5 nm	0.1-3.0 nm
Resolution: z	N/A	N/A	0.01 nm
Magnification range	1X-2x10^3X	10X-10^6X	5x10^3X-10^8X

3.2.5.4 Colour contrast assignment of domain regions

Though the assignment of colour contrast to height difference in AFM height image is straightforward with bright regions depicting hills and dark regions valleys, the colour contrast in a phase image relating to different domains is much more complex and governed by several factors[257,272]. In some reported studies bright regions in phase images were attributed to hard material and dark regions to soft materials[263,273,274,275]. Others have however assigned dark colour to hard domains and bright colour to soft domains[276,277]. Most of the time, a tip-sample indentation examination is required to determine the amplitude and phase signals as a function of the distance between the cantilever and sample regions[263], before contrast assignment can be made with confidence.

In tapping mode (TM-AFM), the difference in tapping cantilever oscillating phase angles is called the phase shift[255,260]. Images recording phase-shift changes are called phase-contrasts. However, the specific sample properties that give rise to phase contrast images remain unclear [255,260,272]. During tapping operation, as the tip approaches the sample, the tip-sample interaction alters the amplitude and the phase angle of the oscillating cantilever. During imaging, the amplitude is maintained at a constant level by adjusting the vertical

position of the cantilever-tip. Therefore for a surface region of larger amplitude damping, the AFM feedback control will move the tip upward to keep the amplitude constant and thus this area is recorded as higher in height image, provided the domain region in question is hard. At the same time, the phase shift ΔΦ with respect to the freely oscillating cantilever is recorded as phase image. Recommended by earlier work[257,264] based on energy model, the phase angle Φ and the amplitude A of a tapping cantilever are related to the average tip-sample power dissipation, $\overline{P}$, by the expression;

$$\overline{P} = \frac{k_0 A^2 \omega_0}{2Q_0}\left(\frac{A_0}{A}\sin\phi - 1\right) \qquad 3.15$$

Where Q_0 is quality factor and ω_0 is natural resonant frequency. In the equation it can be noticed that the sine Φ is directly proportional to changes in energy dissipation as the feedback control keeps the scanning amplitude constant. For a two-phase system, if the phase stays either above or below the "free phase" (90^o) for both domains, the domain with phase angle closer to the "free phase" has the higher energy dissipation. Sine is a symmetric function about 90^o, and symmetric jumps from phase > 90^o to < 90^o are not due to changes in energy dissipation but are caused by a switching between net attractive and net repulsive interaction[264]. In the adhesive films where there exist components of hard nature such as polystyrene (PS) and soft nature such as rubbery adhesive matrix, the bright domains in the phase images are attributed to relatively hard components and dark colour contrast to regions of relatively soft components. This attribution is based on the contrast assignment by the Nanoscope v531r1 software (Digital instruments)[256], reference to the amount of each component in the blends, different tapping forces implemented to examine the extent of deformation of the different domains and reference to reported studies on similar systems[250,263,264]. Knoll et al[263] reported in their work on AFM studies about SBS triblock copolymers that, when tapping setpoint decreased, the phase signal from harder PS domains rose much faster than on softer PB domains. This was the result of larger damping of the cantilever oscillation amplitude during the tip's interaction with the harder PS domains. The contrast of the generated phase images were then bright. When the tip interacted with the PB domains, the oscillation amplitude did not dampen as much, since the tip deformed the PB phase. The corresponding contrast of the PB phase images were then dark[263]. Others[250] have reported similar observations.

3.2.5.5 Morphology investigation with the AFM

The AFM instrument used for the studies was Dimension D3000 with Nanoscope IIIA from Digital Instruments (Santa Barbara, CA) operating in tapping mode (intermittent contact). Commercial silicon cantilever probes from Veeco were used, with spring constants of about 40 N/m and the tip radius of curvature < 10 nm. The measurements were performed at the fundamental resonance frequencies of the cantilevers as automatically tuned by the instrument (Fig. 3.16) ranging between 155 and 200 KHz. Height and phase images were recorded simultaneously for each sample surface examined. The software used for the operation and imaging was the Nanoscope v531r1 version. Irrespective of the scan size chosen for a specific imaging, each image was acquired with the sample/line set by the instrument at 256[256]. This is the number of data points present in the image in the X and Y scan direction. It means that for the images with scan size at 10µm x 10µm, the pixel size is 39 nm (10 /256 = 0.039 µm or 39 nm). Thus features smaller than 39 nm will not be resolved in the 10µm images. For the 5µm x 5µm images, features smaller than ~ 20 nm will not be resolved, and features smaller than ~ 4 nm will not be resolved in the 1µm x 1µm scanned images. Regardless of the pixel size, the feedback loop samples the topography many times at each pixel. Therefore the data displayed at each pixel is the average of the sampling iterations by the feedback loop over the pixel area[256].

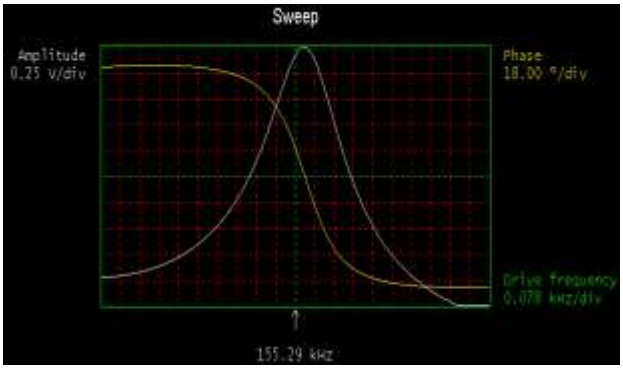

Figure 3.15: A cantilever resonance frequency sweep performed before imaging.

The level of the tapping force used was related to the ratio of setpoint amplitude defined as $r_{sp} = A_{sp}/A_o$, where A_o = cantilever free air oscillation amplitude, A_{sp} = set point amplitude in contact with the surface, as depicted in the illustration in Figure 3.17. For example, for an r_{sp} value close to but smaller than 1, the A_{sp} almost equalled the A_o, and so the tip was very lightly tapping on the surface and the image collected was from the very near-surface feature of a sample. As the r_{sp} decreased from 1 toward 0, the tapping forces increased and

made it possible to image the subsurface film structure. When low set-point tapping amplitudes were used, the tip was prone to stick to the adhesive surface. A tenacious effort was made to collect the images with as minimum tip-sample interaction force as possible, tapping with high r_{sp} values. When a lower r_{sp} was required to reveal the subsurface sample morphology, a small as possible decrements in A_{sp} were applied, to maintain the pristine sample features. This was a very time consuming procedure but the good results obtained were worth the effort.

The images were recorded simultaneously in the topographic height and phase modes. For consistent tapping conditions unless stated, two tapping force levels were used, corresponding to r_{sp} of 0.91- 1.0 (light tapping) and 0.60 – 0.70 (hard tapping). Between these values, different r_{sp} values were employed for moderate tapping. All the measurements were carried out at room temperature.

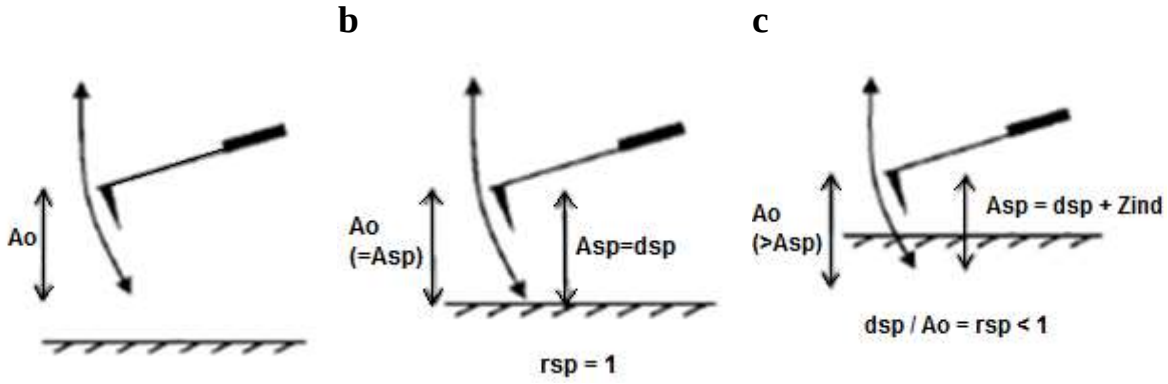

Figure 3.16: The cantilever free air amplitude A_o[278]„ is the (a) oscillation amplitude when there are no external forces interacting with the cantilever. Once tip establishes contact with sample surface, the cantilever oscillation amplitude is defined by setpoint ratio r_{sp}, where $A_{sp} = d_{sp}$, is the setpoint amplitude and a measure of distance between tip and sample. In (c), the tip interacts with the sample surface and the height topology will be interplay of the tip indentation into the sample surface over a distance z_{ind} plus the setpoint value d_{sp}.

3.2.5.5.1 Micro scale domain size quantification

The analysis and calculation of microscale phase separated domain sizes within the adhesive film samples were performed with **an** Able Image Analyser™ (Version v3.6 from Mu Labs). The quantification of the domains was based on the 2-dimensional AFM images as presented. Due to their random and undefined sizes, a fixed threshold value was set for

the smallest well resolved microscale particles observed, as recommended by the software. No threshold was set for the largest particle sizes. The images shown in Figure 3.18 elucidate the procedure for the particle analysis, performed on an AFM phase image of DF645 coated film at 120^{o}C. Based on the threshold criteria set, the software identified all the domains that fell within the criteria window, and calculated their areas in pixels. The units were then converted from pixels into SI-units through measuring the distance between two points of known length, and performing the necessary conversions. In this work, the scanned areas of the samples were utilized for the conversion as they were already known from the AFM images, scanned at 5 µm x 5 µm. To obtain a knowledge of the domain distribution, the domain areas were divided into the categories, "*20-50", "51-100", "101-200", "201-500", "501—"*, depicting the smallest area ranges to the largest area ranges, in pixels. The average particle area ($\bar{A}$) of each defined area category, A_i, was calculated as,

$$\bar{A} = \frac{\sum A_i}{\sum N_i A_i} \qquad 3.16$$

Where N_i is the number of particles belonging to size category, i. The standard size deviation was calculated according to,

$$\bar{A}_{i,var} = \sqrt{\frac{1}{N}\sum_{i=1}^{N}(A_i - \bar{A})^2} \qquad 3.17$$

A total average percentage of domain sizes in each image, j, was calculated by,

$$\bar{D}_{ij=}100 \times \frac{\sum Ai}{\sum_i A_{ij}} \qquad 3.18$$

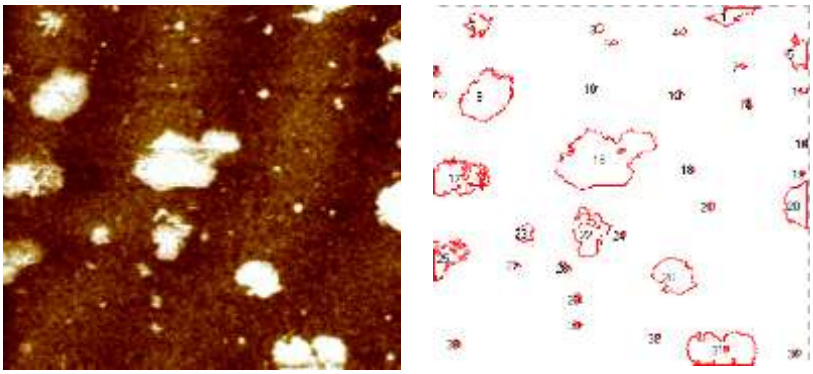

Figure 3.17: An example of particle size analysis. The image to the left is the real AFM phase image of the adhesive film morphology at 5 µm x 5 µm film surface. The corresponding image to the right is the generated analysed film surface by the Image Analyser, with the domain area values given in a table (not shown).

3.2.5.6 Nano scale analysis

The nanoscale domain diameters and inter-domain distances were determined with the AFM Nanoscope IIIa software. A systematic error could be introduced with the determination of some diameters as the AFM tip interaction with domains further from film surface at a certain r_{sp} value, could generate smaller domains than perhaps in reality. Nevertheless this did not affect the general conclusions drawn in the discussions.

The reproducibility of the results was checked by using different types of cantilever tips but with similar cantilever spring constant and different A_o. The results by comparing images with same r_{sp} but different A_o were very reproducible, as long as "fresh and clean" tips were used. With tapping to acquire images on the nanoscale where instrument sensitivity was crucial, reproducibility was sometimes limited by the amplitude noise.

3.2.6 AFM force-distance measurement

Another major application of AFM besides imaging is the measurement of force-distance curves. Here, the AFM tip is approached towards and retracted from the sample surface and the static deflection of the cantilever is monitored as a function of piezo displacement.

AFM force-distance (F-D) measurement is performed to measure long range attractive or repulsive forces between the probe tip and a sample under investigation[279]. The technique has revolutionised the acquisition of information of mechanical properties of a material on the micro-, nano- and even on atomic-scale level[255,260]. For adhesion and elastic modulus investigations, the same force measurement principle is implemented but a different part of the results is extracted for the information of interest.

The measurement is typically performed with the AFM controls set in Contact Mode[260,279]. In simplicity the procedure commences when the electrodes for the z-axis scanner are subjected to a triangular waveform voltage. This action causes the z piezo to extend and contract in the vertical direction, resulting in a relative motion between the cantilever and the sample (Fig. 3.19). The distance and speed that the cantilever tip travels will depend on the magnitude of amplitude and frequency of an applied triangle wavelike voltage pattern. As the cantilever is put into motion, the deflection of its free end (tip location) is measured and plotted at many points as the z-axis scanner extends and retracts in relation to the

sample surface. A laser spot beamed at the back of the cantilever reflects the motion of the cantilever to a detector which records the movement (Fig. 3.19).

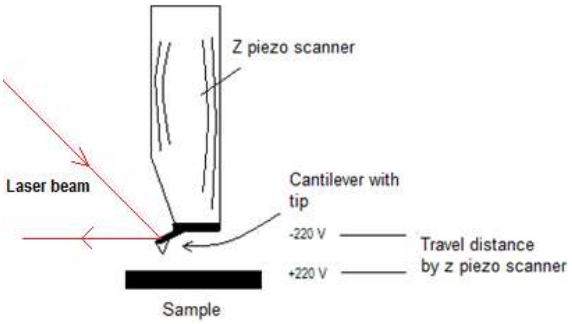

Figure 3.18: Schematic illustration of the piezo travel in force calibration mode

Adhesion force measurement is an experiment involving several steps and the force measurement anatomy illustrated in Figure 3.20 commences[256];

- At starting point A, the piezo extends and the tip descends but no contact with the samples surface is established yet (horizontal red curve). However if the cantilever feels a long-range attractive or repulsive force in this region it will deflect downward or upward.
- At point B, the probe tip is brought very close to the surface of the sample, and if the tip experiences sufficient attractive forces at this distance, it will be pulled down to the surface, explaining the dip at point B. This "jump-into-contact" point is normally due to electrostatic forces (if charged molecular groups are present at the surface) or surface tension (capillary) forces. Analyzing the response of the cantilever gives valuable information about the attractive forces on the sample surface.
- The tip will press the surface once it is in contact with the sample, point C. The cantilever will deflect upwards with different intensity depending on the hardness characteristics of the sample surface. Typically a steep slope implies the tip's interaction with a hard surface where a less steep slope indicates the tip's interaction with a soft deformable surface[252,255,279]. Point C is very important since the slope and shape of the curve at this point provides crucial information about the elasticity of the sample surface.
- After the desired maximum loading point has been reached, the piezo retracts and the tip ascends (retraction curve). At this point D, adhesion and other bonds formed

during contact will cause the tip to stick to the surface some distance past the initial contact point on the approach curve, point B.

- At point E, the tip continues to ascend until the elastic force of the cantilever tip overwhelms the adhesion force of the sample. The tip will finally break free and the force measurement cycle will be completed. The size of the vertical distance of point E and size of the area confined between the extension and retraction curves are proportional to the adhesion force and thermodynamic adhesion energy of the sample.

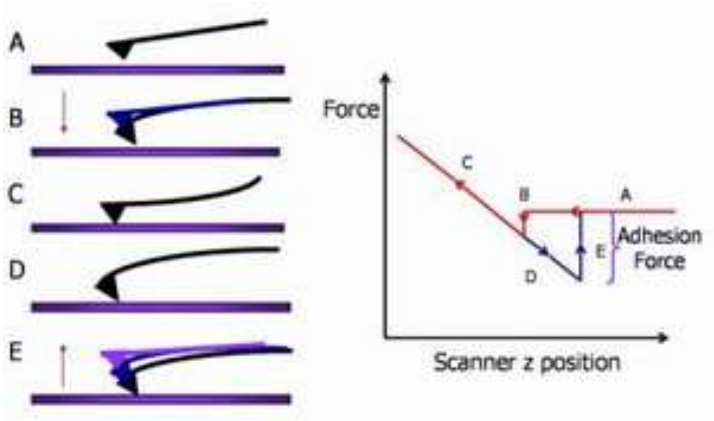

Figure 3.19: Anatomy of a force - distance curve measurement (to the left), illustrating the cantilever tip's behaviour when subjected to external forces, with the plot (to the right) obtained as a result[256].

Usually in AFM force-distance measurements the plot obtained is given as tip-sample interaction vs. tip-sample separation distance, D. The distance generally controlled during the measurement is not the actual D but the piezo displacement Z as shown in the plot in Figure 3.20, which is the distance between the sample surface and the rest position of the cantilever. The relationship between Z and D is given by[279],

$$Z = D + (\delta_c + \delta_s) \qquad 3.19$$

Where δ_s is the deformation of the sample and δ_c is the deflection of the complaint cantilever. The tip-sample force is then given by Hooke's law of elastic deformation according to,

$$F = -k_c \delta_c$$

Where k_c is the spring constant of the cantilever. One does not know in advance the cantilever deflections and the sample deformation during the measurement and the only

distance that one can control is the Z distance, i.e., the displacement of the piezo[279]. Therefore the raw curve obtained by AFM is normally called “force-displacement” instead of “force-distance”.

3.2.6.1 Adhesion force measurement with the AFM

The adhesion force measurements were performed with a NanoWizard II from JPK instruments (Fig. 3.21) mounted on inverted optical microscope Olympus IX 70/70/81. With this setup the experiment could be viewed in real time, through transmission optical microscopy transferred to a computer screen via a camera and that being the reason for the utilization of glass slides as a support for the specimen. The cantilever probe used was commercially available phosphorous doped silicon (Si) type RTESP14 from Veeco. It was rectangular shaped with the following dimensions: length: 115 - 135 µm, width: 30 – 40 µm, thickness: 3.5 – 4.5 µm. The back side was not coated. The resonance frequency was reported to be f_o: 269 – 328 kHz, with a spring constant k_c: 40N/m. The probe was made of Si with a height between 15 - 20 µm and a parabolic tip with radius of 8 – 10 nm. All the data were according to the manufacturer.

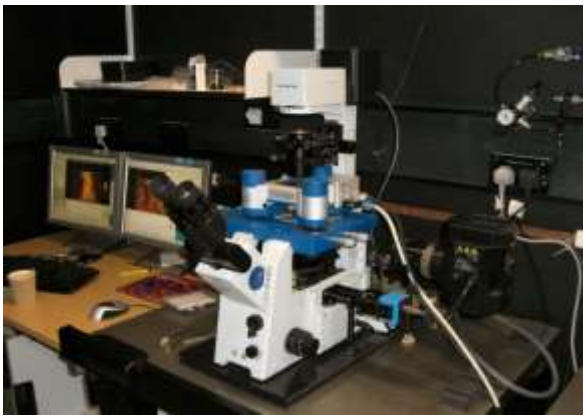

Figure 3.20: The NanoWizard II AFM instrument integrated with computers used for the adhesion force measurements.

The tapping mode of the AFM (TM-AFM) was employed to collect the height and phase topographic images prior to and after the adhesion measurements, to visualise the region of the specimen surface where the force-distance (F-D) curves were collected. The scans were performed on areas of 5X5 μm^2 at a scan rate of 1 Hz. The instrument was then switched to the contact mode (CM) and the necessary calibrations executed for the force-distance tests, without any interference of the AFM stage or sample.

For the calibration process, first a force curve[279,280] was recorded on a hard non-deformable substrate as a reference, to calibrate for the cantilever spring constant and determine the maximum setpoint force to be used for the measurements. This was performed by following the calibration manager of the JPK SPM software calibration process. A freshly cleaned silicon wafer (Si(100) Youngs modulus 179 GPa, MEMSnet®)) was used as the reference substrate. On such a non-deformable hard material, the deflection of the cantilever during the tip-sample indentation (Point C, Fig. 3.20) was equal to the bending of the cantilever. The unloading and unloading curves that were taken overlapped. For elastomeric based materials for instance, the deflection curves and hence indentation curves present a large hysteresis between loading and unloading parts, due to the viscoelastic behaviour[280,281]. The slope of the loading curve with respect to a horizontal line is proportional to the viscoelastic nature of the material, where the less steeper the slope, the softer the material[280,281]. The F-D curves were measured at different regions on the Si wafer, to ensure good reproducibility. After the calibration process, force volumes, i.e. arrays of force curves in a two-dimensional grid across the sample surface were collected on the adhesive samples. The cantilever deflection amplitude (nm) was subtracted from the total Z-piezo displacement for each data set in each force curve. The force-displacement curves were then corrected and plotted as force- distance curves (Section 3.2.6). The force curves were collected over the entire sample surface and each tip-sample measurement was taken at the centre point within the surface area of choice (Index). All the curves were taken with a constant extension/retraction speed set at 10 µm/s and zero seconds dwell time (i.e. tip-sample contact delay time). To further verify the dwell time, all the curves were collected under a trigger mode in which the extension force curve reverses at a pre-assigned relative trigger value of cantilever deflection. To minimise the influence of any excessive contact between tip and the sample, the trigger value was set as small as possible, at 3 nm, so the entire extension and retraction force curves can be considered to be governed by the adhesive interaction between the tip and the samples. All measurements were executed under ambient conditions at room temperature. The procedure was repeated for 3 samples each of a specific coated film to ensure good reproducibility. The measured raw data were exported as ASCII files to Microsoft excel and a JPK custom-designed Matlab, based on an adaptive algorithm was used to quantify the values of the adhesion energies.

3.2.6.2 Elastic modulus measurement with the AFM

The AFM used for the adhesive film surface elastic modulus measurement was an NTEGRA Therma from NT-MDT, Russia (Figure 3.22). The equipment was designed to perform this type of measurement since unlike the JPK instrument (Fig. 3.21), the (x,y,z) piezo scanner is beneath the specimen stage and the cantilever with probe is kept fixed.

During the measurement the stage with sample, is moved up- and down in vertical z-axis to ensure that indentation is performed uniaxially and eliminate lateral drift which might alter the contact area if the cantilever is rather in motion. A commercial silicon (Si) cantilever for force modulation measurement from Vistaprobes was used. The specifications were, length: 125 ± 10 µm, width: 40 ± 5 µm, and thickness: 3 ± 0.5 µm. The probe had a height of 14 ± 2 µm and a parabolic tip with radius of curvature ≤ 10nm, used to avoid penetration of the thin film layer that might lead to inaccurate assessment of the Young's modulus. All the data given were according to the manufacturer.

Though similar F-D methodology as explained above is implemented to carry out elastic modulus measurements, the fundamental theory and concepts for such an investigation is elaborate and prompts mathematical consideration involving several factors. For the exact quantification of the elastic modulus of the samples, it was critical to know the true spring constant, K, of the cantilever. The value depends on the length *L*, width *w*, and thickness *t* of the cantilever and the Young's modulus E of the material by the relationship $K = Ewt^3/(4L^3)$[281]. The elastic modulus of cantilevers typically made from Si and Si_3N_4 are well documented and other methods of calculating the spring constant can also be found in the literature[281]. The length and width can easily be measured using for example the SEM. The thickness of the cantilever is difficult to measure especially if the face of the thickness surface is not entirely perpendicular to the incident electron beam. Thus any small error in the measured cantilever thickness can have a significant impact on the calculated K value due to the power relationship. For these studies a method for determining the rectangular cantilevers K value reported by Sader and co-workers[282] was used and based on the relationship,

$$K = 0.1906 \cdot \rho_f w^2 \cdot L \cdot Q_f \cdot \Gamma_i(f_0) \cdot f_0^2 \qquad 3.19$$

Where *w* and *L* are the width and length of the cantilever, respectively, Q_f and f_0 are the quality factor and the resonance frequency of the cantilever in fluid and ρ_f is the fluid density, all of these parameters are typically used when the cantilever is place in air, Γ_i is

the imaginary part of the hydrodynamic function and only depends on the Reynolds number $Re = \rho_f f_0 w^2 / 4\eta$, where η is the viscosity of the surrounding fluid (air in this case), and is independent of the cantilever thickness and density[282]. The quality factor Q_f is related to the damping ratio (δ), which is a measure of how fast the oscillator is losing energy and can be determined experimentally[282].

Sader's method[283,284] for determining the rectangular AFM cantilever spring constant is relatively simple with a reported high accuracy of around 5%. This is attributed to the cantilever thickness not used in the calculation of the *K* value. For the cantilever used for the measurements, the *L* and *w* were measured by SEM. The measurements were carried out in air at ambient temperature, so the parameters such as density and viscosity of air were taken as $1.18 kg.m^{-3}$ and $1.86x10^{-5}$ $kg.m^{-1}.s^{-1}$ respectively, as required by the fitting software (Nova, NT-MDT, Russia). The cantilever K value was determined exactly to be 17 N/m.

Figure 3.21: The AFM NTEGRA Therma used for the elastic modulus measurement.

3.2.7 Time –of-flight static secondary ion mass spectrometry

At the moment, molecular characterization is steadily gaining interest in analytical micro-analysis. A lot of techniques are currently available for analysis of chemical groups on surfaces of materials. Some of these are x-ray photoelectron spectroscopy (XPS), attenuated total reflection fourier transformed infrared spectroscopy (ATR/FTIR), neutron reflectivity, etc[44]. Perhaps the most exciting for a polymer based sample surface is the Secondary Ion Mass Spectrometry (SIMS). The technique was first developed in 1949 by

Herzog and Viehboek[285], but it was not until the 1970s that its true potential in Surface science was realised as a consequence of work by Benninghoven and his group[286] in Münster, Germany.

Static secondary ion mass spectrometry (S-SIMS) allows the chemical characterisation of the constituents in the upper-most molecular layer of a sample, compared to XPS which probe the 10 nm subsurface layer[287]. Within the range of micro-analytical methods, S-SIMS occupies a rather unique position in that it combines monolayer sensitivity with the capability to generate molecular information. The main advantage of S-SIMS resides in the capability to analyse the pristine surface which is vital in terms of adhesion science, and also to detect information about molecular fragments, not just elemental ratios. In more complex samples such as adhesive multi-blend formulations, S-SIMS provides a distinct advantage over XPS since the latter method requires that all the components of the system and their spectra are known in advance. In contrast, S-SIMS quantification is based on relative peak ratio of two specific ions and this remains valid even if the third component is not known[287].

During an SIMS investigation, high energy primary ions are beamed onto the sample's surface as shown in Figure 3.23. Once they collide with the surface, their energy is transferred to the atoms of the sample under analysis. This creates three major effects, (1) mixing of the upper layers of the sample and the primary ions results in amorphization of the surface; (2) atoms from the primary ion beam are implanted in the sample, and (3) some secondary particles (atoms and small molecules) are ejected from the sample. Among the ejected particles are electrically neutral, as well as positively and negatively charged species. The charged particles of each polarity (secondary ions) can then be extracted from the sputtering area with the help of an electrical field between the sample and an extraction lens. They are then accelerated into a mass spectrometer. Once there, they are sorted by mass (and energy) and finally counted in an ion detector (which can be an electron multiplier, a Faraday cup or a channel plate). The count rates of different secondary ion species give information about the composition of the sample in the sputtered area. Since the size of the sputtered area depends only on the primary ion beam diameter, which is typically in the order of a micrometer, a SIMS analysis has a relatively high lateral resolution[285-288]. The basic SIMS equation is,

$$I_m = I_p Y_m \alpha \theta_m \eta \qquad 3.20$$

Where I_m is the secondary ion current of the species m, I_p is the primary ion flux, Y_m is the sputter yield, α is the ionization probability, θ_m is the fractional concentration of m in the surface layer and η is the transmission of the analysis system. The two fundamental parameters are Y_m and α. Y_m is the total yield of the sputtered particles of species m, neutral and ionic, per primary ion impact. It increases linearly with primary ion influx. It also increases with primary ion mass and energy although not linearly[285-288]. Y_m tends to maximise with energies at around 10 keV. Ionization occurs at, or close to, emission of sputtered particles with the consequence that the matrix participates in the electronic process. This means the secondary ion yield is strongly influenced by the electronic state of the material being analyzed, and it is very sensitive to the electronic state of the atom or the molecule to be ionized and to the matrix from which they are emitted. This is a well known matrix effect problem and brings significant complications when a quantification of SIMS data is required[288].

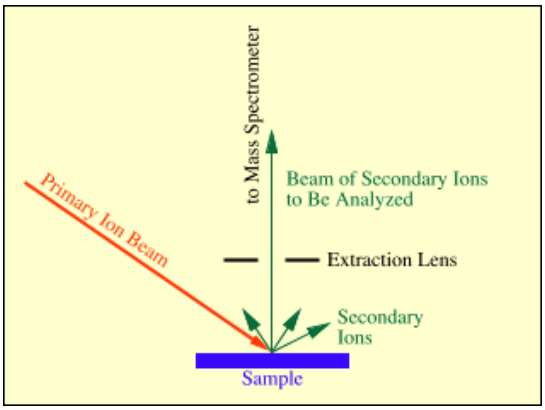

Figure 3.22:An illustration of SIMS experiment set-up where a high energy primary ion beam is directed at an area of the sample surface to be characterized[287].

To provide a better understanding of the process of secondary ion formation for polymers, a wide range of experiments was undertaken by some of the pioneers in the area, such as Briggs, Leggert, and Vickerman[289]. From various approaches a consensus on the overall process has been reached and different fragmentation processes of polymers at the surfaces have been postulated, as shown in Figure 3.24. The model suggests that the primary ion energy is transformed into vibrational energy dissipated within the macromolecules.

In the region close to the point of impact (Fig. 3.24), high energy events leading to the emission of atomic species and uncharacteristic small organic fragments are believed to

prevail. Surrounding the area is a zone, “finger print region” with decreased energy density where structural rearrangements may take place, yielding e.g., polyaromatic moieties. Farther away from the impact point, there is the “monomer region”, where the energy available for rearrangements is low, and the ejection of species minimally rearranged and species on the mass order of the monomers prevail. This region gives rise to larger and structurally most informative fragments.

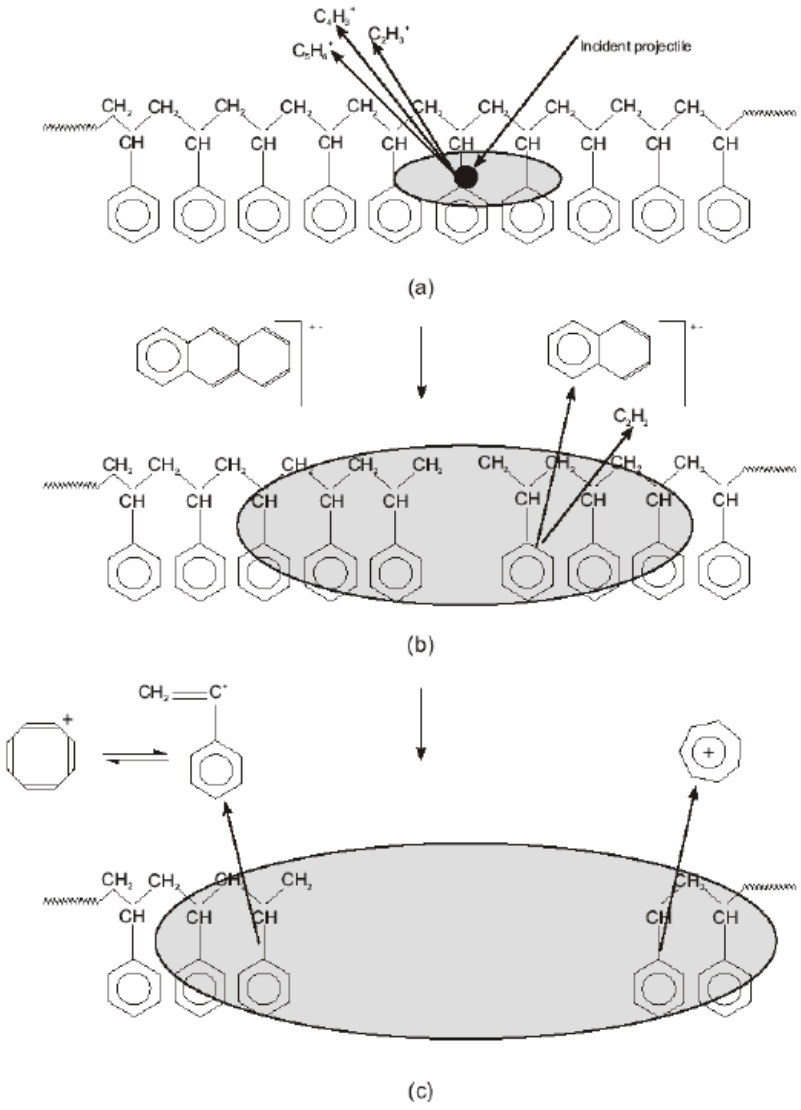

Figure 3.23: Model for ion formation of polymers in S-SIMS involves the existence of three regions in which fragmentation on different levels occurs: (a) violent fragmentation in the impact region, (b) unzipping of larger fragments in the fingerprint region, and (c) simple low-energy fragmentation into large sequences, monomer region. Adapted from Leggert (1998)[289].

3.2.8 Static limit of SIMS

To retain the molecular information in SIMS, it is essential that no primary ion strikes again to an already damaged region. This is achieved by using the static SIMS (S-SIMS) mode, where an extremely low dose of primary ions is used, such that within the time scale of the experiment very much less than 1 % of the top surface layer constituents receive an ion impact[285-289]. Under these conditions on a random impact basis no spot on the surface contributing to the spectrum receives more than one strike. The secondary species generated arise also from a certain area remote from the next point of analytical impact. It is established that each impact physically influences an area of 10 nm^2. This implies that 10^{13} impacts/cm^2 influence all the atoms in the surface. Therefore, the static limit is defined to be $\leq 10^{13}$ ions/cm^2. Any primary ion dose lower than this value is accepted in the static regime of SIMS analysis[287]. Dynamic SIMS involves use of higher primary current density on the sample.

3.2.9 The Mass analyzer

The secondary ions produced are accelerated to 2 keV upwards to an ion mirror where they are reflected downwards to the detection system over a very short distance. Over a flight path of 2 m the secondary ions are separated in mass because, for ions of constant energy, their flight time is proportional to $m^{-1/2}$. This is basically the functionality of the Time-of-flight (ToF) Mass Analyzer. It is the most commonly used analyzer system and has nowadays given the technique the general name of ToF-SIMS. The ToF consists of a combination of drift regions with an ion mirror. The ion mirror utilizes an electrostatic field to reflect secondary ions in order to provide a positive time dispersion, i.e. to increase the flight path of high-energy secondary ions with respect to the lower energy secondary ions[287-289].

3.2.10 Problem with surface charging

The SIMS primary ion beam, secondary ion and electron fluxes produce a net electric charge at the sample surface. If the sample material conducts, the charge is compensated by the current flowing through the sample to the ground. However, insulating samples undergo a surface charge build-up. Sample charging can deflect the primary ion beam (especially when low energy primary ions are used) away from the region of interest so

that the actual bombardment ends. Also the emission of electrons and ions from the surface can be hindered or stopped. Therefore in the case of insulating samples, charging compensation techniques must be used. Bombardment of the sample surface by low energy electrons is the most commonly applied technique for charge compensation[287-289]. Electrons can easily compensate for the positive charge build up.

For further reading about this technique Briggs and Seah have compiled the general SIMS basics and related techniques in their book on surface analysis of organic and inorganic materials[290]. Vickerman and Reed have given a comprehensive overview of S-SIMS applications on polymers with particular attention to the structural assignment of the detected ions[291]. The effects of polymer molecular weight (M_w), casting solvent, ultrasonification (with a non-polymer solvent) and annealing on the TOF-S-SIMS data of monodispersed poly(methyl methacrylate) has systematically studied by Leeson et al[292].

3.2.11 Film chemical nature characterisation with ToF-SSIMS

In this research pristine adhesives film surfaces were analyzed with an S-SIMS analysis using a SIMS IV time-of-flight (ION-TOF-GmbH, Münster) (Figure 3.25), equipped with a Bismuth liquid metal ion gun, a single stage reflectron analyser and electron ionisation gun. The Bismuth 3 cluster ions (Bi_3^+) accelerated at 25 keV bombarded the surface of the samples at an incident angle of 45^o to the surface normal. The target current was approximately 1 pA with a raster area of 200 x 200 μm^2. These conditions resulted in (Bi_3^+) of 1.53 x 10^{12} ions/cm^2 well below the static SIMS accepted limit of $\leq 10^{13}$ ions/cm. Secondary ions were accelerated to 3 keV into a 2m flight tube connected to an Einzel lens and the reflectron, which improved the mass resolution. Charge compensation was necessary to compensate for surface charging created by the positive primary ions and this was adjusted using the pulsed electron flood gun emitting low-energy electrons at 10 eV. The analysis depth was $\leq$ 10 nm and each spectrum was averaged over a 15 s time period. Both positive and negative secondary ions were collected, and all data analyses were carried out with the IonSpec and IonImage (version 4.1) softwares. The information from a wide m/z range were collected and compared.

Figure 3.24: The ToF-SIMS instrument, known as ION-TOF-GmbH used for the surface chemical group characterization of adhesives films.

An illustration (Fig. 3.26) is shown indicating the different depth limitations of some of the diverse material surface characterisation techniques available.

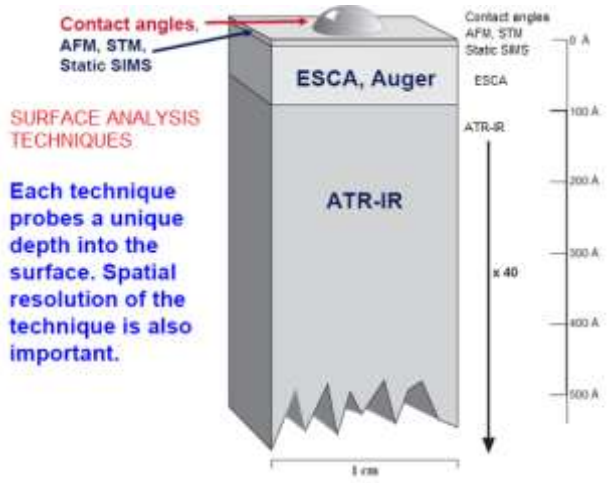

Figure 3.25: Characterisation depth limitations for some characterisation techniques available[256].

Chapter 4

4 Classical investigation of the mechanical properties of PSA and the peel strength to non-woven fabrics

4.1 Introduction

While hot-melt pressure-sensitive adhesives (PSAs) gain significance as structural or semi structural adhesives, the knowledge of their adhesion mechanisms has become increasingly important. When one considers the performance of the end product, there are three distinct factors, peel adhesion[28,204], tack[199] and shear[123,201,206] that can be used to characterize adhesives. The relationship of these characteristics is critical to the understanding of the PSA performance and manufacturing.

As already stated in Chapter 1, the temperature used for coating adhesive films has proved to have a significant impact on the peel performance of the coated adhesive films, with films coated at higher temperatures exhibiting superior peel strengths compared to films coated at lower temperatures. Tremendous amount of work can be found in the literature about the influence of the subcomponents[157,181,293,294,295] of the adhesive blend, as well as the effect of film thickness[296], and film coating method[201], on the peel properties of the finished adhesive product. However a lack of literature on the impact of film coating temperature on the adhesive performance makes this investigation a significant topic for the PSA industry and adhesion science in general.

This part of the study implements classical adhesive characterisation methods such as rotational rheometry and tensile test, commonly utilized by the PSA industry to;

(1) Investigate the effect of film coating temperature on the mechanical property of PSA formulation at end-use condition.

(2) Highlight why these methods are insufficient in obtaining knowledge about the performance of the adhesive coated films.

(3) Measure the adhesion of PSA to three different non-woven fabrics and analyze the effect of bonding rate and fabric surface characteristics to the adhesive peel strength.

4.2 Experimental

4.2.1 Sample preparation and characterization

4.2.1.1 Dynamic shear modulus measurement

The adhesive formulation used for the studies is the DF645 blend and the product specifications are found in Chapter 3, Section 3.1. Bulk adhesive samples of DF645 were annealed for one hour each, at 110^{o}C, 120^{o}C and 160^{o}C, respectively, and allowed to cool to room temperature. The annealing temperatures reflected the temperatures typically used for melt-coating the adhesive films. The cooled specimens were shaped into discs with a diameter of 25 mm and thickness of 2.0 mm. They were then allowed to relax for 24 hours at room temperature to minimise stresses introduced during preparation, before execution of the measurement.

The measurement was firstly conducted by subjecting the samples to a cyclic of 10^{-2} to 10^{2} % strain amplitude (γ_o) at a fixed frequency (ω) of 1 rad/s, to ascertain the linear viscoelastic region (LVR). This was operated in the parallel/parallel plate oscillatory shear mode with a plate diameter of 25 mm and a gap of 2.0 mm by employing the ARES instrument (Fig.3.9). Afterwards a suitable strain value of γ_o =1% was chosen for the time-dependent (frequency sweep) modulus measurements at ω from 10^{-2} to 10^{2} rad/s. All measurements were carried out at ambient temperature of 25^{o}C and RH of 50%, and data reproducibility was checked by repeating the measurements at randomly selected ambient conditions.

4.2.1.2 Tensile testing

Samples of DF645 were annealed for an hour each, at 100^{o}C, 120^{o}C, 160^{o}C and 180^{o}C, respectively. The specimens were then molded as dog-bone shaped tensile specimens with

the gauge dimensions (50 mm x 20 mm x 2.0 mm). Tensile testing was carried out where the samples were strained at a cross-head speed of 300 mm/min at room temperature according to ASTM D412-80, with an Instron 556 and 100N load cell. All the samples were prepared in the same way so any eventual orientation of the base copolymers in the adhesive blend was the same. All measurements were carried out at ambient temperature of 25^{o}C and RH of 50%.

4.2.1.3 Peel Test

Strips of 155^{o}C-coated DF645 (thickness ~10 µm) adhesive film with dimensions 60 by 90 mm on polyethylene (PE) film were rolled on each of the three non-woven fabrics of cotton, nylon and microfibre (also of the same dimension as the adhesive film), with a 2 kg rubber roller. The rolling rates employed were 300 mm/min and 1500 mm/min. The peel tests (Fig. 3.11) were performed within a few minutes of the application to the adherent, to prevent relaxation of the adhesive which could affect the results of the tests. Five peel tests were carried out for each fabric at each rolling rate, from which the maximum and minimum peak peel forces applied were deduced and the average of these forces were calculated from the tensile tester software. The surfaces of the two bonded materials were examined with scanning electron microscope (SEM), prior to and after the peel tests, to examine if the fabrics were removed without leaving residues on the adhesive surfaces and vice versa.

4.3 Results and Discussion

4.3.1 Dynamic shear moduli of DF645 bulk

The dynamic viscoelastic moduli of the DF645 adhesive formulation annealed at three different temperatures was done to quantify the compliance and cohesive strength of the blend at the end-usage condition. Since the coated films were unsuited for the measurements, bulk samples were used instead. The samples were labelled with a suffix specifying their annealing temperatures which was intended to mimic the coating condition of the films. The results presented in this section deals with the adhesive rheological behaviour at room temperature, i.e., below the glass transition (T_g) of polystyrene and therefore polystyrene domains are expected to be rigid[66,82,86,88].

In Figure 4.1 it can be observed that all the bulk samples exhibited similar mechanical properties, with the dynamic shear modulus, G', independent of the strain amplitude in the measurement window. This indicated that the polymer molecules were in their linear viscoelastic region (LVR). A fixed strain γ value of 1 % was chosen to perform the time-dependent modulus measurement of the samples.

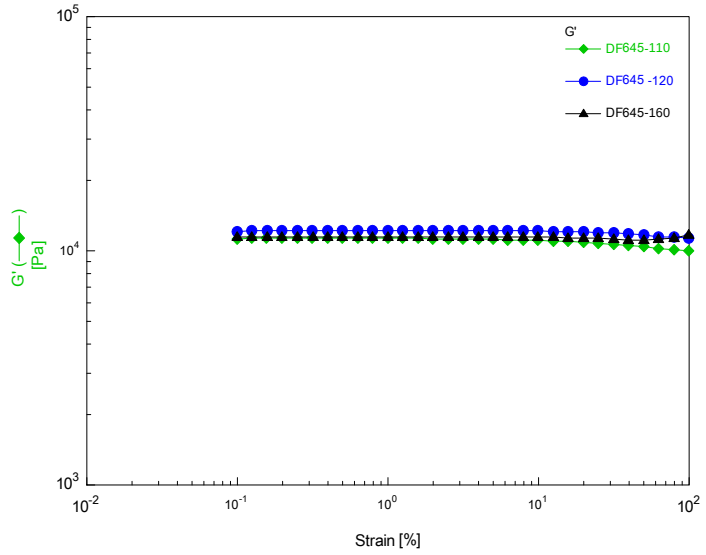

Figure 4.1: Dynamic shear storage modulus, G', as a function of strain amplitude, %, for DF645 bulk samples initially annealed at 110°C, 120°C, and 160°C, respectively, as shown by the legend at the top right corner. The measurements were performed at an oscillatory frequency of 1 rad/s at room temperature.

The frequency measurements were focused on a narrow range of low frequency or terminal region, from 10^{-2} to 10^{2} rad/s since this regime reflects the long-time behaviour[123] of the adhesive during the end-use application. Earlier studies have reported the shear modulus in the low-frequency regime reflects the material's microstructure adopted at a given temperature[104,223,297,298].

All the samples displayed predominantly elastic response with G' virtually independent of ω between 10^{-2} to 10^{0} rad/s and also higher than the dynamic shear loss modulus, G'', as seen in Figure 4.2. The dominant G' is believed to be a result of the entropy elasticity of unique rubbery network of polyisoprene (PI) and poly(ethylene/butylene) (PEB) phase reinforced by polystyrene-rich regions within the adhesive samples. It is clear that molecular segments with a varying range of lengths responded to the stresses applied. At

the low frequencies, below 10^{-1} rad/s, the deformation (strain) being mainly the conformational changes of the chains in response to the changes of shear stress was almost simultaneous with little dragging effect (low G"). As the frequency was further increased up to 10^{-0} rad/s, both G' and G" started to increase at their own pace with G" increasing much faster than G'. This indicated that the adhesive samples were capable of responding to quicker changes of the shear stress. The faster increase of G" implied that movements of molecular chains with a specific length, e.g. the persistence length, started to respond to the frequency of the shear stress, resulting in increasing dragging effect.

The observation in regards to the plateau modulus at the low frequency region is consistent with reported studies on the dynamic mechanical behaviour of triblock copolymer physical gel systems[114,129,299]. In terms of adhesive characteristics, this property is paramount because no creep (flow) should occur at long times and the formulation must exhibit a rubbery-like behaviour at room temperature, once cooled[123].

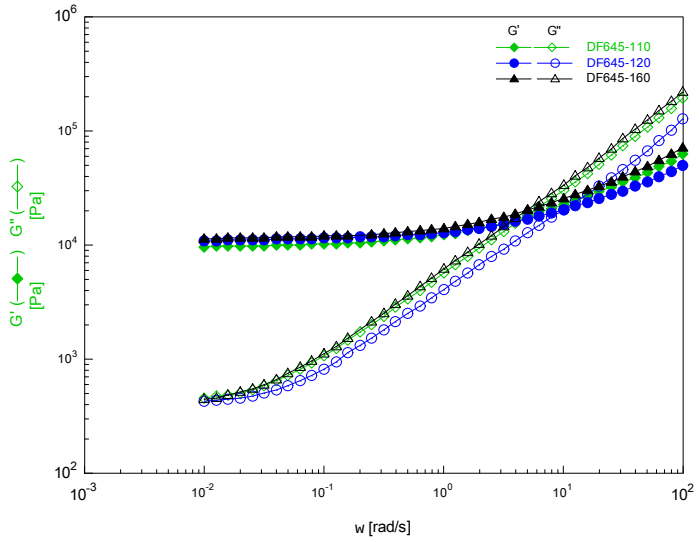

Figure 4.2: The frequency spectra of G' and G'' for DF645 adhesive bulk samples initially annealed at 110°C, 120°C, and 160°C respectively. The measurements were performed at 1% strain.

As the frequency was ramped up, between ~ 10^0 and 10^2 rad/s, the fast rise in G'' continued, even exceeding the slower increase of G'. This insinuated that less relaxations and movements of the polymer chain segments of specific lengths were occurring with the measurements. It is obvious that the adhesive systems underwent a broad transition from "rubber-like" state towards glass transition state. It is envisaged that the movements and

relaxations of the elastomer segments will eventually fail to respond with frequencies beyond the experimentally accessible range. The characteristic relaxation time (τ) corresponding to the elastomer chain segments cooperative movement will be too long to respond to the applied stress. A loss peak (glass transition) in G'' will eventually emerge and G' will level off to a new plateau as a signature of the elastomer chains acquiring the condition of a glassy state.

The measurements have proved that the samples exhibit similar dynamic mechanical properties irrespective of annealing thermal history at small strains. What is still unanswered is the adhesives behaviour during non-linear large strain deformation, equivalent to a debonding process, which is a paramount parameter for judging the product's performance. Investigation of the adhesive large strain behaviour will be presented in Chapter 7 where relationships between the debonding mechanism and adhesive film morphology will be discussed.

4.3.2 Tensile test

The tensile properties of the annealed adhesive samples observed in the stress-strain curves in Figure 4.3 were indicative of elongational behaviour characteristic of elastomers[37], i.e. low modulus and high extensibility. The phenomenon is due to the fact that the elastomer chains (both long and short) of the base triblock copolymers are above their T_gs at ambient condition, enabling the polymer C-C bonds to rotate with low resistance, especially in the presence of mineral oil.

At the initial stages of the deformations (up to ~ 50 mm displacement) (Fig. 4.3), the adhesive sample annealed at 100^{o}C exhibited stresses slightly higher than the adhesive samples annealed at 120^{o}C, 160^{o}C and 180^{o}C, respectively. The proportionality regime of the measurement where stress is proportional to deformation is not conspicuous in the graph, hence the Young's or elastic modulus, E, of the samples could not be determined. As the deformation continued beyond 60 mm displacement, a non-linear upturn in sample stresses was observed. The annealed samples displayed rather similar tensile properties, except the sample annealed at 180^{o}C, where the stress were significantly lower that the other three samples. The results from the measurements are comprised in Table 4.1. According to the mechanical theory of rubber elasticity, the stress-strain for the tetrahedral network structure of rubbers is according to[37,149],

$$\sigma_N = N_e^o RT\left(\lambda - \frac{1}{\lambda^2}\right) \quad 4.1$$

Where σ_N, is the nominal stress, R is the gas constant, T is the absolute temperature, λ is the extension ratio $\lambda = (L/L_o)$, (L and L_o are the lengths of the stressed and unstressed specimen, respectively), and N^0_e, is the number of moles of Gaussian chains in the network per unit volume of rubber. The nominal stress (force divided by the original specimen cross-sectional area) is approximately proportional to λ at high λ because $\lambda >> 1/\lambda^2$. The theory therefore predicts a linear relationship between the stress and the strain, but the upturn in stress at high adhesive extensions, which is similar to observations reported on rubber-based systems[300,301] are due to factors that the theoretical predictions does not account for. In the classical theories, it is assumed that the rubber network is perfectly interconnected, i.e. that no loose chain ends exist but in reality chain ends do exist, and they transfer stress less efficiently than the other inter-connected rubber network part[37,300,301]. The theoretical model does not take into account the complications from intramolecular crosslinking (loops), which might decrease the inter-connectivity of the elastomer network, as well as the effect of crosslinks (both physical and chemical)[37].

There is no one universal relationship to explain the behaviour of rubber-based samples in tensile test measurements. Different relationships fit the experimental observation at different extension ratios. The equation (Equation 4.1) captures the trend in experimental stress-strain data of unfilled rubbers in compression (λ <1) and at low extension ratios (λ <1.2)[151,300]. At higher extension ratios the experimental observations fall below the theoretical curve. The Mooney equation[37,151,300] derived from continuum mechanics is capable of describing the nominal stress-strain data at λ between 1 and 2 as,

$$\sigma_N = 2\left(\lambda - \frac{1}{\lambda^2}\right)\left(C_1 + \frac{C_2}{\lambda}\right) \quad 4.2$$

Where C_1 and C_2 are empirical constants. It may be noted that the Mooney equation is identical with the equation derived from statistical mechanics when $C_2 = 0$. Experiments have shown that for a range of different rubbers C_1 depends on the crosslink density basically as the modulus does according to the statistical mechanical theory, whereas C_2 is approximately constant[300]. Stress-strain data for rubbers swollen in organic solvents analysed by the Mooney equation show that C_1 is practically independent of the degree of swelling, whereas C_2 decreases with increasing degree of swelling approaching C_2=0 at $\nu \sim 0.2$ (volume fraction rubber). Hence highly swollen rubbers (ν< 0.2) behave according to

the statistical mechanical theory[37,151] In this study the observation implies that the tensile strength and elongation at break are independent of sample annealing temperature, up to an annealing temperature of 180°C where the tensile strength deteriorated but the elongation at break increased.

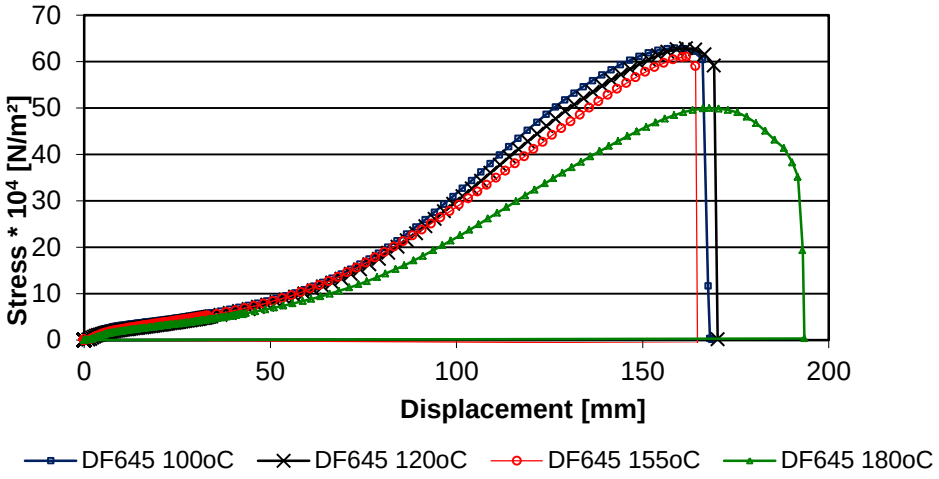

Figure 4.3: Stress-strain curves for adhesive bulk samples initially annealed at different temperatures indicated by the legends. (Courtesy of Dr. Wei Kong, Henkel)

The presence of PS regions serving as physical crosslinks could possibly increase the elongation of the adhesive samples since the structure of the overall material will go from that of individual rubber chains, to presumably chains interconnected via the PS domains plus the eventual plastic deformation of PS domains. That is, the crosslinks could strengthen the response of the material as a unit during large strain deformation[302]. The lowest tensile strength but largest elongation at break measured for the sample annealed at 180°C could be caused by fragmentation of connected network system in the adhesive sample blend. It is also possible that with such a pronounced annealing temperature, the rigid PS domains were extensively diluted by tackifiers/oil, leading to decrease in their strength and as a consequence causing to their pronounced plastic deformations.

Table 4.1: Mechanical properties of the investigated annealed adhesive bulk samples by Tensile Testing

Coating temperature of sample DF645	Tensile Strength * 10^4 [N/m^2]	Maximum Displacement [mm]	Fracture stress * 10^4 [N/m^2]
100^{o}C	63	167	62
120^{o}C	63	169	59
155^{o}C	61	164	59
180^{o}C	50	192	35

At very large elongations (λ>4), other sophisticated theoretical relationships are suggested in the literature to explain the stress-strain behaviour of rubber materials[37,151]. According to M.C. Boye et al.[303], the final steep up-turn of the stress-strain curve for rubber samples as the ultimate strain is approached is due to most of the surviving elastomer chains approaching their full extensions. The process of elongation enhances the alignment of the chains within the elastomers, and cause momentary van der Waals bond formation between segmental chains which leads to crystallization on a local basis within the elastomer sections that can undergo crystallization[303]. The ultimate break occurs possibly due to a weak intermolecular interaction between the aligned chains, defects in the samples caused by chain ends, or final breakage of polymer chains. This open issue related to the coating temperature effect will be further investigated in the following chapters.

4.3.3 Peel test measurements with non-woven fabrics.

4.3.3.1 Effect of the film coating temperature

The peel test results shown in Table 4.2 clearly depict that adhesive films coated at high temperatures underwent stronger adhesive bonds to cotton fabric than adhesive films coated at low temperatures. The film coated at 155^{o}C generated adhesive peel strength approximately three times higher than the adhesive film coated at 120^{o}C. If coated at 130^{o}C the peel force was almost twice as large as the peel force measured for films coated at 120^{o}C. Factors that underline such bond strength differences will be examined in the following chapters.

Table 4.2: Peel strength of DF645 adhesive films bonded to cotton fabric, at peel rate of 300 mm.min^{-1}.

Film coating temperature [^{o}C]	Peel Strength [g/30 mm]
120^{o}C	70.2 ± 14.1
130^{o}C	147.0 ± 26
155^{o}C	218 ± 31

4.3.3.2 Effect of the adhesive bonding rate

As a reminder, the DF645 adhesive films coated at 155^{o}C were used for this part of the studies. The results are enclosed in Table 4.3. The rolling rate employed for bonding the adhesive to the fabric at 300 mm/min generated the highest average peel force compared to the rolling rate at 1500 mm/min, for each of the fabric substrates examined. This indicates that the peel strength depends on the contact time between the adhesive and the substrate, which manifests the viscoelastic nature of the coated adhesive film. Bonding the fabrics to the coated PSA film with the roller, subjects the adhesive to shear stress. At the slow rolling rate of 300 mm/min, the coated film gets adequate time to deform onto the surface of the fabrics, into the cavities and thereby increases the wettability. At the relatively faster rolling rate of 1500 mm/min, relatively more elastic deformation recovers, leaving less plastic deformation into the cavities of the fabrics. As a result, the adhesive bonding strength becomes weaker due to the decrease in contact time and subsequently wettability.

Table 4.3: Average peel force as function of the adhesive bonding rate

Fabric substrate	Average peel force [g] at 300 mm/min	Average peel force [g] at 1500 mm/min
Cotton	340 ± 59	314 ± 38
Nylon	240 ± 90	189 ± 22
Microfibre	80 ± 64	35 ± 11

4.3.3.3 Effect of the substrate surface.

The cotton fabric recorded the highest peel forces to the adhesive, followed by nylon and then the microfibre, as shown in Table 4.3. This trend can be verified by the physical characteristics of the fabrics, presented in the scanning electron microscope (SEM) images in Figures 4.4. A major contributor to the bonding strength superiority is the high inherent roughness of cotton fibres and the pattern of the fabric (Fig. 4.4a). Cotton fibres are ribbon-like and exhibit a surface roughness which will provide a larger efficient surface contact area to impart mechanical interlocking[2,3] than nylon and microfibre. Hence once in contact, the adhesive is able to wet and penetrate the structure of the fabric when pressure is applied and firmly secures the cotton in place. From end-use viewpoint in terms of suitable substrates for the hygiene products application, the cotton fabric is not very good as some of the fibres were adhered to the adhesive film surface after the peel test.

a

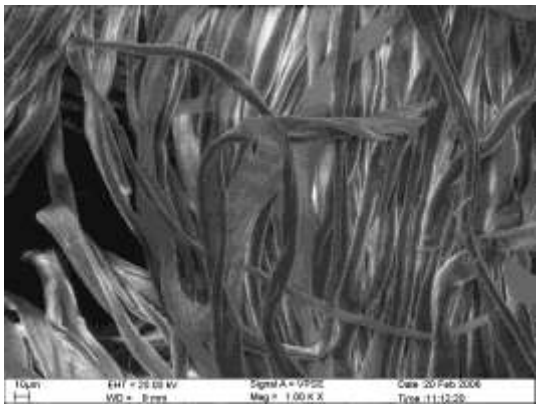

b

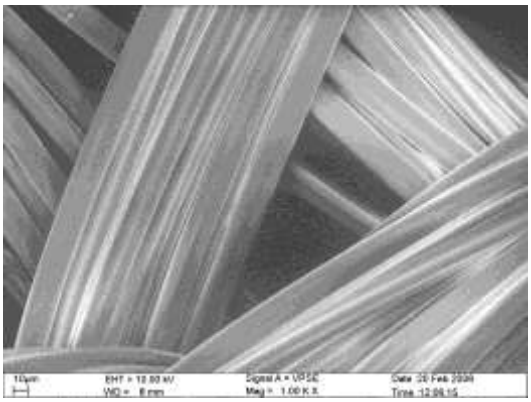

c

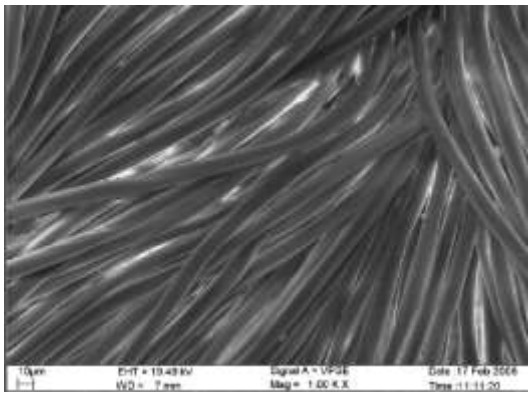

Figure 4.4: SEM micrographs of (a) cotton with a fibre width of approximately 25 µm, (b) nylon fabric consisting of plenty wide cavities, with a fibre diameter of 16 µm. In (c) the fabric structure of microfibre with compactly thin fibres leaving little room for cavities. Each fibre has the diameter of 8 µm. All the images were taken at 1000X magnification.

Nylon generated the second highest peel force of the fabrics (Table 4.3). In Figure 4.4b it can be seen that nylon has a smooth surface, compared to cotton and with a fine weave which is evenly distributed. The examined surface of the adhesive film after the peel test revealed that the nylon fabric was peeled cleanly from the adhesive and vice-versa, without leaving any residues which is a very desirable quality in its end-use application. Nylon has a large effective contact area for adhesion due to the presence and abundance of wide cavities, allowing the adhesive to plastically deform over the region, and establish bonds around the smooth fibre filaments.

The microfibre displayed the lowest bond strength to the PSA of all the fabrics tested (Table 4.3). The extremely smooth surface of the microfibre with tightly packed fibre pattern (Fig. 4.4c) is a key factor to its poor bonding characteristics, leaving only a small effective surface to make interaction with the adhesive. In theory the microfibre should exhibit the largest effective surface area since it has the thinnest fibres. However since the fibres are tightly packed, they prevent the adhesive to spread over wider region as it deforms. Similar to the nylon, microfibre was peeled cleanly without leaving any residues on the adhesive film surface or vice versa.

4.4 Summary

The shear and elongational behaviour of a copolymer based pressure-sensitive adhesive at room temperature was studied and has presented some of the challenges facing the adhesive industry in terms of examining the adhesive product performance. Bulk adhesive samples annealed at temperatures typically employed for film coating showed similar dynamic viscoelastic properties at room temperature. At low frequencies and strain, the adhesive samples displayed storage plateau modulus indicative of solid-like behaviour. This suggests a diminished creep at long times which is a good characteristic during end-use application. The tensile tests performed on the annealed bulk samples also revealed similar properties, except for the bulk sample annealed at 180^{o}C where a significant decrease in tensile strength but increase in elongation was observed.

The above results manifest the intricate nature and property of PSAs since the peel force measurements performed with the same adhesive formulation but as coated films instead of bulk samples, displayed discernible peel strengths with films coated at 155^{o}C exhibiting a

substantial higher peel force as compared to peel forces of the films coated at 130^{o}C and 120^{o}C, respectively.

With the peel test investigation the adhesive to non-woven fabrics, the cotton fabric generated the strongest bonding to the PSA coated film, at the two different rolling rates of bonding but did not peel cleanly. The nylon fabric bonding was not as strong as the cotton fabric bonding but peeled neatly with no evidence of fabric damage. The microfibre had the lowest average peel force at both bonding rolling rates but peeled cleanly just as the nylon fabric.

Though the information obtained with the bulk adhesive sample is useful, it has nevertheless proved to have limitations in judging the performance of the corresponding coated adhesive films. The following Chapters will, therefore, put emphasis on the behaviour and properties of the coated adhesive films by revealing the hierarchical structure and phase transitions of the films with corresponding adhesion nature down to the nanoscale level.

Chapter 5

5 Thermal Phase Transition and Viscoelastic Behaviour of Styrene-based hot-melt Pressure Sensitive Adhesive Films

5.1 Introduction

In Chapter 4, adhesive bulk property investigations performed on samples with different thermal histories suggested that examining the bulk property alone is not sufficient to judge the performance of PSAs, as the results did not reflect on any potential discrepancy in sample microstructure that might have evolved at the different annealing temperatures, unlike work based on pure copolymer systems[223,297]. This part of the studies investigates the structure and property of the films directly in order to understand their adhesion variation to the coating conditions, and provide clear answers to the adhesive developers and product manufacturers. The bonding and debonding that correspond to adhesion of PSAs have been reported to relate to the viscoelastic behaviour of the bulk adhesive[293-296]. Therefore evaluating the viscoelastic behaviour of the adhesive film can give an insight into the end-use and predict the performance of the product.

Due to the relatively small amount of base block copolymers used in PSA formulations, thermal transitions demonstrative of the copolymer segmental mobility can be difficult to detect. The Dynamic Mechanical Thermal Analysis (DMTA) or shortly Dynamic Mechanical Analysis (DMA), was used to evaluate the viscoelastic behaviour of the adhesives coated films due to its sensitivity to respond to subtle molecular mobility[145,234]. The technique is actually deemed unsuitable for the adhesive films since the films are naturally sticky and very complaint whilst the DMA is appropriate for specimen in solid state or with a solid support. Traditionally when measuring viscoelastic properties of adhesives with DMA, the sample material is either placed in shear clamp geometry or a

supporting film is required for running in the tension mode[232]. Sometimes the problem with the shear experiment is that the adhesive can be too sticky for the geometry. With the supporting film, the issue is an intricate sample preparation procedure that makes it difficult to obtain reproducible measurements[232].

Steel material pockets from Perkin Elmer[304,305,306] adjusted and employed for the DMA investigation of the adhesive films proved very successful. The pocket is simply a piece of stainless steel that the adhesive film is attached inside and folded, before mounting into the DMA instrument. This made it possible for heating the specimen through the melt while preserving its geometry and without contaminating the equipment. According to the manufacturer the material pocket[305] is very effective for the determination of transition temperatures, but does not permit quantitative measurement of dynamic moduli, due to the stiffness of the pockets which contributes very strongly to these values. The objectives with this study were therefore to:

- To characterize the effect of coating temperature on the viscoelastic property of hot-melt PSA films and the correlation to the adhesion strength.
- To quantify the activation energy involved in the glass transitions of phase separated domains within the adhesive coated film with good bonding property.
- To characterize the effect of the coating temperature on the viscoleastic property of PSA films of adhesive blends with different triblock base copolymers and polystyrene contents.
- To compare the viscoleastic properties of different PSA films coated at different temperatures, and the relationship with the measured adhesive peel strength.

5.2 Experimental

5.2.1 Materials and sample preparation

The three hot-melt PSA formulations termed as DF645, 7M8 and DFC600 were supplied by Henkel as thin coated films sandwiched between silicone release papers. Details of the subcomponents of each blend system are found in Section 3.1. The films were melt-coated onto silicon release liner at a line speed of 300m/min, resulting in film thickness of around 10 μm with a total mass of adhesive per surface area liner of 30g/m^2. The adhesive films of DF645 and DFC600 were coated at 120^{o}C and 155^{o}C, respectively. Film coatings of 7M8

were prepared at 130^{o}C and 165^{o}C, respectively. Bulk uncoated samples were also received. Pure samples of the triblock copolymers and the resins of the DF645 blend system were also received as granules. The preparation of specimens of the raw materials and adhesives varied because of their different physical properties.

For the adhesive film sample preparation, well defined rectangular-shaped specimen geometry with the dimension (length × width × thickness = 17.45 × 4.0 ×1.0 mm) was measured with callipers and cut with a pair of sharp scissors. The length was cut parallel to the direction of the film coating. The silicon paper on one side of the pristine adhesive film was then removed with tweezers and the freshly untouched adhesive surface was adhered on one side of the opened material steel pocket without shearing. The other silicon paper was then removed and a newly shaped film was attached on top of the previous film through the same procedure. After piling up 20 layers of films, the pocket was closed and the specimen was allowed to relax at room temperature for 24 hours before execution of the measurement.

Granules of the block copolymers SIS and SEBS were packed into a rectangular-shaped aluminium mould with the dimension given above and heated in an oven at 160^{o}C for only 3 minutes, to ensure thermal degradation did not come into effect. The temperature choice was based on the inability to shape the copolymers at any lower temperature for that short heating period of time. It is noteworthy to mention that the thermal prehistory treatment of the copolymers could alter their viscoelastic properties but since they were solely used for reference purpose, the preparation procedure was justified. The solid samples were then removed from the aluminium moulds, but not inserted into the material pockets as they were solid sheets. The DMA measurement was carried out some days after the preparations. Both mid-block and end-block resins came as brittle granules, and were grounded into powder and then applied into the material pockets.

Prior to each DMA measurement, the material pocket with sample was placed on a flat glass table and a clean flat metal disc weighing 7 kg was placed on top of the pocket for 30 minutes, before mounting it in the DMA clamps. This was done to ensure a reproducible sample thickness of 1 mm since there would have been variations in the results if the material pockets were hand tightened. The manufacturer suggested tightening with pliers but the implementation of the weight proved to generate repeatable results. It was also necessary to leave 5 cm of free space at each side of the sample in material pocket to

ensure the specimen was not tightened under the DMA clamp screws. For accurate reproducible measurement results, consistent sample dimension was crucial and for this reason, the material pocket proved advantageous as the sample in the form of powder or soft adhesive film under measurement was confined within the geometry. An illustration of the material pocket is shown in Figure 5.1.

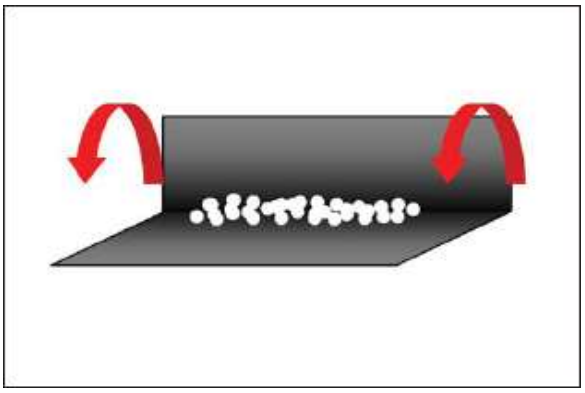

Figure 5.1: Sample granules inserted in steel material pocket as used for the DMA measurements[305].

5.2.2 DMA measurement

Before the phase transition investigations, a suitable oscillatory amplitude of 15 µm was established within all the specimens' linear viscoelastic region (LVR). For the phase transitions measurements, a temperature ramp test was employed where the sample's response was monitored at a constant frequency and constant amplitude of deformation. Data were taken at the equipment's default setting of 0.5 s/pt. Constant frequency of 1 Hz was used and the experimental conditions were;

1. Initial temperature: -90^{o}C
2. Motor drive : On
3. Equilibrate at: - 85^{o}C
4. Data Storage: On
5. Ramp 3^{o}C/min to 170^{o}C
6. End of method

With the above set-up, it was possible to open the DMA furnace and tighten the clamp screws that could loosen due to the equilibration at -85^{o}C, before the furnace was closed again and the measurement continued. The heating and cooling rates were controlled with liquid nitrogen and the temperature accuracy monitored by thermocouples fixed just

underneath the specimen in the DMA furnace. All the necessary calibrations to the instruments and test set-up were performed before the measurements.

For the activation energy measurement, multifrequency/temperature mode was chosen, where the experimental conditions were the same as previously, with the exception of the measurements carried out at 5 discrete frequencies.

5.3 Results and Discussion

The results in the following sections firstly highlight the thermal dynamic mechanical behaviour of the pure components of the DF645 blend formulation, followed by a presentation of the coated films. The activation energy quantification is then presented, and finally a comparison between DF645, 7M8, and DFC600 is discussed. Due to the application of the steel material steel pocket, only the tan δ (Equation 3.5, Chapter 3) measurement as function of temperature was useful for these studies.

5.3.1 Thermal dynamic mechanical studies of the constituent block copolymers

The temperature dependence of tan δ for the SEBS (Kraton G 1650) is observed in Figure 5.2. The two relaxations peaks are typical for block copolymers with two incompatible sequential[169,170]. The broad T_g peak from around -55^oC to -20^oC with peak maximum at -37^oC is ascribed to the slippage of entanglement units of the polyethylene/butylene (PEB) rubbery domains. The T_g peak beginning at around 89^oC with peak maximum at 98^oC is attributed to the relaxation of rigid polystyrene (PS) phase. The broadening of the peaks is due to the ease at which different polymer segments rearrange as a result of the heating. Chains that are constrained have more restricted motion than unconstrained chains. The soft rubbery chains far from the glassy PS domains have more freedom of movement than rubbery chains adjacent to PS domains. These latter chains become more rigid and thus need a higher energy for relaxation than their more flexible counterparts far from PS segments, creating a broadening transition peak effect. A similar broadening effect applies to the PS segments where rigid PS chains adjacent to flexible rubbery PEB chains move at a lower temperature than PS chains in the bulk of PS domains. Different lengths of polymer chain segments would also move at different temperatures. Published viscoleastic

studies on properties of Kraton G 1650 have reported T_g to be –37°C for PEB domains and 100°C for PS domains[166]. Others have reported[307] –42°C for rubbery T_g and 98°C for PS domains T_g. Results observed in the literature are consistent with values obtained in this study. The agreement of current results with literature is taken as good support for the quality of the measurements with the DMA.

Above the T_g of the PS, the tan δ curve showed a crooked pattern. This happened because of the elongation of the specimen bar due to the substantial molecular mobility with the heating. The data points after the T_g point of the PS is therefore not valid as consequence of changes to specimen geometry, and will not be discussed any further since they are of no relevance to the study.

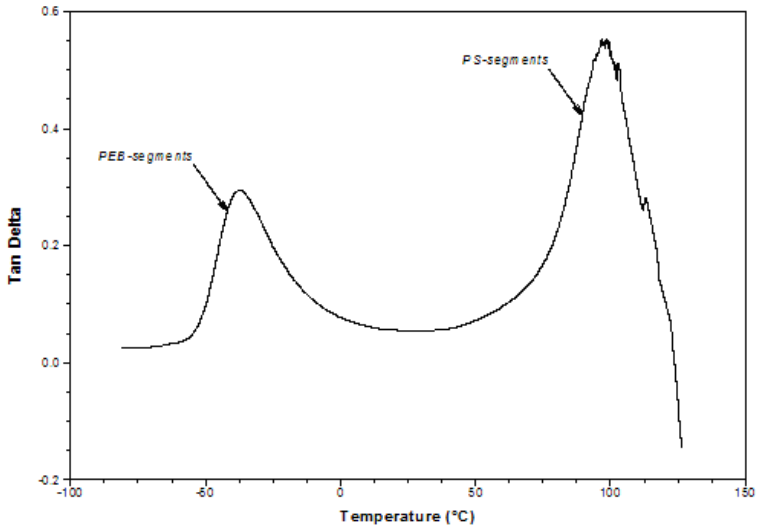

Figure 5.2: Tan δ measurement of SEBS block copolymer bulk sample shows two distinct peaks of Tgs at low temperatures for PEB segments and high temperature for PS segments.

Figure 5.3 shows the tan δ as function of temperature for the SIS (Vector 4114). A broad T_g peak from -65°C to -25°C with maximum at -58°C is attributed to polyisoprene (PI) chain relaxation, and the peak at 98°C is assigned to PS segmental relaxation. The trend is similar to the SEBS and this is expected since both copolymers have discernible chemically incompatible blocks. The T_g for homopolymer 1,4-cis polyisoprene as reported in polymer data handbook[64] range from (-74°C) to (-60°C). The T_g of the PI measured here is expected to be higher due to the presence of PS domains which would restrict the mobility of some PI chains. Just as the measurement of the SEBS, the data points after the Tg of PS are not valid due to elongation of the specimen bar.

The weight percentages of the PS in both triblock copolymers were smaller than the weight percentages of the elastomer blocks but the T_g peaks relating to PS domains seem to dominate in both measurements. This is also assigned to changes in specimen length due to intensification of molecular mobility as the measurement ramp temperature approached 100^{o}C. To ascertain this ambiguity, other measurements were carried out with thin samples of the SIS inserted in material pockets. The results as shown in Figure 5.4 correlated well with the expected T_g transition profile and reproducible with the measurement of SIS without the material pocket (Fig. 5.3). A very weak shoulder peak appeared at around -11^{o}C to 0^{o}C adjacent to the T_g for PI (Fig. 5.4), which is presumably a PI-PS interphase layer[308] relaxation. The results also vindicate the use of material pocket as it did not have any impact on the T_gs of the block copolymer segments. If anything it actually improved the sensitivity of the measurements as the interphase relaxation could be identified. The T_gs measured for the block copolymers are summarised in Table 5.1.

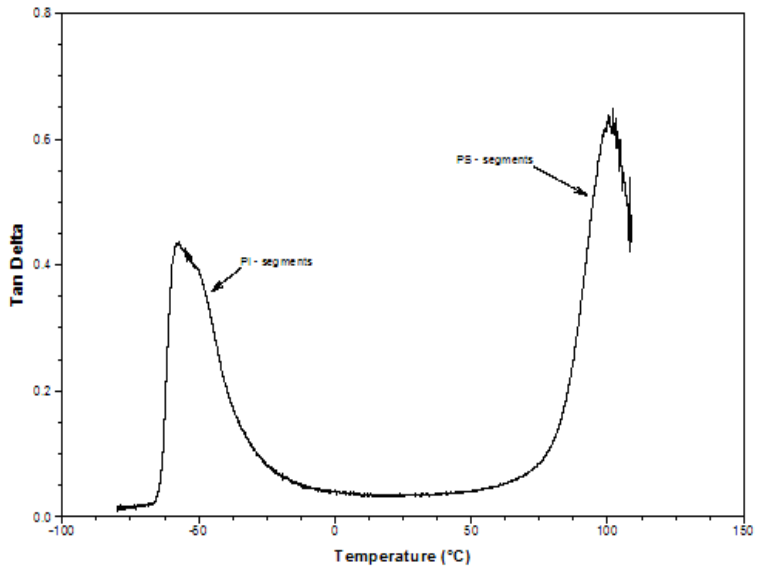

Figure 5.3: Tan δ measurement of block copolymer 1,4-*cis* styrene-*b*-isoprene-*b*-styrene(SIS) showing the T_g peak for PI at low temperature and Tg for PS at high temperature

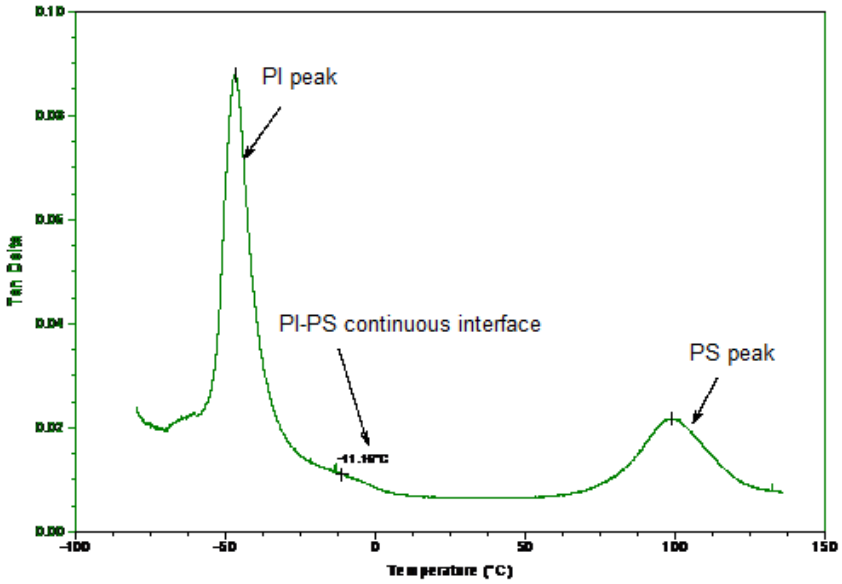

Figure 5.4: The tan δ spectrum for SIS triblock copolymer in material pocket is consistent with the measurement without the material pocket (Fig.5.3).

5.3.2 Thermal dynamical mechanical studies of the constituent middle block and end block tackifiers

The results of the midblock resin in the material pocket as shown in Figure 5.5 reveal a distinct loss maximum peak at 50^{o}C. Additional measurements were run with the empty steel material pockets to verify that the steel pockets did not have phase transitions in the temperature range of interest (Fig. 5.5, bottom line).

The measurement for the endblock resin displayed chain relaxation peak at around 55^{o}C (Figure 5.6). The M_w for alpha-methyl styrene (AMS) in the formulation is between 1000-2000 g/mol. Han et al[186] have reported T_g for AMS of similar M_w (1200g/mol) to be (54^{o}C). Both the tan δ peaks for the resins are broad and convoluted. This is assigned to the nature of the short-chain lengths of the resin oligomers. As a result, both resins are hard and brittle at temperatures below their T_gs and flow like liquid at temperatures above their T_gs, a characteristic similar to the behaviour of organic small molecules.

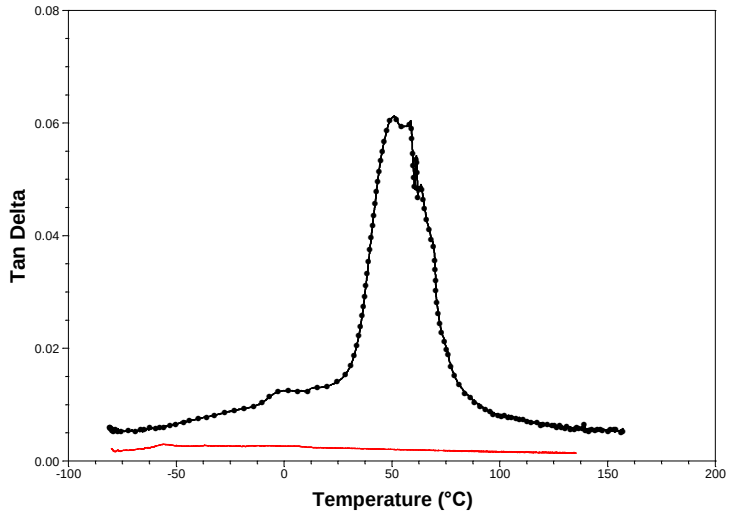

Figure 5.5: The tan δ as a function of temperature for midblock tackifier resin in material pocket. The bottom solid line is the measurement of an empty material pocket.

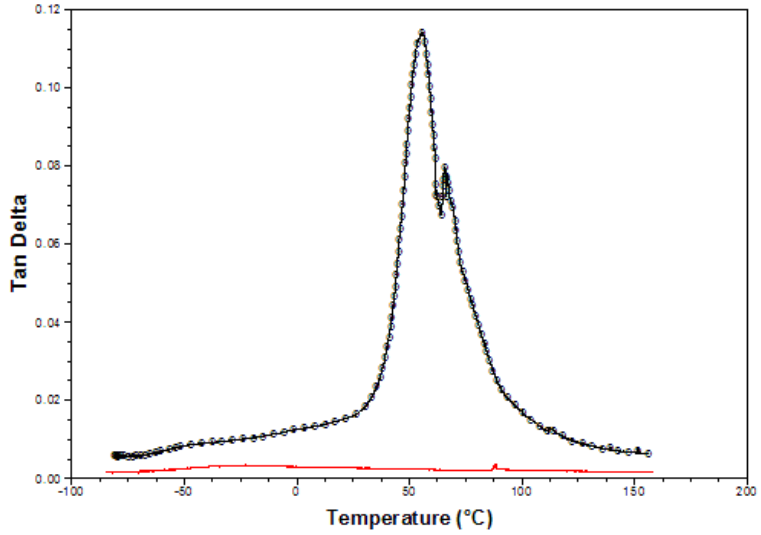

Figure 5.6: The tan δ as a function of temperature for endblock tackifier resin in material pocket (patterned curve), and the measurement for an empty material pocket (bottom solid curve).

5.3.3 The effect of coating temperature on phase transitions of DF645 coated films.

The importance of compatibility of hydrocarbon tackifying resins in adhesive systems has long been recognised. Investigations to quantify tackifier compatibility have explored

mixed T_g measurements, as well as a wide and pragmatic variety of tack measurements. If a base polymer and a tackifier are compatible, a single T_g is observed for the mixture and the tan δ peak will be shifted to a higher temperature due to the contribution from the higher tackifier resin T_g or vice versa, as already explained in Section 2.6.1.2. The Fox equation (Equation 2.35) has been reported to provide a fairly good prediction of T_g for a binary blend system provided the T_gs of the individual components can be determined[19,161]. Lloyd M. Robeson has comprised other equations[42] for predicting T_g of mixtures where he discusses a Schneider proposed virial-like expansion expression involving two variables:

$$\frac{T_{gb} - T_{g1}}{T_{g2} - T_{g1}} = (1 + K_1)\emptyset_2 - (K_1 + K_2)\emptyset_2^2 + K_2\emptyset_2^3 \qquad 5.1$$

Where $K_1 = K^*_1 / (T_{g2} - T_{g1})$ and $K_2 = K^*_2 / (T_{g2} - T_{g1})$. K^*_1 is related to the interaction energy difference between hetero and homo contacts; K^*_2 involves the energetic effects on the binary contacts of the molecular environments. K_1 and K_2 can be employed as data fitting parameters. Pressure-sensitive adhesive systems are not straightforward binary polymer blends but complex blended systems where molecular interplay between the multiple copolymers, multiple tackifying resins and mineral oil all contribute to the nature of the glass transition. There is therefore no simple relationship between the structure of the base copolymers used and the T_g of the adhesive formulation. This difficulty prompted the examination of the pure components where possible, to identify discrepancies and connections in thermal transitions between the raw materials and the blended samples. As elucidated in Section 2.6.1.2, the choice of a suitable resin for mixing with a specific block copolymer domain based on mutual solubility parameters has been found experimentally to be more complex than it was known to the adhesive industry[186-189]. Midblock compatible resin has been found to also associate with the endblocks of the block copolymers[187,188,189] and the endblock compatible resin also mixes with the copolymer midblocks[186,188,189]. With the reported observations in mind, four possibilities of resin distribution with respect to the two phases of both the SIS and SEBS block copolymers in the adhesive blend system are postulated as follows;

1. Both resins can partition into the PS phase.
2. Both resins can partition into the elastomer phase of PI and PEB.
3. Both resins can mix into both the elastomer and the PS phase.
4. Both resins can form separate phases.

The presence of the paraffin oil will only decrease the T_gs of the other subcomponents due to its plasticizing effect. Meanwhile the decrease in T_g of the adhesive rubbery phase by the paraffin oil will influence the increase of the T_g by the resins. The challenging task was therefore to identify which resin associated most with which copolymer phase, under the influence of the film coating temperature. The pristine uncoated bulk sample was investigated mainly for this purpose, to be used as reference.

The bulk uncoated DF645 sample (Figure 5.7, maroon/star curve) revealed a profound primary relaxation at -13^oC, attributed to the T_g of the adhesive continuous elastomer/oil/resin phase, as it appeared between the T_gs measured for the separate components. The observation is a synergistic effect by the contribution from all the subcomponents in the adhesive system including the PS. The shoulder peak around 12^oC indicated phase separation in the blend system but its origin is not yet understood. It could be the transition of phase separated midblock tackifier-rich domains. Since the resin content is highest in the DF645 formulation (56-wt %), it is plausible that once solubility with midblock copolymer (10-wt % in total) phase is saturated[309], the residual resin would phase separate into resin-rich domains. It could also be the T_g of poorly dispersed large phase-separated copolymer agglomerates, where PS is dispersed and plasticized by elastomer/paraffin oil. The rigid PS chain structure could then restrict the surrounding elastomer segmental relaxation to a certain degree, and as a consequence the thermal relaxation of the intermixed regions would occur at a slightly higher temperature than the continuous rubbery adhesive matrix. Another possible reason could be the relaxation of the interface between elastomer-styrene as observed in the spectrum for SIS (Fig. 5.4), whose volume fraction in the blend has increased due to accumulation of resins at the interface[310], shifting the T_g from -11^oC to 12^oC. In Chapter 6, the morphology studies of the blends will help clarify this ambiguous relaxation peak.

At high temperature, a very weak broad peak between 68^oC to 91^oC assigned to PS segmental relaxation is observed. Lee[311] tested the viscoelastic properties of a PSA based block copolymer, and suggested that the T_g of PS is not revealed in the thermal analysis for a styrene content less than 14%. For now let's assume that this is also a possibility since the total triblock PS content is only wt-6% in the formulation.

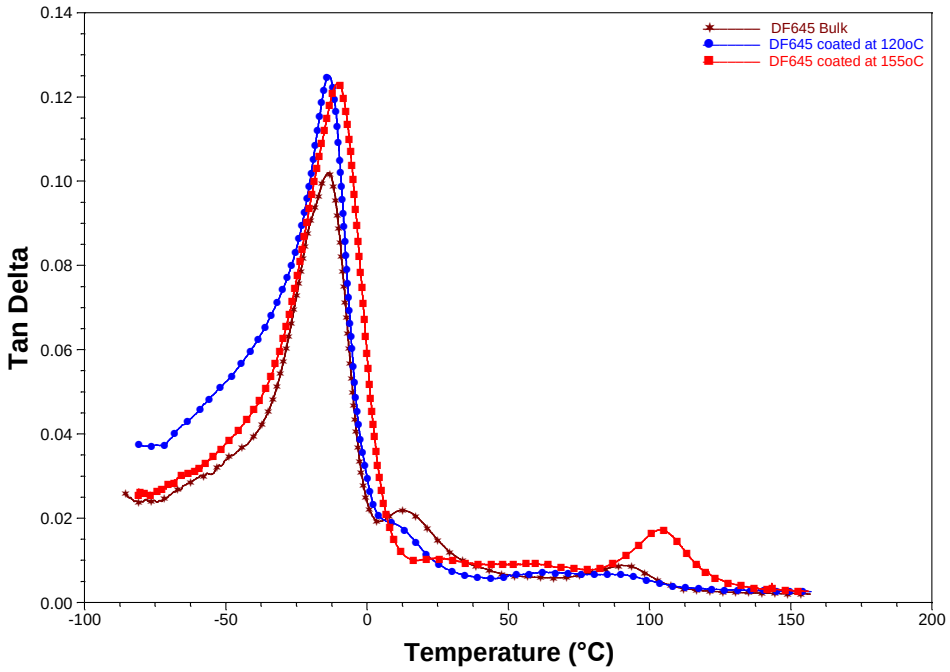

Figure 5.7: The tan δ as function of temperature for bulk DF645 sample, with the corresponding films coated at 120 and 155 ^{o}C, respectively.

The DF645 coated film at 120^{o}C (Fig. 5.7, blue/circular curve) revealed a similar trend as observed for the bulk uncoated sample. A significant T_g transition is observed at around –14^{o}C attributed to the T_g of the adhesive continuous phase. However the peak is broader as compared with that for the uncoated bulk sample, suggesting a diffuse rubbery phase separation and a larger viscoelastic dissipation during transition. A small tailing peak at 12^{o}C is identifiable, more or less similar to that as observed in the temperature scan of the uncoated bulk sample. A weak broad peak between 55^{o}C to 91^{o}C assigned to the relaxation of PS-rich regions is also observed.

The film coated at 155^{o}C (Fig. 5.7, red/square curve) revealed an adhesive matrix T_g at -10^{o}C, +4^{o}C higher than the matrix T_gs of the uncoated bulk and coated film at 120^{o}C. The Fox Relationship is not suitable for predicting the T_g of such a complex multi-blend system due to the synergistic effect, but it does help to interpret trends in location of the T_g. Rewriting the relationship given in Equation 2.35 based on only the elastomers and resins contribution to the matrix T_g yields,

$$T_{g,matrix} = \frac{T_{g,resin} * T_{g,elastomer}}{(T_{g,elastomer} * x_{resin} + T_{g,resin} * x_{elastomer})} \qquad 5.2$$

The relationship implies that increasing the x_{resin} in the elastomer phase increases the $T_{g,matrix}$. The increase in $T_{g,matrix}$ for film coated at 155^{o}C insinuates improved compatibility of perhaps the midblock resin and elastomer domains. The explanation is justified by the fact that the PS is chemically incompatible with the elastomers (Figures 5.2 to 5.4) and the paraffin oil (T_g = -118^{o}C)[312] will only reduce the $T_{g,matrix}$. The subtle tailing peak after $T_{g,matrix}$ observed for bulk and film coated at 120^{o}C is non-existent. This strongly indicates that it could be due to phase separated midblock-rich relaxation which has disappeared as more midblock resins have swollen up the triblock elastomer network. This is a significant effect of the film coating temperature.

A well defined peak from 92^{o}C to 128^{o}C and with maximum at 102^{o}C is assigned to relaxation of the PS segments. The results suggest a more uniform and homogenous nature of PS-rich regions within the film coated at 155^{o}C. Lees[311] observation whereby he reported that the T_g of PS is not revealed in thermal analysis for styrene content less than 14% in viscoelastic studies of PSAs, is not consistent with this observation, as the PS content was fixed in all the samples. The results of the measurements are comprised in Table 5.1.

Table 5.1: The glass transition temperatures of the subcomponents and the adhesive samples of the DF645 formulation.

Sample DF645	$T_{g,matrix}$ ^{o}C	T_g (PS), ^{o}C
SIS (wt-40% PS)	-58 (PI)	98
SEBS (wt-30% PS)	-37 (PEB)	98
Middle block resin	50	
End block resin	55	
Pristine Bulk	-13	68 - 91
Film coated at 120^{o}C	-14	55 - 91
Film coated 155^{o}C	-10	102

5.3.3.1 Self-assembling of multi-phase structure within coated films of hot-melt PSAs

The ability of polystyrene PS in low content triblock copolymers to self-assemble into micelles in a solvent that preferentially dissolve the elastomer midblock has already been mentioned (Section 2.4.1). Based on the above phase transition observations the PS are

assumed to be enriched in phase separated copolymer domains within the continuous rubbery-rich phase of the adhesive system. The core of these domains could predominantly consist of the PS large blocks, where the surroundings could be enriched by the elastomer blocks extending into the rubbery/oil/resin continuous adhesive phase. Since the PI and PEB segments are covalently bonded to the PS segments, they may plausibly form either loops/hairpins, bridges and dangling chain ends (Fig. 2.9), depending on the most thermodynamically favourable conformation for the elastomer chain in question[94,113]. These network systems will be discussed further in Chapter 6 when the morphology studies are presented. Nevertheless it is relevant raising the topic here since the kind of network present in the different temperature coated films contributes to the phase transitions observed in the thermal dynamic mechanical studies.

Given the lower endblock resin T_g (Figure 5.6) than the T_g for PS of the base triblock copolymers (Fig. 5.2 – 5.4), an ideal compatibility the two components should generate a T_g in-between their measured T_gs. The broad peak observed in the temperature range between 55^{o}C to 91^{o}C for DF645 coated at 120^{o}C and 68^{o}C-91^{o}C for the bulk sample could therefore be intermixed PS/AMS-rich regions within the adhesive film matrix. The observation is an indication of an incomplete phase separation between the PS and the continuous elastomer-rich adhesive matrix. Kraus and Rollman[297] have reported about ABA triblock copolymers that the nature of the interface domain boundaries is diffuse and intermixed as the block copolymers become shorter. Others have reported that a low molar mass PS dissolves in AMS whilst a high molar mass PS will phase separate[186]. Due to the low coating temperature of 120^{o}C where the adhesive blend viscosity is high, it construes that short chain triblocks within copolymer-rich regions would diffuse into the matrix and blend with AMS, whilst large triblocks with high degree of polymerisation (N), will still be trapped within the copolymer-rich cores. As a result the PS-rich regions are differently plasticized by the presence elastomer/oil. All these factors are plausible contributions to the diminished nature of the PS T_g for the low-temperature coated film.

Interestingly, the film coated at 155^{o}C displayed a distinct T_g peak for PS-rich-copolymer domain relaxation at 102^{o}C and meanwhile no broad peak was observed in the middle temperature region as seen for the bulk and coated film at 120^{o}C (Fig. 5.7). It has been reported that a necessary requirement for viscous flow in styrene-diene block systems is when PS detaches from domains and re-attaches to others[162]. This means that the processing temperature should be above the PS flow temperature at which all the triblock

copolymers with different sizes are able to move. The thermal energy at the higher film coating temperature is sufficient to induce such a segmental mobility where the flow will facilitate PS-PS chain connections through the strong π-π interaction of its benzene rings. Poorly dispersed copolymer regions are now assumed to be extensively dispersed, allowing more elastomers/oil/resins into the continuous adhesive matrix. The PS block mobility could also promote PS domain self-assembly as the blocks move and re-connect to new blocks in motion. This would then result in a more enriched PS phase separated copolymer domains where PS blocks are organised more efficiently compared to that of the low temperature coated film and the bulk samples. Hence such a phase would require a higher energy barrier to initiate PS cooperative segmental mobility, resulting in the higher PS T_g (Table 5.1). At the same instance, the increased elastomer volume fraction in the adhesive matrix would serve in improving the miscibility with especially the midblock resins and reduce the fraction of residual separated resin-rich regions. All these incidences could take place simultaneously as a result of a higher film coating temperature, and together contribute to a profound difference in adhesive film morphology. In adhesive blends based on SIS and SBS copolymers, it has been observed that high degree of tack is only obtained if mid-block resins are compatible with polydiene segments and incompatible with the polystyrene segments, providing the polydiene-resin form the continuum phase, with the polystyrene phase forming phase separated domains[188,189,309].

Based on the film coating temperature, it is hypothesized that the condition at a high coating temperature whereby PS segments move from one domain and re-attach to another domain should generate higher ratio of elastomer chain bridges to loops/hairpin and dangling conformations. For the film coated at a low temperature, the elastomer loop/hairpin conformations would dominate due to the limited mobility of the PS blocks. Such a morphology discrepancy would have a tremendous impact on the mechanical property of the coated films whereby bridging of PS-rich-copolymer domains suggest a more elastic-like 3-dimensional network property than lack of domain connectivity. In a study by Tanaka and Edwards[313] on the viscoelastic properties of physically cross-linked network systems, they reported that the stress transfer by the elastomers chains interconnecting PS domains is very efficient since the stress is transmitted from one PS junction to the other along the elastomer chain. The stress transfer by elastomer chain loops was negligible as it could only happen through friction of loops with surrounding chains implying much higher strains at the local adhesive film areas. These characteristics will be investigated in Chapters 6 and 7.

In terms of the location of the endblock AMS resin, it is envisaged to be enriched within the PS-rich-copolymer regions where it would contribute to denser packing of the PS and at the interface of PS-rubbery matrix since it has been reported to have chemical affinity for both PI and PS[186]. This is not a surprise given that AMS comprise a vinylic group just like PI and benzene group just as PS. The possibility that the midblock HDCPD is also found in the PS-rich-copolymer regions is not discredited as it was reported to have affinity for PS under certain conditions[188,189]. A large intermixed interfacial region between rigid PS phase and rubbery phase would actually contribute to the outstanding property that the adhesive manufacturer pursues since the energy dissipation during a debonding process would be improved[314,315,316].

The above concept is a simplified theoretical explanation to a probable adhesive morphology, where the rationale is based on the viscoelastic phase transition observations, complemented with information from the literature review. In reality, things are more complex and much more factors need to be considered before a comprehensive elucidation of the adhesive film morphology developed at different temperatures can be made. For instance, a reliable account of the thermodynamic interaction between each binary interactions by evaluating χ for segment-segment interaction is needed (Section 2.4). The χ for the PS alone should include $\chi_{PS\text{-}OIL}$, $\chi_{PS\text{-}PI}$, $\chi_{PS\text{-}PEB}$, $\chi_{PS\text{-}midblock\ resin}$, $\chi_{PS\text{-}endblock\ resin}$, and each χ by itself is a function of temperature (Equation 2.23). Defining χ for each component in the blend system will generate an intricate matrix equation system with computer simulation[316] only being the option of solution. Such information could not be obtained in the literature, but the results obtained with the DMA studies, together with the information acquired from earlier studies hopefully justifies the tentative explanation.

5.3.4 Activation energy involved with T_gs of DF645 coated films.

The activation energy involved for the molecular rearrangement that gave rise to the T_gs of the DF645 coated film at 155^{o}C was acquired with dynamic multifrequency/temperature measurements (Figure 5.8 and 5.10). The reason for the film choice was to acquire knowledge of the energy involved in developing the morphology of the adhesive film with good bonding property. The time-dependant polymer cooperative segmental mobility as

function of temperature follows the Arrhenius equation used in many situations to investigate diverse molecular energy dynamics[317, 318,319] according to,

$$F = Ae^{-\frac{E_a}{RT_g}} \quad 5.3$$

$$In(F) = In\left(Ae^{-\frac{E_a}{RT_g}}\right) \quad 5.4$$

$$In(F) = \ln(A) - \frac{E_a}{RT_g} \quad 5.5$$

Where *F* is a frequency applied for a test run, *A* is the pre-exponential factor, *Ea* is the activation energy and "*R=8.314 J*K^{-1}*mol^{-1}*" is the gas constant. T_g is the temperature at which the maximum loss is observed at the frequency *F*. Plotting *ln (F)* as function of $1/T_g$ gives a linear relationship (Figure 5.9 and 5.11) where:

$$-\frac{E_a}{R} = slope \quad 5.7$$

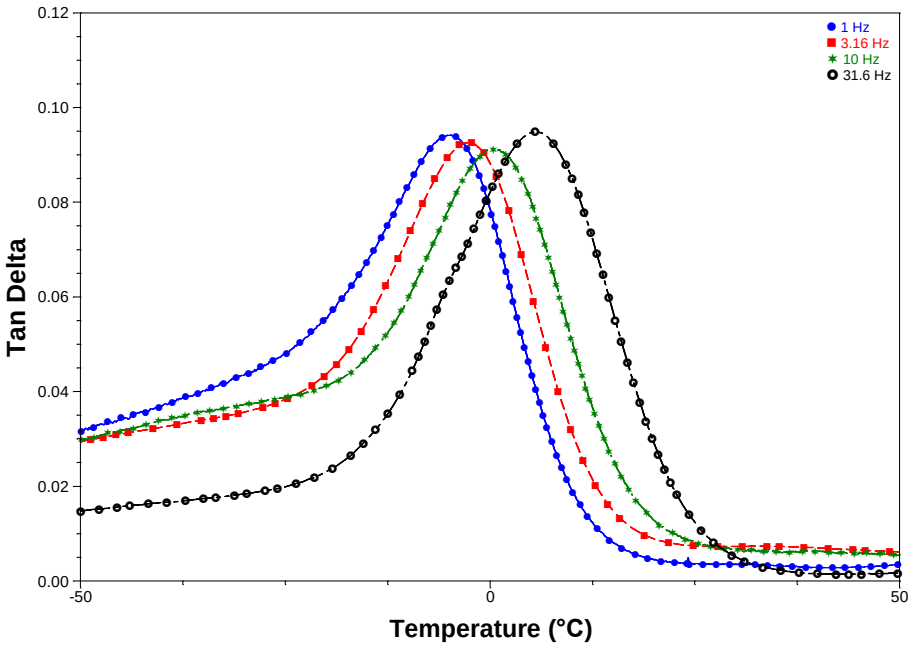

Figure 5.8: The dependence of the adhesive matrix tan δ as a function of temperature and frequency. The frequencies are shown in the legend at the top right corner.

Table 5.2 shows data points from the plot for calculating the E_a for the adhesive matrix T_g and Table 5.3 shows data transition points for the PS-rich phase T_g. The E_a for the rubbery matrix relaxation was 39 Kcal*mol^{-1}(164 KJ*mol^{-1}) and 48 Kcal*mol^{-1} (201 KJ*mol^{-1}) for the PS-rich phase, respectively. These are the energy barriers the adhesive film had to overcome within the measurement set conditions in order to undergo the structural reorganisation to generate the transition peaks. There has not been any study previously reported on the same blend system so it is impossible to compare the E_a values. In reported studies about homopolymer styrene, the E_a for PS relaxation was reported to be 83 Kcal*mol^{-1} (348 KJ*mol^{-1})[320]. Gao et al reported[321] in their work a value of 77 Kcal*mol^{-1} for PS where they implemented Dynamic dielectric analysis (DEA) for the thermal relaxation investigation. The deviations from literature are expected since the earlier studies were based on pure polystyrene systems.

Table 5.2: The T_g values of the rubbery matrix at different frequencies

Frequency [Hz]	Temperature [^{o}C]
1	-6.76
3.16	-3.68
10	1.29
31.6	5.92

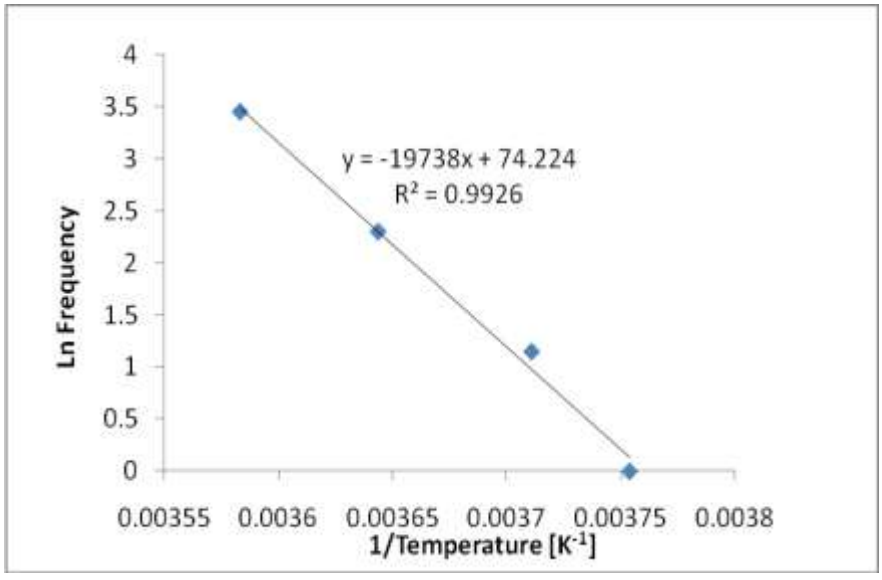

Figure 5.9: The Arrhenius plot for the T_g of the adhesive rubbery matrix at different measurement frequencies.

Gao[321] stated that the E_a values reported in their work was still lower than the energy involved with PS segmental sliding. The reason for the low Ea value obtained in this study for PS segmental mobility is assigned mainly to the presence of elastomer/oil that will increase the free volume and hence ease rearrangement of PS-segments, especially for the chains at the interface to the rubbery matrix. As for the E_a involved in the rubbery matrix T_g, it is fair to imply that the presence of the tackifiers can restrict elastomer entanglement sliding due to the filler effect, and give rise to a higher E_a barrier than if the system was purely rubbery. On the other hand mineral oil will ease mobility by increasing the free volume in the elastomer segments but the tremendous increase in matrix T_g suggests a dominant effect by resins.

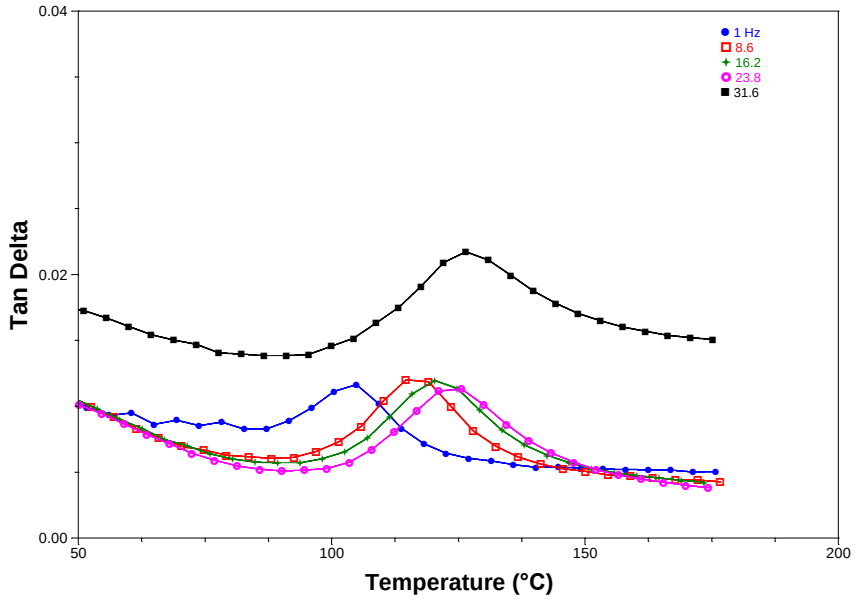

Figure 5.10: The dependence of the PS-rich tan δ as a function of temperature and frequency. The frequencies are shown in the legend at the top right corner.

Table 5.3: T_g values of the PS-rich domains at different frequencies

Frequency [Hz]	Temperature [°C]
1	104.55
8.6	116.99
16.2	121.43
23.8	124.10
31.6	126.23

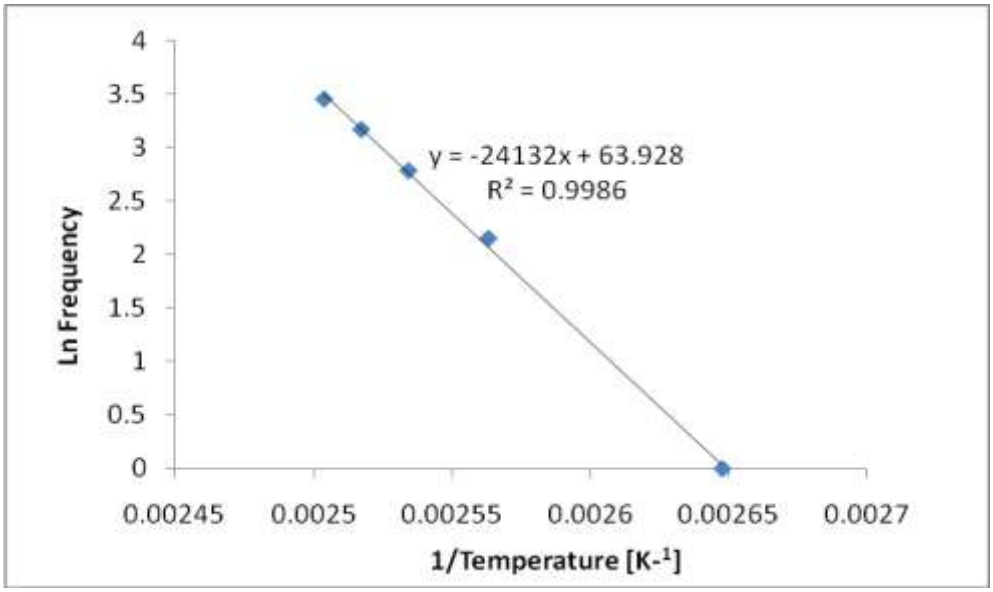

Figure 5.11: The Arrhenius plot for the T_g of PS-rich phase at different measurement frequencies.

5.3.5 Phase transitions of three different adhesive blends films and the relationship to peel strength

This section underlines the difference in thermal transitions of DF645 coated films compared to coated films of the 7M8 and the DFC600 adhesive blend systems. The effect of film coating temperature on the phase transitions for the coated films of the 7M8 and DFC600 blends is consistent with the observations made for the DF645 blend system. Unless relevant, the discussions will only relate to the differences in the blend formulations, and their relationship to alterations in thermal transition peaks (See Section 3.1.1 for the details of the formulations). For simplicity, the impact of mineral oil is neglected as it is fixed in all the blend systems. Two principles are discussed in this section, (a) shifts in T_gs, and (b) tan δ peak heights according to Equation 3.5.

5.3.5.1 The phase transitions of the adhesive films coated at low temperatures

In Figure 5.12, the T_g for the matrix of 7M8 coated at 130^{o}C is lower (~ -5^{o}C) than the $T_{g,matrix}$ for DF645 coated at 120^{o}C. Due to the higher styrene content, 7M8 had to be coated at slightly higher temperature to achieve adequate flow for successful film coating. The difference in the matrix T_gs implies that the endblock AMS with higher M_w in 7M8

has become less compatible with the rubbery-rich matrix and associated more with the PS-rich-copolymer regions. As given in Equation 5.2, decreasing resin volume fraction in the rubbery matrix will result in lower $T_{g,matrix}$. Han et al.,[186] observed in their studies that an AMS with a $M_w \geq 2000$g/mol entirely associated with the PS endblocks of SIS. Ghosh et al[166].and others[322], have reported similar observations in studies about the effect of block molecular weight on SEBS viscoelastic property. The matrix tan δ peak height (~ 0.125) of the DF645 is higher than that of the 7M8 (~0.095). This insinuates a relatively larger energy loss during the $T_{g,matrix}$ transition for the DF645 coated film compared to the 7M8 coated film. Nevertheless all the tan δ values are relatively low, implying a dominant elastic-like property of all the coated films.

There are very weak broad transitions, almost non-existent between 51^{o}C to 84^{o}C, and 97^{o}C to 133^{o}C for the 7M8 coated film (Figure 5.12). This again suggests partial plasticization of PS-rich-copolymer regions. The observation comes as a surprise as a higher M_w polystyrene of the triblocks are assumed to phase separate efficiently due to the stronger segregation power,χN,[72-78]. However the coating temperature proves to be a key factor as the thermal energy was not adequate to facilitate PS segmental mobility which could result in a more uniform phase separated regions. The T_gs for the coated films have been comprised in Table 5.4.

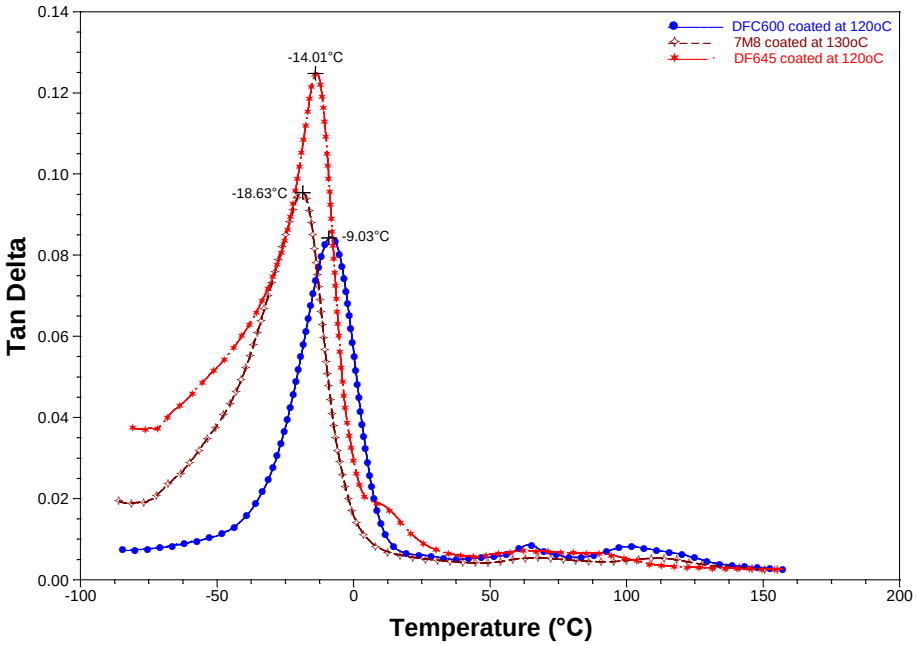

Figure 5.12: The tan δ-temperature curves for adhesive films coated at low temperatures as function of adhesive blend formulations. The legend at the right corner designates each film blend with coating temperature.

The $T_{g,matrix}$ of DFC600 coated at 120°C is +5°C higher than that of DF645 coated at 120°C (Fig. 5.12 and Table 5.4). The tailing transition peak (around 12°C) which was conspicuous for DF645 coated at 120°C is also non-existent, implying a diminished presence of probably phase-separated midblock resin-rich regions or larger partitioned copolymers agglomerates.

Table 5.4: The main phase transitions of the different PSA films coated at low temperatures.

Sample	$T_{g,matrix}$ °C	T_g (PS), °C
DF645 coated at 120°C	-14	-
7M8 coated at 130°C	-19	-
DFC600 coated 120°C	-9	102

The higher polydiene content in the DFC600 formulation possibly contributes to improving the elastomer miscibility with the midblock resins and yields a better diluted entanglement matrix, which gives rise to the higher $T_{g,matrix}$. This is consistent with the

earlier reported work[309] and also the synergistic effect of all the subcomponents within the blend system. The studies in Chapter 6 and 7 will help clarify the differences in the three blend systems.

The tan δ peak of the DFC600 coated film is also lower than that of the DF645 and 7M8 coated films, suggesting less energy dissipation during transition. It is envisaged that the higher presence of *cis* -C=C- bonds could promote the film elasticity. Hence during the thermally activated segmental mobility transition, the sample's ability to store elastic energy per measurement cycle is enhanced and a relatively lower $T_{g,matrix}$ peak height is observed as a result. Further explanation will be given after the morphology studies in regards to the effect of the polydiene segments.

After the T_g of the rubbery matrix, the DFC600 coated film revealed a small thermal relaxation peak at around 72^oC. This could be a domain-boundary mixing effect[323]. The SIS has lower M_w than the SBS in the DFC600 blend system. The PS of triblock SIS copolymers is then likely to be more plasticized, leading to that relaxation peak. The T_g transition between 89^oC and 128^oC with maximum ~102^oC is ascribed to the T_g of PS-rich-copolymer regions.

The peel force values reported for the films of the different blend systems coated at low temperatures are comprised in Table 5.5. The DFC600 coated film has superior peel strength as compared to coated films of 7M8 and DF645, respectively. Apart from the relatively highest DFC600 film matrix elasticity, the PS-rich-copolymer domains seems to be more uniform (Define PS T_g, Fig. 5.12) which could contribute to the DFC600 film's highest peel strength compared to those of the other low-temperature coated blend films.

Table 5.5: Peel strength of films of the three hot-melt blends coated at low temperatures

Adhesive film	Coating temperature [^oC]	Average peel load [N/30mm]
DF645	120	31.78 ± 0.17
7M8	130	32.16 ± 8.66
DFC600	120	94.80 ± 9.90

5.3.5.2 The phase transitions of the adhesive films coated at high temperatures

The phase transitions of the DF645 compare with the 7M8 and DFC600 coated at high temperatures are shown in Figure 5.13, with the T_g values in Table 5.6. It is apparent that sufficient thermal energy promotes uniform assembling of PS-rich-copolymer domains within the coated film matrix. The T_g relating to PS block segmental relaxation for the 7M8 coated at 165^{o}C is expected to be highest due to the highest PS M_w [1166] used in the blend. The $T_{gmatrix}$ of the 7M8 is slightly lower than the $T_{gmatrix}$ of the DF645 (Fig. 5.13) and this is similar to the trend of the films coated at low temperatures (Fig. 5.12), with the explanation already given above.

Another significant observation is the higher $T_{g\ matrix}$ for the 7M8 coated at 165^{o}C compared to the 7M8 coated at 130^{o}C (Tables 5.4 and 5.6). It is possible that as the PS-PS interactions increase during the high film temperature coating, the endblock AMS affinity decreases towards the PS of the triblock copolymers. Therefore higher fraction of AMS will be in the continuous rubbery adhesive phase and hence contribute to increasing the $T_{g,matrix}$ of the high temperature coated film (See Section 5.3.3.1)

The DFC600 coated film at 155^{o}C displayed a broad shoulder peak between -73^{o}C and -41^{o}C (Fig. 5.13). This suggests some separation of rubbery-rich continuous phase. During the self-assembling of the PS-rich-copolymer domains at the high coating temperature, the elastomer segments are assumed to be more exposed within the adhesive due to the extensive PS segmental mobility. The tailing peak could be some rubbery rich phase within the continuous adhesive matrix of rubbery/resins/oil. Further investigation into the origin of the peak is needed to establish its impact on the film's adhesive peel strength.

After the adhesive matrix T_g peak around -11^{o}C (Table 5.7), the DFC600 coated film exhibited a weak shoulder peak at 17^{o}C possibly due to some interfacial layer relaxation as explained in Section 5.3.1.3. The defined transition peak found between 85^{o}C to 129^{o}C with peak maximum at 99^{o}C, is assigned to the relaxation of a more homogenous PS-rich-copolymer domains within the adhesive film matrix.

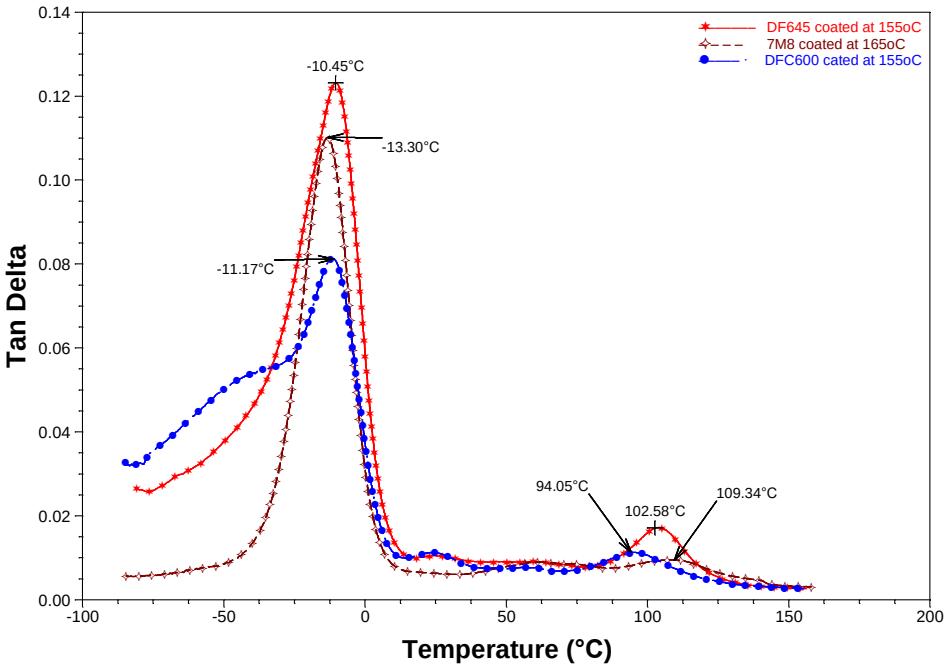

Figure 5.13: The tan δ-temperature curves for adhesive films coated at high temperatures as function of adhesive blend formulations.

Table 5.6: Major phase transitions of hot-melt PSA films coated at high temperatures.

Sample	$T_{g,matrix}$ °C	T_g (PS), °C
DF645 coated at 155°C	-11	103
7M8 coated at 165°C	-13	109
DFC600 coated 155°C	-11	94

As shown in Table 5.7, the highest peel force is measured for the DFC600 coated film is ascribed which manifests the adhesion improvement due to the presence of high concentration of polydiene which partly serve in improving the rubbery compatibility with the resins. Film structure studies in Chapter 6 will shed more light on the influence of the polydiene segments on coated film nature.

Table 5.7: Peel strength of films of the three hot-melt blends coated at high temperatures

Adhesive film	Coating temperature [^{o}C]	Average peel strength [N/30mm]
DF645	155	82.56 ± 12.25
7M8	165	128.60 ± 18.90
DFC600	155	139.10 ± 13.60

5.4 Summary

This work has underlined the possibility of predicting adhesive property by investigating the coated films viscoelastic behaviour with DMA, through the implementation of material pockets. The method has proved to be effective for determination of transition temperatures as the steel pocket did not exhibit thermal transitions in the measurement range. With the interrelation of the phase transition, viscoelasticity and surface adhesion of the three adhesives, a further in-depth understanding of the formulation-structure-properties is presented.

Two distinct phase transition peaks were observed with the DMA measurements for the adhesive films coated at high temperatures. A thermal transition peak was visualized around 120^{o}C for the thermal relaxation of the adhesive rubbery matrix and another peak at around 98^{o}C for the relaxation of phase-separated PS-rich-copolymers regions within the film matrix. The PS phase separation reflects the superior peel strength of the high-temperature coated films since the PS transition peak was very weak for films coated at low temperatures. This suggests extensive plasticisation of the PS-rich-copolymer regions within the low-temperature coated films.

The change of block copolymer in blend appears to be effective in improving the adhesion of the coated films and also minimising their dependency on the coating temperature. In replacing SEBS with SBS in the DFC600 blend system, the film coated at high temperature did not display much higher peel strength than the film coated at low

temperature, unlike the DF645 and 7M8 blend systems. The addition of more *cis*-C=C bonds from the SBS seems to have,

- Promoted the compatibility of the rubbery polymer phase with the resin tackifiers through weak attractions of the electron-rich double bonds and the alicyclic resins.
- Imparted more elasticity to the film matrix which was observed by low tan δ peak height during the T_g transition of the film matrix of both the low- and high-temperature coated films.

The use of more polystyrene with higher molecular weight (M_w) in the adhesive formulation made the film's adhesion behaviour very sensitive to the coating temperature since higher temperature is essential for efficient self-assembling of the PS-rich-copolymer regions. In the 7M8 blend system with higher styrene content and M_w compared to the other blend formulations, the film adhesion was found to deteriorate significantly if the film was coated at low rather than at high temperature.

Chapter 6

6 Micro- and nanoscale morphology investigation of hot-melt PSA films with atomic force microscopy

6.1 Introduction

In Chapter 5, thermal dynamic mechanical studies performed on coated films from the three different hot-melt pressure-sensitive adhesive (PSA) blends revealed complex phase behaviour of the adhesive samples. Two major glass transition (T_g) peaks were observed for each of the blends. A defined T_g peak observed at low temperatures (below room temperature) attributed to the thermal relaxation of the adhesive matrix and a high temperature T_g peak (~100^oC) assigned to thermal relaxation of polystyrene (PS) rich copolymer separated domains within the film matrix. Additional weak T_g peaks were also identified, especially for films coated at low temperatures. The emergence of these peaks was an indication of a further phase separation within the adhesive coated films.

Through the employment of atomic force microscope (AFM), this Chapter is aimed at reviewing, (1) the adhesive film morphology on a micro- and nanoscale level and (2) to attain further knowledge of the adhesive film structure to support the viscoelastic studies. Since the surface adhesion and properties of the coated films are bound to be dependent on their structure generated by a specific manufacturing condition, the purpose of this Chapter is first, to recognise this fact and then to define its importance to the peel performance. Coating temperature effect on film morphology is presented, followed by the annealing effect on film morphology. The fundamental differences behind the microphase and nanoscale film morphologies are discussed.

Time-of-flight static secondary ion mass spectroscopy (TOF S-SIMS) is employed to investigate the chemical group nature at the near-surfaces of the coated films. Understanding the delicate balance between bulk chemical composition on one hand, and the surface free energy on the other hand, leading to the desired surface structure and film adhesion are paramount to the adhesive manufacturer.

6.2 Experimental

6.2.1 Sample preparation and characterisation

The three hot melt PSA formulations used for the studies were the commercial adhesive products DF645, 7M8 and DFC600 supplied by Henkel as thin coated films on polyethylene (PE) film substrates. The compositions of the formulations and film coating process information are found in Chapter 3.1. The adhesive films of DF645 and DFC600 were coated at 120^{o}C and 155^{o}C, respectively. Film coatings of 7M8 were prepared at 130^{o}C and 165^{o}C, respectively.

6.2.1.1 Atomic force microscope

Small pieces (1 cm x 1 cm) of pristine coated films on PE substrates with surfaces covered by silicon paper were cut with a pair of clean scissors. Each sample was firmly placed on a steel disc with double sided tape and mounted onto the AFM sample holder. The holder consisted of a large magnetic metal disc on an adjustable metal holder, where it was magnetically attached. Prior to the examination, the silicon papers were removed meticulously with a clean pair of tweezers. The surfaces of the free-standing adhesive films were also examined to ensure that the AFM images obtained were not influenced by the PE films used as supporting substrates for the coated adhesive films. All the film surfaces examined were the surfaces that would eventually be placed into contact with adherends during end-use application, and all the measurements were performed at room temperature. See Section 3.2.5.5 for extensive characterisation procedure.

6.2.1.1 ToF S-SIMS analysis

The pristine coated specimens on the PE substrates were cut into 7 x 7 mm^2 squared samples. Double-sided tapes were adhered to the metal substrates and the PE sides were attached to the tapes resting on top of the metal substrates. Prior to the specimen's insertion in the SIMS instrument, the silicon release paper on the surface to be characterized was removed with clean tweezers. All the samples were not pre-treated but examined as pristine adhesive films. See Section 3.1.11 for extensive characterisation procedure.

6.3 Results and Discussion

The results are presented according to the following order;

- Film morphology on the microscale is presented, followed by film morphology on the nanoscale.
- Thermodynamic concepts and the literature reported studies are employed to elucidate the observed film morphologies.
- The impact of long time annealing on film morphology is presented.
- The observations from S-SIMS chemical group analysis of coated adhesive surfaces are presented.

6.3.1 Effect of coating temperature on microscale film morphology

6.3.1.1 DF645 adhesive coated films

Unless stated all the AFM height images are placed on the left with corresponding phase images placed on the right. In the tapping mode (TM) AFM images shown in Figures 6.1 and 6.2, the DF645 films coated at 120^oC comprised of phase-separated agglomerates randomly dispersed within the adhesive matrix. The images were acquired with moderate tapping (r_{sp} = 0.87) and the height images suggest that the agglomerates exist at the film surface but yet beneath the uppermost surface layer. One major problem with TM-AFM on soft materials is the distinction between the real surface topography and an apparent one due to lateral variations in the indentation depth of the tip[263,254] into the sample surface. The observation made from this work is that when very light tapping forces were

employed, the height images revealed virtually uniform adhesive film surfaces, irrespective of the blend formulation investigated. The corresponding phase images displayed a homogeneous layer of a relatively soft phase. This is expected given the elastomers forming the continuous phase together with paraffin oil have lowest surface energies in the blend systems[64,324]. Unfortunately it was not possible to distinguish and measure the depth of the surface thicknesses, unlike reported work on pure triblock copolymer systems. Knoll et al[263], have reported a 7 nm thick uppermost layer of polybutadiene (PB) blocks on AFM studies of pure styrene-butadiene-styrene (SBS) triblock copolymers. Hoichang et al.[196] investigated the near-surface morphology of an SBS based hot-melt PSA with transmission electron microscope (TEM). They reported a thin homogenous uppermost PB layer of < 15 nm. Others have reported similar results on triblock copolymer systems where the polymer block chains with lower surface energy covered the free air surface even when the components with a higher surface energy formed the matrix[250,325,326]. Hence all the height images acquired with moderate tapping are not related to real surface roughness but interplay between the real surface topography and tip indentation into the soft uppermost film surfaces, which was necessary to reveal the informative sub-surface film morphologies. The bright colour contrast of the agglomerates in the phase images suggests that they are relatively harder than the continuous film matrix (See AFM, Section 3.2.5.4).

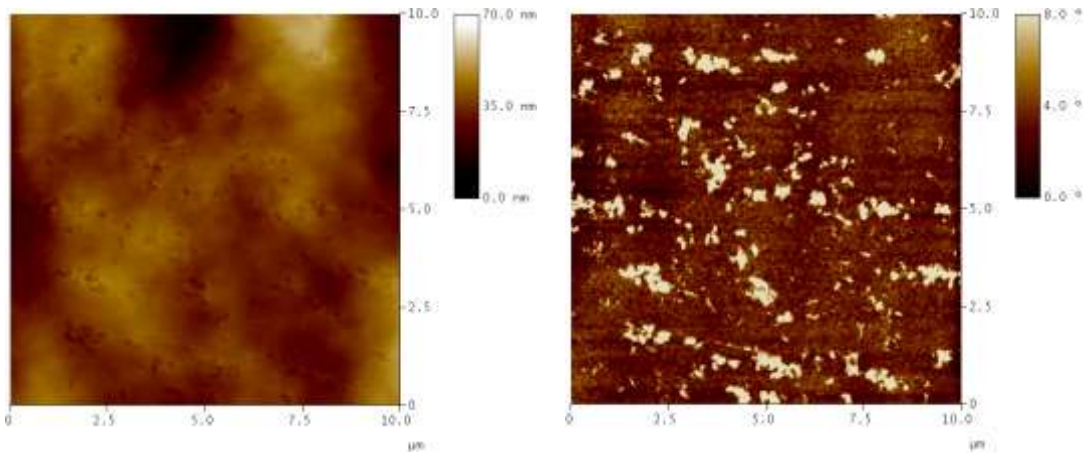

Figure 6.1: The surface morphology of DF645 film coated at 120°C. The height image (left) and the phase image (right) revealed phase-separated relatively hard agglomerates dispersed within the adhesive matrix. The scan size is 10 µm x 10 µm. The height and phase difference scale bars are placed to the right of each image.

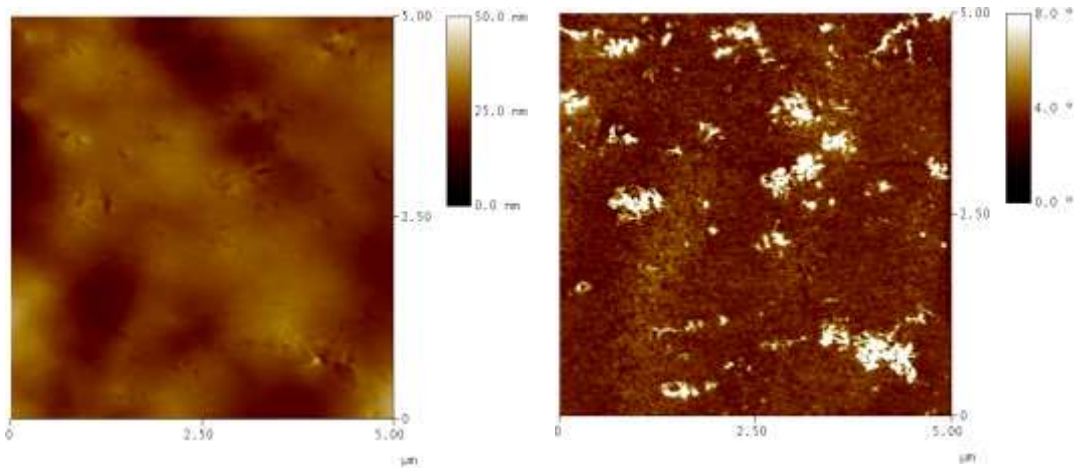

Figure 6.2: The surface morphology of DF645 adhesive film coated at 120^{o}C, at scan size 5 µm x 5 µm of film surface area.

The film morphology of DF645 coated at 155^{o}C (Figures 6.3 and 6.4) revealed microscale phase-separated agglomerates similar to that of the film coated at 120^{o}C. The agglomerate size distributions in the different temperature coated films are presented in Figure 6.5. The analysis was performed on 25 images from each sample scanned at 5 µm x 5 µm (See Section 3.2.5.5.1 for size distribution quatification). As observed in the size statistic diagrams (Fig. 6.5 a-d), the agglomerates were larger and occupied a larger film surface area in the film coated at 120^{o}C than the film coated at 155^{o}C. The standard deviations (Fig. 6.5a,b) suggest a broad size distribution of the largest agglomerate micro-domains, coexisting with the smaller domains. In the film coated at 155^{o}C, the smallest agglomerates increased in amount and the largest agglomerates decreased in sizes, with narrower standard deviation compared to the film coated at 120^{o}C. Also the total number and sizes of the agglomerates reduced sharply compared to film coated at 120^{o}C (Fig. 6.5d). Figure 6.5e shows the random agglomerate presence within the coated films, where 25 randomly selected films of each film coating are compared. The agglomerates are a vindication that the formation of relatively hard micro-phase regions within the adhesive film is more pronounced when films are coated at low temperatures rather than at high temperatures.

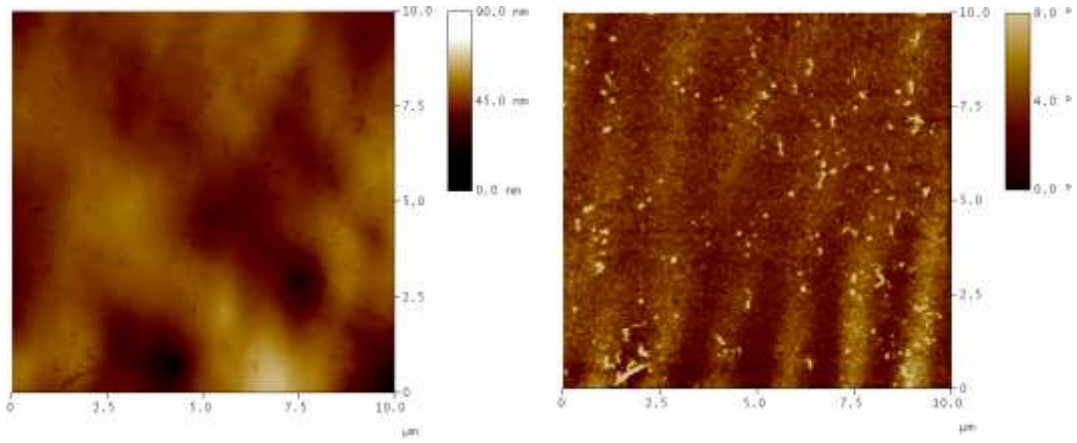

Figure 6.3: The film morphology of DF645 film coated at 155^{o}C revealed smaller and relatively hard agglomerates similar to those of the than as observed for films coated at 120^{o}C. The adheive matrix appeared to exhibit heterogenous mechanical characteristics. The scan size is 10 µm x 10 µm.

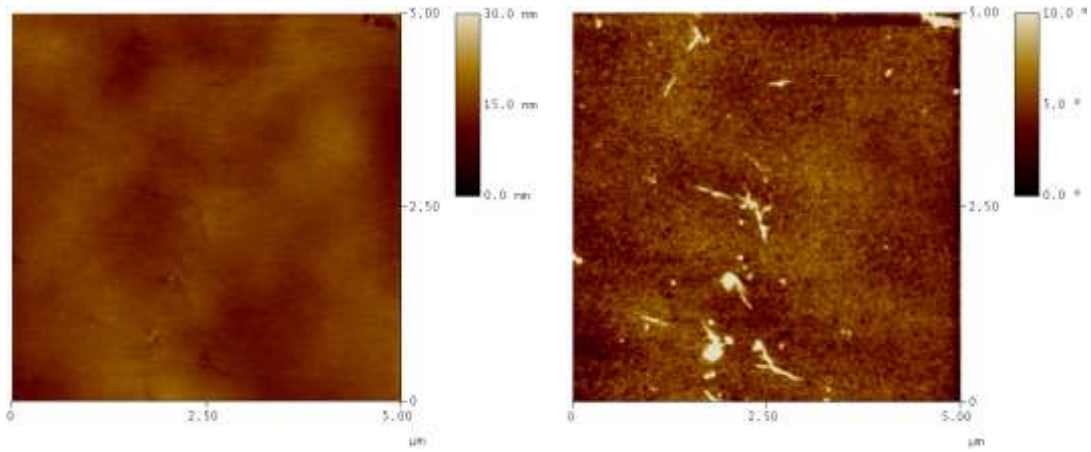

Figure 6.4: The film morphology of DF645 film coated at 155^{o}C at 5 µm x 5 µm scan size.

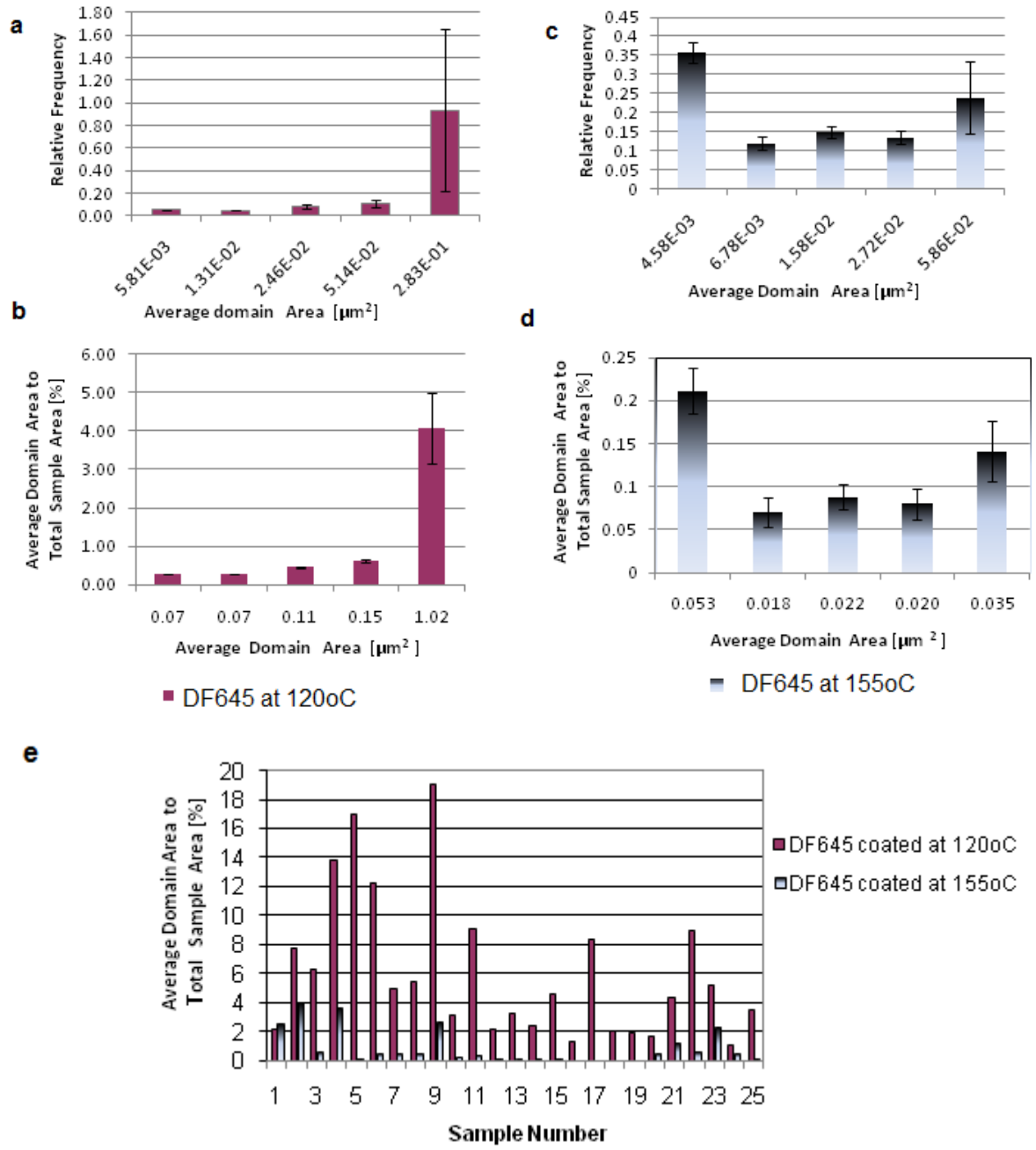

Figure 6.5: The microphase separated agglomerate size distribution in the DF645 coated films at 120°C (uniform colour) and 155°C (colour gradient), respectively. In (a) the number distribution of domains within the film coated at 120°C is presented, where in (b) the total corresponding domain area of each domain-area category to the total sample surface area is shown. In (c) the number distribution of domains within the film coated at 155°C is presented, and (d) the total corresponding domain area of each domain-area category to the total sample surface area is shown. In (e), the random area distribution of the micro domains in the different coated films is shown.

The multiple thermal transition peaks observed for each coated film in the thermal dynamic mechanical studies presented in Chapter 5 correlate well with the film morphologies. It was suggested (Chapter 5) that, residual resin-rich regions could be formed due to saturated miscibility with midblock copolymer elastomer phase[309,327], as the midblock resin content is highest in the DF645 formulation (56-wt %). Some of the agglomerates were also suggested to be copolymer partitioned aggregates, partly due to poor blend mixing of the relatively high viscous blend especially at the lower film coating temperatures. As a consequence, when quenched from the molten temperature to room temperature, the copolymers inevitably form some separated regions with the film matrix. The fact that the agglomerates exhibit harder mechanical nature than the continuous film phases further supports the explanation since PS are rigid at ambient temperature, as well as the pure tackifiers. Unfortunately it was not impossible to establish the chemical natures of the agglomerates with the standard TM-AFM utilized. It has been reported that relatively hard microphase regions can reduce the adhesion strength of adhesives by serving as stress accumulation or flaw regions within the films during a large strain debonding process[328].

Another interesting observation is the sinusoidal pattern seen in the phase images especially for the DF645 coated at 155^{o}C (Fig. 6.3). The pattern does not correlate with the topological height image and is therefore not caused by film surface roughness. The intermediate colour contrast of the stripes implies that the adhesive matrix exhibit local regions of intermediate mechanical characteristics than the relatively soft continuous larger film matrix. This could have been caused by different flow of some molecules at the film coating process.

6.3.1.2 7M8 adhesive coated films

The TM-AFM images at moderate tapping force of 7M8 coated film at 130^{o}C (Fig. 6.6) revealed relatively hard agglomerates with the coated film matrix, similar to the DF645 coated samples. The rubbery continuous matrix displayed local regions of different mechanical characteristics proved by the stripes in the phase image, just like the DF645 coated films. In Figure 6.7 two different tapping forces implemented for imaging the coated film surface demonstrated a discrepancy in the uppermost to subsurface film morphology. When a light tapping force, with r_{sp}= 0.98 was used (Fig. 6.7), a rather soft free film surface was observed as stated earlier. When the tapping force was increased to

r_{sp}=0.78 (Fig. 6.7b), a film subsurface morphology exhibiting the relatively hard agglomerate regions dispersed within the film matrix is seen.

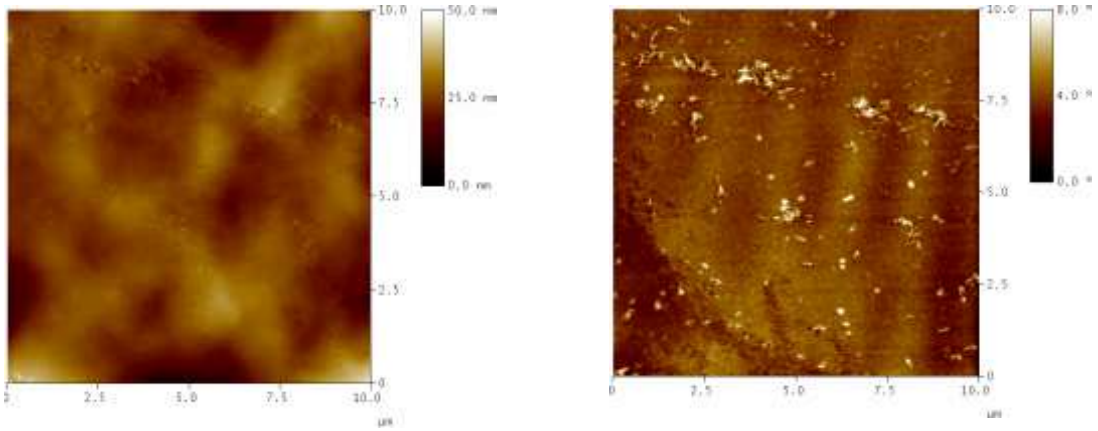

Figure 6.6: 7M8 adhesive blend coated at 130^{o}C exhibited a film morphology of relatively hard microphase separated agglomerates dispersed within the continuous adhesive matrix (bright domains in phase image, right). The stripes (phase image) insinuates that the matrix exhibited regions of different mechanical properties. Scan size is 10 x 10µm.

a

b

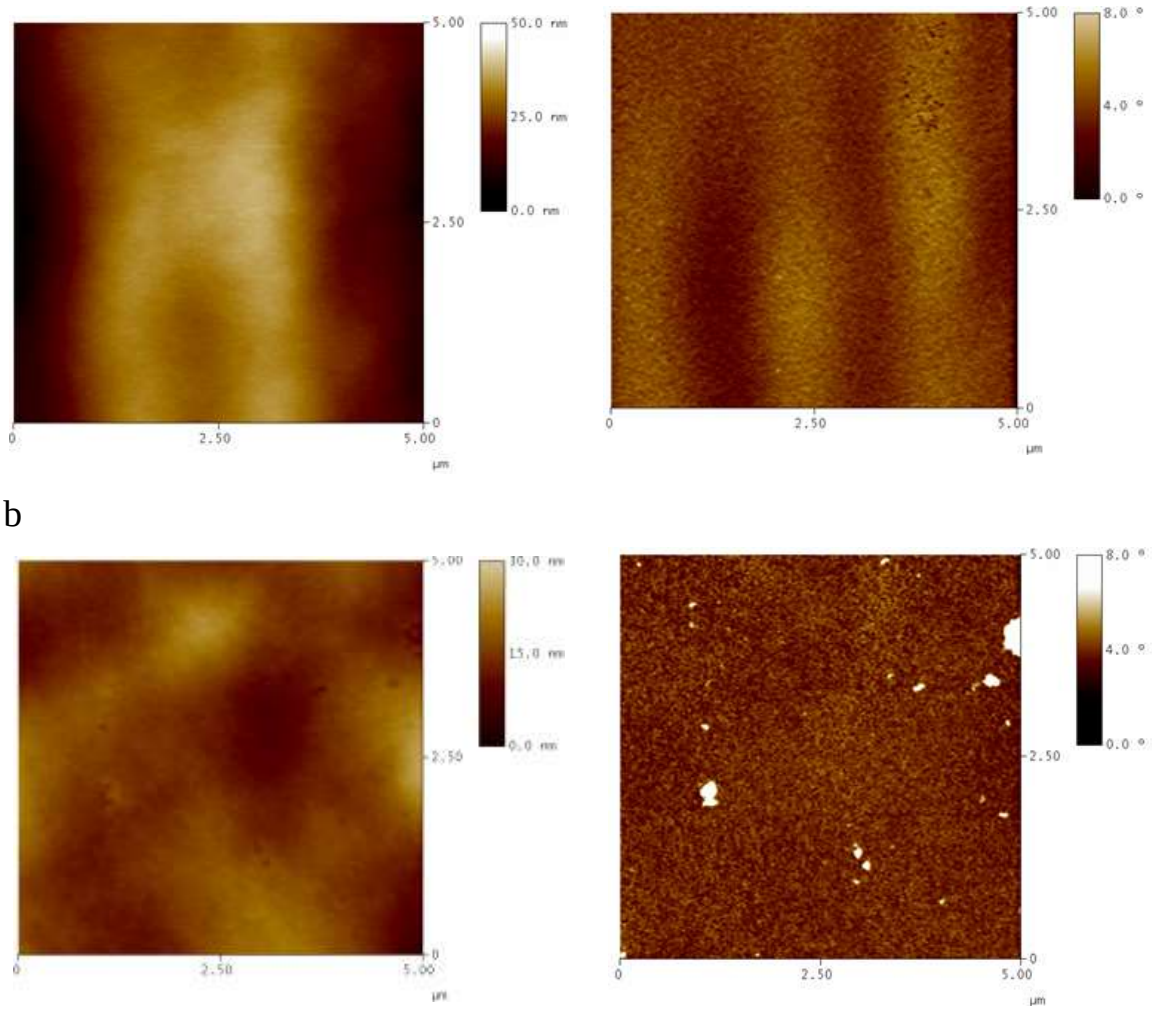

Figure 6.7: TM-AFM images of the same surface area of 7M8 coated at 130^{o}C. In (a) a light tapping force (r_{sp}= 0.98) revealed the uppermost film morphology of a continuous relatively soft phase (phase image, right). As the tapping force was increased (r_{sp}=0.78) in (b), a film sub-surface morphology comprising of relatively hard agglomerates dispersed within the film matrix is revealed. Scan sizes are 5 x 5 µm.

In Figures 6.8 and 6.9, the AFM images of 7M8 film coated at 165^{o}C revealed film morphologies (phase images, to the right) comprising of the relatively hard microphase separated agglomerates but yet much fewer than the observation made for the film coated at 130^{o}C (Fig. 6.6 and 6.7). The random distribution of the agglomerates was confirmed when some of the film surface areas imaged showed none of the separated aggregates (Fig. 6.9). For this adhesive system, adequate images could not be collected for agglomerate size distribution quantification due to the limited research time.

A significant difference observed between the 7M8 and the DF645 coated films was the scanning conditions necessary to reveal the sub-surface film morphologies. Higher r_{sp} values, closer to 1, were able to unveil the subsurface film morphology of the 7M8 samples but not the DF645 film series. This implies that the 7M8 samples could be stiffer and less tacky[278] which is not surprising given their highest PS content of the three different adhesive formulations. From a practical point of view any stiffening of the adhesive film surface would have impact on the adhesion performance because it would decrease the wetting of the adherend but yet impart stronger holding power due to the larger PS presence.

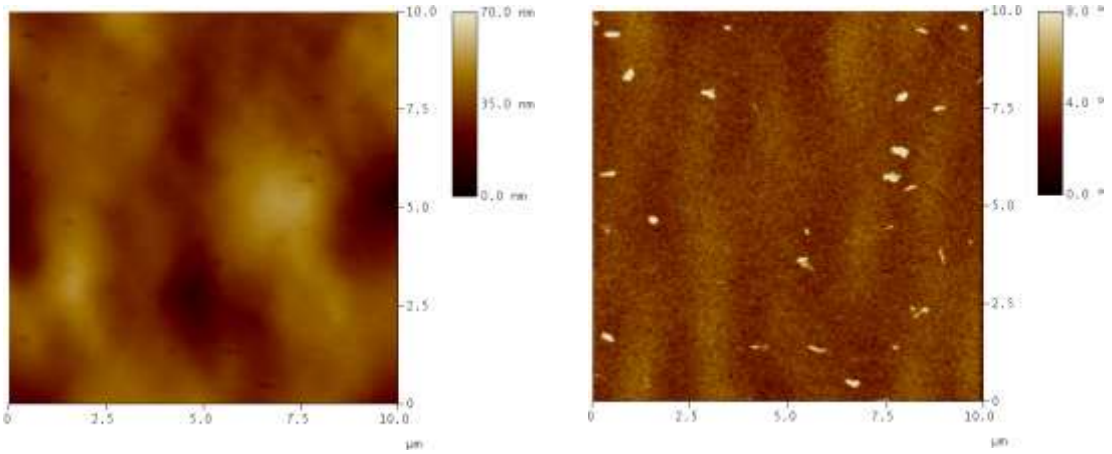

Figure 6.8: When coated at 165°C, the 7M8 film morphology comprised of fewer relatively hard agglomerates compared to films coated at 130°C. Moderate tapping with scan size 10 x 10 µm was used for the AFM imaging.

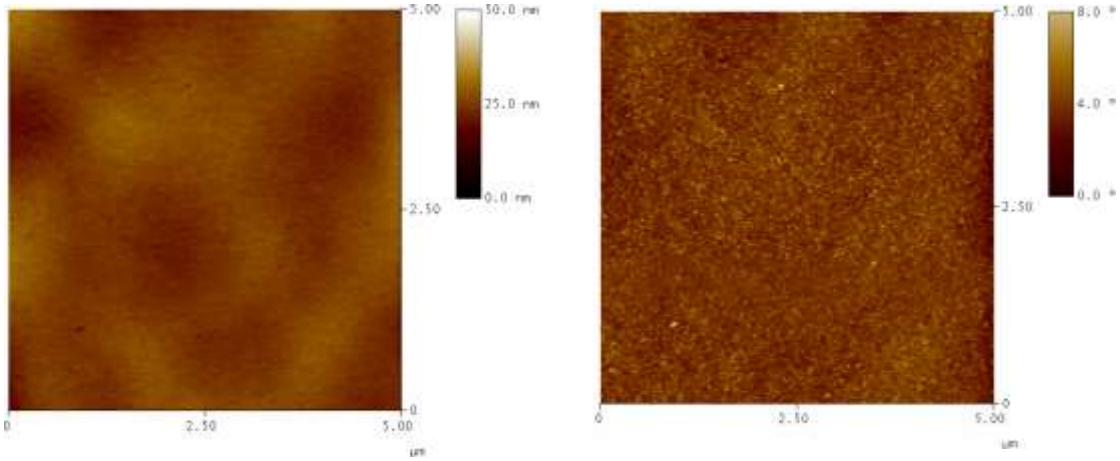

Figure 6.9: Some areas of the film surface of 7M8 coated film at 165°C had no agglomerates, as the phase image to the right indicates. The tapping was perfoemd on ffilm surface area of 5 x 5 µm.

6.3.1.3 DFC600 adhesive coated films

In Figures 6.10 and 6.11, the phase images of DFC600 films coated at 120^{o}C showed film morphologies with virtually non-existent phase separated micro agglomerates. A similar observation is made for the films coated at 155^{o}C, as shown in Figures 6.12 and 6.13, irrespective of the film area investigated. This is a significant discrepancy to the DF645 and 7M8 adhesive formulations. Moreover the continuous adhesive film matrices of the DFC600 film series appeared to exhibit more of the intermediate mechanical characteristics rather the relatively soft matrix phases of the DF600 and the 7M8 films. This property seems more pronounced in the phase images of the coated film at 155^{o}C (Figures 6.12 and 6.13). In an earlier study[309] highlighted in Chapter 5, it was suggested that the polydiene segments of triblock copolymers improved the compatibility of the rubbery segments with the tackifying resin, provided they formed the continuous phase with the polystyrene phase separated. The DFC600 adhesive blend has the highest polydiene content of the three different adhesive formulations. The compatibility improvement can be due to attractive van der Waals interaction between the electron-rich double bonds of the polydiene segments and the alicyclic groups of the resin as suggested in Chapter 5. The observation made here, is also further indication that some of the microphase separated agglomerates in the DF645 and 7M8 film blends are actually residual resin-rich regions due to the saturated miscibility with the elastomeric phase.

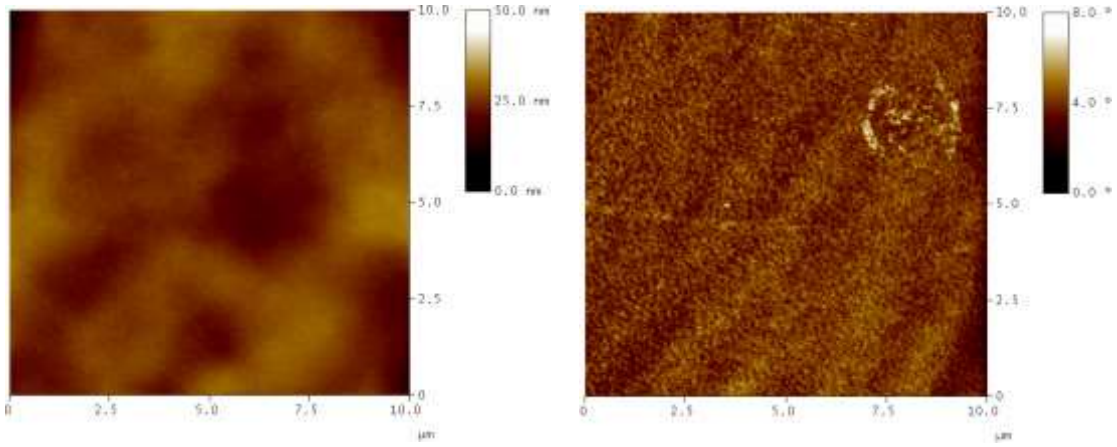

Figure 6.10: TM-AFM image of DFC600 coated at 120^{o}C virtually exhibit none of the microphase separated relatively hard aggolmerates as seen in the film samples of the DF645 and the 7M8 blend systems. Scan size is 10 x10 µm.

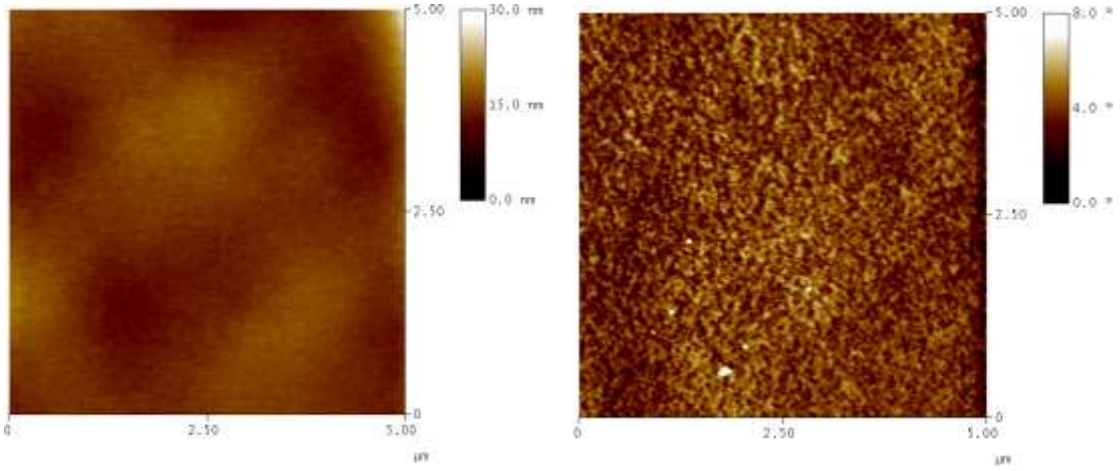

Figure 6.11: TM-AFM image of DFC600 coated at 120^{o}C revealed a continous film matrix consisiting of further phase separation on a higher scale. Scan size is 5 x 5 µm.

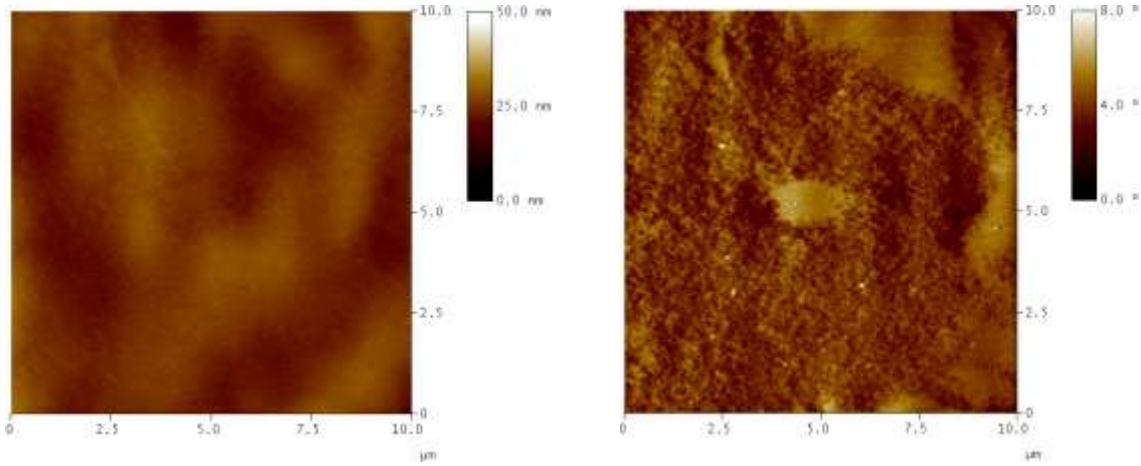

Figure 6.12: TM-AFM image of DFC600 coated at 155^{o}C showed an adheisve film matrix with no agglomerates just like the film coated at 120^{o}C. The film matrix exhibited continuous regions of less soft mechanical nature as suggested by the different colour contrasts. The scan size is 10 x 10 µm.

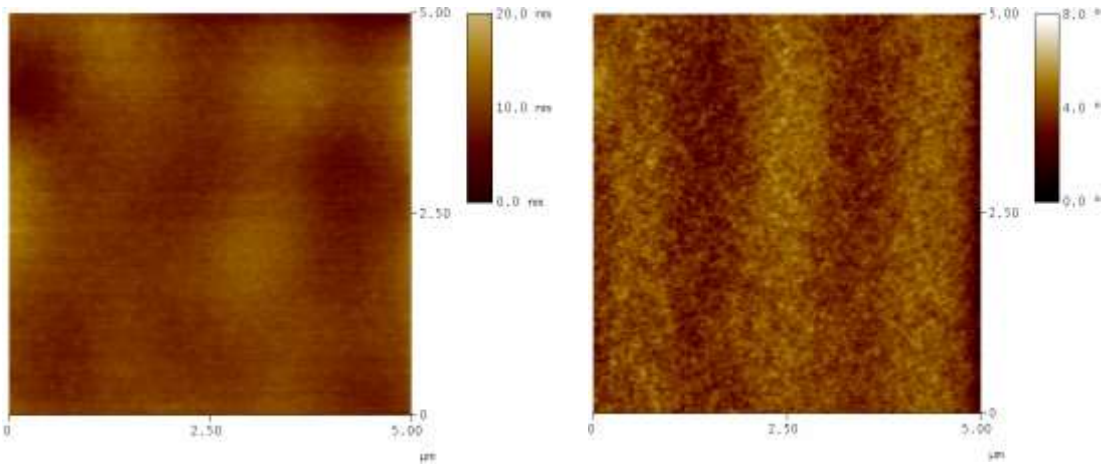

Figure 6.13: TM-AFM image of DFC600 coated at 155^{o}C a homogenous film matrix with continuous areas of slightly different mechanical charctistics. The scan size is 5 x 5 µm.

6.3.2 Effect of coating temperature on nanoscale film morphology

Unless relevant for the discussion the TM-AFM height images in this sections are omitted since the sample surfaces appeared very smooth on this scale and there was no difference in the height topographies of the different coated films. The image contrast on this scale was very sensitive to the tip-sample interaction between attractive and repulsive forces regimes (Chapter 3, AFM section). This will be highlighted in the explanation where need be.

6.3.2.1 DF645 adhesive films

The effect of the coating temperature on the nanoscale film morphologies of the DF645 blend samples are presented in Figure 6.14. With moderate tapping at r_{sp} = 0.78, the phase images revealed nano-sized mostly spherical domains of harder nature within the softer adhesive rubbery matrix. When coated at 120^{o}C (Fig. 6.14a), the domains were fewer, less uniform in geometry and more randomly distributed than when coated at 155^{o}C (Fig. 6.14b) where some local short range domain order could be observed. The domains are assigned to PS-rich-copolymers regions presumably functioning as physical crosslinks for the midblock elastomer chains within the continuous adhesive phase of

elastomer/resins/paraffin oil molecules. In chapter 5, the T_g peaks observed for the PS segmental relaxations do confirm this phase separation. The well-defined PS T_g peak observed for the film coated at 155^{o}C reflects the superior domain abundance, with a more homogenous nature, when compared to those formed if the film is coated at 120^{o}C.

A meticulous tapping approach was required to reveal the organised nanoscale structures as the specimen seemed to be very sensitive to changes in the tapping condition. Evidence of the sample sensitivity is presented in the AFM images of DF645 coated at 155^{o}C (Figure 6.15). When a light tapping force of r_{sp}= 0.90 was used, a well defined PS-rich-copolymer domains was seen and appeared to extend towards the free air film surface, suggested by the height images to the left (Fig. 6.15a). When the setpoint amplitude was decreased to r_{sp} = 0.69 (Fig. 6.15b), the organised surface features were distorted completely, soft film surface nature.

a b

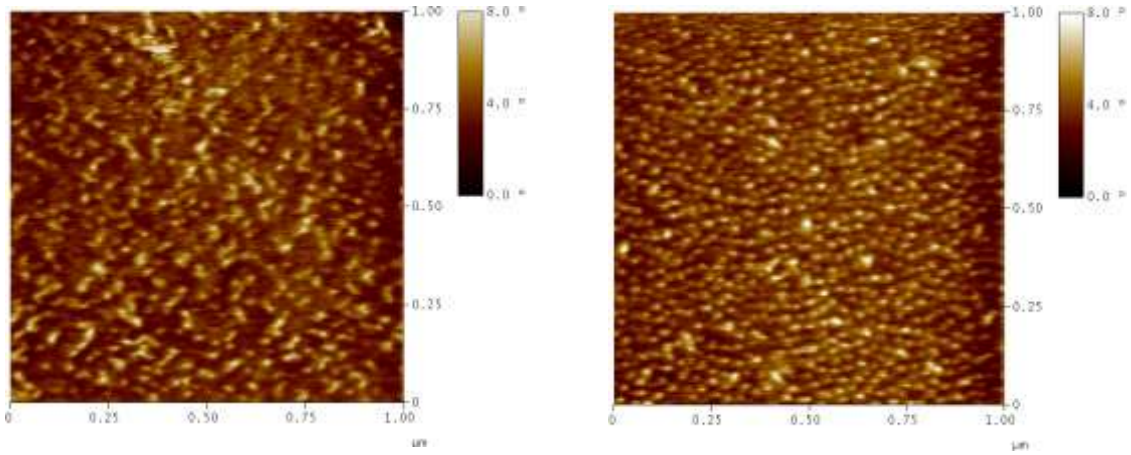

Figure 6.14: The phase images from the TM-AFM revealed rigid phase-separated PS-rich-copolymer domains dispersed within the DF645 adhesive film matrix. In (a) the morphology of the film coated at 120^{o}C and (b), the film morphology of the adhesive coated at 155^{o}C. The scan sizes are 1 x 1 µm.

a

b

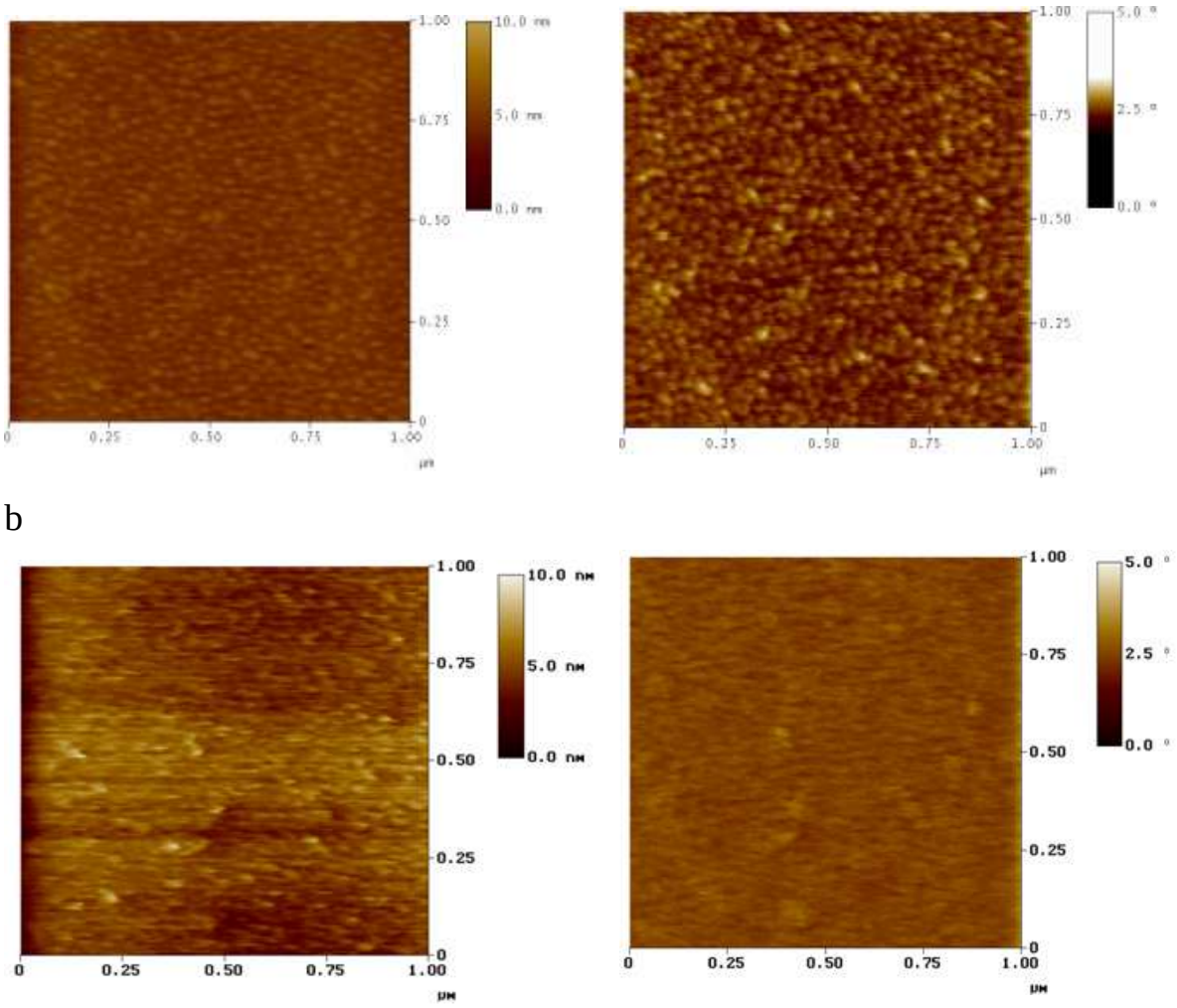

Figure 6.15: AFM images of DF645 coated at 155°C. When (a) light tapping force was applied, a film morphology of densely packed PS-rich-copolymer spheres (phase image to right) protruding from the film surface as shown in the height image (left) is revealed. When the tapping force was increased significantly in (b), the organised features were entirely distorted. Scan sizes are 1 x 1µm.

6.3.3 7M8 adhesive films

The AFM images collected at different tapping forces for a film coated at 130°C are presented in Figure 6.16. At light tapping (Fig. 6.16a) with r_{sp} = 0.96, a film surface morphology of phase-separated PS-rich-copolymer domains dispersed within the adhesive matrix is observed. The domains appeared to extend above the film matrix (height image), reflecting the fact that the matrix deformed more readily than the domains, similar to the

DF645 films. As the tapping force was increased (Fig. 6.16b), with $r_{sp} = 0.78$, the relatively soft matrix was pushed further down to enhance the boundaries of the rigid PS-rich-copolymer domains. This significant observation was not always consistent. The AFM image collected for 7M8 coated at 165^{o}C presented in Figure 6.17 suggests that the tip pushed through the uppermost soft matrix to reveal the subsurface PS-rich domains. The phenomenon is probably due to local differences in domain inter-connected network systems, which either promotes elasticity or imparts a region of a more viscous nature. A rubbery phase of dominant elastic nature will resist more to plastic deformation and therefore recover at a quicker time-scale after the tip-sample interaction is removed. The images generated will then reveal the domains existing further down than the continuous rubbery matrix. If the local rubbery matrix is of a more viscous nature, it is plausible that the slow recovery or permanent deformation of the rubbery layer after removal of tip-sample interaction will result in a phase image whereby the domains seemingly extend towards the film's free air surface.

a

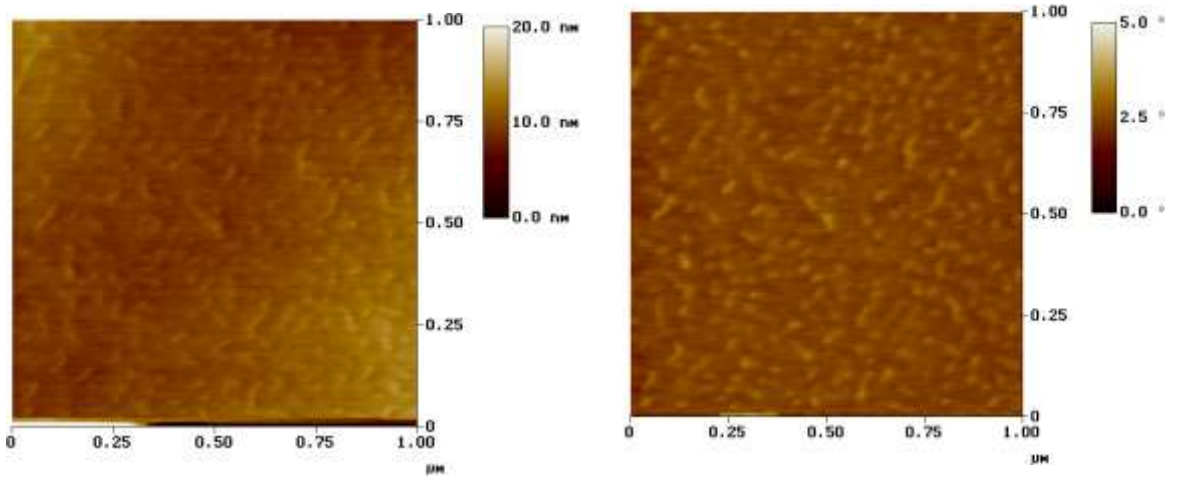

b

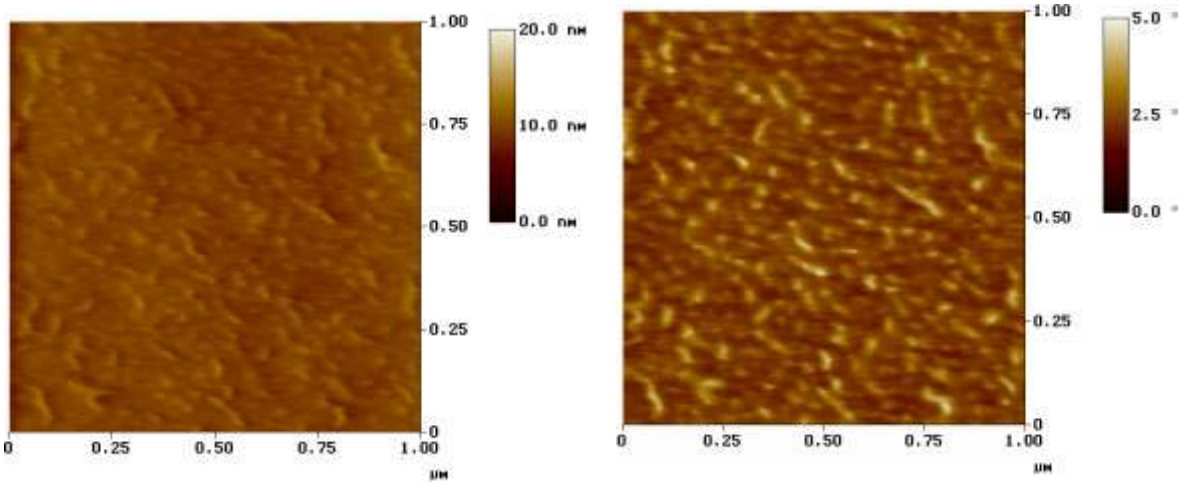

Figure 6.16: AFM images of 7M8 coated film at 130^{o}C revealed, (a) film surface morphology of phase separated PS-rich domains seemingly extending from film matrix. When the tapping force was increased further in (b), the rubbery phase is pushed further down to enhance the nano-domain boundaries. Scan sizes are 1 x 1 µm.

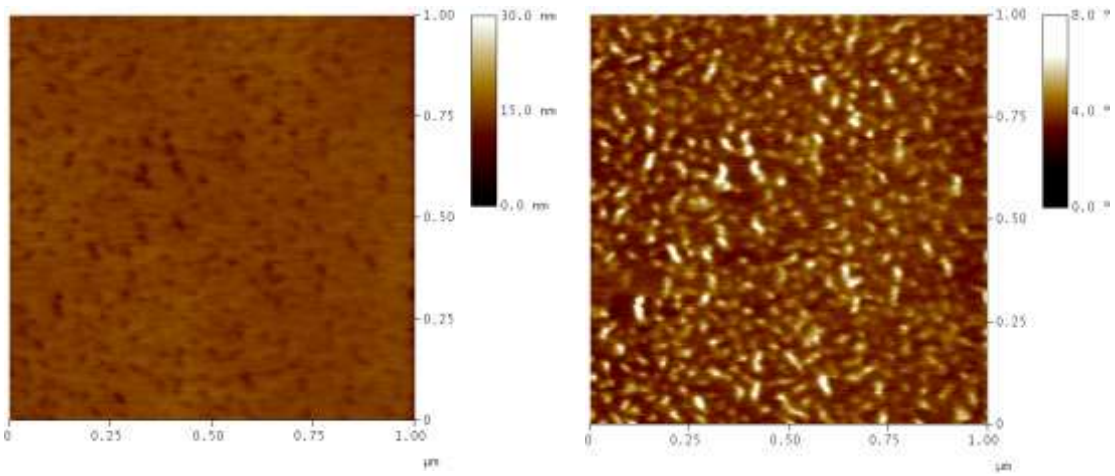

Figure 6.17**: The AFM images with moderate tapping for 7M8 coated at 165^{o}C show that the PS-rich-copolymer domains were pushed further down in the film matrix as indicated by the height image. The observation is presumably due to faster viscoelastic recovery of continuous rubbery phase. Scan size is 1 x 1 µm.**

Displayed in Figure 6.18 is the effect of the coating temperature on the nanoscale film morphology of the 7M8 adhesive films. In the phase image of the film coated at 130^{o}C (Fig. 6.18a), it can be seen that the relatively hard PS-rich-copolymer domains are much fewer than the domains formed when the film is coated at 165^{o}C (Fig.6.18b). The temperature effect is consistent with the DF645 blend but a dramatic difference is the domain sizes. The films seem to exhibit domains of both spherical- and small rod-shaped morphologies. This is expected given the highest styrene content used in the 7M8 blend formulation compared to the other two blend formulations. It has already been presented in Chapter 2 (Section 2.4) how block copolymers form different energetically favourable morphologies in a selective solvent, to minimise repulsive interactions with the continuous system[72-82,329]. The specific morphology formed depends on the incompatible polymer's content, among other factors. In an SIS triblock system Hamley et al[75] found that the incremental addition of polyisoprene (PI) homopolymer caused phase-separated PS phase to change from lamellar morphology at high local concentration, to rod-like and spherical domains at low concentrations. However their sample was a pure triblock system unlike the systems studied in this system which consists of resins and oil. This is an interesting observation, which implies that the presence of elastomer-compatible oil and resins in the adhesive do not influence the thermodynamic driving force for phase separation of the chemically incompatible rubbery and styrene segments.

a b

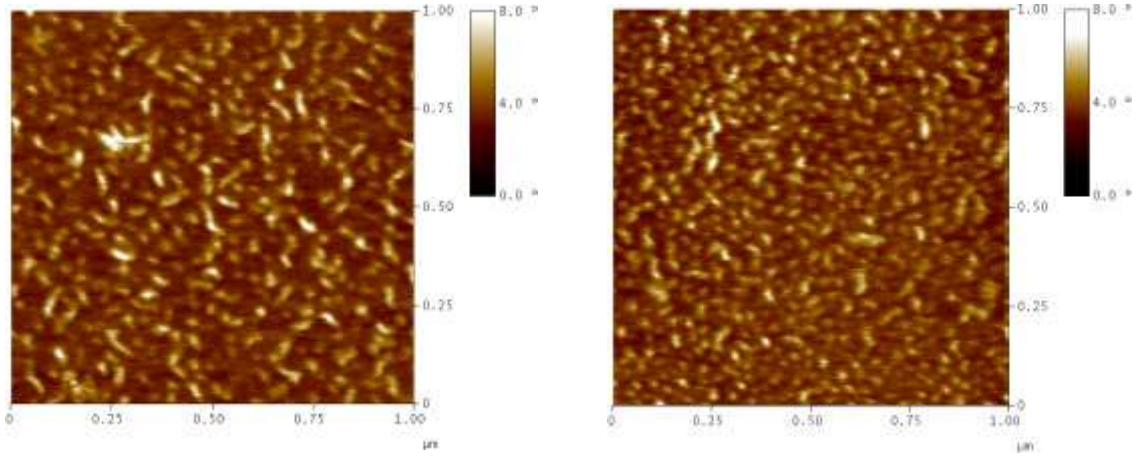

Figure 6.18: AFM phase images of 7M8 film coated at (a) 130^{o}C exhibited much fewer PS-rich-copolymer phase-separated domains, than observed in (b), for the film coated at 165^{o}C where higher domain presence is seen. Scan sizes are 1 x 1µm.

6.3.3.1 DFC600 adhesive films

The film morphology of DFC600 coated at 120^{o}C exhibited an uppermost surface of a relatively soft layer at light tapping (r_{sp} = 0.91), observed in Figure 6.19a. When the tapping force was increased to r_{sp} = 0.79 (Fig. 6.19b), the film morphology of phase-separated PS-rich-copolymer domains dispersed within the adhesive matrix is visualized. A similar observation was made for the film coated at 155^{o}C (Fig. 6.20a), where light tapping of r_{sp}= 0.96 revealed a uniform relatively soft rubbery surface. Increasing the tapping force to r_{sp}= 0.79 a film subsurface morphology (Fig. 6.20b) of densely populated phase-separated PS-rich-copolymer domains unfolded. Both the continuous adhesive matrices of low and high coated films comprised of areas of relative soft and intermediate mechanical characteristics, as the colour contrasts suggested.

The physical explanation of the matrix colour contrast characteristics could be related to the forces governing the tip-sample interaction[260-264] (Section 3.2.5.4). For a given tapping force level when the AFM tip begins to touch the virtually flat adhesive surface, it gives a deeper indentation on the soft rubber-rich layer than on the hard PS-rich-copolymer domains. With r_{sp} value close to 1, the tip-sample interaction was dominated by van der Waals attractive force (see AFM section, Chapter 3). Due to the rubber-like and adhesive nature of the sample surface, the attraction could cause longer contact time between tip and

sample, giving rise to larger amplitude damping of the oscillation[263] and making the uppermost matrix regions appear relatively bright. In some respect the contrast of the uppermost layer reflected the local adhesion strength, which do not seem to be as uniform for DFC600 coated at 120^{o}C (Fig. 6.19a), compared to DFC600 coated at 155^{o}C (Fig. 6.20a).

The effect of coating temperature on adhesive film morphology is presented in Figure 6.21. The PS-rich-copolymer domains were fewer and larger in the film coated at 120^{o}C (Fig. 6.21a) than in the film coated at 155^{o}C (Fig. 6.21b) where some short range ordering of the domains could be found. Though the coating temperature effect is not as profound on the DFC600 system compared to the DF645 and 7M8 blend systems, it nevertheless influenced the nano-domain self-assembly.

a

b

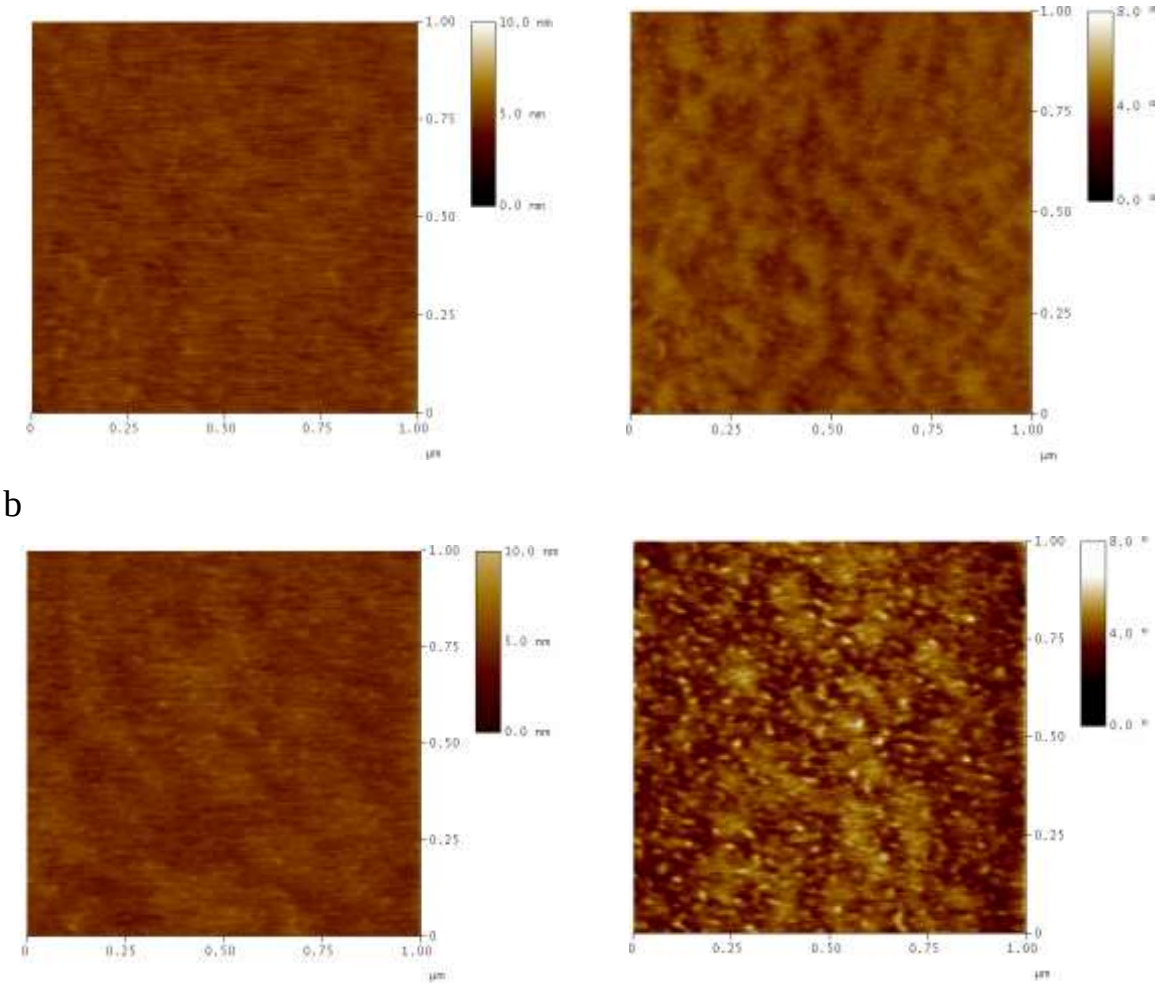

Figure 6.19: AFM images of the film morphology of DFC600 coated at 120^{o}C, (a) where light tapping revealed the near-surface film nature and (b) moderate tapping revealed the sub-surface film structure. The Scan sizes are 1 x 1µm.

a

b

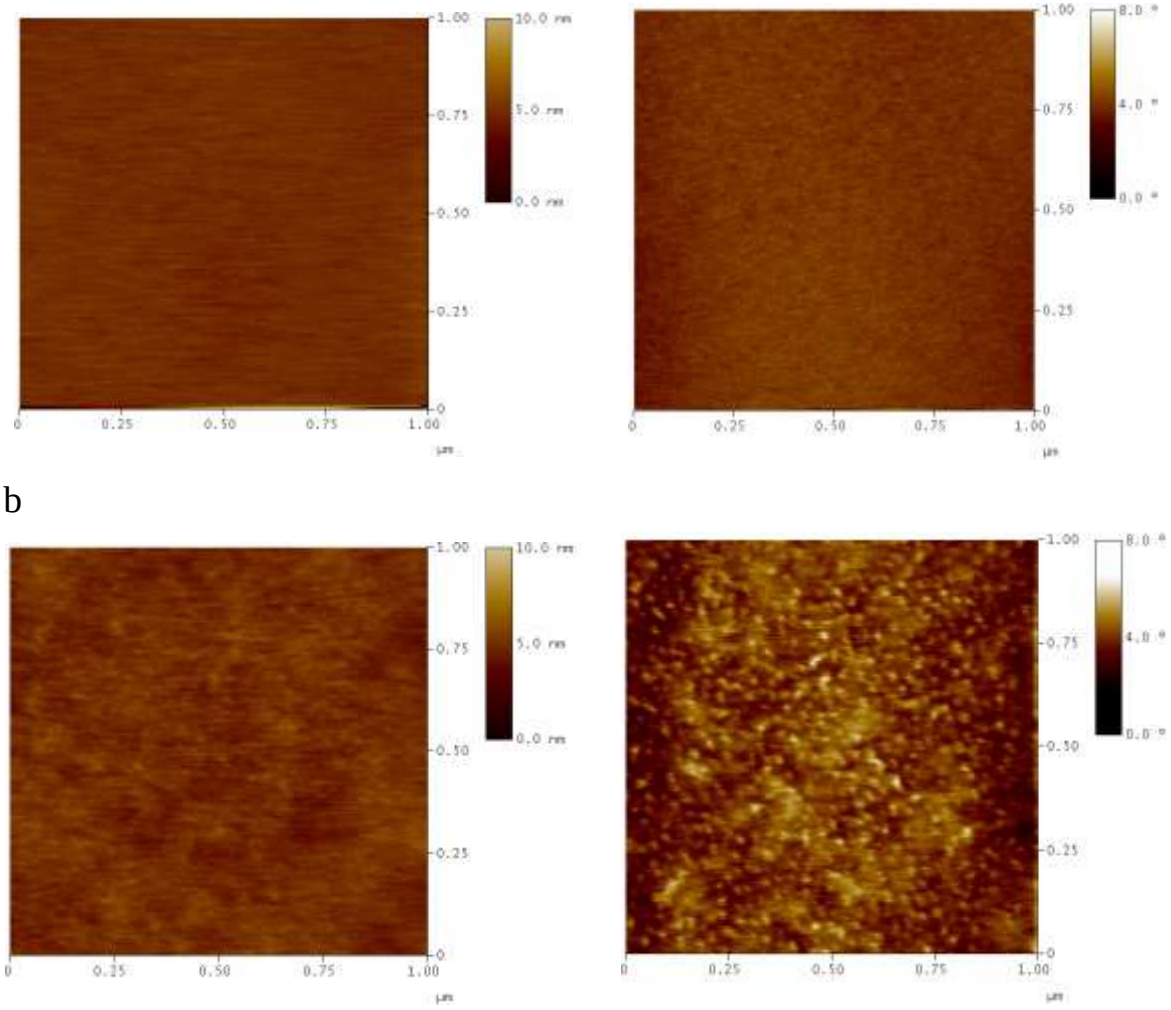

Figure 6.20: AFM images of the film morphology of DFC600 coated at 155^{o}C, (a) where light tapping revealed the near-surface film nature and (b) moderate tapping revealed the sub-surface film structure. The Scan sizes are 1 x 1µm.

a b

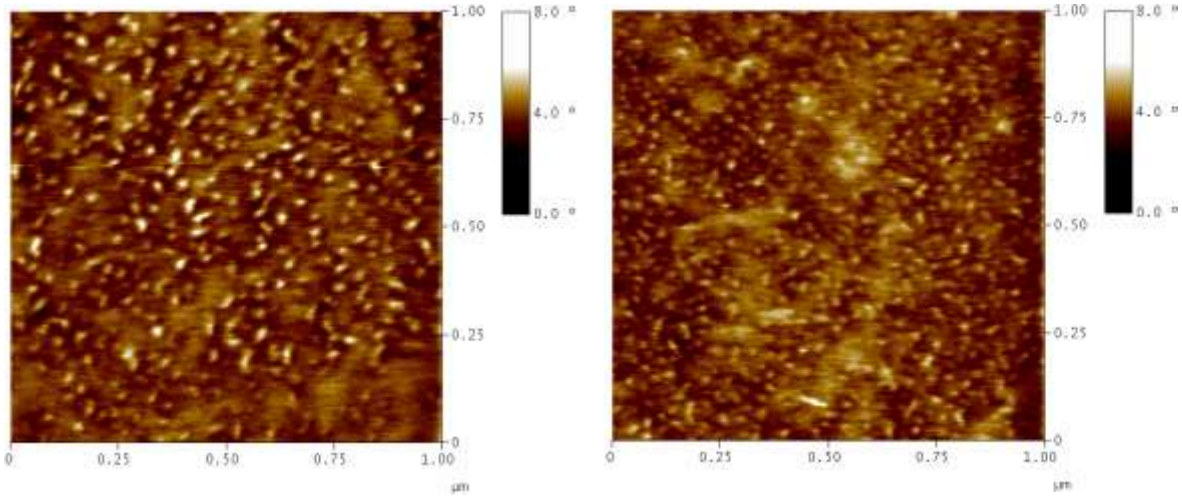

Figure 6.21: Phase images of DFC600 revealed the film morphologies of, (a) film coated at 120°C comprising larger and fewer PS-rich-copolymer domains than (b) the film coated at 155°C. The matrix areas (colour contrast between dark and bright) are implicit of intermediate mechanical characteristics. The scan sizes are 1 x 1µm.

6.3.4 Discussion of film morphologies and the impact on adhesive properties

The information obtained with the TM-AFM indicates that the discrepancies in the adhesive film morphologies are strongly connected to the film thermal history. It has already been explained how the microphase separated agglomerates could be tackifier-rich domains formed by surplus midblock resin due to saturated miscibility with copolymer elastomeric phase. Some agglomerates could also be copolymer-rich partitioned regions caused partly by poor blending of the relatively high viscous adhesive at the lower coating temperatures. The fewer agglomerates observed in the films coated at higher temperatures support the explanation, as well as its diminished presence within the films of the DFC600 blend system which has the highest polydiene content.

On the nanoscale the films coated at higher temperatures consisted of much more PS-rich-copolymer phase-separated domains with some sporadic presence of local short-range order within the adhesive matrices than the films coated at low temperatures, irrespective of the blend system. The difference in the film morphologies demonstrated by the AFM

phase images seemed to have taken place at the different coating temperatures and frozen in place due to the rapid cooling from molten state to room temperature. As explained in Chapter 2, the driving force behind the nanophase domain assembling is a thermodynamically collective and complex range of entropic and enthalpic interactions between the different sub-components of the blends. The existence of the rigid PS-rich-copolymer domains is due to repulsive interactions between the chemically incompatible PS endblocks of SEBS, SBS and SIS, and the midblock elastomers (PI, PB and PEB) swollen by resin oligomers and paraffin oil within the continuous adhesive phases. These interactions depend on the magnitude of the thermodynamic incompatibility factor, χN, and the volume-fraction composition of the copolymers[72-82] (Section 2.4). The χ between any two binary interactions of the different components in the blends is temperature dependent and a controlling factor in these studies, for the PS-rich-copolymer phase separation. The χ_{AB} for any binary interaction can be evaluated from the Hildebrand solubility parameter (δ)[56-58] (also given in Section 2.4) according to,

$$\chi_{AB} = \frac{(\delta_A - \delta_B)^2}{K_B T} \qquad 6.1$$

Where K_B and T are the Boltzman constant and absolute temperature, respectively. For instance segregation will occur more readily between styrene and isoprene with increasing $\chi_{styrene/isoprene.,}$ as δ_{PS} = 9.10 $(cal/cm^3)^{1/2}$ and δ_{PI} = 7.9 $(cal/cm^3)^{1/2}$ at 25^oC[64]. Polystyrene-rich domain self-assembling is therefore affected by the coating thermal history, which directly influences the domain network and the rubber-like adhesive behaviour of the coated films.

The quantification of the domain diameters, spacings (smallest distance between centres of adjacent domains) and their amount per 1 x 1 μm^2 film area are presented in Table 6.1. The characterisation was performed on the 2D phase images collected with the TM-AFM. Quantification errors would possibly come from the fact that (1) the fracture trajectory in the phase images does not produce a cross-fracture across the equators of domains, and (2) as a two-dimensional projection of a three-dimensional nano structure, the nearest neighbours of any given domain in the images do not necessarily lie in the same plane in three dimensions, thereby precluding accurate assessment of inter-domain spacing. Small-angle X-ray scattering (SAXS) experiment would have provided more accurate spacing and domain radius measurements. However characterising these samples with the technique simply failed due to a lack of any domain long-range order that is required and

found for instance in pure triblock systems[98]. Nevertheless the results correlate well with reported domain diameters and spacing[113,330], of other styrene based thermoplastic elastomer gel (TPEG) systems. Since the domains in the phase images are well resolved, their amounts per 1x1 μm film surface areas were accurately quantified. Hoffman et al[99]., have reported a PS micellar domain diameter of ~ 13.2 nm and inter-domain spacing of ~ 36 nm in an SEBS(Kraton G 1650) gel system with up to 10 wt-% copolymer content. In the adhesive systems it is plausible that the domains comprise of some oil, resins and elastomer molecules. The average M_n of the linear triblocks used in the blend systems is ~ 110,000 g/mol with PS ~ 33 wt-% (Table 3.1). The weight of a PS monomer is 104 g/mol and this gives an average number of PS monomers, N, per chain = 349 in the adhesive systems. Assuming theta condition (i.e. the condition in a mixture where the polymer chains are just compatible with the solvent and expand to reduce unfavourable segment-segment interactions), the rms end–to-end distance of the polymer coil with N monomers is given by[331]:

$$\langle R^2 \rangle^{1/2} = R_o = N^{1/2} C_\infty^{1/2} l \qquad 6.2$$

Where C_∞ which is the expansion factor, is 9.85 at T ~ 300 K in various solvents for polystyrene[64] and l is the length of the C-C single bond which is ~1.54 Å. The relationship gives a PS coil radius of ~ 9 nm. If the hard nano-domains within the adhesive films were purely PS micelles, their sizes should even be smaller than the calculated value as the paraffin oil is a poor solvent for PS. The observed nano-domain sizes are larger value (Table. 6.1) within experimental uncertainty. Therefore the terminology by addressing them as PS-rich-copolymer domains rather than PS micelles gives a better reflection of reality. This further suggests that the nature of the domain cores move towards PS homogeneity with the coating temperature, due to their decrease in sizes (Table 6.1) and the conspicuous PS T_g transition peaks (Chapter 5). It is not excluded though that the interfacial region, i.e. intermixed domain corona could have become larger.

At the relatively low coating temperatures, close to the T_g of PS, the long range mobility of the PS segments is restrained despite the oil molecules increasing the free volume and the highly mobile elastomers all serving to facilitate the PS movement. The reason is mainly due to the relatively stronger segregation power (Equation 6.1) and the limited thermal force. The morphology formed when the molten film was frozen into place preserved the size, shape and distribution of the domains at the melt state. The larger domain sizes (Table

6.1), together with the weak PS T_g peaks (Chapter 5) reflect a more intermixed domain core nature frozen into place. The domains can then potentially be weaker in their ability to distribute stresses when the film sample is subjected to external forces due to the higher presence of other components (paraffin oil/tackifiers/elastomer) within the domain cores[103,105,154]. It is not excluded that the larger sizes could as well be caused by a higher number of PS chain segments within the assembled domains, especially in the case of the 7M8 blend system where a higher PS content[166] was used.

The question then arises as to the kind of elastomer structural arrangement that should take place in these systems coated at different temperatures. One of the properties that make a styrene based triblock copolymers favourable in a hot-melt PSA formulation is the copolymers ability to maintain its network structure even at temperatures above the T_g of the polystyrene[97-99]. The larger inter-domain spacings (Table 6.1) also observed for the films coated at low temperatures suggest that some PS-rich-copolymer domains are effectively isolated and with lack of inter-connected network by the elastomer segments. This is due to the relatively large entropic penalty that will arise from extensive stretching of the elastomers[94] causing a reduction in their conformational entropy. With a higher fraction of possible elastomer loop/hairpin chain conformations (Section 2.4.1) and some dangling chain ends, the stress transfer during a debonding process would majorly be made through friction of the local surrounding chains[313]. Such a stress transfer mechanism is inefficient compared to that controlled by elastomers, bridging the PS-rich-copolymer domains. It therefore appears that the reduction in the population of PS-rich-copolymer domains with decreasing coating temperature is responsible for the formation of midblock elastomer networks that are less effective at transmitting stresses within the coated films. The above elucidation would be true for the DF645 and 7M8 blend systems.

The situation with the DFC600 blend system is envisaged to be slightly different. Though the inter-domain spacing is also relatively large for the DFC600 coated at 120^{o}C, there still seems to be a better network system within the film compared to the low-temperature coated films of the DF645 and the 7M8 blends. This is because of the higher polydiene content is the DFC600 formulation. It has already been mentioned how the polydienes improve the dilution of the resins in the elastomeric entanglement network, as reported in some studies[123,187,309]. Since the double bond segmental units are restricted of freedom of rotation around the σ-bonds, substantial entropic penalty could arise if the polydiene elastomer chains underwent further loop/hairpin conformations by back-folding[94]. It is

believed that the system would rather choose to form dangling chain ends with PS ends blocks extending into the rubbery matrix to gain some extra translational entropy. Hence interconnected network system could be formed by such adjacent dangling chain ends if their concentration becomes high enough. Such PS block connections are perhaps too small to be resolved by the AFM phase images. The contribution of the polydienes to the film adhesive property could be;

1. An increase of the tack characteristics due to the high presence of resins within the elastomeric phase
2. An improved dissipation of strain energy during a debonding process via extra inter-connected network through adjacent polydiene-induced PS-rich chain ends.

Therefore the dependency of the film's property with the formation of the PS-rich-copolymer physical crosslinks under the influence of the film coating temperature is not as significant for the DFC600 system. The peel force for DFC600 coated at 120^{o}C is 3 times higher than that of DF645 and 7M8 low temperature coated films (Table 5.5). The film matrices of the DFC600 samples (Fig. 6.21) exhibit more of intermediate mechanical characteristics which could be a reflection of the enhanced tacky nature.

Table 6.1: Estimation of PS-rich-copolymer domain population, diameter and inter-domain distance of the adhesive films coated at different temperatures.

Adhesive film sample	Average domain diameter [nm]	Average domain population/ μm^2	Average inter-domain spacing [nm]
DF645 coated at 120°C.	32 ± 5	287 ± 77	45 ± 12
DF645 coated at 155°C.	24 ± 5	521 ± 39	32 ± 6
7M8 coated at 130°C.	35 ± 12	245 ± 46	50 ± 15
7M8 coated at 165°C.	26 ± 6	482 ± 29	33 ± 8
DFC600 coated at 120°C.	27 ± 6	310 ± 14	40 ± 11
DFC600 coated at 155°C.	22 ± 5	432 ± 32	33 ± 9

At the high film coating temperatures, i.e. DF645 and DFC600 coated at 155°C, respectively, and 7M8 coated at 165°C, the lower viscosity of the molten blends due to increase in the molecular kinetic energy make the systems evolve towards a more thermodynamic equilibrium-like film state. In Chapter 5 a literature report[162] was highlighted where flow in incompatible triblock copolymer systems was stated to be caused by PS blocks moving from domains and re-associating with other domains and thereby maintaining the dynamic equilibrium-state network (Section 5.3.3.1). This condition could generate more of elastomer bridges than the loop/hairpin conformations especially as the average domain spacing has decreased (Table 6.1). In binary blends based on PS-PI block copolymers, the segregation power between the PS and PI chains was

found to decrease with increasing temperature[86-89], as indicated by Equation 6.1. This condition would also promote the PS chains confined within copolymer agglomerates to be pulled out more easily into the elastomer rich matrix and undergo additional PS-rich regions. Upon quenching, the altered morphology would be frozen in-place and thereby distinguish the high-temperature-coated from the low-temperature-coated film morphologies (Table 6.1). Energetically it seems that the elastomer conformation that will dominate within the system is perhaps the stretching entropic penalty associated with the chain bridging topology. Though the enthalpic interactions between the domains would increase due to their higher presence which would lead to more unfavourable contacts, the environment would still favour the elastomer chain bridges and loop-induced entanglements connecting the nano-domains. This is because of the smaller average domain spacings (Table 6.1), allowing bridging and entanglements of neighbouring chain loops without any substantial chain stretching. The interfacial area of the nano-domains enriched in elastomer/oil/resin due to the incompatibility, would become larger[332] as the domains are closer, which is a good property in terms of energy dissipation during a debonding process. Furthermore the interface (corona) could serve in repelling the nano-domains from each other through limited interpenetration of the surrounding elastomer chains. The phenomenon, known as steric stabilization is found to occur in incompatible block copolymer systems and generates an effective stabilization of the phase separated domains[87].

With the elastomer chain bridging and loop-induced entanglement interactions, the interconnected network structure would be over a larger volume and generate an efficient dissipation of stresses over a wider region from one domain junction to the other[113,313,333]. This will have a tremendous impact on the elasticity of the coated films. This property will be investigated in Chapter 7. The DFC600 coated at 155^{o}C could exhibit substantial additional interconnections via the polydiene-induced PS chain ends and probably explains the smallest domain sizes (Fig. 6.21, Table 6.1) as more PS form the chains ends due to the higher mobility at the film molten state. For

An estimation of the distribution of the domains per 1 μm^2 film surface area was made to gain an insight into the volume and surface area occupied by the rigid regions. The assumption is based on a cross-section film surface and takes into account the nano-domain sphere surface directly in contact with the rubbery matrix. With the volume of a hemisphere, $2/3\pi r^3$, and the curved surface area of a hemisphere, $2\pi r^2$, where r is the radius of the sphere, an estimate was made and is given in Table 6.2. The thickness of the

monolayer thin film is approximated to the average domain diameter of each sample. For the calculation of the PS volume fraction in the blend formulations, the density of polystyrene, 1.04 g/cm[64] was used. The wt-% PS of the copolymers is 6%. This gives a PS volume percent of 5.8 vol%. The estimated volume percentages (vol-%) of the PS-rich-copolymer spheres of all the coated films (Table 6.2) are higher than the total PS vol-% in the formulations. This increase of the volume is taken as the presence of other components dispersed within the PS-rich nano-domains[105]. Interestingly the values are larger for the films coated at lower temperatures which validate the earlier suggestion made in reference to the higher presence of elastomers/resins/oil imbibed within the nano-domains of the low temperature coated films. The possibility that fewer PS chains exist within the nano-domains of the high-temperature coated films is valid since the domains have increased in amount (Table 6.1).

The domains also occupy a large surface area in all of the coated films. The large surface area contact to the rubbery matrix is envisaged to maximise their reinforcement as physical crosslinks. For the films of the DF645 and 7M8 coated at high temperatures, the domain surface areas are slightly higher than that of the films coated at low temperatures, respectively. In reverse, their surface areas within the DFC600 coated at high temperature is slightly smaller compared to that coated at low temperature. This again would confirm the DFC600 system's less-sensitivity to the film coating temperature in regards to adhesion performance. The domain surface areas were actually expected to be much larger for films coated at higher temperatures as smaller particles exhibit larger effective surface. The unexpected values (Table 6.2) could arise from two fundamental factors. There could be a competition between maximising the reinforcement of the physical crosslinks in terms of their number and surface contact to the soft matrix, as well as maximising the adhesion in terms of large volume ratio of the continuous rubbery multi-component phase. The adhesive reaches an optimised balance easily when coated at a high temperature.

Table 6.2: Estimation of PS-rich-copolymer domain volume fraction and surface area per 1µm x 1µm film surface area, in relation to film coating temperature.

Adhesive film sample	Volume fraction of PS-*r*-Co[a] domains (%)	Surface area of PS-*r*-Co[a] domains (%)
DF645 coated at 120°C	8.4	47.0
DF645 coated at 155°C	6.4	48.0
7M8 coated at 130°C	9.3	47.7
7M8 coated at 165°C	7.2	50.4
DFC600 coated at 120°C	5.1	34.7
DFC600 coated at 155°C	4.1	33.4

[a] PS-rich-copolymer

6.3.5 Effect of annealing on film morphology

6.3.5.1 Micro scale film morphology

The effect of an annealing period of four weeks at a temperature of 40°C on the morphologies of adhesive films initially coated at low temperatures is presented in this section. During the annealing period, it is assumed that self-diffusion of some triblock copolymer segments[334,335] with specific chain lengths, mobility of oil molecules, tackifying resins and other related relaxations[336], contribute to the improved adhesive film morphology. These processes seem to be very dependent on the annealing condition (temperature, time).

The microscale phase images of the annealed DF645 coated at 120°C and 7M8 coated at 130°C are presented in Figures 6.22a and 6.23a, respectively. The relatively harder agglomerates appear to disperse within the film matrix with the surrounding region exhibiting more of an intermediate mechanical characteristic and perhaps more tacky. Jeusette et al[327], reported in their work on an acrylate copolymer-based PSA with rosin-ester resins that a long annealing time caused kinetically trapped resin agglomerates within the adhesive matrix due to the rapid quenching process, to diffuse to the film's uppermost surface. These could partly have happened during the aging period, resulting in an improved miscibility of the resins and polymer elastomer chains at the near film surfaces. Such a process could be governed by the surface energy differences of the different components within the multi-blend systems[337].

a **b**

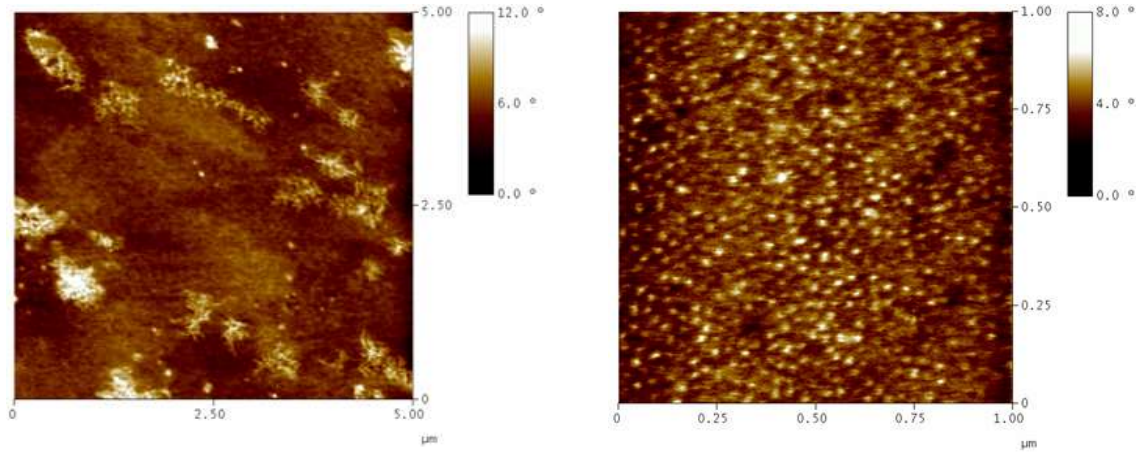

Figure 6.22: AFM phase images performed at moderate tapping revealed film surface morphologies of annealed D645 coated at 120^{o}C at (a) microscale with scan size 5 x 5 µm, and (b) nanoscale with scan size 1 x 1 µm.

a b

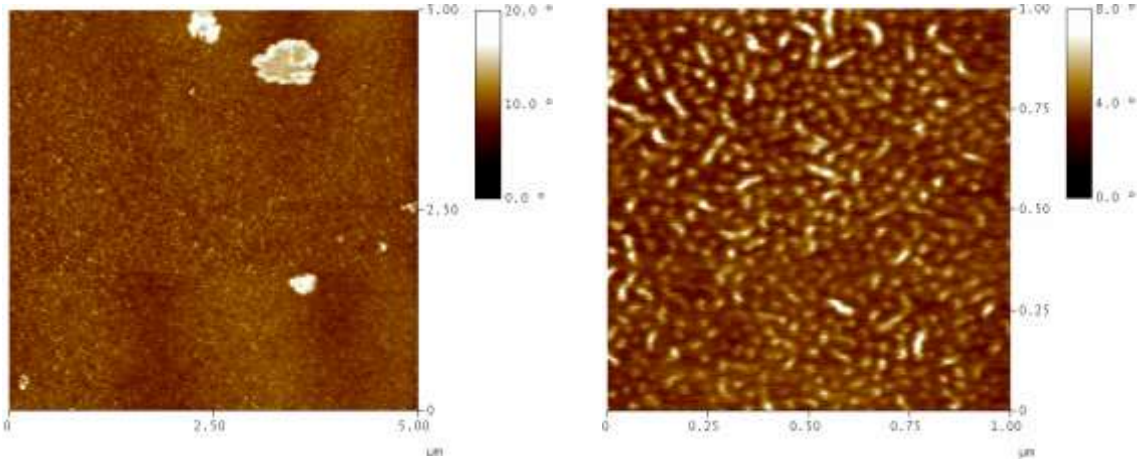

Figure 6.23: AFM phase images performed at moderate tapping revealed film surface morphologies of annealed 7M8 coated at 130^{o}C at (a) microscale with scan size 5 x 5 µm, and (b) nanoscale with scan size 1 x 1 µm.

6.3.5.2 Nano scale film morphology

The nano scale film morphologies of DF645 initially coated at 120^{o}C and 7M8 at 130^{o}C, respectively, are presented in Figure 6.22b and 6.23b. In the phase image of the DF645 film, densely populated PS-rich-copolymer domains dispersed within the continuous rubbery adhesive matrix is observed. For the 7M8 film, both spherical- and small rod-like domains are revealed as expected, due to the higher PS content in the formulation. The

improved film morphologies are reminiscent of those initially coated at high temperatures. The PS-rich domain amount per 1x1 μm^2 film surface area, domain diameters and inter-domain spacing characterisations are presented in Table 6.3. During the annealing, it appears that kinetically constrained molecular states initially locked by the rapid cooling, are released and allowed to re-organize into the preferred thermodynamic feasible morphological structures seen. The domains have almost doubled in amount when compared to the equivalent unannealed film samples (Table 6.3). It is also noted that the average diameter of the nano-domains have become smaller but yet larger than for films coated at high temperatures, insinuating different self-assembling stages.

The organisation of PS-rich-copolymer self-assembly by thermally-induced diffusion mechanism[334,338] is a slow process and could not occur during the annealing period. The diffusion, D, of a spherical particle is generally obtained by the Stokes-Einstein equation according to[87],

$$D = \frac{k_B T}{6\pi\eta R} \qquad 6.3$$

Where $k_B T$ is an estimate of the translational energy per particle, k_B is the Boltzmann constant, R is the gas constant, T the absolute temperature, and η the viscosity of the fluid. The D, for a polymer particle[87,] can be as low as ~ 10^{-18} m^2s^{-1}. In a work by Helfand et al[336], they suggested that for a polymer A chain to diffuse from a polymer B domain, it will require an activation free energy F^* of,

$$F^* = \chi N_s + \frac{3}{2}\frac{1}{N_s}\frac{d_B^2}{b^2} \qquad 6.4$$

Where χ is the Flory-Huggins interaction parameter, N_s is the degree of polymerisation of the diffusing chain (polymer A), *b*, is the statistical length of a monomer in the pure polymer, and d_B is the distance of travel. The first term was described to be the energy of polymer A chain in polymer B domain, and the second term is the stretching free energy of the polymer A units. Based on the slow mobility of the block copolymers, the re-distribution of the resins and oil molecule diffusion are speculated to majorly contribute to the dispersion of the large agglomerates which seemingly result in the organisation of more PS-rich-copolymer nano-domains during the annealing period. The diffusion process of the oil which would affect the inter-domain spacing and a more uniform domain nature due to oil expulsion could be facilitated by concentration gradient. Fouchet et al[339] have reported that the diffusion process of mineral oil in styrene-butadiene polymer films follows Fick's

third law in the temperature range between 20°C and 111°C. Fickian behaviour obeys the relationship[339],

$$\frac{M_t}{M_{sat}} = \frac{kt^{[1/2]}}{z} \quad 6.5$$

And

$$k = \frac{4}{z\pi}\sqrt{D} \quad 6.6$$

Where M_t is the amount of solvent absorbed by the polymer at time *t*, M_{sat} is the equilibrium sorption-desorption amount at infinite time, z is the polymer section thickness, and D is the diffusion coefficient which is reported to be $1.51*10^{-13}$ (m^2/s) at ~42°C. They further reported that a polymer with an open structure (low crosslinking density) and high chain mobility (low T_g) has faster mineral oil absorption-desorption rate. The polymer polarity influence was attributed to the increase in the solubility parameter difference between the polymer and the mineral oil[340] (Chapter 2.3.3).

Hotta et al[333] studied the stress relaxation in transient networks of symmetric SIS triblock systems. They reported a characteristic temperature (T^* ~ 30°C) well blow T_g (PS), where PS chains were pulled out from phase separated PS domains, and reconnected to different network domains under an applied stress. The characteristic time-scale for the PS chain recombination was found to be much faster than the release rate, since the free PS chains were diluted in the PI matrix, and therefore had a high mobility until they recombined with the other glassy domains. Shorter PS segments could move during the film annealing (40°C, 4 weeks) and presumably form new self-assembled PS-rich domains. By experimentally finding the most efficient annealing condition, i.e., lowest free energy pathway for rubbery matrix multi-component dynamic-equilibrium and for PS-rich-copolymer self-assembling will be beneficial for improving adhesive film properties at low coating temperatures.

Table 6.3: Effect of annealing condition on the nano scale PS-rich-copolymer domain characteristics.

Adhesive film sample	Average domain diameter [nm]	Average amount of domains/μm^2	Average interdomain distance [nm]
DF645 coated at 120^{o}C	32 ± 5	287 ± 77	45 ± 12
DF645 coated at 120^{o}C and annelaed	28 ± 5	488 ± 14	37 ± 7
7M8 coated at 130^{o}C	35 ± 12	245 ± 46	50 ± 15
7M8 coated at 130^{o}C and annelaed	29 ± 7	458 ± 12	42 ± 10

Estimation of the domain volume fractions and surface areas within the annealed film matrices are shown in Table 6.4. Comparatively the volume fractions seem to have increased with the annealing. The observation is not consistent with the effect of the film coating temperature where the volume fraction decreased(Table 6.2). Presumably this could be due to the formation of new PS-rich-copolymers domains and adding to the already existing ones. With the adequate annealing time for ordering, the microscopic structure organisation is revealed better by the TM-AFM. The domain surface area values are also much higher, confirming that the long time annealing improved the arrangement of the nano-domains within the thin film layers, generating lattices where glassy regions interact more with rubbery matrix.

Table 6.4: Estimation of nano-domain volume fraction and surface area per 1 x 1 μm^2 annealed film surface area.

Adhesive film sample	Volume Fraction of **PS-*r*-Co**[a] domains (%)	Surface Area of **PS-*r*-Co**[a] domains/Film Surface Area (%)
DF645 coated at 120^{o}C	8.4	47.0
DF645 coated at 120^{o}C and annealed	9.8	62.0
7M8 coated at 130^{o}C	9.3	47.7
7M8 coated at 130^{o}C and annealed	10.2	62.2

[a] PS-rich-copolymer

6.3.6 Chemical group analysis on surfaces of coated films

The purpose with this part of the work was to examine the few nanometres of the uppermost top layer of the hot-melt PSA films with different thermal processing histories, and establish any discrepancies in the chemical groups and their relationship to the adhesion property. The samples investigated were labelled as:

- **Sample A = 7M8 film coated at 130^{o}C.**
- **Sample B = 7M8 film coated at 130^{o}C, and annealed at 40^{o}C for 4 weeks.**
- **Sample C = 7M8 film coated at 165^{o}C.**

Positive ions collected from a wide ion mass spectra range have been compiled in the order given above, to make the elucidation tractable. The molecular structures of the based triblock copolymers in the 7M8 formulation are shown in Figure 6.24.

The mass spectra for m/z ≤ 50 are presented in Figure 6.25. This low mass range provides information from the primary ion impact region, generating secondary ion fragments from the film sub-layer region and the uppermost film surface. The significant silicone (Si) peak at m/z = 28 reflects the remnants of the silicone release papers peeled off from the film surfaces. Positive ion fragments characteristic for polyethylene[291] (PE) are $C_2H^+_5$ observed

at m/z = 29, $C_3H^+_5$ at m/z = 41 and $C_3H^+_7$ m/z = 43. In a reported work about triblock copolymer surfaces by Galuska[341], the $C_2H^+_5$ and the $C_3H^+_5$ ions were attributed to a protonated ethylene monomer ion and ethylene monomer plus an additional methylene group. These ions were associated with chain-ends of PE homopolymer formed through sigma ionization[342]. In the adhesive films the source of these ion fragments could be from the alkane hydrocarbon units of paraffin oil, or from the PEB segments of the SEBS, presumably the ethylene side groups. The observation is an evidence of the rubbery nature at the surfaces of the three coated films due to their high relative peak intensities and with similar abundance for all the samples. The ion $C_3H_3^+$ fragment peak at m/z = 39 is presumably from the midblock resin tackifier. A similar positive ion fragment has been reported on studies of pressure-sensitive adhesives where low H/C ratios corresponded typically to the alicyclic ring structures of the midblock compatible resin[327].

a

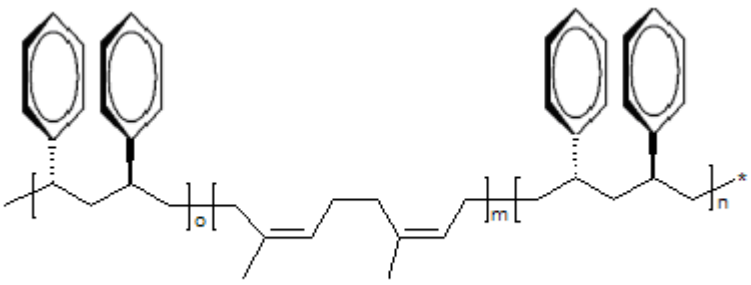

PS-block-poly(1,4-cis isoprene)-block-PS

b

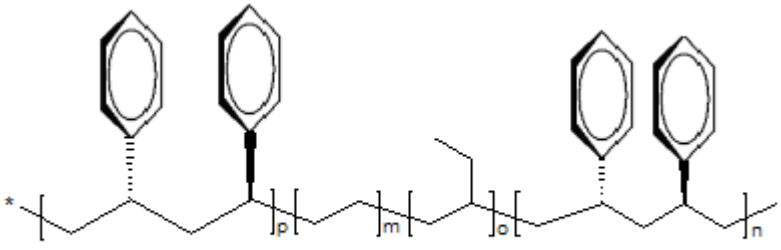

PS-block-poly(ethylenebutylene)-block-PS

Figure 6.24: The illustrations of the triblock copolymer segmental units of the 7M8 blend system showing (a) styrene-*b*-isoprene-*b*-styrene (SIS) and (b), styrene-*b*-ethylenebutylene-*b*-styrene (SEBS).

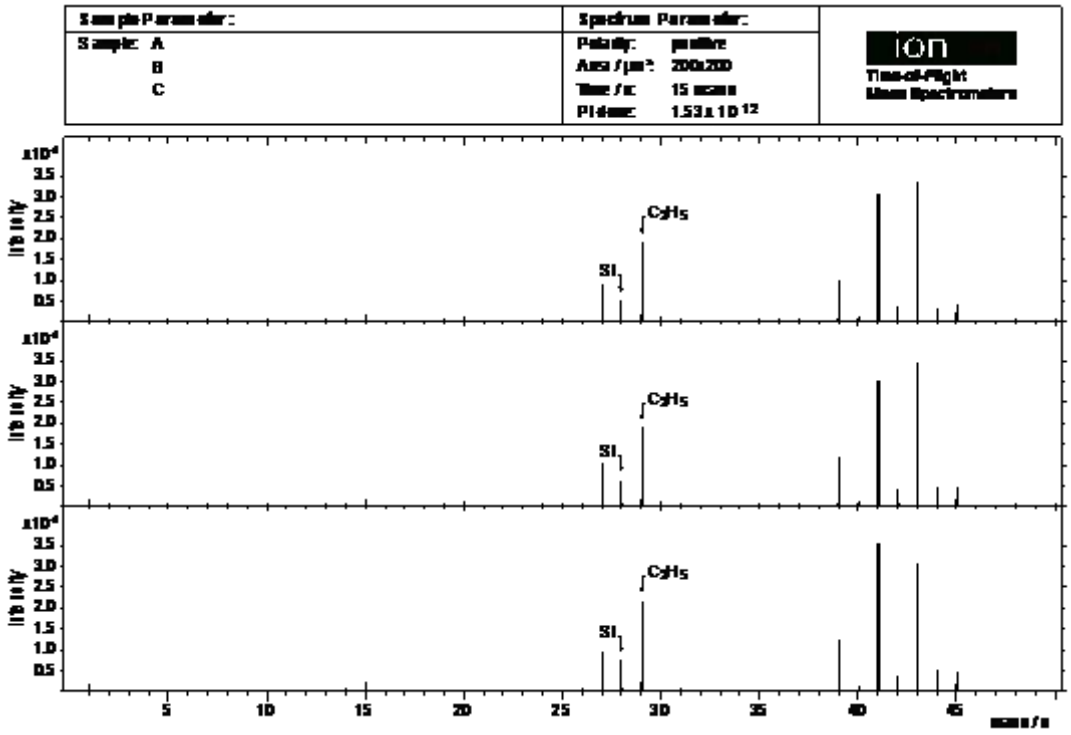

Figure 6.25: Mass spectra in the low m/z range at ≤ 50 for the samples of A = 7M8 coated at 130°C, B = 7M8 coated at 130°C and annealed, and C = 7M8 coated at 165°C.

In Figure 6.26, characteristic peaks of polyisoprene (PI), polystyrene (PS) and tackifiers can be observed. Extensive studies of TOF-SIMS on styrene-isoprene block copolymers by Mehl et al[343], Hasegawa et al[337] and others[79,344], have reported the uppermost surfaces of the block copolymers to be entirely occupied by PI block layers due to their lower surface energies. Characteristic PI peaks[341-344] in these spectra range are m/z = 55, 68, 69, 81 and 93, and for PS[341-344] m/z = 51, 63 and 91. The PS ion fragment $C_4H_3^+$ at m/z = 51 has a very weak relative intensity. Galuska[341] reported in his studies that the relative intensity of this ion increased as the M_w of PS increased and that the ion was formed during fragmentation of the main PS backbone chains. In the current samples the main PS backbone chains are assumed to exist inside the phase separated PS-rich-copolymer domains which should reside beneath the uppermost rubbery surface layer and therefore giving the ions large escape depths[289-291]. The very weak peak intensity signal supports this assumption. The next significant PS ion fragment is the $C_7H_7^+$ at m/z = 91. This ion is known as the tropyllium ion[341,343] and it is a protonated styrene monomer minus a methylene group. It is a characteristic of a hydrogenated end group of PS polymer (R-CH_2-

C_6H_5) and is formed through allylic cleavage[342]. The relative intensities observed in the spectra are larger by a factor of 2 compared to the PS ion fragments at m/z = 51. The sources of PS in the adhesive blends are SIS, SEBS and the α-methyl styrene (AMS) endblock resin. The PS endgroup chains of the triblock copolymers have already been postulated to exist inside the PS-rich-copolymer domains and hence give them large escape depths. However the high relative peak intensities of the tropyllium ions imply a relatively short escape depth for these ions and are assigned to AMS ion fragments. This suggests the resin's presence in the continuous adhesive rubbery matrix.

The high relative peak intensities observed at m/z = 55 for $C_4H^+_7$ and m/z = 67 for $C_5H_7{}^+$ are assigned to the midblock resin tackifier and paraffin oil fragments[345], due to their high contents in the formulation and lower surface energies. Protonated butadiene monomers (PI fragment without methylene side group) can also generate the m/z = 55 peak[341,343]. The large relative intensity peak at m/z = 69 of ion fragment $C_5H_9^+$ is characteristic of the protonated isoprene monomer[341,343] or midblock resin fragments[327]. Its relative peak intensity is actually larger by a factor of approximately 1.5 in the spectrum of 7M8 coated at 165°C (Spectrum C) than 7M8 coated at 130°C (Spectrum A). After annealing the 7M8 coated at 130°C (Spectrum B), the peak intensity of this cationized ion increased by a factor of 1. The peak of the $C_5H_7^+$ ion is also larger in 7M8 coated at 165°C and 7M8 annealed than 7M8 coated at 130°C. This could indicate a higher presence of some elastomers, oil or resins at the uppermost film surface of 7M8 coated at 165°C or annealed than the 7M8 coated at 130°C. Hasegawa and Hashimoto[337] showed in their study with transmission electron microscopy (TEM) that, by slowly evaporating the solvent from a PS-PI diblock copolymer blend over several days, the uppermost surface enrichment of the PI domains was promoted. Jeusette et al[327] also implemented ToF-SIMS investigation to study the surface of annealed PSA and reported the presence of phase separated resin-rich agglomerates at the adhesive near-surface that increased in concentration with the aging time.

A high peak intensity of $C_4H^+_9$ at m/z=57 relates to a protonated butylene from presumably the PEB segments of SEBS. The Relatively high peak intensities at m/z = 73, 83, and 95 are not characteristic peaks of any of the triblock copolymers and are probably from the midblock resin. The peaks could also originate from paraffin ion fragments due to the oil's low surface energy[345]. Surface energy values of some constituents in the adhesive formulation are presented in Tables 6.5.

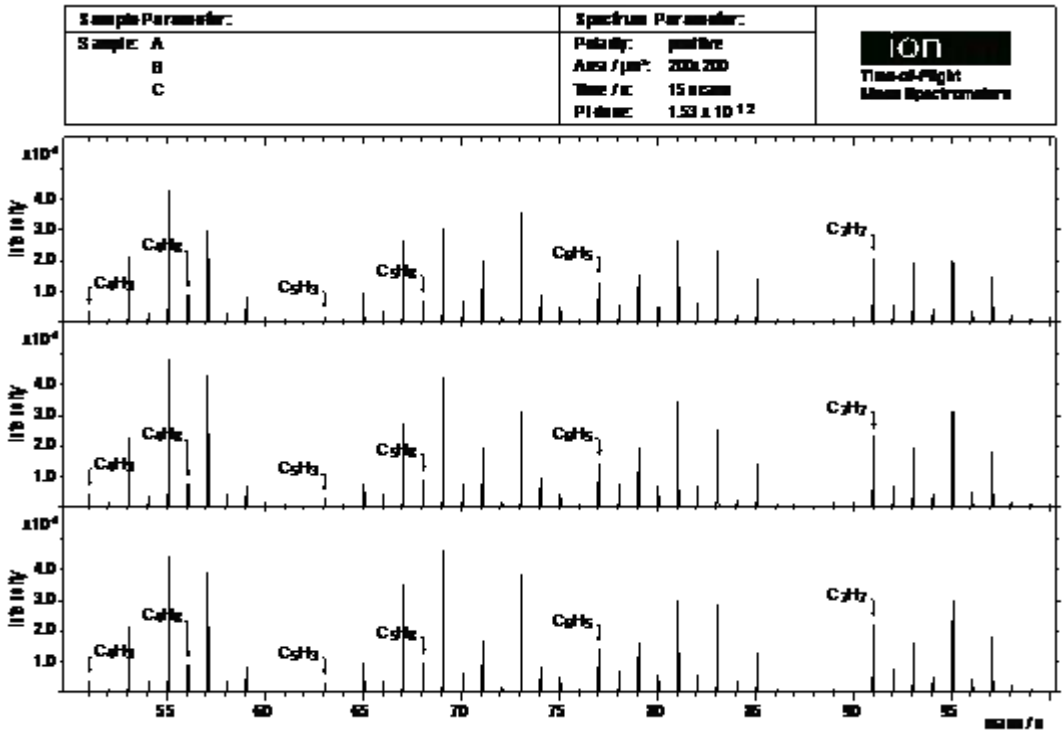

Figure 6.26: Mass spectra in the low m/z range from 50 to 100 for the samples of A = 7M8 coated at 130°C, B = 7M8 coated at 130°C and annealed, and C = 7M8 coated at 165°C.

Table 6.5: The surface energies of some of the constituents in the adhesive formulations are listed.

Adhesive constituent	Surface free energy at 20°C [dyn.cm^{-1}]	Reference
Paraffin oil	26	Dirac[346]
Polyethylene – linear	35.7	Polymer Data Handbook[65]
Polyisoprene	30 - 32	Mehl, Herkules[344]
Poly (α-methyl styrene)	39.0	Polymer Data Handbook[65]
Polystyrene	40.7	Polymer Data Handbook[65]

In Figure 6.27 characteristic PI ion peaks[341,343] are m/z = 119 and 121 and PS peaks[341,343] are m/z = 115 and 117. The higher PI relative peak intensities compared to the PS peaks is

taken as higher PI enrichment at the uppermost sample surfaces. Mehl et al[343]., also reported in their work that the relative ion yield of PS is 8.8 times greater than the ion yield of PI in ToF-SIMS investigation. In other words if PS was presence on the surface as much as PI, its ion peaks would definitely be much higher and also appear at the high-mass range. The high relative peak intensity at m/z = 105 is $C_8H_9^+$ and ascribed to AMS ion fragments without the methylene group. The component appears to be higher on the surfaces of sample C and B than A. The high relative peak intensity at m/z = 147 reflects a low H/C ratio ion fragment of a ring structure which presumably originates from the midblock resin.

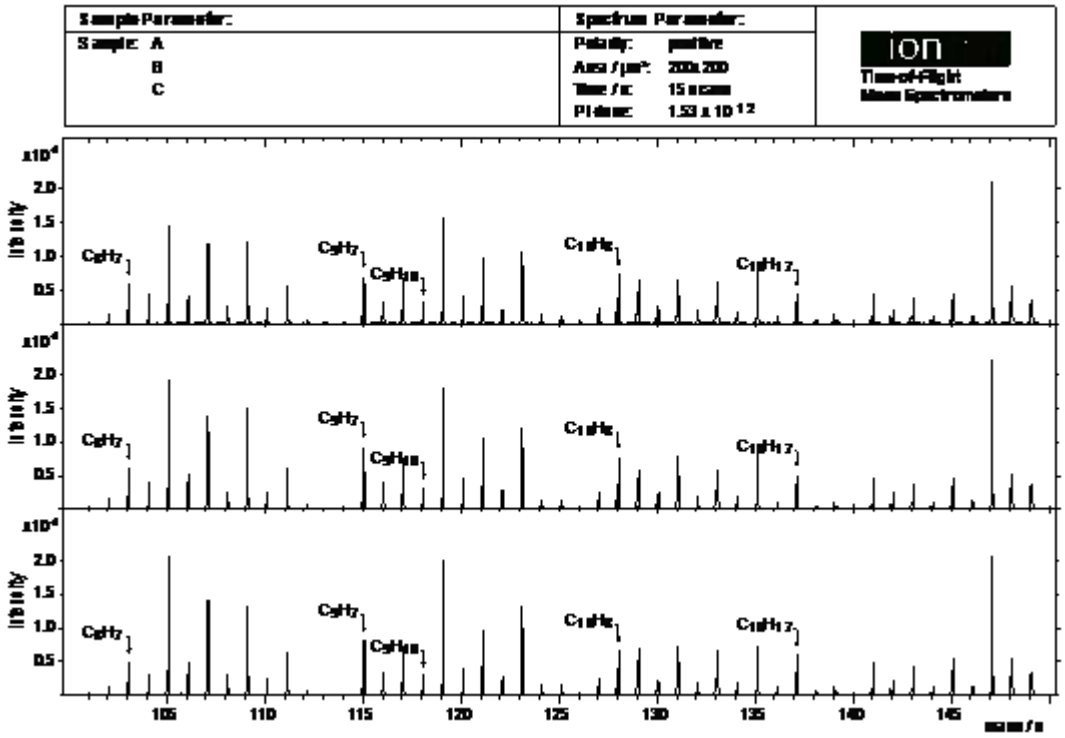

Figure 6.27: Mass spectra in the m/z range from 100 to 150 for the samples of A = 7M8 coated at 130°C, B = 7M8 coated at 130°C and annealed, and C = 7M8 coated at 165°C.

Towards the relatively high ion mass region (Figure 6.28), the only relative peak intensities as an indication of triblock base copolymers are the much less prominent signals of PI at m/z= 177 and PS at m/z = 193. Their weak intensities suggest that the absolute uppermost surfaces of the adhesive films, up to 10 Å[347], are enriched in oil possibly due to its low surface energy (Table 6.5).

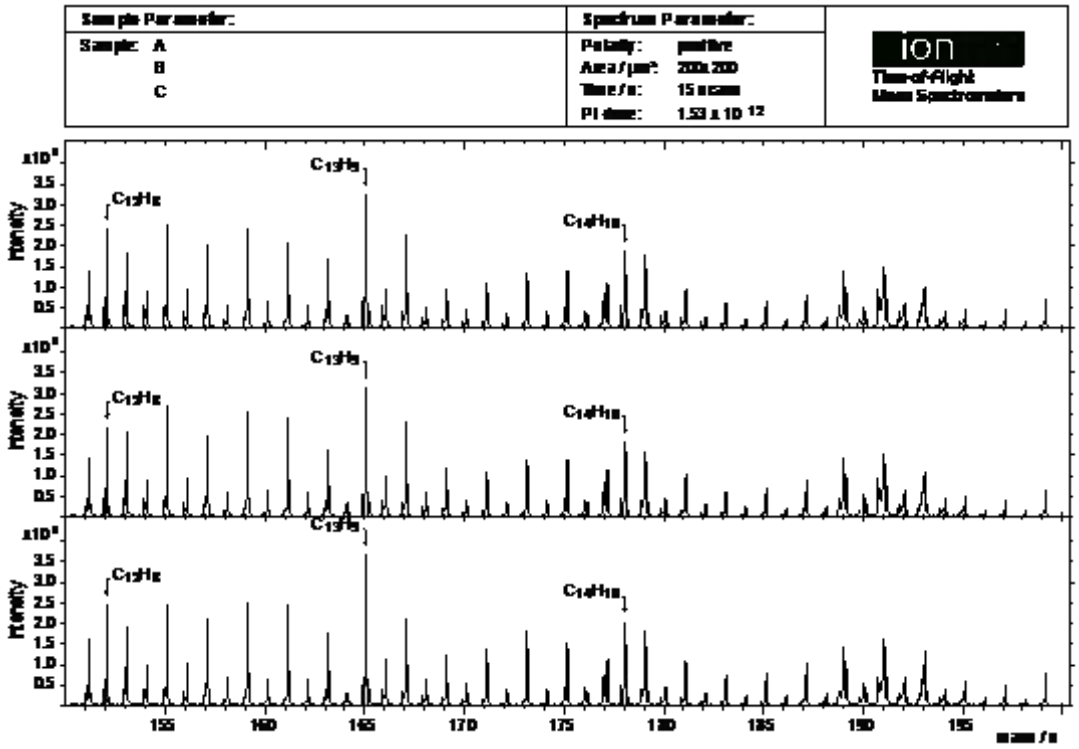

Figure 6.28: Mass spectra in the m/z range from 150 to 200 for the samples of A = 7M8 coated at 130°C, B = 7M8 coated at 130°C and annealed, and C = 7M8 coated at 165°C.

In Figure 6.29 the high relative peak intensities at m/z = 207 and 221 could be from the oil but the true origin is not known. A Thorough examination of spectra regions up to m/z= 700 (not shown here), as well as an examination of the negative ion spectra showed a striking similarity in terms of the molecular presence on the surfaces of the 7M8 adhesives films, irrespective of the processing history.

It is noteworthy to mention that the SIMS investigations were carried out on adhesive surfaces of 200 x 200 µm^2. Therefore the results do not necessarily reflect a potential discrepancy in chemical nature on the micro- and nanoscale regions as revealed by with the AFM. On a macroscale, it can be claimed with confidence that there are no chemical group discrepancies on the surfaces of the adhesive coated films, but constituent quantitative differences do exist. The results from this investigation have demonstrated that valuable information about the surface composition of PSA systems can be provided by S-SIMS analysis.

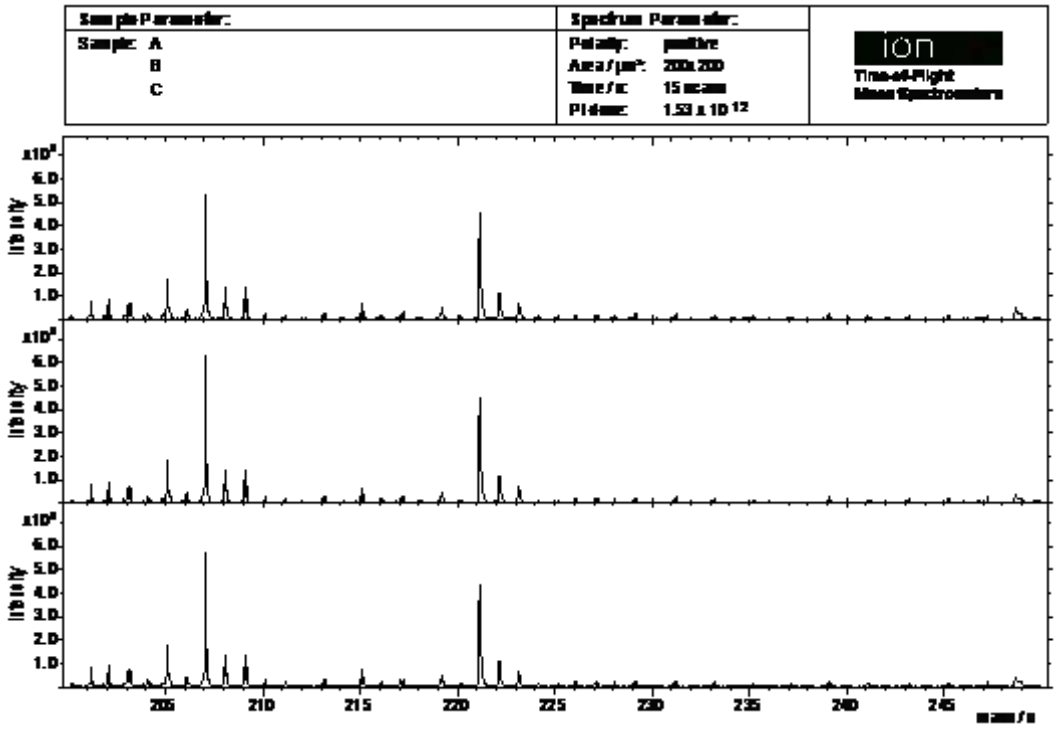

Figure 6.29: Mass spectra in the m/z range from 200 to 250 for the samples of A = 7M8 coated at 130^{o}C, B = 7M8 coated at 130^{o}C and annealed, and C = 7M8 coated at 165^{o}C.

6.4 Summary

The capabilities of TM-AFM for contributing to adhesion science by providing new and important information on a highly local scale have been presented. The technique has provided numerous insights into the micro- and nanoscale morphology of multi-blend adhesive films with different processing thermal histories. The work has proved that though conventional TM-AFM height images do not necessarily reflect the real surface topography of soft adhesive films, the phase images however give a true account of the film morphology. This is a quick and convenient way to investigate the quality of the blending process and partly predict product end-use performance.

In the case of DF645 and 7M8 blend formulations, the TM-AFM topographies revealed phase separated micro-sized agglomerates within the coated adhesive films. When the film was coated at low temperatures the agglomerates were bigger in sizes and more abundant than when the film was coated at a higher temperature. These agglomerates were possibly

residual tackifier-rich and partitioned copolymer-rich regions. For the DFC600 formulation, the agglomerates were non-existent irrespective of film coating temperature.

On the nanoscale, the adhesive coated films of all the blend systems consisted of relatively hard phase-separated PS-rich-copolymer domains dispersed within the film matrix. The domains appeared smaller in sizes (~ 25 nm), had shorter inter-domain spacing (~ 33 nm) and were more abundant when the film was coated at a higher temperature. The low temperature films exhibited fewer domains, with an average size of ~ 30 nm and spacings of ~ 45 nm. In part the discrepancy in film morphology is due to the preparation process, which involved melting at high temperatures and subsequently quenching to ambient temperatures, thereby freezing the architecture formed at the melt state. When the DF645 and 7M8 films initially coated at low temperatures were annealed at 40^{o}C for 4 weeks, the film morphologies improved significantly where the amount of domains per micrometre squared film area doubled.

It seems that the two principal morphological elements that dictate the adhesion properties of the coated films are (a) the population of the PS-rich-copolymer domains and (b) the domains interconnection either by elastomer chain bridges and elastomer chain entanglement junctions possibly formed by adjacent polydiene-induced dangling chain ends. The latter is especially true for the DFC600 blend system with the highest polydiene content. Due to this phenomenon the interconnected network structure is dominant even for the low-temperature coated film, which makes the film's property least sensitive to the coating temperature. The reduction in the population of the PS-rich-copolymer domains with decreasing film coating temperature seemed to be responsible for the formation of elastically inactive elastomer network systems, mainly for the DF645 and 7M8 coated films.

The capability of ToF S–SIMS to generate and detect ionized oligomers has provided a unique potential in examining pristine adhesive surfaces. On the microscale no chemical group discrepancies were observed at the uppermost adhesive film surfaces, irrespective of the processing thermal history. The relative peak intensities did suggest quantitative differences of an oil-rich rubbery thin layer covering the uppermost adhesive film surfaces. For high-temperature coated and annealed films, the relative peak intensities of PI ion fragments appeared higher than found for the low-temperature coated films.

Chapter 7

7 Adhesion force and elastic modulus of coated hot-melt pressure-sensitive adhesive films on a nano-scale level

7.1 Introduction

In Chapter 6, adhesive film morphologies on micro- and nano-scales were revealed with tapping-mode atomic force microscope (TM-AFM). A film structure comprising PS-rich-copolymer phase-separated nano-domains dispersed within the continuous adhesive matrix could be observed for all the blend systems. For films melt-coated at high temperatures or annealed, the domains were more abundant and exhibited shorter spacings compared to the films melt-coated at lower temperatures. Based on the results, the domain interactions either by elastomer chain bridges or entanglement junctions formed by adjacent rubbery segments is believed to differ significantly in the different coated films.

The surface and bulk properties investigated with classic test techniques in Chapter 4 proved that the industrial procedure in judging the adhesive's peel performance on the macroscale is not adequate. For a fundamental understanding of the mechanisms by which these tack-promoted PSAs undergo bonding, one must understand and inter-relate the complex physics occurring at each scale level. This part of the studies extends the concept of investigating the adhesive peel behaviour to a local scale with contact areas on the nanometer range. Through the employment of AFM, the work aims to quantify the surface adhesion exclusively attributed by molecular structure and morphology of the coated film surface. The adhesion of the film in response to the morphology formed at different coating and annealing conditions are studied. Similar AFM methodology is implemented to examine the elastic modulus of the coated film surfaces.

7.2 Experimental

The DF645 and 7M8 adhesive blends were supplied by Henkel as free-standing coated films sandwiched between silicone-release papers (See Chapter 3.1 for details of the blends). The films were melt-coated at 30g/m^2 (total mass of adhesive per surface area paper) onto the silicon-release paper moving at a line speed of 300 m/min, which resulted in film thicknesses of around 10 μm. The adhesive films of DF645 were coated at 120^{o}C and 155^{o}C, respectively, and films of 7M8 were prepared at 130^{o}C and 165^{o}C, respectively. Additional samples of the aforementioned DF645 coated at 120^{o}C and 7M8 coated at 130^{o}C, respectively, were annealed in an oven at 40^{o}C for 4 weeks.

The pristine free-standing films were cut into the shapes of 7 x 7 mm^2. The silicon release papers on one side of the specimens were meticulously removed with clean tweezers and the tacky film surfaces were adhered to freshly cleaned microscope glass slides (for adhesion force measurement) and metal discs (for elastic modulus measurement) without shearing the samples. Afterwards the samples were then fixed in the AFM stages, and the other silicon release papers on the surfaces to be investigated were removed prior to the measurements, in an attempt to minimise contaminants on the film surfaces. It is important to mention that the adhesive surfaces studied were the surfaces to be exposed to substrates during end-use application. The identification was made possible since the silicon papers sandwiching the free adhesive films were of different colours, to distinguish the surfaces to be exposed at the end-use from the surface usually adhered to the PE-film substrate. Extensive description of the adhesion force and elastic modulus characterisations are given in Sections 3.2.6.1 and 3.2.6.2, respectively. All the measurements were performed at room temperature and condition.

7.3 Results and Discussion

The images collected with the TM-AFM are presented as 2-dimensional as obtained from the tapping mode. Firstly images of each sample surface are introduced, followed by the corresponding force modulation measurements in similar sequence as the investigations were taken.

7.3.1 Effect of film coating temperature on adhesion force

7.3.1.1 7M8 adhesive series

In the images of sample 7M8 coated at 130^{o}C (Figure 7.1), the height image (left) suggests a relatively rough film surface with brighter colour contrast indicating elevated regions and darker colour contrast of depressed regions. The corresponding phase image reveal microphase separated agglomerates of mechanically harder nature randomly dispersed within the continuous softer adhesive film matrix. Such characteristics of the adhesive coated samples have already been explained in Chapter 6 with the morphology studies and therefore briefly mentioned here. In Chapter 6, the agglomerates were believed to be residual midblock resin-rich and/or partitioned block copolymer regions partially due to poor blending. The limited solubility between the resins (~ 56 wt-% in the blend) and elastomer polydiene segments (~ 10 wt-% in the blend) and the limited mobility of copolymer segments as effect of the low film coating temperature, result in a film morphology from a more favourable thermodynamic state.

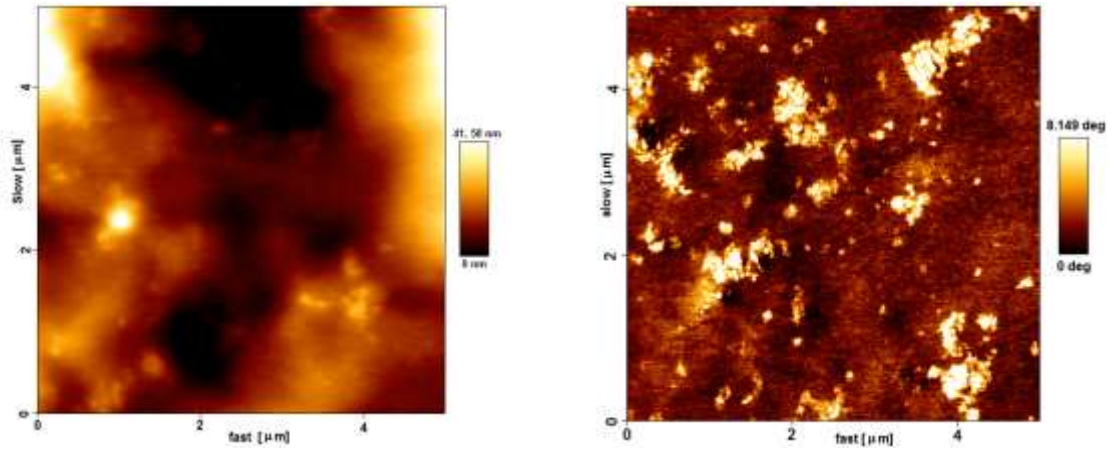

Figure 7.1: AFM images of 7M8 coated at 130 ^{o}C revealed relatively hard phase-separated agglomerates within the adhesive film matrix. The height image is to the left and the corresponding phase image to the right. Scan size is 5x5 µm^{2}.

In Figure 7.2 the phase image of the 7M8 coated at 130^{o}C is again showed, with gridlines depicting the areas on the sample surface that the force –distance (F-D) measurements were carried out. The AFM tip was allowed to touch the centre point within each grid (index) before it was withdrawn and the resulting force values recorded. On this 7M8 coated film sample, 64 adhesion force curves were collected. Starting at the bottom left grid designated as Index 0, the measurement proceeded in a horizontal pattern until the

first each row was finished and then continued from the row above in a reverse direction until ending at the film surface region designated as Index 63 was measured.

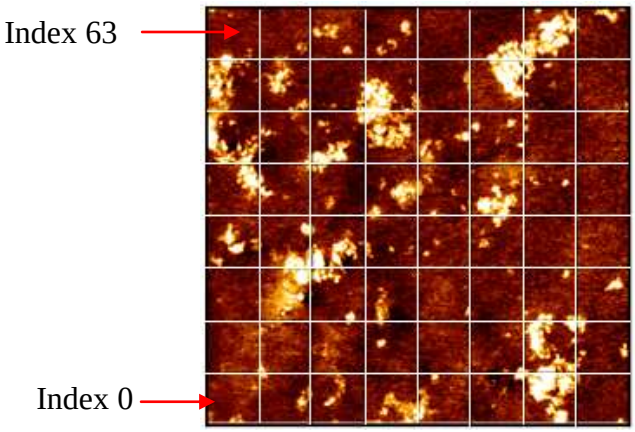

Figure 7.2: The same phase image of Figure 7.1 with the grids explaining the areas on the film surface where the 64 tip-sample adhesion measurements were collected. The measurement was commenced at the bottom outermost left grid designated as Index 0, and continued horizontally until the first row was done, and then proceeded from the next grid above in reversed horizontal direction until the centre point of the Index 63 area region was measured.

For further introduction of the experimental results, a couple of relevant moments with the measurements are firstly explained. Two or three force curves collected for each sample will be presented as it is unnecessary to present all the force curves measured for each sample due to their similarities for each specific film sample in question. The y-axis is the cantilever deflection and the x-axis is the piezo travel distance. In the force curves shown in Figure 7.3 for the 7M8 film coated at 130^{o}C, sinusoidal oscillation patterns of the extension zero line are registered as the tip approached the sample surfaces. Theoretically the horizontal lines[279,281] (Section 3.2.6) should be straight as the tip at this point is far away from the sample surfaces and hence no forces should be interacting with it. The superimposed oscillation typically occurs if there is optical interference between the laser beam reflecting off the upper face of the cantilever (Fig. 3.19) and the laser beam that inevitably passes the cantilever and scatters off the sample surface to the detector[279]. As the approached the specimen surface (Index 6, Fig. 7.3), it jumped to contact with the sample (extension line) at a piezo distance of z ~ 9600 nm. This was the consequence of an induced mechanical instability since the gradient of the tip-sample attractive interaction force exceeded the force constant of the cantilever. The contact point of the jump-in is not as conspicuous here as reported in the literature[250,255,256,260,279], probably due to the high stiffness of the cantilever used, giving rise to a diminished deflection and also as a result of the high speed measurement condition set[259]. Once contact was established the tip was

pulled into the sample by the adhesive interaction and the cantilever bent upwards until the pre-set trigger value was reached. The process was then reversed and the tip begun its withdrawal (retraction line) from the sample surface. At the initial retraction process, no data points were recorded as observed in the F-D curves (Fig. 7.3). This occurred with all the measurements irrespective of film coating temperature and adhesive blend system. Sun and Walker[348] have reported with AFM studies on the viscoelastic response of poly(dimethylsiloxane) (PDMS) that, the omission of first data points with tip retraction was dependent on the tip-sample contact-time. They noticed that a longer dwell time (pre-set contact-time) caused a larger gap between the end of the extension curve and the beginning of the retraction curve. They believed that the sample relaxation was the cause to the gap. In these measurements the dwell time was set to zero and kept constant for all the samples. Therefore it is believed that the missing data points in these measurements was caused by the intrinsic sample adhesive which held on firmly to the tip and made it withdraw some time after the piezo withdrawal had begun.

As the piezocrystal exerted a further pulling force on the cantilever, the sample which was still holding on to the tip caused the cantilever to bend downwards due to the adhesion force. This occurred with the piezo retraction until a minimum deflection point at around a retraction distance of z ~ 9600 nm was reached, where a pull-off or jump-out was observed (Fig. 7.3). This jump-out will normally be associated with the zero line, i.e. when the tip detaches from the sample surface but the cantilever is again pulled as the tip was still in contact with the film surface, seen in the trajectory of the jump-out part of the retraction curve. Further jumps were again recorded until contact was definitely broken at z ~ 11000 nm and the tip bounced back to the zero line (extend and retract curves overlapped). The maximum difference between the vertical deflection of the cantilever at the contact (Extend) and noncontact (Retract) straight lines at the jump-out point is the pull-off or adhesion force[250,255,256,260,279,348].

Further information can be extracted from the force curve of the film region of Index 6 (Fig. 7.3). During a force-distance measurement as explained in Section 3.2.6, the slope generated with the tip-sample contact usually reflects the hardness of the sample surface[252,279,348]. In the extension contact curve between z~ 9600 nm and z ~ 9300 nm, it appeared that firstly, the tip-sample interaction was relatively soft (less resistance to the tip) and as the tip extension proceeded, the interaction became relatively hard (more resistance to the tip). This could not be caused by the impact from the steel AFM sample-

support as the samples are relatively thick on this scale (thickness ~ ≤ 10 μm). In a reported study[349] where similar double-slopes were observed, the authors attributed the phenomenon to the tip's interaction with first a fibre or membranous structure that then slipped way from the probe and lead to the second contact point. In this work though the distortions of the contact point curves presumably reflects the inhomogeneity of the film surface property where the viscoelastic/adhesion nature appear to vary locally.

Another force-distance (f-d) measurement collected at a relatively soft film matrix region (Index 59, Figures 7.3) displayed similar characteristics to the measurement at the relatively hard agglomerate region (Index 6). At the retraction tip-sample pull-off point of the Index 59 sample region (Fig. 7.3), a small one-step tip-detachment unfolded, followed by the multi-step viscous pull-offs similar to that of the Index 6 region. This would continue until finally the elastic force of the cantilever overwhelmed the adhesion force of the sample, resulting in the total breakage of the tip–sample contact. The force curve measurement performed at a third region (Index 48, Figs. 7.4) exhibited a one-step tip jump-out but with similar force magnitude as the two force curves presented above. The trends noticed in the other 60 force curves collected were consistent with the ones shown here (Figures 7.3 and 7.4). Another noteworthy observation is that at the experimental measurement time-scale, the sample did not regain its original shape, indicated by the deformation, δ, (Index 6, Fig. 7.3) after the tip withdrawal. This demonstrates the viscous-like characteristics of the film near-surface.

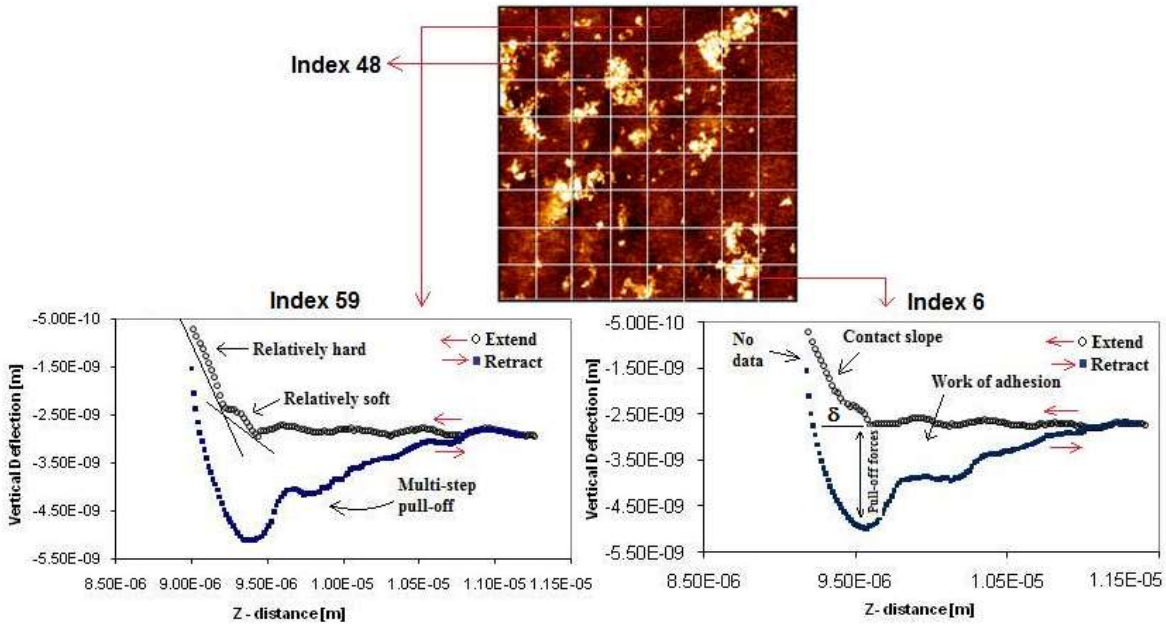

Figure 7.3: The F-D curves measured at bright agglomerate and soft matrix areas are similar in adhesion nature. The inserted phase image highlights the regions (Index) on the sample surface where the measurements were collected. The area of the confined region between the extension and the retraction curves is equivalent to the work of adhesion, i.e. the energy exerted by the cantilever probe to detach from the film surface. Other explanations are also given in the curves. The horizontal gap, δ, indicates the sample surface deformation.

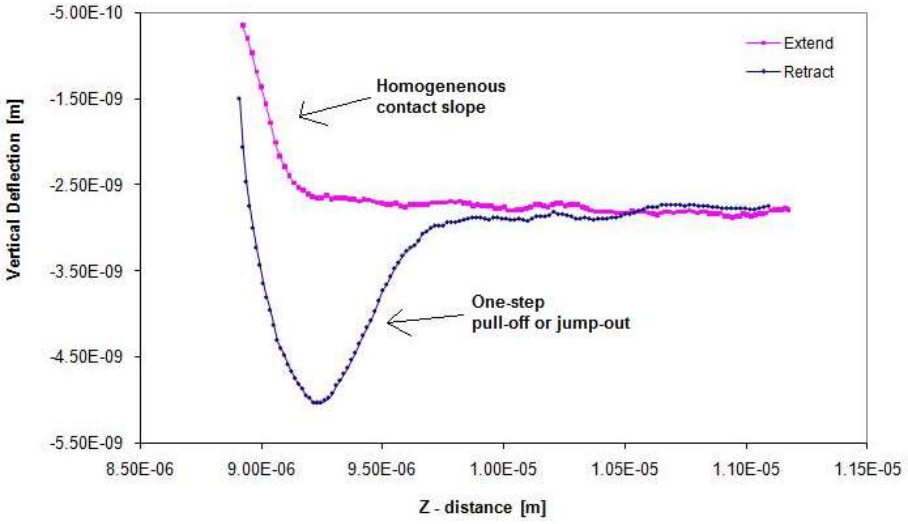

Figure 7.4: The Index 48 region (Fig. 7.3) displayed an F-D curve of homogenous deformation as the tip was pulled into the sample (extension curve) and a one-step tip jump-out from the sample surface (retraction curve).

The results above reflect an intricate nature of the tip debonding mechanism from the coated adhesive film surface. Whilst a one-step tip jump-out is observed in some film surface regions, other areas exhibited a multi-step tip jump-out. Remarkably the debonding behaviour is independent of the mechanical characteristics of the phase-separated agglomerate regions within the coated film (Fig. 7.3). As far as this work goes, this is the first time such heterogeneous complex force curves have been measured on adhesive samples. This infers that the tip was not directly interacting with the sample's subsurface morphological information revealed in the AFM phase images. Rather the tip was directly interacting with the uppermost tackifier-promoted rubbery/oil-rich thin adhesive surface as suggested by the results presented in Chapter 6. However the mechanical characteristics of the surface and hence the interfacial adhesion is due to the synergistic effect mainly contributed by the film subsurface morphology as will be proved eventually.

Height and phase images of the surface of 7M8 film coated at 165^{o}C are shown in Figure 7.5. A vital significant difference in the film morphology compared to the film coated at 130^{o}C is revealed. The micro-phase separated agglomerates within the continuous film matrix are almost non-existent. This observation has also already been known and discussed in Chapter 6.

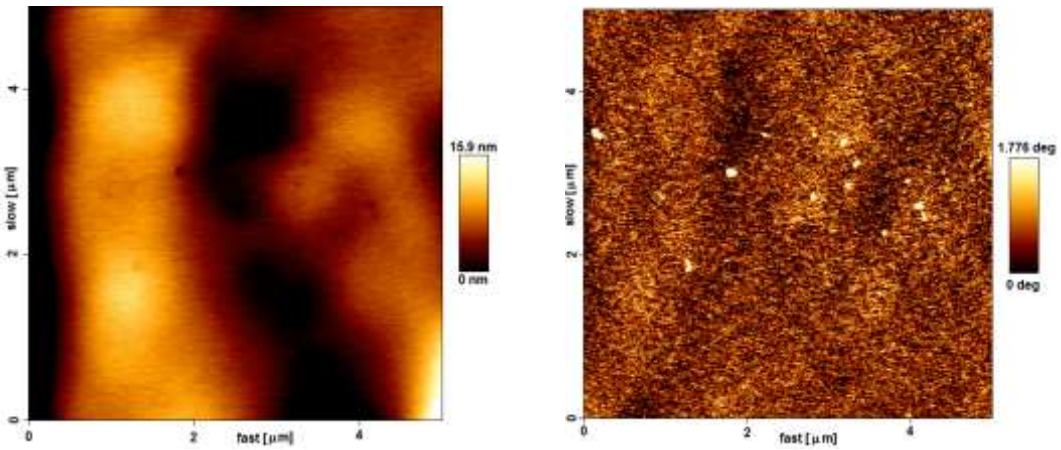

Figure 7.5: The AFM images of 7M8 film coated at 165^{o}C revealed a rather flat surface topography (left) and a phase image (right) of very few phase-separated relatively hard agglomerates(bright regions) within the film matrix. Scan size is 5 x 5 µm^{2}

Two of the 64 adhesion force measurements collected for the film coated at 165^{o}C are shown in Figure 7.6 with the phase image describing the areas of the measurements. In both the F-D curves of Indexes 9 and 33, a similar oscillation approach pattern unfolded as

the tip moved towards the sample surface, just as the measurements for the film coated at low temperature (Fig. 7.3). Once tip–sample contact was established (extend curve, Index 9) at approximately z ~ 8 000 nm, a homogenous cantilever upward-deflection occurred as the tip was pulled into the sample by the adhesion-induced attractive forces. This occurred until the maximum applied load was reached where the process was reversed. At the beginning of the piezo retraction, data points were again missing with the tip withdrawal, for the same reasons given above. During the tip–sample pull-off point (between the minimum retraction point and the horizontal line), a one-step debonding process is observed with much larger tip jump-out gap compared to the results obtained for the film coated at 130^{o}C (Fig. 7.3). The hysteresis between the extension and retraction curves once again manifests the adhesion of the film sample. The area relating to the work of adhesion is also much larger than measured for the low temperature coated film (Fig. 7.3). This indicates that the tip was in contact with the sample at a much longer piezo travel distance (Z) than it was for the film coated at 130^{o}C (Fig. 7.3). The discrepancy in the magnitude of the force measurements strongly indicates that the film surface adhesion is strongly dependent on film coating temperature, even at bonding contact areas on the nanometre range. The repeatable behaviour of the tip-sample jump-out also reflects a more homogenous adhesive film nature, which subsequently insinuates a more uniform thermodynamic equilibrium-like film subsurface morphology as seen. The observation made here is consistent with results and conclusion drawn from Chapters 5 and 6. The plots also suggest very viscous-like film surface nature (gap between the extension and retraction curves at the horizontal zero-line) with almost no sample recovery at the measurement time-scale, similar to the low-temperature coated film (Fig. 7.3).

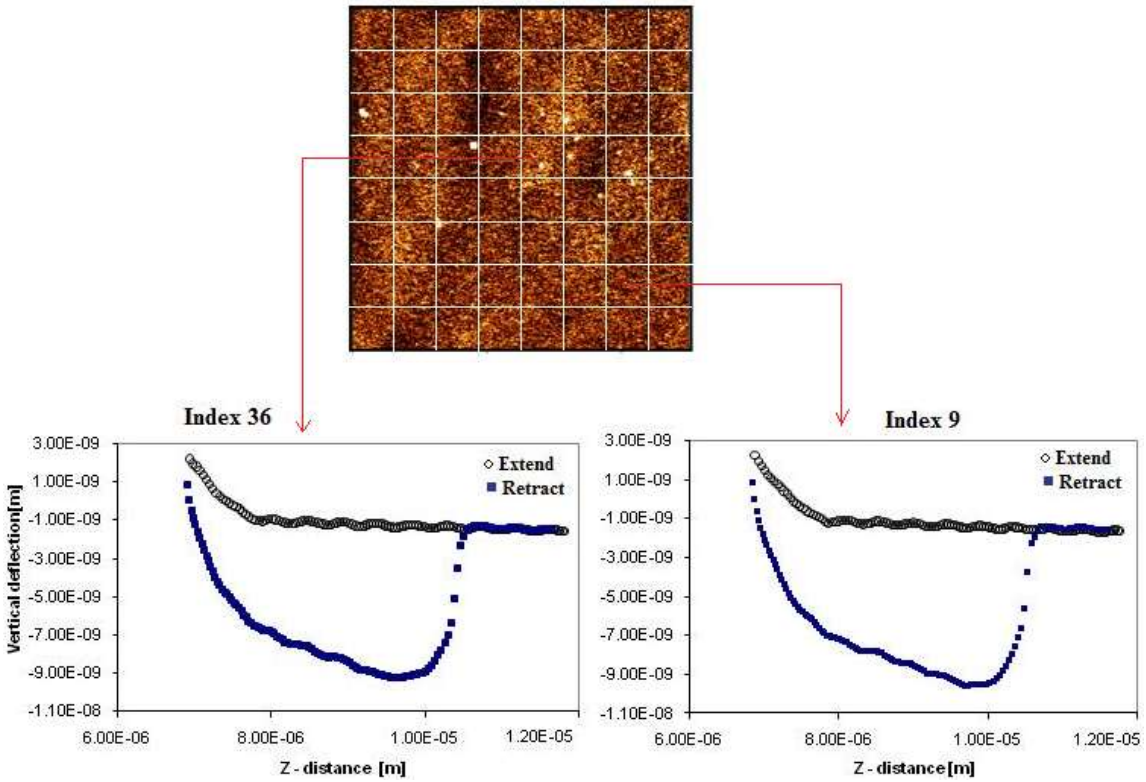

Figure 7.6: Two selected F-D curves measured on the film surface of 7M8 coated at 165^{o}C imply homogeneous adhesion property irrespective of the film surface region. The indexes and gridlines designate the region on the phase image of the film surface where each measurement was taken.

7.3.1.2 DF645 adhesive series

The coating temperature effect on the adhesion characteristics of the DF645 film series are presented in this section. There are some similarities to the 7M8 film series, albeit that more force measurements were collected for these samples. The TM-AFM phase image of DF645 film coated at 120^{o}C (Fig. 7.7) exhibited phase-separated relatively hard agglomerates dispersed within the film sub-surface morphology. The agglomerates were more than observed for the film coated at 155^{o}C (Fig. 7.9). Such property of the DF645 blend under the influence of film coating temperature has already been presented and discussed in Chapter 6. Once again the results with the F-D measurements as shown in Figure 7.8, suggest that the tip was not directly interacting with the film sub-surface morphologies revealed in the AFM images. It is noteworthy to mention however that the complexity of the pull-off curves of the tip-sample adhesion of film coated at 120^{o}C (Figures 7.8) is not as pronounced as observed with the measurement of 7M8 coated at 130^{o}C. This could support the argument about the adhesive film's pronounced sensitivity

to the coating temperature with increase in the PS content, as used in the 7M8 blend. Nevertheless the adhesive strength trend between the films coated at high temperature compared to the films coated at low temperature was consistent with the 7M8 film series.

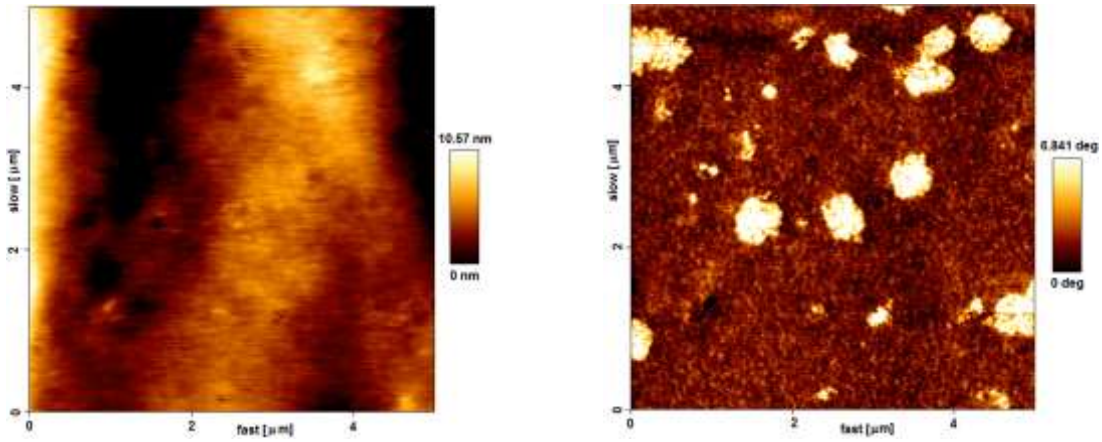

Figure 7.7: The TM-AFM images of DF645 film coated at 120°C show seemingly smooth film surface with height range (left image) of ~ 11 nm and a phase image (right) of phase-separated relatively-hard agglomerates dispersed within the film matrix. Scan area is 5 x 5 µm^2.

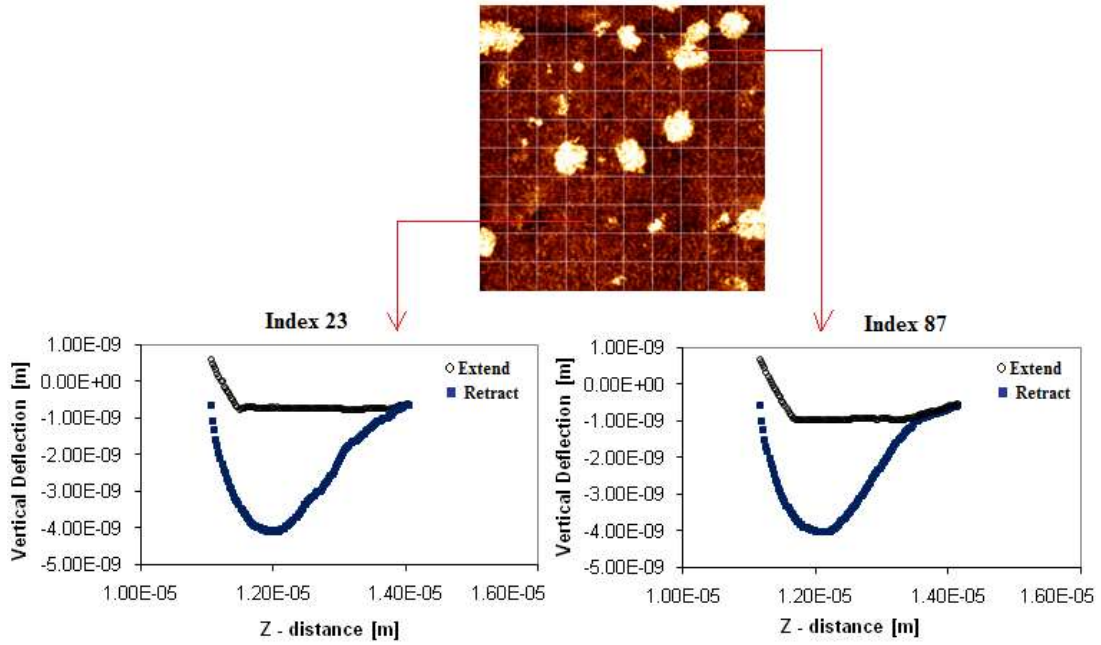

Figure 7.8: Two F-D curves collected at different phase-separated areas of the film surface as depicted by the arrows, clearly generated similar adhesion forces and energies. This insinuates that the film surface adhesion property is not directly related to the films local phase-separated mechanical characteristics as seen in the phase images.

Similar to the 7M8 coated at 165°C, the DF645 coated at 155°C (Figure 7.10) also displayed a one-step tip-sample contact breakage, with adhesion forces and work of adhesion which are of significantly larger than the DF645 film coated at 120°C (Fig. 7.8).

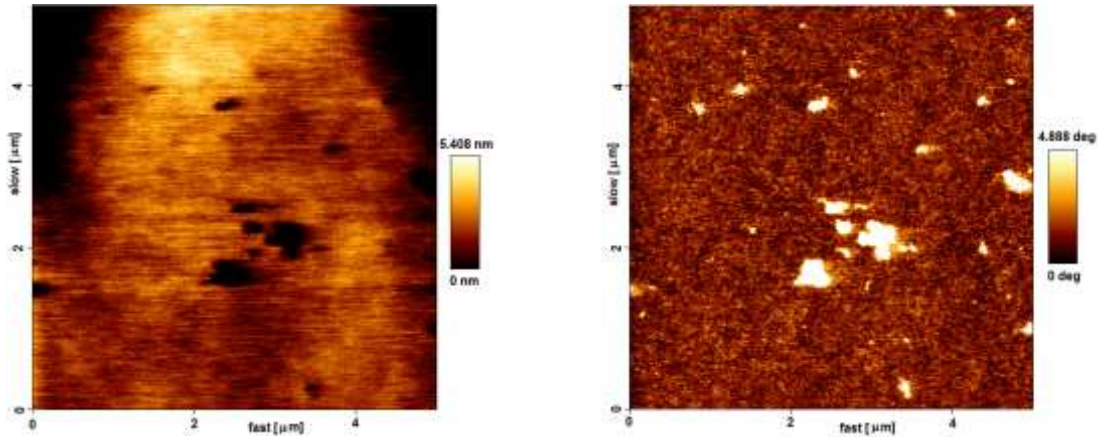

Figure 7.9: TM images of DF645 film coated at 155°C displaying a relatively smooth film surface (height topology, left image), and the phase image (right) comprised of less microscale phase-separated relatively hard agglomerates dispersed within the continuous film matrix. Scan area is 5x5 µm^2.

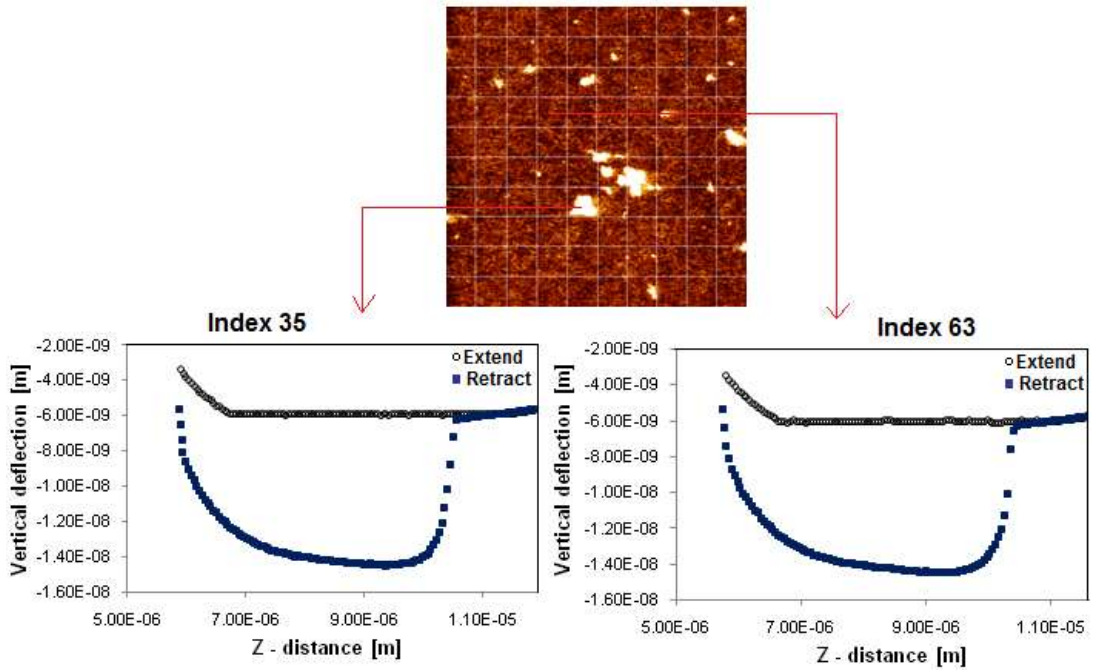

Figure 7.10: Two adhesion force measurements collected at different regions of both relatively hard agglomerate and matrix sub-surface areas of DF645 coated at 155°C show similar adhesion properties.

In Chapter 6, morphology studies with TM-AFM and surface chemical group analysis with ToF-SSIMS indicated that the surfaces of the coated adhesive films were enriched in rubbery/oil continuous phase. It must be mentioned that for all the TM-AFM images shown in this Chapter, further phase separations consisting of the PS-rich-copolymer

domains exist on the nano-scale level, as already presented in Chapter 6. The results obtained with the F-D curve measurements clearly indicate adhesion behaviour independent of the microscale phase-separated agglomerate regions. This is a strong support for the existence of the rubbery/oil-rich layer covering the uppermost film surfaces. It appears then that the formation of the nano-domains with corresponding elastomer network system is responsible for the significant tip-sample adhesion differences presented above.

7.3.2 The effect of the film annealing condition on adhesion force

7.3.2.1 7M8 and DF645 annealed samples

The AFM images collected on the 7M8 film coated at 130^{o}C and annealed at 40^{o}C for 4 weeks are presented in Figure 7.11. It is obvious that the agglomerates are fewer and the continuous film matrix appears more homogenous and reminiscent of the morphology of the film initially coated at high temperature. The observation has already been explained in Chapter 6. The improved adhesion property indicative of high tip-sample pull off force and the larger adhesion energy are shown in Figures 7.11. Similar to the high-temperature coated films (Figures 7.6 and 7.10), the AFM probe seemed to have been in contact with the annealed sample surface at a much bigger piezo retraction distance, visualized in the forces curves (Fig. 7.12). The film adhesive nature is again independent on the agglomerate region (Fig. 12) but another significant difference to the film unannealed film (Fig. 7.3) is the more homogenous tip-sample adhesion nature, demonstrated by the extension contact point slopes and retraction tip jump-out curves (Fig. 7.12).

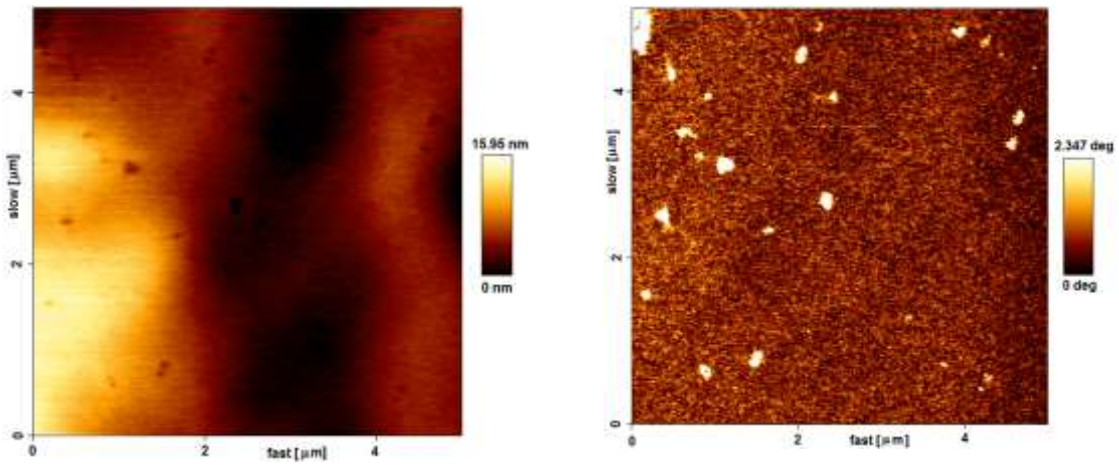

Figure 7.11: TM-AFM images of the 7M8 film coated at 130 ^{o}C and annealed for 4 weeks at 40^{o}C revealed a significant morphology improvement. The height image (left) and phase image (right) show less microscale phase-separated agglomerates dispersed within the more homogenous film matrix. Scan size is 5 x5 µm^{2}.

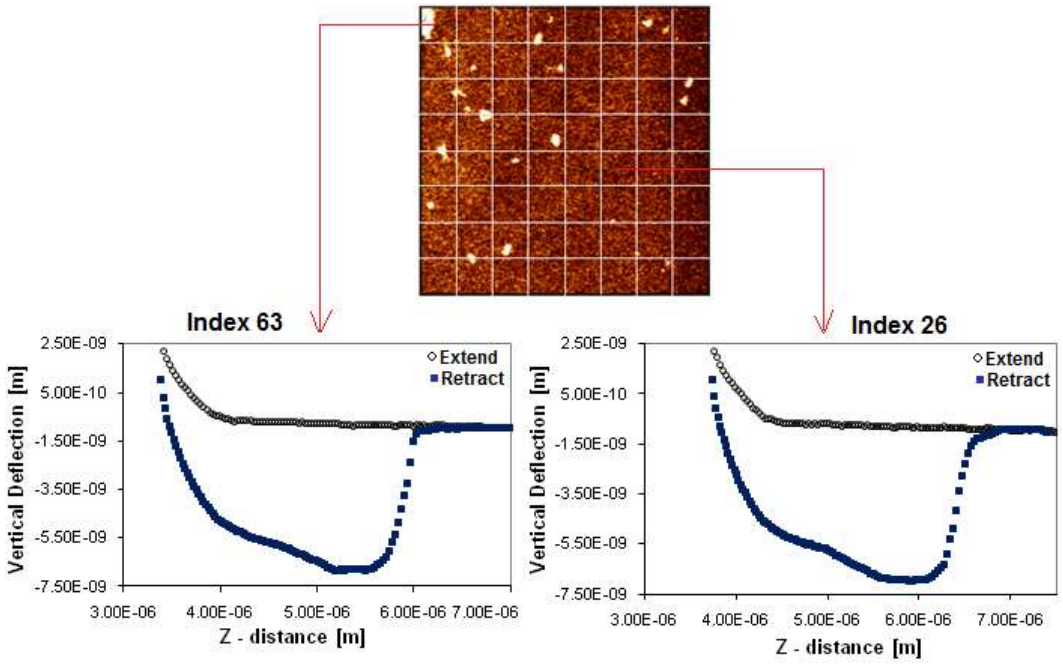

Figure 7.12: Two different force-distance curves measured on the film surface at different regions show reproducible large adhesion forces and adhesion energies for the 7M8 annealed sample.

The annealing effect on the DF645 coated film initially coated at 120^{o}C is presented in Figure 7.13. It is clear that the relatively hard microphase-separated agglomerates disperse into the film matrix and acquire the more intermediate mechanical characteristics, as explained in Chapter 6 (Section 6.3.5). The F-D curve measurements presented in Figures

7.14 is a vindication of the enhanced adhesion nature of the annealed DF645 coated film, presumably caused by the improved mixing of the residual resin-rich or copolymer aggregates during the long-time annealing. In the F-D curves (Fig. 7.14) the results again imply that the film surface adhesion was independent on the micro-phase separated agglomerates (curves of Index 6 and Index 33 film areas). This again suggests the tip's interaction with the thin rubbery/resin/oil-rich surface layer but the improvement of the surface nano-scale film morphology is crucial of the near-surface film layer characteristics.

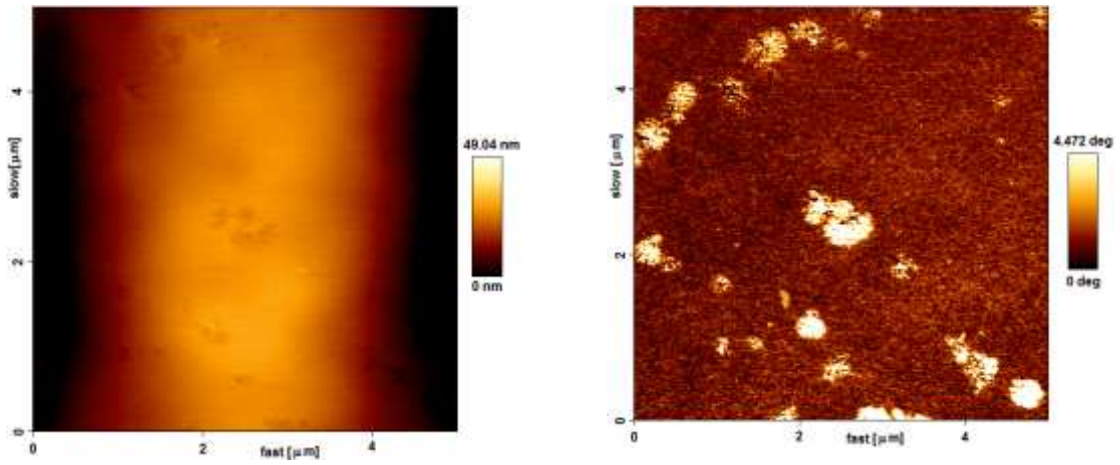

Figure 7.13: The TM-AFM images of the DF645 film coated at 120 ^{o}C and annealed for 4 weeks revealed the hard agglomerates (phase image, right) seemingly dispersing within the continuous adhesive film matrix. Scan size is 5 x 5 µm^{2}.

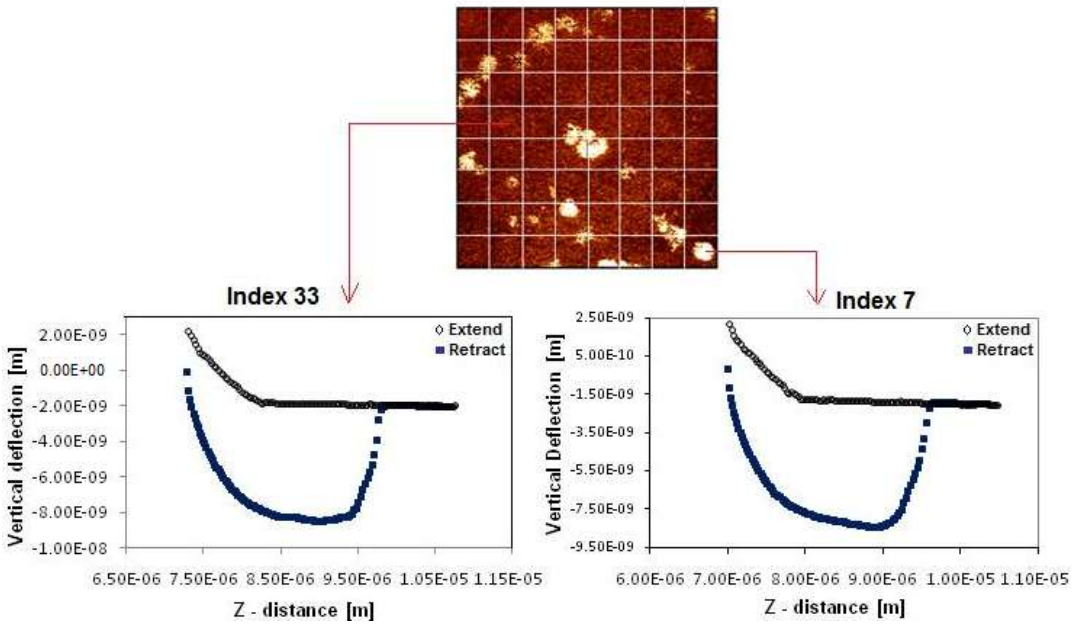

Figure 7.14: The grid lines on the phase image (Fig. 7.13) depict the film surface regions of discernible mechanical characteristics where the adhesion measurements were collected. The adhesion nature is very similar irrespective of film subsurface local region property.

The adhesive formulations are blend systems of high molecular block elastomers and polystyrenes, bulky oligomers of middle-block-compatible and endblock-compatible tackifiers and mineral oil. The molecular dynamic mechanisms resulting in the improved film morphology during the annealing could be caused by different relaxations and diffusion processes. Each of the different copolymer chain segments will for instance inherit a unique specific characteristic relaxation time and/or a diffusion process which would depend on the nature of the chain, the chain's environment and the annealing condition (temperature and time). Since the adhesive blends are polymer based, they appear to exhibit the characteristics of viscoelasticity relating to the time-temperature superposition principle[142]. This means that the adhesives annealed at a low temperature for a long time should behave similarly to those heated at higher temperatures for short times and melt-coated. The polymer chain dynamic relaxation is governed by an energy barrier that obeys Arrhenius relationship[350,351] according to,

$$k_i = Aexp\left(-\frac{E_a}{RT}\right) \qquad 7.1$$

Where k_i is the relaxation rate constant, A is the pre-exponential constant, E_a is the activation energy, R is the gas constant, and T is the absolute temperature. Since the elastomer chains are above their T_g, their segmental motions are on the time-scale of nanoseconds[351] and much faster than the relaxation times of the PS segments. With presence of resins diluting the elastomer entanglement network and the oil serving as a plasticizer, the polymer segmental mobility dynamics could this respect will not explicitly obey the relationship in Equation 7.1. In Chapter (Section 6.3.5), a couple of possible mechanisms resulting in the altered annealed film morphology are suggested.

For all the adhesion force curves collected, there was no evidence of any residual adhesive that might have come off the film surfaces and stuck to the cantilever tip during the measurements. TM-AFM images taken immediately after each F-D measurement revealed a slight alteration to the domain positions due to an inevitable thermal drift of the cantilever[279,349]. The images neither showed artifacts of repeatable uniform features typically associated with debris stuck to the tip[352]. Assuming there were adhesive residues adhering to the tip with the measurement as the sample's cohesive failure, there would have been tremendous differences in the force curve magnitudes from one grid region to the next, as more adhesive accumulated on the tip. The absence of such measurement artifact is taken as a good evidence of a strong sample cohesive strength. The tip-sample bond fracture was mainly caused by adhesive interfacial failure[353,354].

7.3.3 Quantification of adhesion force and thermodynamic work of adhesion

The adhesion force obtained at the tip-sample contact breakage can typically be calculated according to the following relationships;

$$F_{adhesion} = F_{pull-off} \quad 7.2$$

$$F_{pull-off} = k \cdot \delta_c \quad 7.3$$

Where $F_{pull\text{-}off}$ is the force exerted by the sample on the cantilever (which is equivalent to the force exerted by the cantilever on the sample, i.e. equalling to the adhesion force), k and δ_c are the cantilever constant and the cantilever deflection at the jump-out, respectively[252,261,279,348,349]. The above equations are valid if the debonding process is

considered purely elastic. Due to the viscoelastic nature of the adhesive samples, where sample plastic deformation contributed largely to the adhesion behaviour, a significant error will be introduced if the aforementioned relationships are implemented to quantify the adhesive peel force. For stiff materials with low surface energy, Derjaguin, Muller and Toporov (DMT)[355] have derived the mechanical contact between two bodies as,

$$F_{adh} = 1.5\pi R W_{adh} \tag{7.4}$$

$$W_{adh} = 2(\gamma_1\gamma_2)^{\frac{1}{2}} \tag{7.5}$$

Where γ_1 represents the sample surface free energy, γ_2 is surface energy of the of the substrate and R is a small contact radius in the nanometre range. The DMT theory is also based on continuum elastic theories and assumes smooth surfaces with no plastic deformation or viscoelastic phenomena. Forces acting between the contact bodies outside the contact surface are not taken into account in the elastic theories. These forces could be significant for the film adhesion behaviour due to the probable chain network system within the blend matrix. Perhaps a better adopted relationship for treating complaint adhesive materials is proposed by Sun and Walker[348]. Their contact relationship is based on Griffith's criterion and Sneddon's method where the Si tip is modelled as a hyperboloid according to,

$$\delta = \frac{aA}{2R}\left[\frac{\pi}{2} + arcsin\left(\frac{(\frac{a}{A})^2 - 1}{(a/A)^2 + 1}\right)\right] - \sqrt{\frac{2a\pi(1-\upsilon^2)w_o}{E}} \tag{7.6}$$

And

$$P = \frac{2E}{1-\nu^2}\left[\frac{A}{2R}\left[aA + \frac{a^2 - A^2}{2}\left(\frac{\pi}{2} + \arcsin\left(\frac{\left(\frac{a}{A}\right)^2 - 1}{\left(\frac{a}{A}\right)^2 + 1}\right) - a\sqrt{\frac{2a\pi(1-\upsilon^2)w_o}{E}}\right]\right]\right] \tag{7.7}$$

Where δ and P are the indentation and the load, respectively. R is the tip radius of curvature, A = R cot(α), where α is the tip's semivertical angle, ν is the Poisson ratio of the sample, E is the elastic modulus of the measured sample surface, a is the contact radius, and w_o is Dupre's work of adhesion. These equations require exact knowledge of the tip-sample contact radius, the cantilever spring constant and the modulus of the tip-sample contact region. In the standard AFM force-displacements curves used in these studies,

there is no direct way to deduce the contact area or indentation depth[279,,356] (Section 3.2.6). This is because;

- The contact surface between the AFM silicon tip and adhesive film surface will depend on the volume of sample or topological chain conformation that adheres to the tip [348,357].
- The soft adhesive sample will most likely buckle and wrap around the tip due to hydrophobic and viscoelastic forces[279], altering the contact area from measurement to measurement.
- Creep and hysteresis effects cause the tip to travel deeper into the specimen even after maximum pre-set applied load[279,358] and this would affect contact depth. Non-linear detector response is known to be another source of artifact that affects the tip-sample contact depth[358].

Another common problem that can affect the tip-sample contact area is that the tip is inclined at a small angle with respect to the direction perpendicular to the sample surface[359]. The ramification will be a larger contact area if the tip interacts with regions lying below the surface's x-y plane, as the side of the tip will touch the specimen first before the tip apex. This however will only generate larger variations in the values for each specific sample and do not influence the discrepancy across the different samples adhesion nature. Based on the above reasons, the adhesion force and work of adhesion determinations are based on the data obtained from the measurements and plotted as presented in the figures. The tip-sample contact area (tip radius < 10 nm) is very small and sample surface roughness could contribute to increase the adhesion force by increasing the contact area[197]. This has been accounted for in the discussions.

The values as measured and calculated from the F-D curves are presented in Table 7.1. The mean adhesion force $\bar{F}$ and the variance $\Delta F = \sqrt{\frac{1}{N}\sum_{i=1}^{N}(F_i - \bar{F})^2}$, with N being the number of force curves and F_i being the individual adhesion forces were determined, as well as the average adhesion energies. Though the absolute values should be considered semi-quantitatively within experimental error, the discrepancy between the samples is very meaningful. This lies in the fact that that same measurement conditions were applied to all the samples of a specific blend. In fact the only variable parameter was the film's processing history (coating temperature or annealed). Hence the eventual errors from the measurement are assumed to be consistent for all the samples. In Table 7.1, 7M8 films coated at 165^{o}C exhibit roughly a ~3 times improved adhesion force and a ~12 times

higher adhesion energy than when coated at 130^{o}C. After annealing the low-temperature coated film, there were ~3 times and the adhesion energy was ~8 times higher. For the DF645 series, the adhesion force is ~2.5 times higher and the adhesion energy is ~6 times better for film coated at 155^{o}C compared to films coated at 120^{o}C. After annealing the low-temperature coated film, the improvement in adhesion force and energy were twice as much. The standard deviations in the calculated values reflect alterations in the tip-sample contact area for reasons stated above. As the samples are commercial adhesives, no information is found in literature about AFM interaction with similar multi-blend systems. An attempt to identify specific mechanism of energy dissipation during the debonding will therefore involve some speculation.

It is anticipated that using different techniques to investigate the adhesion behaviour of different samples on a macroscopic scale should be equally the same as the investigation on a nanoscopic scale with AFM. In comparison with the peel test results for the 7M8 and the DF645 coated films to cotton fabrics, presented in Chapter 5, the peel force was ~ 4 times higher for 7M8 coated film at 165^{o}C than for the film coated at 130^{o}C. For the DF645 coated at 155^{o}C, the peel force was ~2.6 times higher than for the film coated at 120^{o}C. This suggests that the chemical adhesion contribution to the product's adhesive strength is significant, compared to the contribution from mechanical adhesion/interlocking which depends mostly on sample surface roughness[360].

The results presented in these studies strongly indicate very distinguishable strain energy dissipation mechanisms by the adhesive films during the tip debonding. As far this work goes no systematic studies have been published regarding the practical adhesion of plastically or viscoelastically deformable sample attached to a rigid/rough AFM substrate. Sun et al[348]., have mapped force-displacement curves on poly(dimethylsiloxane) at different ramp rates and tip-sample dwell times. With slower ramp rate and longer dwell time, they observed larger adhesion-induced indentation and an increase in hysteresis between the extension and retraction force curves. They attributed the observation to energy dissipation dominated by viscoelastic relaxation processes within the polymer bulk and polymer relaxation at the tip-sample interface. On the basis of discussions about macroscopic measurements of adhesive performance[23,211-216] it has been noted that the peel strength increases with increasing peeling velocity because viscoelastic losses within the bulk of the adhesive are controlled by the deformation rate. From the peel, tack, and shear tests, the viscoleastic losses with the formation of fibrils is assigned as the fundamental

reason for good peel behaviour (Chapter 2.6.3). The relationship between the thermodynamic work of adhesion, W_{thermo} which is determined with pull-off experiments[361] and the practical adhesion, W_{adh}, with peel, shear tests, etc., is $W_{adh} = W_{thermo} (1+\phi)$. The, ϕ, is a dissipation function depending on the test parameters (e.g. crack propagation, temperature, rate and adherend deformation) and adhesive bulk parameters (e.g. thickness and viscoelasticity)[211,214,217,218]. The observations therefore suggest that more efficient and faster energy dissipation mechanisms occurred within the high-temperature coated and annealed samples compared to the low-temperature coated films. Hence the molecular stress relaxations at the film surface and within the film morphology (of high-temperature coated and annealed) could be faster and more efficient.

As confirmed by the force curve plots (E.g. Figures 7.3, 7.6 and 7.12), it is apparent that the tip stayed in contact with the high-temperature coated and the annealed films longer than with the low-temperature coated films, until the tip-sample contact breakage. The tip jump-outs are also larger as seen in the plots. Since the tip is on the end of a complaint cantilever, a high pull-off is equivalent to a substantial cantilever bending during tip detachment. These observations reflect stronger intrinsic surface adhesion exhibited by the high-temperature coated and the annealed films compared to the low-temperature coated films. It is though not understood yet whether fibrilisation or cavitation of the sample preceded the tip jump-outs and contributed to the discrepancy in peel strengths as the investigation offered no means of visualizing the debonding mechanisms in real time at the nanometre range.

Table 7.1: The results from the AFM force-distance measurements presenting the quantification of the adhesion force and energy values.

Adhesive films	Amount of force curves	Average adhesion force, x $k^{(b)}$ [N]	Average work of adhesion x $k^{(b)}$ [Nm]
7M8 coated at 130°C	49	2.15 ± 0.14	1416 ± 226
7M8 coated at 130°C, and annealed.	49	5.83 ± 0.27	11406 ± 880
7M8 coated at 165°C	49	6.92 ± 0.76	16580 ± 2907
DF645 coated at 120°C	90	3.45 ± 0.1	5324 ± 242
DF645 coated at 120°C, and annealed.	49	6.34 ± 0.22	12058 ± 711
DF645 coated at 155°C	90	8.76 ± 0.17	33544 ± 1633

(b) Cantilever spring constant

7.3.1 Studies and discussions of the complex nature of the retraction force curves

7.3.1.1 Role of rubbery phase

The synergistic contribution from all the film subcomponents with corresponding relaxations of specific characteristic times all contribution to the adhesive strengths

measured for the different coated films. The probable stretching of the adhesive film during the debonding can be described by a thermodynamic balance between work of adhesion and the sample cohesive energy. Based on the results and explanations given above, a tentative effort is made to explain the roles of surface chemical nature, the film hierarchical structure and block copolymer chain dynamics behind the intricate nature of the debonding processes.

The adhesive films are highly hydrophobic consisting mainly $–CH_n-$ groups. The Chemical group analysis with ToF-SIMS presented in Chapter 6 revealed similar chemical nature on the surfaces of the adhesive films irrespective of processing thermal history. This is not a surprise given the fact that each PSA sample series are of the same blend formulation. The tip used for the force measurement was made of silicon (Si) atoms. When exposed to air, Si is known to form a thin layer of silicon dioxide (SiO_2) at the Si-air interface[357]. Hence charged SiO^- groups can exist on the Si tip surface, but their contribution to adhesion as electrostatic attractive forces should be minimal as no charged groups were used in the blend systems. Hydrogen (H) bonding is not expected at the tip-sample interface, as H must be directly bonded to one of the atoms with high affinity for electrons such as oxygen (O), nitrogen (N) or fluorine (F) for the force to be in effect. Van der Waals forces are assumed to be dominant for the tip-sample attraction[357]. Meniscus forces generated by thin layer of water found on most surfaces have been reported to contribute to adhesion forces[279]. The presence of water layer should be consistent for the samples under the same measurement conditions and moreover earlier studies have reported that the adhesion force of a hydrophobic surface is independent of the air humidity[362].

In mixtures consisting of dangling polymer chains in the solution, steric forces have been reported to contribute to the surface adhesion forces. Steric force[279] arises when a rigid surface is pressed against a surface of dangling polymer chains. The rigid surface can confine the dangling chains in a well-defined volume creating a repulsive entropic force, “steric” or “overlap” force. These forces could be in effect at the tip-sample interfacial contact. On the basis of qualitative considerations of solubility parameters, the release of PS segments into the film matrix at higher temperature due to the decrease in segregation power is assumed to increase the rubbery concentration in the matrix. This is because of the triblock structure and the outcome could be stronger steric forces for films coated at higher temperatures and annealed than films coated at low temperatures.

Three models are proposed to describe the adhesive peel nature observed with the force-distance measurements. The Models are postulated with support form the phase transition observations in Chapter 5, the film morphologies presented in Chapter 6 and information about copolymer physical network systems found in the literature[99-105,147-151]. The adhesive systems are hypothesized to be semi-interconnected, i.e. there are sections within the films where PS domains acting as physical crosslinks are interconnected with the elastomer chains into a network and there are sections where the domains are effectively isolated. Based on the results presented in Chapter 6, there appears to be a higher fraction of inter-connected network system within the high-temperature and annealed films than within the low-temperature coated films. What dictates the interconnection are the domain spacings and the presence of polydiene, as hypothesized in Chapter 6.

The illustration depicted in Figure 7.15a, Model A depicts an adhesive film-morphology with higher fraction of effectively isolated PS-rich-copolymer domains. This is due to the relatively larger domain spacing making elastomer bridging thermodynamically unfeasible (Chapter 6). Such a system is presumed to be dominant within the low-temperature coated films of the DF645 and 7M8 adhesive blends. When the film matrix is subjected to the cantilever force, the stress dissipation can mainly occur through friction and slippage of the elastomer chains and possibly resin conformer re-organisations at the strained region. The stresses are therefore largely localised due to the lack of long-range network system. Assuming an absence of other molecular mechanisms for energy dissipation, the mechanical energy absorbed by the sample system from the cantilever and stored reversibly will be relatively low until the maximum threshold limit is reached. The sample will then detach from the probe as a result and relatively low adhesion force and corresponding adhesion energy are measured in effect.

In Model B (Figure 7.15b), a film morphology is depicted where the abundant presence of phase separated PS-rich-copolymer domains enable domain inter-connections by elastomer chain bridging[94] and adjacent loop entanglement interactions. Since the film matrix is dominated by the domain-interconnection, it is assumed that the independent network deformation of the matrix system in the proximity of the tip-sample contact region can be distributed over a macroscopic region. When the film surface layer is stressed during the tip withdrawal, the mechanical energy can then be transmitted primarily along the elastomer chains from a domain junction to the other over the wider film matrix area. The energy dissipation mechanism within a system of Model B would be highly efficient as

more units are involved in the several relaxation processes. Even though rubbery chains in the surroundings of the rigid PS domains are restrained from easy mobility since denser crosslinked polymer networks are known to lower the mobility of the chain segments[363] , perhaps the dilution effect of the resins still imparts large freedom of motion to the elastomers, giving them short relaxation times and overriding the confinement effect of the rigid nano-domains. As such the rubbery chains at the film's near-surface could still exhibit quicker relaxations and contribute to the efficient energy dissipation within the high-coated and annealed film samples.

In a system lacking suitable inter-domain distances thermodynamically feasible for elastomer chain bridging, the presence of resin-diluted polydiene-induced PS dangling chain ends are speculated to contribute to the domain inter-connectivity, as illustrated in Model C (Fig. 7.15c). This could occur since the polydiene elastomer segments might not undergo chain loop by back-folding[94] due to the already decrease in entropy of the restrained free rotation caused by the π-π bonds. This phenomenon was postulated in Chapter 6 for the DFC600 blend system where the adhesive peel is relatively good even for the low temperature-coated film. The DFC600 system did have the highest polydiene content in the blend formulation.

a

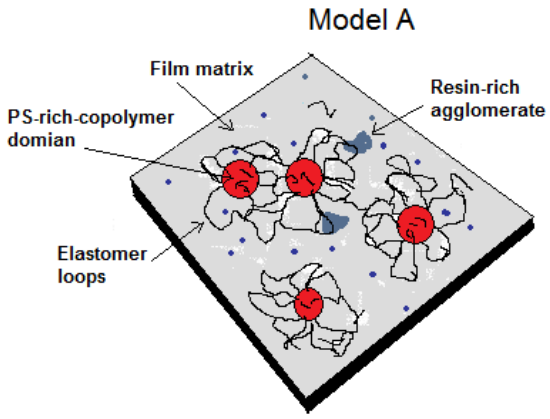

b

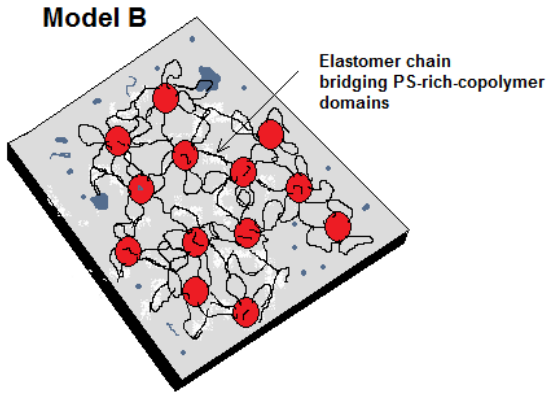

c

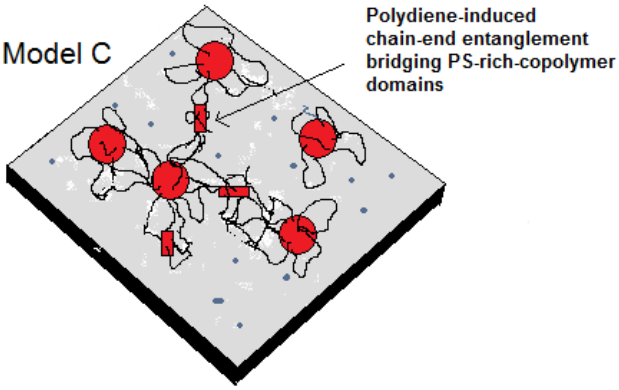

Figure 7.15: Schematic illustration depicting (a) the pre-dominant network architecture of the adhesive matrix of low temperature-coated film, (b) the predominant matrix of high-temperature coated and annealed films. In (c) polydiene--induced dangling PS chain-end entanglements contributing to the network system by inter-connecting the nano-domains at distances energetically unfavourable for elastomer chain bridging.

From the observations made of the samples coated at low temperatures (7M8 at 130^{o}C and DF645 at 120^{o}C), the force curve trends suggest inefficient energy dissipation mechanism as the cantilever probe detach from the film surface at relatively short piezo withdrawal distances. The tip jump-out process also appeared to occur as a gradual detachment (especially for 7M8 coated at 130^{o}C, Fig. 7.3) rather than a large sharp discontinuity as seen for the high-temperature coated and annealed films. The central arguments drawn is that the film surface possibly elongated by fibril formation or single elastomer chain extensions due to the film matrix's system inability to dissipate the contact region stresses over a wider area. As the piezo exerted further pulling force and the tip-sample distance increased, the viscoelastic force of some of the film layer or single matrix chains tethered to the tip became larger. In such a case the tethered sample would longer adhered and consequently detached from the tip (first multistep level of pull-off part). The outcome was be a new equilibrium position (horizontal line, Fig. 7.3) for the cantilever, but the tip was still a distance away from the initial zero-force horizontal start position since as some sample was still attached to it. The process went on until the spring constant exerted by the piezo-cantilever exceeded the gradient of the intermolecular forces between tip and sample. The tip would then detached from the sample and bounced back to its initial zero force line, for the next f-d curve in the next region (Index) to be collected.

Similar observations have been reported by Portigliatti et al[364]., about the adhesion behaviour between an AFM tip and single latex particles. They discovered that upon retraction of the tip, viscoelastic and plastic energies were dissipated in a volume, which could extend to several neighbouring particles. If the stress could not propagate to the neighbouring particles, it was dissipated by the pulling out of filaments from the particle, which was indicated by multiple tip jump-outs in the force-displacement curves. Ortiz et al[397]., measured the entropic elasticity of poly(methacrylic acid) by stretching the polymer chains with an AFM tip and they reported similar multistep retraction curves assigned to the lengths of the stretched chains. The observations made in these studies suggest that the 7M8 sample coated at low temperature inherit discernible local adhesion nature. When the tip interacted with the regions where one-step pull-off was observed (Fig. 7.3), it is assumed that the film layer or single chains detached simultaneously. The fundamental film subsurface morphology (Chapter 6) that underpins strong adhesion characteristics was inefficient in dissipating the strain energy as depicted in Model A (Fig. 15).

For the high-temperature coated and annealed films (Figures 7.6, 7.10, 7.12, 7.14) the cantilever tip demonstrated an abrupt one-step detachment process with larger pull-off forces. The observation manifests uniform and homogenous nature of the film surface layers which interacted with the Si tip at the contact regions. During the debonding processes of these films from the tip, the matrix chains binding resins/oil act in synchrony as a result of the predominant interconnections, as explained with Model B (Figure 7.15b). It is further assumed that more elastomer chains exist at the coated film surfaces due to the higher PS micelle/μm^3 amounts in the films (See Chapter 6, section 6.3.4 and 6.3.5), and that the elastomer chains are relatively more entangled. The rationale is based on the notion that, each self-assembled PS-rich copolymer domain will have a certain amount of elastomer chains in its surrounding[94]. With a fixed film free volume, the best way for efficient packing in a confined space would be through entanglements, resulting in a finite length of the network chains.

As piezo retraction proceeded the extension of the entanglements is successfully trapped which meant large sliding of the chains across each other is prevented. The Si tip was effectively held firmly and larger cantilever deflections were observed (Figures .6, 7.10, 7.12, 7.14) with the piezo retraction. This perhaps also explains the higher intrinsic adhesion of the films surface of high-temperature and annealed samples. The cantilever force exerted on at the local contact region was further dissipated through the interconnections. As the piezo retraction proceeded further, it got to a point where the strain energy exerted on film matrix chains reached a maximum. The network chains between successive entanglements could then be stretched fully. The repercussion was simultaneous breakage of the tip-sample contact and the tip bounced back in a one-step elastic-like nature to the initial zero force line for the next force measurement to take place. Oesterhelt et al[365], have reported about how single strands of poly(ethylene glycol) in water were pulled by the AFM. They stated that that the water molecules were likely to form fluctuating intramolecular bridges, shortening the net polymer length and making them resist substantial extension during the tip retraction process.

7.3.1.2 Role of PS domains

Although the rubbery/resin/oil film matrix surfaces establish the direct contact to the cantilever tip, the dissipation of the large strain energy during the tip debonding processes would be majorly controlled by the polystyrene-rich regions. Hence it is also important to

consider the stress distribution from the PS perspective. The amount and nature of the phase separated PS-rich-copolymer domains are acknowledged to be essential for the film's cohesive force and peel resistance. In styrene-elastomer based thermoplastic gel systems, the authors reported the presence of imbibed rubbery/oil within PS phase-separated micelles[103-105]. This in effect will have an impact on the property of the domains functioning as physical crosslinks for the rubbery matrix.

By implementing models of rubber elasticity (Section 2.5.1) Schlegel et al.[154], characterised the stress-strain behaviour of a multi-graft copolymer of PS and PI. They reported that if the PS domains were ordered in homogenous lamellae or cylinder phases enclosed by a PI phase, the stress distribution within the PS phase would be homogenous and highly efficient. If the PS regions were disordered due to the presence of imbibed PI serving as local stress maxima points, they became very sensitive to stresses and failed easily. A similar phenomenon could unfold within the adhesive samples. The more uniform the domain cores are, the better they will function as stress distributing junctions during film debonding process. For the films coated at high temperatures, the distinct T_g peaks attributable to the PS domain relaxation observed in the DMA measurements (Chapter 5) support this view. The smaller domain sizes revealed by the AFM phase images (Chapter 6) partly reflects an improved chain ordering within the PS-rich-copolymer domains of high-temperature coated and annealed films. The films coated at lower temperatures with larger nano-domain sizes and diminished T_g (PS) insinuates a relatively heterogeneous domain nature with potentially poorer stress distribution ability.

The wisdom from these results is that the debonding process is comprised of viscous and elastic parts coming from both, the adhesive soft matrix of elastomer/resins/oil and the glassy PS-rich-copolymer domains. The contribution of the viscous deformation alone has to be considered in two ways, firstly the PS phase due to local exceeding of the yield stress, and the matrix elastomer chains. The elastic part can be expected firstly from the contribution of the elastomer phase due to the chain bridging of the glassy nano-domains and the interconnections by possibly the polydiene-induced entanglements. The glassy nano-domains serve as obstacles to the viscoelastic flow of the matrix phase during the debonding process. An increase of the obstacles can be expected firstly by an efficient distribution of the PS-rich-copolymer domains as explained in Chapter 6, and also by the PS undertaking different thermodynamic feasible phases as a result of variation in its local

concentration. 7M8 coated at 165°C has actually displayed very high peel strength values (not shown here)[366], probably as a result of the higher styrene content in the formulation.

7.3.1 Elastic modulus determination of thin coated films

The use of nano indentation to measure mechanical properties can be related to the contact theory originally considered in the 19th century by Hertz[367] and Boussinesq[368]. Hertz analysed the problem of the elastic contact between two spherical surfaces with different radii and elastic constants. Boussinesq developed a method based on a potential theory for computing the stresses and displacements in an elastic body loaded by a rigid axisymmetric indenter. A development of Boussinesq's work has been contributed by Sneddon[369] where he derived general relationships between the load, displacement, and contact area for any punch that can be described as a solid of revolution of a smooth function. Oliver and Pharr[370] made a critical improvement to the indentation technique, who applied Sneddon's method to determine the contact area at maximum load and function of unloading depth.

For the elastic modulus determination, the tip is allowed to penetrate into the sample, where both elastic and plastic deformations occur. Plastic deformation will make the sample conform to the indenter shape up to the contact depth h_c, as illustrated in Figure 7.17a where h_{max} is defined as the maximum indentation depth and h_s the elastic displacement or sink-in depth[371,372]. During the tip withdrawal from the sample surface, the first phenomenon that occurs is the elastic recovery of the zone near the contact area. The gradient S (Fig. 7.17b) of the initial portion of the unloading stiffness curve provides the elastic parameters for the sample. The relationship of moduli obtained from an indentation measurement by a rigid indenter is[369-372,]

$$\frac{1}{E_r} = \frac{1-\nu_i^2}{E_i} + \frac{1-\nu_s^2}{E_s} \qquad 7.8$$

Where E_r is the reduced modulus, E_i and ν_i are the Young's modulus and Poisson's ratio of the indenter, and E_s and ν_s are the same parameters for the sample. For samples that are much softer than the indenter, $E_i >> E_s$ and the above equation can be rewritten as:

$$E_s = E_r \cdot (1-\nu_s^2) \qquad 7.9$$

a b

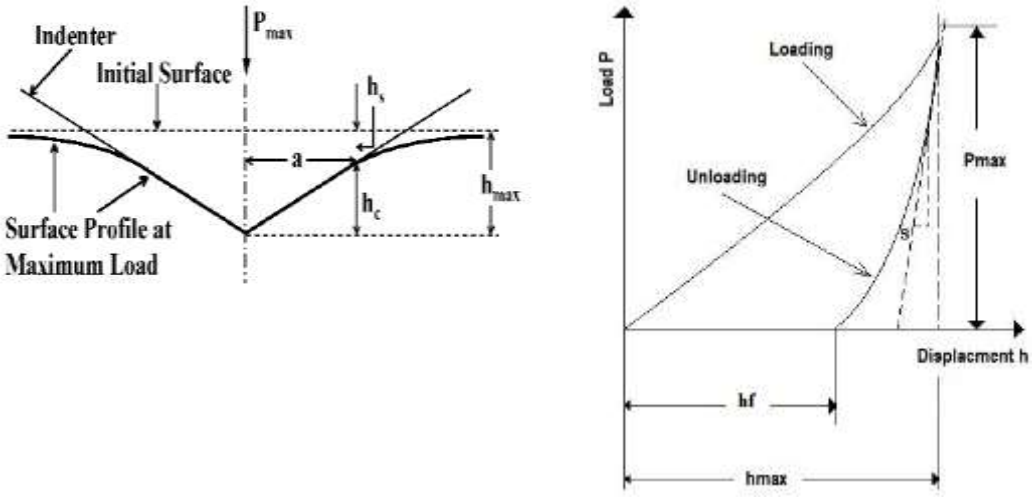

Figure 7.16: Sketch of (a) the indentation profile of the AFM tip, and (b) loading and unloading curves including the elastic contact slope, S and final depth hf[371].

The constituents of the adhesive blend that exhibit a viscoelastic property are mainly the triblock copolymers, hence value for Poisson's ratio has been chosen as 0.4 which is between that of 0.35 for rigid polymeric material like polystyrene and 0.5 for elastomers[373]. According to the Sneddon's theory of the punch of a hard indenter on a deformable surface, E_r is directly proportional to S between the tip-sample contact area of the unloading curve at the maximum load P and indentation depth h_c as[374,374,375,376]:

$$S_{(i)} = \frac{dP_{max}}{dh_c} = \frac{4\sqrt{R_C}}{3} E_r \, {\Delta h_c}^{1.5} \qquad 7.10$$

Where R_c is the radius of curvature of the tip if the apex is assumed to be parabolic, h_c, is the height of the penetration contact depth and $S_{(i)}$ depicts S for each indentation measurement i. A correlation of the S factor is required due to the bending of the cantilever itself, through the relationship[377],

$$S_{conv.} = \frac{S_{cantilever} S_{sample(ij)}}{S_{cantilever} - S_{sample(ij)}} \qquad 7.11$$

$$S = S_{conv.} K = \frac{S_{conv.} \cdot k}{S_{cantilever}} = \frac{k \cdot s_{sample(ij)}}{S_{cantilever} - S_{sample(ij)}} \qquad 7.12$$

Where $S_{cantilever}$ is the slope measured on the non-deformable silicon substrate, to obtain the deflection of the cantilever. $S_{sample(ij)}$ is the slope for measurement point *i* of each sample surface *j*, *k* is the cantilever spring constant and has already been determined exactly to be 17 N/m (See Section 3.2.6.2). The *K* (nN/nA) is a conversion factor and comes about because the Nova software (NT-MDT, Russia) records the vertical axis of the load in nano-amps (nA) and this value has to be converted to nN according to[377,378],

$$K = \frac{k}{S_{cantilever}} \tag{7.13}$$

The force values are then multiplied by *K* to convert them from nA to nN. Since the adhesive sample is assumed to buckle around the tip with a potential sample pile-up (i.e. when material is forced up along the sides of the tip) due to the soft nature of the film surface, h_c is determined as[376,379],

$$\Delta h_c = \Delta h_{sample} - \Delta h_{tip} \tag{7.14}$$

Where Δh is the penetration depth between maximum load and tip-sample contact point. Fifteen indentation measurements on each sample surface were collected and the values are comprised in Table 7.2. The Shear elastic modulus *G'* is finally determined according to[382,]

$$G' = \frac{E_s \cdot 2(1-v)}{3} \tag{7.15}$$

It must be stated that the Sneddon theory used for the elastic modulus quantification describes an infinitely hard indenter with a special geometry and a flat, deformable substrate. The JKR model[279,380] registers a better insight into nano-mechanical evaluation of adhesives since the model is suitable for highly viscoelastic systems with low stiffness and indenters with large tip radii. The relationship between the applied load, P, and the contact radius, r_a is determined as,

$$\frac{r_a^3 k}{R} = P + 3\pi\sigma R + \sqrt{6\pi\sigma RP + (3\pi\sigma R)^2} \tag{7.16}$$

Where k is the elastic constant, σ is the surface energy and R is the radius of the indenter. Due to limited research time and available funds there was no opportunity for accurate

determination of the surface energy and hence the implementation of the JKR model. Error with the quantification of the elastic modulus will arise from the definition of the initial points of the unloading slope since data points were missing for reasons given earlier. The unique nature of the blend systems and further uncertainty with the determination of the indentation depth makes it unreasonable to compare the values obtained in this work with values found in the literature. Wensheng et al.[378], have reported G' values of 4.27 MPa for polybutadiene surface and 1000 MPa for polystyrene, obtained by nano indentation studies with AFM. The values presented in this work are expectedly much smaller since the specimens are not homopolymer systems.

Table 7.2: Quantification of the elastic moduli for DF645 adhesive coated films.

Sample DF645	Slope S [nN/nm]	Youngs Es [KPa]	Shear G' [KPa]
Film coated at 120^{o}C	4.46 ± 0.34	16.8 ± 0.4	6.7 ± 0.4
Film coated at 155^{o}C	7.24 ± 0.84	11 ± 1.5	3.9 ± 0.6

The film coated at 155^{o}C appears to exhibit an easier deformable surface than the film coated at 120^{o}C. Crosby and Shull[381] suggested in their work that for an adhesive to show outstanding bonding properties, a large average molecular weight between entanglements (M_e) for the base elastomer is required, and this value is inversely proportional to the plateau elastic modulus G'(modulus at end-use condition). Other studies have also highlighted this relationship[23,176,208]. The film surfaces have proven to be rubbery-rich, as evidenced by the phase images (Chapters 6) and the force curves not directly relating to the phase-separated regions characteristics (7.3 to 7.13). In contrast, it is worthwhile to mention that the tensile and the dynamic storage moduli measurements presented of the bulk adhesives annealed at the different temperatures for coating the films do not show such an obvious difference. This may further support the notion of discernible properties of the films and the corresponding bulk samples.

7.4 Summary

The studies presented in this Chapter have provided new and important structure-and-adhesion information of copolymer-based pressure-sensitive adhesives (PSAs) on a highly local scale. With the implementation of an atomic force microscope (AFM), it has been possible to perform straightforward adhesion investigation of pristine commercial adhesive

surfaces. The ability to use the same AFM probe for sample imaging combined with the capability to switch back and forth from the imaging to force mode measurement allows a straightforward identification of the film's local morphology and adhesion properties.

The work has demonstrated that desired bonding and debonding of PSA:s based on styrenic triblock copolymers are dominated by the viscoelastic characteristic of the coated adhesive film even on a local bonding region on the nanoscale range. Though the AFM tip appeared to have interacted directly with the films' rubbery/resin/oil-rich near-surfaces, the fundamental characteristics governing the adhesive bonding nature involves the synergistic effect of mainly the film's subsurface morphology. This effect consists of;

1. The abundance of PS-rich-copolymers domains dispersed within the adhesive continuous matrix and function as physical crosslinks.
2. The inter-connections of the domains by elastomer bridging if the domain-spacing allows elastomer bridging without entropic penalty.
3. The inter-connections of the domains by resin-rich polydiene-induced PS-rich dangling chain ends through entanglement junctions with similar neighbouring chains. These entanglement inter-connections might occur even at domain-spacings thermodynamically unfeasible for elastomer bridging.

The inter-connected network system when extending over a larger film area is profoundly vital for the energy dissipation within the coated film when the film is subjected to external stresses. The force-distance curve measurements with AFM cantilever tip have conclusively verified adhesive strength superiority by films coated at high temperatures, where much higher adhesion forces and larger adhesion energies were obtained in comparison with corresponding adhesive films coated at lower temperatures. This is due to the inter-connections dominating the stress distribution mechanism within the high-temperature coated films. In the low-temperature coated films where there appears to be a higher fraction of PS-rich-copolymer domains effectively isolated due to the low domain presence, the film's ability to distribute internal stresses is deteriorated significantly and the adhesive peel strength is suppressed as a result.

When the low temperature coated films were annealed at 40^{o}C for 4 weeks, the adhesion property improved tremendously, almost equalling the adhesion force and adhesion energy values measured for the films coated at high temperatures. The long time annealing seems

to have promoted the self-assembly of the PS-rich-copolymer domains and hence the re-establishment of some inter-connected network system.

Adhesive film surface modulus measurement with an AFM nano indentation technique proved that films coated at high temperatures exhibit a lower surface modulus than films coated at low temperatures. Such property suggests that the high-temperature coated films could exhibit rubbery chains at the near surface with shorter relaxation times to release internal stresses probably due to a better dilution of the resins within the rubbery phase.

Chapter 8

8 Conclusion and future work

8.1 Conclusions and Future work

8.1.1 Conclusions

Adhesion is a surface physico-chemical phenomenon and can be briefly determined by two factors. The first factor is the energy of the deformation of the viscoelastic adhesive, which comes into play until rupture or separation occurs from the bonding to substrates. The second factor is that the two bonding surfaces must be brought into contact with each other for molecular attraction forces to come into play (wetting). This responsibility partly lies with the surface nature of the substrate and the interaction of the adhesive with the substrate. In this research work a systematic investigation of the properties of coated films of different commercially available pressure-sensitive adhesives (PSAs) has been carried out. This has been done in an attempt to understand the underlying factors that govern the adhesion performance from macro- to nanoscale. For comprehensive knowledge of the viscoelastic behaviour and optimization of the adhesive's performance, one must understand and inter-relate the complex physics occurring at each scale level during end-use. The adhesive systems utilized in this research were multi-component blends where contradicting effects of the some of the blend components and close T_gs made it difficult to instantly identify patterns of subcomponent compatibility. Nevertheless the results obtained are enlightening and suggest that adhesive films with different thermal histories exhibit distinguishable peel performance even on bonding areas on the nanometre scale. The conclusions from the studies are:

- **Hierarchy of surface structure of PSA films.**

With TOF S–SIMS, the uppermost surfaces of the PSA films were characterised on a macroscopic scale of 250 x 250 mm^2. The results have shown from a chemical group

standpoint that adhesive films of the same blend system exhibit similar chemical groups on the film surfaces irrespective of the film's preparation thermal history. Relative ion peak intensities suggested an enrichment of the rubbery/resin/oil matrix on the uppermost film surfaces, presumably driven by molecular surface energetics. Subtle discrepancies in peak intensities indicated more enrichment of the aforementioned on the surfaces of films coated at high temperature or annealed compared to low temperature coated films.

Beneath the near-surface tapping mode (TM) AFM revealed adhesive film morphology of phase-separated micro-sized agglomerates coexisting with nano-sized domains within the soft coated film matrices. The micro-sized agglomerates seemed to be residual resin-rich regions and partitioned block copolymer aggregates. The nano-sized domains were PS-rich-copolymer self-assembled domains. The micro-sized agglomerates were found within the coated films of the DF645 and 7M8 blend systems, but were non-existent in the coated films of the DFC600 blend system. For the 7M8 coated films, the matrices comprised of both spherical- and small rod-shaped PS-rich-copolymer domains and this was expected given the highest styrene content in the 7M8 blend system.

- **Multi-component self-assembly, phase transition and separation.**

The results from the viscoelastic property investigation with DMA were consistent with the AFM film morphology observation. For the coated films of all the blend formulations, two major phase transition peaks were observed. A conspicuous T_g peak observed at low temperatures (~ -11^oC) for the thermal relaxation of the adhesive rubbery matrix and a T_g peak (~100^oC) indicative of the thermal relaxation of the PS-rich-copolymer domains. In the case of the 7M8 and DF645 films there were further weak peaks which could be the thermal relaxations of the micro-sized agglomerates. The tan δ peak heights of the adhesive matrix T_g of both high- and low-temperature coated films of the DFC600 blend system were the lowest of all the adhesive samples. This suggests a relatively dominant elastic-like film matrix nature during the thermal transition. The observation has been attributed to the high polydiene content in the DFC600 formulation which is envisaged to promote the elasticity of the adhesive coated films.

- **Adhesion at nanoscale with corresponding nanostructure, viscoelasticity and elasticity.**

Adhesive peel strength measured with an AFM force-distance method explicitly showed that the coated films exhibit distinguishable peel properties even on nanometre scale

bonding contact areas. The films coated at high temperatures displayed superior adhesive peel strengths compared to the equivalent adhesive samples coated at low temperatures. The stronger intrinsic adhesion of the high-temperature coated films is assigned to the synergistic effect of:

1. Inter-connected network system whereby elastomer chains binding oil and resin molecules connect the PS-rich-copolymer domains either through chain bridging and entanglement junctions due to high domain number density and short inter-domain spacings. This morphology majorly governed the energy dissipation within the coated films during the debonding by transmitting the peel-off stresses over wider film areas.
2. Improved dilution of resins within the elastomer phase which could result in quicker stress relaxations of the rubbery chains. The lower surface modulus measured for high-temperature coated films compared to low-temperature coated films could be the result of this phenomenon.

The relatively low presence of PS-rich-copolymer domains found within the low-temperature coated films is envisaged to generate film morphology with low fraction of domain inter-connected network. The outcome is a suppression of the film's ability to distribute internal stresses efficiently. Therefore low adhesion peel forces and adhesion energy values were measured for the low-temperature coated films. After long-time annealing of the low-temperature coated films, the adhesive peel performance improved significantly. This was due to the improvement of the film morphology that was reminiscent of the high-temperature coated film morphology.

- **The effect of temperature on film morphology and adhesion**

The adhesive film morphology and subsequently peel characteristics is strongly connected to the film's processing thermal history. In the case of DF645 and 7M8 blend formulations, the aforementioned microphase-separated agglomerates were bigger in sizes and higher in presence within the films coated at low temperatures compared to the films coated at higher temperatures. When the low-temperature coated films were annealed, the agglomerates appeared to disperse into and acquire similar mechanical characteristics as the film matrix. The agglomerates were not found within the films of the DFC600 blend system and it is concluded that the high concentration of polydiene segments enhanced the

rubbery miscibility with the resin agglomerates, which could facilitate the PS domain self-assembly.

On the nanoscale the formed PS-rich-copolymer domains were abundant, smaller in diameter and with short domain spacings within the continuous matrices of the high-temperature coated films. Within the films coated at low temperatures, the nano-domains were much fewer, bigger in sizes and with larger inter-domain spacing. The discrepancy in adhesive film molecular architecture was a combination of;

- The film preparation process which involved melting at high temperatures and quenching to ambient temperatures, thereby preserving the formed morphologies at the melt sate.
- The segregation power, χN, between mainly the PS and the rubbery phase. Since N is fixed in the adhesive blends, the, χ, which is inversely related to temperature crucially contribute to the domain self-assembly.

There seems to be a competition between maximising the reinforcement of the PS-rich-copolymer domains in terms of their number and surface areas (they function as physical crosslinks) and maximising the adhesion in terms of large a volume ratio and contact surface of the multi-component rubbery matrix. The adhesive reached an optimised balance easily when coated at high temperatures. The long-time annealing improved the film morphology and adhesion of the low-temperature coated films. The copolymer-based PSA formulations inherit the characteristics of viscoelasticity, showing the time-temperature superposition principle. This means that the adhesives annealed at a relatively low temperature for a long time should behave similar to those heated at a higher temperature for a short time.

The morphology and peel behaviour for the DFC600 films did not depend as much on coating temperature compared to the 7M8 and DF645 samples. It was probably due to the improved compatibility between the polydiene-enriched elastomer phase and the alicyclic resins presumably via Van der Waals attractions. The polydiene could further promote the physical interconnections of the PS-rich-copolymer domains through entanglement-junctions of adjacent chains. Since double bonds are restricted from freedom of rotation around the σ-bonds, substantial entropic penalty could arise if the polydiene-elastomer chains underwent further restraint by back-folding into loop conformations. It is believed that the system would rather choose to form dangling chain ends where PS end blocks

would extend into the rubbery film matrix to gain some extra translational entropy. Therefore nano-domain inter-connections could occur easier as a result of a large volume of entangled dangling chain ends within the film matrix, resulting in a wider network system. Even when the DFC600 was coated at low temperature, its peel force was roughly 3 times higher than that of the low-temperature coated films of the 7M8 and DF645 blend systems.

- **The role of the end-block tackifier and the optimization of the PSA formulation**

Though the location of the endblock tackifier resin within the film matrix and its involvement in the self-assembling of the PS domains could not be directly confirmed, the alteration of the tackifier was found to have an effect on the structure and properties of the adhesives. In the case of the 7M8 formulation where higher content of a styrene-based resin was used, the adhesive film was found to be very sensitive to the coating temperature. The adhesive peel strength deteriorated significantly if the coating temperature was not high enough to enhance the mobility of the PS chains and facilitate the self-assembly of the nano-domains. It is assumed that if the resins are enriched at the PS and rubbery matrix intermixed interface, the phase-separated interfacial property will improve and the energy dissipation during a debonding process will be enhanced. Factors that facilitate the formation of the physical crosslink network system like for instance the introduction of components like the polydienes or thermal energy to promote the PS-rich-copolymer self assembly, the peel strength of the coated adhesive film will be improved.

- **Novel combined techniques for characterising PSA coated films**

In Chapter 4, classical mechanical property investigations performed on adhesive bulk samples with different thermal histories suggested that though the temperature effect is not as crucial on the mechanical characteristics of the bulk adhesive, it is extremely significant on the properties of the corresponding coated films. The possibility to directly measure the properties of the coated films is paramount to the adhesive industry. The investigation of the viscoelastic behaviour of the adhesive coated films with DMA by enveloping the soft thin films in steel material pockets proved very successful. The method allowed the determination of the transition temperatures but did not permit a quantitative measurement of the complex dynamic modulus due to the high stiffness of the pockets.

The studies also provided new and important structure information about adhesives on a highly unexplored scale. With TM-AFM, it was possible to perform a straightforward morphology investigation of the tacky pristine adhesive surfaces. The technique demonstrated that height images do not necessarily reflect the real surface topography of soft adhesive samples. The phase images do give a true account of the film morphology and it is a quick way to investigate the quality of the blending process and partly predict product end-use performance.

AFM force-distance measurement also highlighted a quick way of investigating the microscale and nanoscale adhesive peel properties with no specimen pre-treatment, as required with other techniques.

8.1.2 Future work

There are a couple of avenues that lays the foundation for future studies based on the results presented in this thesis work. No doubt each of the formulations studied could be manipulated to maximise one or more adhesive properties and that for each blend studied, the optimal formula will probably be different. This will however require time and tremendous amount of work. Naturally an adhesive blend could be prepared with a triblock copolymer consisting of three incompatible blocks such as ABC in a B selective solvent. Such a system is assumed to generate very high fraction of B elastomer chains bridging phase-separated A-rich and B-rich domains, resulting in a film with profound elastic-like properties at end-use condition. The ability of the rubbery chains to bridge the rigid PS-rich-copolymer domains in addition to entanglements is postulated to contribute largely to the peel performance of the tackifier-promoted adhesive films. Future studies could therefore be directed towards investigating the fraction of for instance elastic chains which are elastically active (i.e. bridging PS domains).

8.1.2.1 Dynamic viscoelastic studies of the network system

For all the bulk samples annealed at the different temperatures in Chapter 4, an elastic plateau modulus was observed at the low frequency (long times) range indicative of network structure as reported in earlier studies[123]. It is known that ordered copolymer melts exhibit non-terminal relaxations on a time scale longer than the longest relaxation time of an individual chain. Therefore, the shear modulus in the low-frequency reflects the

material's microstructure adopted at a given thermal history[223]. It would be interesting to find out the plateau modulus at the low frequency regime for the thin adhesive coated films. Thin films can be prepared and piled up to the equivalence of ca 2mm. The adhesive samples can be annealed for approximately one hour each at the different coating temperatures and then quenched in liquid nitrogen or ice/water slurry to freeze the morphologies developed at the molten state. Two sets of measurement protocols can be followed; (1) amplitude strain sweep to ascertain the linear viscoelastic region and (2) frequency sweeps at different fixed temperatures to study the relaxation characteristics of the molecular architecture of the triblock copolymer based systems. Such information would be useful in defining optimal film annealing condition.

In the studies by Derail et al[123] they reported that the low frequency plateau modulus decreased with the volume fraction of isoprene in an SIS/SI system. The samples behaviour at the lowest frequencies was reported to correspond to the relaxation of the polyisoprene of SI trapped in an SIS network. The plateau modulus is known to scale linearly with the reciprocal of the molecular weight between entanglements, M_e ,according to [382]

$$G_N^o = \frac{4}{5}\frac{\rho k T N_A}{M_e} \qquad 8.1$$

Where *k* is the Boltzman's constant, ρ is the polymer density, N_A is the avogadros constant and T is the temperature in Kelvin. The value of M_e can give an insight into the resin compatibility with the rubbery phase and reflect the dissipation power of the elastomeric phase.

8.1.2.2 AFM morphology studies of the network system

Scanning force microscopy (SFM) has been applied to detect in situ conformational transitions of single polymer molecules adsorbed on a substrate surface. In the report by Gallyamov et al[383], they studied the reversible collapse-decollapse of cylindrical poly (methacrylate)-graft-poly (n-butyl acrylate) brush-like polymers exposed to different solvent vapours with different surface tensions in real time with SPM. The micro-molecules on mica tended to assume a compacted globular conformation when exposed to the vapour of compounds, which due to their amphiphilic nature adsorb on mica and lower the surface energy of the substrate (e.g. alcohol). By contrast, the macromolecules adopted

extended two-dimensional worm-like conformations when in the vapours of compounds having high values of surface tension (e.g. Water). The dynamics of the collapse and spreading of the macromolecules were observed directly and in real time. They attributed the observation to the tendency in competition in the spreading on the substrate surface between the macromolecules and the co-adsorbed vapour molecules. If the brush-like macromolecules succeeded in the spreading, they acquired an extended conformation. Otherwise they collapsed in order to reduce the surface area per molecule. These brush-like structures could be viewed in real-time with the SPM. Similar procedure could be implemented in an attempt to view the network conformation existing in the different adhesive morphologies.

Solutions of the film could be prepared by film casting the adhesive in toluene which is a very good solvent for styrene, and then such as in hexane or chloroform which has low surface tension or vapours of mineral oil.)[384]. The films can e.g. be prepared by producing a 20 wt % adhesive/toluene solution, then depositing on mica and allow to dry for room temperature for 24 hours. The different network systems can then be viewed with TM-AFM, perhaps at 150 x 150 nm^2 scan size at room temperature.

8.1.2.3 Bonding between PSA and non-microfibre

From the point of view of suitable substrates for hygiene products application, the future trend is directed towards microfibre due to its strength and aesthetics. From consumer and future perspective, the fabric is interesting but the adhesive bonding to microfibre has to be promoted by for example improving the wettability between the adhesive sample and the microfibre substrates. In Chapter 4, this factor seemed to be the reason for the poor bonding the microfibre and the PSA film. Continuation of this work could be directed towards patterning for instance the surface of the coated adhesive film with patterned release silicon-liner to promote contact to microfibre. To micro-pattern large arrays of tip-like sub-micrometre features on coated PSA should improve the effective contact area between microfibre and the adhesive surface. These patterns could be made on the silicon release paper and transferred during the coating process. Adhesion enhancement by division of the contact area has been demonstrated experimentally by Peressadko and Gorb[385,386]. A patterned surface made out of polyvinylsiloxane (PVS), was found to have significantly higher adhesion on a glass surface than a smooth sample made out of the same material.

References

[1] Benedek. I., "*Pressure Sensitive Adhesive and Applications 2nd edition*", 2004, New York, Marcel & Dekker, p. 11

[2] John Comyn, "Adhesion Science", 1997, p. 10.

[3] A.J. Kinloch, "*Adhesion and Adhesives, Science and Technology*", 1987

[4] S.S. Voyutskii, "*Autohesion and Adhesion of High Polymers*", John Wiley and Sons, New York, 1963

[5] R. M. Vasenin, "*Adhesion, Fundamentals and Practice*", McLaren and Son, London, 1969, p. 29

[6] Alphonsus V. Pocius," *Adhesion and Adhesives Technology, An Introduction*", 1997, p. 125.

[7] B. V. Deryaguin, V. P. Smilga, "*Adhesion, Fundamentals and Practice*", Mclaren and Son, London, 1969, p. 152

[8] C. Kemball, "Adhesion", edited by D. D. Eley, Oxford University Press, London, 1961, p. 19

[9] A. J. Staverman, "*Adhesion and Adhesives*", Vol. I, edited by R. Houwink and G. Salmon, Elsevier, Amsterdam, 1965, p. 9

[10] W. C. Wake, Royal Institute of Chemistry Lecture, Series 4, 1966, 1

[11] L. Pauling, "*The Nature of the Chemical Bond*", Cornell University Press, New York, 1960

[12] R. J. Good, "*Treatise on Adhesion and Adhesives*", Vol. I, edited by R. L. Patrick, Marcel Dekker, New York, 1967, p. 15

[13] J. Israelachivili, "*Intermolecular and surface forces",* London Academic press, New York, 1991

[14] A.J. Kinloch, "*Review The science of adhesion, Part 1 Surface and interfacial aspects*", Journal of Material Science 15, 1980, 2141-2166

[15] Costantino Creton, *"TACK"*, Comprehensive Adhesion Science, Vol. II, The Mechanics of Adhesion, Rheology of Adhesives and Strength of Adhesive Bonds, May 10th 2001

[16] A.J. Kinloch, "*Adhesion and Adhesives, Science and Technology*", 1987, Chapter Seven.

[17] Pressure Sensitive Tape Council, Glossary of Terms, 2001

[18] *http://industrial-adhesives.globalspec.com/LearnMore/Materials_Chemicals/Adhesives/Pressure_Sensitive_Adhesives*

[19] Satas D., "*Handbook of Pressure Sensitive Adhesive Technology, 2nd Edition*", 1989, Van Nostrand Reihold Co., New York

[20] V.L. Vakula and L.M. Pritykin, "*Polymer Adhesion, basic physico-chemical principles*", 1991, pages 291 and 316.

[21] Alphonsus V. Pocius, *"Adhesion and Adhesives Technology, An Introduction"*, 1997, p. 237.

[22] Don Satas, "*Hand book of Pressure –Sensitive Adhesive Technology*", 1982, chapter 3.

[23] A. Zosel, "*The effect of fibrillation on the tack of pressure sensitive adhesives*," International Journal of Adhesion & Adhesives 18 (1998) 265-271

[24] Alfred J. Crosby, Kenneth R. Shull, "*Adhesive Failure Analysis of Pressure Sensitive Adhesives*", Journal of Polymer Science: Part B: Polymer Physics, Vol. 37, 3455-3472, 1999.

[25] Liliane Leger, Costantino Creton, "*Adhesion mechanisms at soft polymer interfaces*", Phil. Trans. R. Soc. A. 2008, 366, 1425-1442

[26] Peter L. Drzal, Kenneth R. Shull, "*Adhesive Failure of Model Acrylic Pressure Sensitive Adhesives*", The Journal of Adhesion, 81, 2005, 397-415

[27] Michiharu Yamamoto, Fumiko Nakano, Tomoko Doi, Yataka Moroishi, "*Synthesis and PSA performance study for novel acrylic and butyl acrylate block copolymers*", International Journal of Adhesion & Adhesives 22, 2002, 37-40

[28] Zosel A., J. Adhes., 1989, 30, 135-149

[29] Henkel, Slough, United Kingdom

[30] Istvan Benedek, *"Pressure-Sensitive Adhesives and Applications"*, Second Edition, Revised and Expanded, 2004

[31] L. Mandelkern, " *An Introduction to Macromolecules*", Springer-Verlag, New York, 1972

[32] W.J. Burlant, A. S. Hoffman, "*Block and Graft Polymers*", Van Nostrand Reinhold Co., New York, 1960

[33] McCrum N. G., Buckley K., Gagg. C., "*Principles of Polymer Engineering*", Oxford University Press, 1997

[34] J. M. G. Cowie, "*Polymers: Chemistry & Physics of Modern Materials, Second Edition*", 1991

[35] A. Ravve, "*Organic Chemistry of Macromolecules*", Marcel-Dekker, Inc., New York, 1967

[36] *http://www.pprc.org/pubs/techreviews/hotmelt/hmdefin.html*

[37] L. R. G. Treloar, "*The Physics of Rubber Elasticity*", Oxford University Press, 1975

[38] L. H. Sperling, "*Introduction to physical polymer science*", Fourth Edition, A John Wiley & Sons, Inc. Publication, 2006

[39] G. Odian, "*Principles of Polymerization*", 2004, Wiley-Interscience

[40] C. Li Pi Shan, S. Yalvac, C. Diehl, G. Marchand, C. Rickey, T. Karjala, "*Development of Olefin Copolymers for Pressure-Sensitive Adhesives*", PSTC, May 2007, Orlando, FL

[41] Marcin Karbarz, Zbigniew Stojek, Costas S. Patrickios, "*ABA triblock copolymer-based model networks in the bulk: Effect of the number of arms on microphase behaviour*", Polymer 46, 2005, 7456-7462

[42] Lloyd M. Robeson, "*Polymer blends, A comprehensive review*", Hanser Gardner publications, 2007

[43] J. M. G. Cowie, "*Polymers: Chemistry & Physics of Modern Materials, Second Edition*", 1991, chapter 8

[44] Richard A. L. Jones and Randal W. Richards, "*Polymers at surfaces and interfaces*", 1999, Cambridge university press

[45] Paul J. Flory, "*Thermodynamics of high polymer solutions*", Journal of Chemical Physics, August 1941, Vol. 9, Issue 8

[46] Maurice L. Huggins, "*Solutions of long chain compounds*", Journal of Chemical Physics, May 1941, Vol. 9, Issue 5

[47] Shibayama M., Yang h., Macromolecules, 1985, 18, 2179

[48] A.Y. Grosberg, A. R. Khokhlov, "*Statistical Physics of Macromolecules*", New York, 1994, AIP Press

[49] A. Sariban, K. Binder, Journal of chemical physics, 1987, 86, 5859

[50] F.S. Bates, J. H. Rosedale, Physical Review Letters, 1990, 65, 1893

[51] J. Dudowiwicz, K. F. Freed, Macromolecules, 1991, 24, 5076

[52] K. S. Schweizer, J.G. Curro, Advances in Polymer Science, 1994, 116, 321

[53] R. P. Kambour, J. T. Bendler, Macromolecules, 1983, 16, 753

[54] Takeo, Araki, Qui Tran-Cong, Mitsuhiro Shibayama, "*Structure and Properties of Multiphase Polymeric Materials*", 1998, Marcel Dekker, INC, New York

[55] Rosen S. L., "*Fundamental principles of polymeric materials*", 1993, John Wiley & Sons, New York

[56] Hildebrand J.H., "*The Solubility of Non-Electrolytes*", New York, Reinhold, 1936

[57] John, Burke, "*Solubility Parameters: Theory and Application*", The Book and Paper Group Annual", Vol. 3, 1984, http://cool.conservation-us.org/coolaic/sg/bpg/annual/v03/bp03-04.html

[58] Charles M. Hansen, "*Hansen Solubility Parameters A User's Handbook"*, Second Edition, 2007, Taylor & Francis Group, LLC

[59] Van Krevelen, D.W., "Properties of Polymers: The Correlation with Chemical Structure", New York, 1990

[60] P. A. Small, J. Appl. Chem., 3, 71, 1953

[61] K. L. Hoy, J. Paint. Technol., 42, 76, 1979

[62] K. K. Chee, "*Temperature Dependence of Solubility Parameters of Polymers*", Malaysian journal of chemistry, 2005, Vol. 7, No. 1,

[63] John, Burke, "*Solubility Parameters: Theory and Application*", The Book and Paper Group Annual", Vol. 3, 1984, http://cool.conservation-us.org/coolaic/sg/bpg/annual/v03/bp03-04.html

[64] James E. Mark, *" Polymer Data Handbook*", Oxford University Press, Inc., 1999

[65] I. W. Hamley, "*Ordering in thin films of block copolymers: Fundamentals to potential applications*", Progress in Polymer Science, Elsevier, 2009

[66] Koray Yurekli, Ramanan Krishnamoorti, "*Dynamics of block copolymer micelles*", Macromolecules, 2002, 35, pp. 4075-4083

[67] M. Szware, M. Levy, R. Mikovich, J. Am. Chem. Soc., 78, 1956, 2656

[68] M. Hefft, J. Springer, Macromol. Chem. Rapid Commun., 11, 1990, 397

[69] V. Percee, M. Lee, J. Macromol. Sci. A, 29, 1992, 723

[70] T. Kodaira, K. Mori, Makromol. Chem., 193, 1992, 1331

[71] R. Bohnert, H. Finkelmann, Macromolecular Chemistry and Physics, 1994, 195, 689

[72] Frank S. Bates, Glen H. Fredrickson, "*Block Copolymer Thermodynamics: Theory and experiment*", Annual review of physical chemistry, 1990, 41

[73] Eric Raspaud, Didier Lairez, Mireille Adam, *"Triblock Copolymers in Selective solvent. 2. Semidilute solutions, macromolecules"*, 1996, 29, 1269-1277

[74] Ludwik Leibler, "*Theory of Microphase Separation in Block Copolymers*", Macromolecules, 1980, 13, 1602-1617

[75] Hamley I. W., "*The Physics of Block Copolymers*", Oxford University Press, New York, 1998

[76] Glenn H. Fredrickson, Frank S. Bates, "*Dynamics of Block Copolymers: Theory and Experiment*", Annu. Rev. Mater. Sci., 1996, 26:501-50

[77] Xiao-jun Li, M . Schick, "*Self-assembly of copolymers and lipids*", Condensed Matter Physics, 2001, Vol. 4, No. 2(26), pp. 325-333

[78] Mark Douglas Whitmore, Jaan Noolandi, "*Theory of phase equilibria in block copolymer-homopolymer blends*", Macromolecules, 18(2), 2486-2497

[79] E. Helfand, Macromolecules, 8, 1975, 552

[80] T. Ohta, K. Kawasaki, Macromolecules, 1986, 19, 2621

[81] D. J. Meier, Appl. Polym. Symp., 24, 1974, 67

[82] Chang Dae Han, Nitin Y. Vaidya, Do Kim, "*Lattice disordering/ordering and demicellization transitions in highly asymmetric polystyrene-block-polyisoprene*", Macromolecules, 2000, 33, 3767-3780

[83] Damian A. Hajduk, Sol M. Gruner, Erramilli, "*High-Pressure Effects on the Order-disorder transition in block copolymer melts"*, Macromolecules, 1996, 29, 1473-1481

[84] I. Goodman, "*Developments in block copolymers*", Applied Science Publishers, London, New York, 1982

[85] Chang Dae, Deog Man Baek, "*Effect of volume fraction on the order-disorder transition in low molecular weight polystyrene-block-polyisoprene copolymers. 1. Order-Disorder transition temperature determined by rheological measurements*", Macromolecules, 1995, 28, 5043-5062

[86] Ashish K. Khandpur, Stephan Forster, Frank S. Bates, "*Polyisoprene-Polystyrene Diblock Copolymer Phase Diagram near the Order-Disorder Transition*", Macromolecules, 1995, 28, 8796-8806

[87] I. W. Hamley, "*Introduction to Soft Matter, Polymer, Colloids, Amphiphiles and Liquid Crystals*", John Wiley & Sons, Ltd, 2000

[88] Nitin Y, Vaidya, Chang Dae Han, Do Kim, "*Microdomain structures and phase transitions in binary blends consisting of highly asymmetric block copolymer and a homopolymer*", Macromolecules, 2001, 34, pp. 222-234

[89] I. W. Hamley, K. A. Koppi, J. H. Rosedale, F. S. Bates, K. Almdal, K. Mortensen, Macromolecules, 26, 5959, 1993

[90] Aniket Bhattacharya, S.D Mahanti, Amitatabha Chakrabarti, "*Network pattern formation in phase separating polymer solutions: A molecular dynamic study*", Physical review letters, 1998, Vol. 80 (2)

[91] Xiaofeng Ren, Juncheng Wei, "*Triblock copolymer theory: free energy, disordered phase and weak segregation*", Physica D, 2003, 178, 103-117

[92] Stephen Forster, Ashish K. Khandpur, Jin Zhao, Frank S. Bates, "*Complex phase behaviour of polyisoprene-polystyrene diblock near the order-disorder transition*", Macromolecules, 1994, 27, 6922-6935

[93] R. Kleppinger, M. Van Es, N. Mischenko, M.H.J. Koch, H. Reynaers, "*Physical gelation in a triblock copolymer solution: In situ study of stress-strain behaviour and structural development*", Macromolecules, 1998, 31, 5805-5809

[94] Mai Ngugen-Misra, Wayne L. Mattice, "*Micellization and gelation of symmetric triblock copolymers",* Macromolecules, 1995, 28, 1444-1457

[95] Hermans, P. H. In Colloid Science II; Kruyt, H. R., Ed.; Colloid Science II; Elsevier Publishing Inc.: Amsterdam, 1949; Vol II, pp. 483-651

[96] Eugene Helfand, Z.R. Wasserman, "*Block copolymer theory. 5. Spherical Domains*", Macromolecules, 1978, 11 (5), 960-966

[97] A. N. Semenov, J.F. Joanny, A.R. Khokhlov, "*Associating polymers: Equilibrium and linear viscoelasticity*", Macromolecules, 1995, 28, 1066-1075

[98] R. Kleppinger, K. Reynders, N. Mischenko, N. Overbergh, M.H.J. Koch, K. Mortensen, H. Reynaers, "*A high-temperature cubic morphology in triblock copolymer gels*", Macromolecules, 1997, 30, 7008-7011

[99]T. Durrchmidt, H. Hoffmann, "*Organogels from ABA triblocks copolymers*", Colloid polym. Sci., 2001, 279:1005-1012

[100] Jose R. Quintana, Esperanza Diaz, Issa Katime, "*Physical gelation of polystyrene-block-poly(ethylene/butylene)-block-polystyrene copolymer in paraffinic oil. Oscillatory shear compression measurements*", Macromol. Chem. Phys., 1996, 197, 3017-3026

[101] Kenneth R. Shull, Alfred J. Crosby, Cynthia M., "*Adhesion of triblock copolymer-based thermoreversible gels and pressure sensitive adhesives*", Mat. Res. Soc. Symp., 2002, Vol. 629

[102] N. P. Balsara, M. Tirrell, T. P. Lodge, "*Micelle formation of BAB triblock copolymers in solvents that preferentially dissolve the A block*", Macromolecules, 1991, 24, 1975-1986

[103] Jin Kuk Kim, Marissa A. Paglicawan, Sung Hyo Lee, Maridas Balasubramanian, "*Influence of Hydrocarbon Oils on the Physical Gelation of Poly(styrene-b-(ethylene-co-butylene)-b-styrene) (SEBS) Triblock* Copolymers", Journal of Elastomers and Plastics, 2007, Vol. 39, 133

[104] M. B. Kossauth, D. C. Morse, F. S. Bates, "*Viscoelastic behaviour of cubic phases in block copolymer melt*", J. Rheol. Vol., 1999, 43, issue 1, p 167-199.

[105] Jonathan H. Laurer, Rudy Bukovnik, Richard J. Spontak, "*Morphological Characteristics of SEBS thermoplastic elastomer gels*", Macromolecules, 1996, 29, 5760-5762

[106] Watanabe H., Kotaka T., Polym. J., 1982, 14, 739-747

[107] Liebler L., Orland H., Wheeler J. C., J. Chem. Phys. 1983, 79, 3550-3557

[108] Hashimoto T., Shibayama M., Kawai H., Watanabe H., Kotaka T., Macromolecules, 1983, 16, 361-371

[109] Mortensen K., Pedersen J. S., Macromolecules, 1993, 26, 805-812

[110] Brown W., Schillen K., Hvidt S., J. Phys. Chem., 1992, 96, 6038-6044

[111] B. Ohlsson, B. Tornell, Polym. Eng. Sci., 36, 501, 1996

[112] L. S. Flosenzier, J. M. Torkelson, Macromolecules, 25, 735, 1992

[113] J. H. Laurer, J. F. Mulling, S. A. Khan, R. J. Spontak, J. S. Lin, R. Bukovnik, "*Thermoplastic elastomer gels. I. Effects of composition and processing on morphology and gel behavior*", 1998, Journal of polymer science: Part B: Polymer physics, Vol. 36, 2379-2391

[114] Wilder E. A., Hall C. K., Khan S. A., Spontak R. J., Recent Res. Dev. Mater. Sci., 2002, 3, 93-115

[115] Abdallah D. J., Weiss R. G., Adv. Mater., 2000, 12, 1237-1247

[116] Halperin A., Zhulina E. B., Europhys. Lett., 1991, 16, 337

[117] Zhulina E. B., Halperin A., Macromolecules, 1992, 25, 5730

[118] Watanabe H., Kotaka T., Polym. J., 1982, 14, 739

[119] Hashimoto T., Shibayama M., Kawai H., Watanabe H., Kotaka T., Macromolecules, 1983, 16, 361-371

[120] Watanabe H., Kotaka T., Macromolecules, 1983, 16, 1783

[121] Wanka G., Hoffmann H., Ulbricht W., Colloid Polym. Sci., 1990, 268, 101

[122] Mortensen K., Pedersen J. S., Macromolecules, 1993, 26, 805-812

[123] C. Derail, A. Allal, F.X. Gibert, C. Marin, *"Rheological properties of Hot-melt pressure-sensitive adhesives (hmpsas) based on styrene-isoprene copolymers. Part 1: A rheological model for [SIS-SI]"*, The Journal of Adhesion, 79, 2003, 825-852

[124] R. L. Patrick, "*Treatise on adhesion and adhesives*", Materials, 1969, (Marcel Dekker, New York), Vol. 2, p. 129

[125] Hadjichristidis N., Pispas S., Floudas G. A., "*Block Copolymer Synthesis Strategies, Physical Properties and Applications*", John Wiley and Sons, Inc., New Jersey, 2003, pp. 419

[126] Laurer J. H., Mulling J. F., Khna S. A., Spontak R. J., Lin J. S., Bukovnik R, Journal of Polymer Science Part-B-Polymer Physics, 1998, 36, 2513-2523

[127] King M. R., White S. A., Smith S. D., Spontak R. J., Langmuir, 1999, 15, 7886-7889

[128] Jose R. Quintana, Esperanza Diaz, Issa Katime, "*Physical gelation of polystyrene-block-poly(ethylene/butylene)-block-polystyrene copolymer in paraffinic oil. Oscillatory shear compression measurements*", Macromol. Chem. Phys., 1996, 197, 3017-3026

[129] Polizzi S., Stribeck N., Zachmann H. G., Bordeianu R., Polymer Composites, 1988, 434-442

[130] Ceauescu E., Bordeianu R., Ghioca P., Buzdugan E., Stancu R., Cerchez I., Pure Appl. Chem. 1984, 56, 319-328

[131] Stribeck N., Basecke P., Polizzi S., Colloid & Polymer Science, 1989, 267, 687-701

[132] Watanabe H., Kuwahara S., Kotaka T., J. Rheol., 1984, 28, 393-409

[133] Sato T., Watanabe H., Osaki K., Macromolecules, 2000, 33, 1686-1691

[134] Spontak R. J., Wilder E. A., Smith S. D., Langmuir, 2001, 17, 2294-2297

[135] Laurer J H., Bukovnik R., Spontak R. J., Macromolecules, 1996, 29, 5760-5762

[136] King M. R., White S. A., Smith S. D., Spontak R. J., Langmuir, 1999, 15, 7886-7889

[137] Jackson N. R., Wilder E. A., White S. A., Bukovnik R., Spontak R. J., Journal of Polymer Science Part-B Polymer Physics, 1999, 37, 1863-1872

[138] Yu J. M., Jerome R., Macromolecules, 1996, 29, 8371-8378

[139] Spontak R. J., Wilder E. A., Smith S. D., Langmuir, 2001, 17, 2294-2297

[140] Vega D. A., Sebastian J. M., Loo Y., Register R. A., "*Phase behaviour and viscoelastic properties of entangled block copolymer gels*", Journal of Polymer Science Part B: Polymer Physics, 2001, 39, 2183-2197

[141] Pocius A. V., "*Adhesion and Adhesives Technology: An Introduction*", 1997, Hanser-Gardner Publishers, Munich, Germany

[142] Ferry, J. D. "Viscoelastic Properties of Polymers", 3rd Ed., Wiley, New York, 1980

[143] F. Bueche, "*Physical Properties of Polymers*", John Wiley & Sons, New York, 1962

[144] Hata T., "Mechanisms of Adhesive Failure", Journal of Adhesion, Vol. 4, pp. 161-170

[145] L. R. G. Treloar, "*The Physics of Rubber Elasticity*", Chapter 1, Oxford University Press, 1975

[146] Hepburn C., "Polyurethane Elastomers", 2nd Ed., Elsevier Science Publishers, New York, 1992

[147] Thomas A. Vilgis, "*Rubber Elasticity and Inhomogeneities in Cross-Link Density*", Macromolecules, 1992, 25, 399-403

[148] Martijn van der Schuur, Reinoud J. Gaymans, "*Influence of Chemical Crosslinks on the elastic behaviour of segmented block copolymers*", Polymer, 46, 2005, 6862-6868

[149] James E. Mark, Burak Erman, Frederick Roland Eirich, "*Science and Technology of Rubber, Second Edition,*" 1994, Academic Press Ltd, United Kingdom

[150] J. M. G. Cowie, "*Polymers: Chemistry & Physics of Modern Materials, Second Edition*", 1991, chapter 14

[151] Michael Rubinstein, "*Elasticity of Polymer Networks*", Macromolecules, 2002, 35, 6670-6686

[152] G. Heinrich, "*Long-time relaxation of polymer networks*", Macromolecules, 1992, 25, 404-407

[153] Gilmer T., Williams M. J., J. Chem. Ed., 1996, 73(11), 1062

[154] R. Schlegel, U. Staudinger, M. Thunga, R. Weidisch, G. Heinrich, D. Uhrig, Jimmy W. Mays, H. Iatrou, N. Hadjichristidis, "*Investigations on mechanical properties of PI-PS multigraft copolymers*", European polymer journal, 45, 2009, 2902-2912

[155] Alexandra Roos, Costantino Creton, "*Linear Viscoelasticity and Non-Linear Elasticity of Block Copolymer Blends Used as Soft Adhesives*", Macromol.Symp. 2004, 214, 147-1546

[156] Benedek I, Heymans L.J, "*Pressure sensitive adhesive adhesives technology*", New York: Marcel Dekker, Inc.; 1996

[157] C. Derail, M.N. Cazenave, F.X. Gibert, C. Marin, *"Rheological properties of Hot-melt pressure-sensitive adhesives (hmpsas) based on styrene-isoprene copolymers. Part 2: Innovative molecular design from predictive formulation"*, The Journal of Adhesion, 80, 2004, 1131-1151

[158] M.N. Cazenave C. Derail, F. Leonardi, C. Marin, *"Rheological properties of Hot-melt pressure-sensitive adhesives (hmpsas) based on styrene-isoprene copolymers. Part 3: Rheological behaviour of different block copolymers with high diblock content"*, The Journal of Adhesion, 81:623-643, 2005

[159] Benedek I, Heymans L.J, "*Pressure sensitive adhesive adhesives technology*", New York: Marcel Dekker, Inc.; 1996

[160] Jagisch F.C., Tancrede J.M, "*Handbook of pressure sensitive adhesives*", Satas & Associates, 1999

[161] Hansen, D. R, E. E. Ewins, D. J. St. Clair, "*Formulating Guide for Adhesives and Sealants*", Kraton Polymers, 2000, pp. 47

[162] Kraus G., Hashimoto T., "*Structural Changes in Melts of Butadiene-Styrene and Isoprene-Styrene Block based Pressure-Sensitive Adhesives*", J. Appl. Polym. Sci., 44, 1745-1757

[163] Hansen, D. R, E. E. Ewins, D. J. St. Clair, "*Formulating Guide for Adhesives and Sealants*", Kraton Polymers, 2000, pp. 47

[164] Sims C. L., "*New Styrene Block Copolymers to Extend the Performance Range of PSA Tapes and Labels*", PSTC Annual Technical Proc., 105-136

[165] R. Adhikari, R. Godehardt, W. Lebek, R. Weidisch, G. H. Michler, K. Knoll, "*Correlation between Morphology and Mechanical Properties of Different*

Styrene/Butadiene Triblock Copolymers: A Scanning Force Microscopy Study", J. Macromol. Sci.-Physics, B40(5), 833-847, 2001

[166] Subiman Ghosh, Anil K. Bhowmick, Namita Roychowdhury, G. Holden, "*Influence of block molecular weight on the properties of styrene-ethylenebutylene-styrene block copolymers"*, Journal of applied polymer science, 2000, Vol. 77, 1621-1628

[167] I. Benedek, "*Development and Manufacture of Pressure-Sensitive Products*", Marcel Dekker, New York, 1998

[168] Johnston J. "*Tack-Known by Many Names, It's Difficult to Define*", Adhesive Age, Vol. 26, No. 12, 34-38

[169] Zosel A., "Built to Last", Adhesive Age, Vol. 43, No. 8, pp. 34-40

[170] Landrock H., "*Adhesive Technology Handbook*", 185, USA, Noyes Publication

[171] Hu F., Olusanya A., Lay L. A., J. Urquhart, L. Crocker, " *A Finite Element Model for the Assessment of Loop Tack for Pressure-Sensitive Adhesive Tape and Labels*", Report 8, National Physical Laboratory, UK, 1998

[172] Creton C., L. Leibler, "*How Does Tack Depend on Time of Contact and Contact Pressure?*", Journal of Polymer Science: Part B: Polymer Physics, Vol. 34, pp. 545-554

[173] Zosel A., "*Shear Strength of Pressure-Sensitive Adhesives and its Correlation to Mechanical Properties*", Journal of Adhesion, Vol. 44, pp. 1-16

[174] Aubrey D. W., Sheriff M., Journal of Polymer Science, Polymer Chemistry Edition, 1978, 16, 2631-2643

[175] Class J.B., Chu S. G., J. Appl. Polym. Sci., 1985, 30, 825-842

[176] H. J. Kim, Mizumachi H. J., J. Adhes., 1995, 49, 113-132

[177] W. Brockmann, R Huther, "*Adhesion mechanisms of pressure-sensitive adhesives*", Int. J. Adhesion and Adhesives, 16, 1996, 81-86

[178] Caiyun Wu, Guozhang Wu, Chifei Wu, *"Dynamic mechanical properties in blends of poly(styrene-b-isoprene-b-styrene) with aromatic hydrocarbon resin"*, Journal of applied polymer science, 2006, Vol. 102, 4157-4164

[179] Emmett P. O'Brien, Louis T. Germinario, Gary R. Robe, Tim Williams, Doug G. Atkins, Debbie A. Moroney, Mark A. Peters, "*Fundamentals of hot-melt pressure-sensitive adhesive tapes: the effect of tackifier aromaticity*", J. Adhesion Sci. Technol., 2007, Vol. 21 (7), pp. 637-661

[180] Kelly Brown, Jacob, C. Hooker, Costantino Creton, "*Micromechanisms of Tack of Soft Adhesives Based on Styrenic Block Copolymers*", Macromol. Mater. Eng., 2002, 287, 163-179

[181] Creton.C, "*Pressure Sensitive Adhesives: An Introductory Course*", 2003, Materials Research Society. www.mrs.org/publications/bulletin/

[182] Hansen, D. R, E. E. Ewins, D. J. St. Clair, "*Formulating Guide for Adhesives and Sealants*", Kraton Polymers, 2000, pp. 47

[183] P. A. Mancinelli, "*New Development in Acrylic HMPSA Technology*", in TECH 12, Advances in Pressure-Sensitive Tape Technology, Technical Seminar, Proc. Itasca, IL, May, 1989

[184] B. H. An, "*Escorez® Hydrocarbon Tackifier Resins*", ExxonMobil Chemical, The Society of Adhesion and Interface, Korea, August 2001

[185] Istvan Benedek, "*Pressure-Sensitive Formulation*", VSP BV, 2000, The Netherlands

[186] Chang Dae Han, Jinhwan Kim, Jin Kon Kim, " *Viscoelastic behaviour of mixtures of a block copolymer and a homopolymer*", macromolecules, 1989, 22, pp. 3443-3451

[187] Dong-Hyuk Lim, Hyun-Sung Do, Hyun-Joong Kim, *"PSA performances and viscoelastic properties of sis-based psa blends with H-DCPD tackifiers"*, Journal of applied polymer science, 2006, Vol. 102, 2839-2846

[188] Jin Kon Kim, Du Yeol Ryu, Kyung-Hee Lee, "*The aromatic hydrocarbon resins with various hydrogenation degrees Part 1. The phase behaviour and miscibility with polybutadiene and with polystyrene*", Polymer 41, 2005, 5195-5205

[189] Du Yeol, Ryu Jin Kon Kim, "*The aromatic hydrocarbon resins with various hydrogenation degrees Part 2. The adhesion and viscoelastic properties of the mixtures of resins and block copolymers* ", Polymer 41, 2000, 5207-5218

[190] S. Giordano, C. Padori, A. Riva, L. Vitalini Sacconi, Adhesive Age, 1994, November, 32-38

[191] N. D. Keyzer, Adesione, 2, 13-24, 1992

[192] C. Galan, C. A. Sierra, J. M. Gomez Fatou, J. A. Delgado, "*A Hot-melt Pressure-Sensitive Adhesive Based on Styrene-Butadiene-Styrene Rubber. The Effect of Adhesive Composition on the Properties*", Journal of Applied Polymer Science, Vol. 62, 1263-1275, 1996

[193] Lakrout H., C. Creton, D. Ahn, K. R. Shull, "*Influence of Molecular Features on the Tackiness of Acrylic Polymer Melts*", Macromolecules, 2001, 34, 7448-7458

[194] Gay C., L. Leibler, "On Stickiness", Phys. Today, 1999, 52(11), p. 48-52

[195] Piau J., C. Verdier, B. Lazhar, "*Influence of Rheology and Surface Properties in the Adhesion of Uncross-linked Pressure Sensitive Adhesives*", Rheol. Acta, 1997, 36, 446-461

[196] Hoichang Yang, Unnyoung Sa, Minjeong Kang, Hyeon Soo Ryu, Chang Yeol Ryu, Kilwon Cho, "*Near-surface morphology effect on tack behaviour of poly(styrene-b-butadiene-b-styrene) triblock copolymer/rosin films*", Polymer, 47, 2006, 3889-3895

[197] Cliche A., P. Pareige, C. Creton, "*Role of Surface Roughness in Controlling Adhesion of a Soft Adhesive on a Hard Surface*", C. R. Acad. Sci. Paris: Polymers at Interface, 2000, 1(9), p.1-8

[198] A.J. Steven-Fountain, A.G. Atkins, G. Jeronimidis, J.F.V Vincent, D.F. Farrar, R.A. Chivers, "*The effect of flexible substrates on pressure-sensitive adhesive performance*", International Journal of Adhesion and Adhesives, 22, 2002, 423-430

[199] Kinnsuke Hino, Toshio Ito, Mitsuo Toyama, *" Morphological studies on wettability and tackiness of pressure-sensitive adhesives*", John Wiley & Sons, Inc., 1975

[200] P.C. Pandey, H. Shankaragouda, Arbind Kr. Singh "*Nonlinear analysis of adhesively bonded lap joints considering viscoplasticity in adhesives*", , Department of Civil Engineering, Indian Institute of Science, Bangalore, 560 012, India, Received 24 January 1997, accepted 4 August 1998 accepted

[201] A.E. O'Connor, C.W. Macosko "*Melt versus Solvent Coating: Structure and Properties of Block-Copolymer-Based Pressure-Sensitive Adhesives*", Journal of Applied Polymer Science, Vol. 86, 3355-3367, 2002.

[202] Ick Kyung Sung, Kwan-Suk Kim, In-Joo Chin, "*Dynamic mechanical and morphological study on model pressure sensitive adhesive based on poly(styrene-b-butadiene-b-styrene),*

[203] Sheriff M., Aubrey DW., *"Viscoelasticity of rubber-resin mixtures"*, Journal of polymer science part A- polymer chemistry, 1978, vol. 16, issue 10, 2631-2643

[204] Sheriff M., Aubrey DW., *"Peel adhesion and Viscoelasticity of rubber-resin blends"*, Journal of polymer science part A- polymer chemistry, 1980, vol. 18, issue 8, 386-389

[205] J. B. Class, S. G. Chu, "*The viscoelastic properties of rubber-resin blends. II. The effect of resin molecular weight*", Journal of applied polymer science, 2003, vol. 30 issue 2, 2003, 815-824

[206] Dahlquist C. A., "*Pressure Sensitive Adhesives*", in Treatise on Adhesion and Adhesives, R. L. Patrick (ed,), Marcel Dekker, New York, Vol. 2, pp. 219-270

[207] Christensen S. F., Flint S. C., "A Practical Criterion for Rheological Modelling of the Peeling of Pressure-Sensitive Adhesive", Journal of Adhesion, Vol. 72, pp. 177-207

[208] Lakrout H., Creton C., "*Micromechanics of Flat-Probe Adhesion Tests of Soft Viscoelastic Polymer Films*", Journal of Polymer Science: Part B: Polymer Physics, 2000, Vol. 38, pp. 965-979

[209] Chang E. P., "*Viscoelastic properties of pressure-sensitive adhesives*", Journal of Adhesion, Vol. 60, pp. 233-248

[210] Kaelble D. H., Trans. Soc. Rheo., 1969, 9(2):135

[211] Crosby A. J., Shull K. R., Lakrout H., C. Creton, "*Deformation and Failure Modes of Adhesively Bonded Elastic Layers",* J. Appl. Phys., 2000, 88, 2956-2966

[212] Plaut R. H. S. Suherman, D. A. Dillard, Williams N. L., "Elastic Analysis of the Loop Tack Test for Pressure-Sensitive Adhesives", Journal of Adhesion, Vol. 76, pp. 37-53

[213] A. Zosel, Int. J. Adhes. Adh., 1998, 18, 265-271

[214] Alfred J. Crosby, Kenneth R. Shull, "*Debonding Mechanisms of PSAs*", Adhesive Age, Jul 1999, Vol. 42, No. 7, p. 28

[215] A. N. Gent, J. Schultz, J. Adhesion 3, 281-294, 1972

[216] Alphonsus V. Pocius *Adhesion and Adhesives Technology, An Introduction,* 1997, p. 237

[217] Don Satas, "*Handbook of Pressure –Sensitive Adhesive Technology*", 1982, Chapter 3.

[218] Gent A. N., Lindley P. B., Proc. Roy. Soc., 1958;A249: 195

[219] Gent A. N., Wang C. J., Mat. Sci., 1991;26:3392

[220] Junko Asahara, Naruhito Hori, Akio Takemura, Hirokuni Ono, "*Crosslinked Acrylic Pressure-Sensitive Adhesives. I. Effect of the Crosslinking Reaction on the Peel Strength*", Journal of Applied Science, 2003, Vol. 87, 1493-1499

[221] Frank Sosson, Antoine Chateauminois, Costantino Creton, "*Investigation of Shear Failure Mechanisms of Pressure-Sensitive Adhesives,*" 25 August 2005, DOI: 10.1002/polb.20619, www.interscience.wiley.com

[222] Hayashi Y., Hata T., J. Adhes. Soc. Japan, 1984, 20, 4

[223] C.Y. Ryu, S. Lee, D.A. Hajduk, T.P. Lodge, "*Structure and Viscoelasticity of Matched Asymmetric Diblock and Triblock Copolymers in the Cylinder and Sphere microstructures*", Journal of Polymer Science: Part B: Polymer Physics, Vol. 35, 1997, 2811-2823

[224] Fumiko Nakano, Tomoko Doi, Yataka Moroishi, "*Synthesis and PSA performance study for novel acrylic and butyl acrylate block copolymers*", Michiharu Yamamoto, International Journal of Adhesion & Adhesives 22, 2002, 37-40

[225] http://www.patentstorm.us/patents/5418052-description.html

[226] http://www.freepatentsonline.com/6797766.html

[227] Dr Donn DuBois, Dr. Noel De Keyzer, Dr Martin Dupont, *"High performance styrenic block copolymers featuring a novel hybrid midblock phase*", 2005, Adhesives & sealants council meeting.

[228] http//:www.pnas.org/cgi/content/full/92/23/12768

[229] Bodil Wesslén och Bengt Wesslén, ”*Polymer Teknologi, Syntetiska Polymrer och Polysackarider*”, Lund 1997, p. 75.

[230] Nakajima T, Kajiwara K, McIntyre J. E., “*Advanced Fibre Spinning Technology*”, Woodhead Publishing, pp. 187-188

[231] Barbara Flanagan, “*The Case of the Missing Microfiber*”, I. D. April 22, 2008

[232] *Dynamic Mechanical Analysis Basics: Part 1 How DMA works”*, www.perkinelmer.com, 2007

[233] Hang Gao, Julie P. Harmon, “*Para-substituted polystyrenes: Stress relaxation, creep, dynamic mechanical and dielectric analyses”,* Thermochimica Acta 284, 1996, 85-102

[234] Dynamic mechanical analysis basics: “*Part 2 Thermoplastic transitions and properties*”, 2007, www.perkinelmer.com

[235] Danch A, “*Some comment on nature of the structural relaxation and glass transition*”, Journal of thermal analysis and calorimetry, 2003, Vol. 91, issue 3, 733-736

[236] Turi, Edith A, “*Thermal characterisation of polymeric materials, 2nd Edition, Vol. I*”, Academic Press, Brooklyn, New York, p. 529

[237] Chang Dae Han, “*Rheology and Processing of Polymeric Materials*”, Volume I Polymer Rheology, Oxford University Press, Inc., 2007

[238] A. Franck, “*Application of Rheology of Polymers*” TA Instruments Germany, AN009

[239] Formulas, Applicable to the TA Instruments ARES and RSA III, TA Instruments, Revision B, Issued September 2004

[240] Cagle.V.C, “*Handbook of Adhesive Bonding”,* USA: McGraw-Hill, 1973, pp. 8

[241] Samuel Akogyeram, Anette Lindell, Ronny Lindell, Hakan Person, “*Studying the effect of ozone flow rate on the adhesion between pe-film and Al-foil*”, Project work, Lund Institute of Technology, 2004.

[242] http://www.testedandproven.com/standards_material.html

[243] http://www.usc.edu/dept/materials_science/ccr/4research-projects/poster01.htm

[244] http://www.force-gauge.net/test_grips4.htm

[245] http://www.xinst.com/results_peel.htm

[246] Adhesives: www.textturetechnologies.com/adhesives_applica. Texture Technologies [20 Nov 2005].

[247] Jeffree C. E., Read N. D., “*Ambient- and Low-temperature scanning electron microscopy*” In Hall J. L., Hawes C. R., “Microscopy of Plant Cells., London, Academic Press, pp. 313-413

[248] Von Ardenne Manfred, "*Das Elektronen-Rastermikroskop. Praktische Ausfuhrung*", Germany, Zeitschrift fur technische Physik 19, 407-416

[249] G. Binnig, C. F. Quate, "*Atomic force microscope*", Physical review letters, 1986, Vol. 56 (9), pp. 930-933

[250] Sergei N. Magonov, "*Characterisation of polymer surfaces with atomic force microscopy*", Annu. Rev. Mater. Sci., 1997, 27:175-222

[251] S. Kopp-Marsaudon, Ph. Leclere, F. Duborg, R. Lazzaroni, J. P. Aime, "*Quantitative measurement of the mechanical contribution to tapping-mode atomic force microscopy images to soft materials*", 2000, 16, 8432-8437

[252] Adriana Paiva, Nina Sheller, Mark D. Foster, "*Study of the surface adhesion of pressure-sensitive adhesives by atomic force microscopy and spherical indenter tests*", Macromolecules, 2000, 33, 1878-1881

[253] C. Daniel Frisbie, Lawrence F. Rozsnyai, Aleksandr Noy, Mark S. Wrighton, Charles M. Lieber, "*Functional group imaging by chemical force microscopy*", Science, New series, Vol. 265 (5181), pp. 2071-2074

[254] Y. Martin, C. C. Williams, H. K. Wickramasinghe, "*Atomic force microscope-force mapping and profiling on a sub 100-Å scale*", J. Appl. Phys., 61, 4723, 1987

[255] E. Meyer, " *Atomic force microscopy*", Progress in surface science, Vol. 41, pp. 3-49, 1992

[256] John Thornton, "*Scanning probe microscopy training notebook. Version 3*", Digital Instruments, 2000

[257] Ricardo Garcia, Ruben Perez, "*Dynamic atomic force microscopy methods*", Surface science reports, 2002, Vol. 47, 197

[258] Atomic force microscopy: A guide to understanding and using the AFM, Galloway Group, Spring 2004

[259] F.L: Leite, C.E: Borato, W.T.L da silva, P. S. P. Herrman, O.N. Oliveira Jr.,"*Atomic Force Spectroscopy on Poly(o-ethoxyaniline) Nanostructured Films:Sensing Nonspecific Interactions"*, Microsc. Microanal. 13, 1-9, 2007

[260] S. N. Magonov, "*Atomic force microscopy in analysis of polymers*", Encyclopedia of analytical chemistry, R. A. Meyers Ed., John Wiley & Sons Ltd., 2000, pp. 7432-7491

[261] Genaro Zavala, "*Atomic force microscopy, a tool for characterisation, synthesis and chemical processes*", Colloid % Polymer science, 2008, Vol. 286 (1), 85-95

[262] K. L. Babcock, C.B. Prater, "*Phase imaging: Beyond topography*", Veeco Instruments Inc., 2004, www.veeco.com/library/application-notes

[263] A. Knoll, R. Magerle, G. Krausch, "*Tapping mode atomic force microscopy on polymers: Where is the true sample surface?*", Macromolecules, 2001, 34, pp. 4159-4165

[264] You Wang, Rui Song, Yingshun Li, Jingshu Shen, "*Understanding tapping-mode atomic force microscopy data on the surface of soft block copolymers*", Surface science, 2003, 530, pp. 136-148

[265] F. J. Giessible, Appl. Phys. Let., Vol. 76, 2000, 1470

[266] Phase Imaging: Beyond Topography, www.veeco.com/search_more.php?type=appnotes&search_term=phase

[267] Toshio Ando, Noriyuki Kodera, Eisuke Takai, Daisuke Maruyama, Kiwamu Saito, Akitoshi Toda, "*A high-speed atomic force microscope for studying biological macromolecules*", 2001, PNAS, Vol. 98 (22), 12468-12472

[268]Ohnesorge F.M., Hörber J.K., Häberle W., Czerny C.P., Smith D.P., Bining G., "*AFM review study on pox viruses and living cells*", Biophys. J., 1997, Vol. 73 (4), 2183-94

[269] Rostislav V. Lapshin, "*Feature-oriented scanning methodology for probe microscopy and nanotechnology*", 2004, Nanotechnology, Vol. 15 (9), pp. 1135-1151

[270] Rostislav V. Lapshin, "*Automatic drift elimination in probe microscope images based on techniques of counter-scanning and topography feature recognition*", 2007, Measurement in science and technology, Vol. 18 (3), pp. 907-927

[271] Digital Instruments Online Application Notes, 9/7/99. http://www.di.com/appnotes/Phase/PhaseMain.html

[272] Javier Tamayo, Ricardo Garcia, "*Effects of elastic and inelastic interactions on phase contrast images in tapping-mode scanning force microscopy*", Apply. Phys. Let. 1997, 71 (16), pp. 2394-2396

[273] S. N. Magonov, V. Elings, V. S. Papkov, "*AFM study of thermotropic structural transitions in poly(diethylsiloxane)*", Polymer, 1997, 38, 297

[274] R. Adhikari, R. Godehardt, W. Lebek, R. Weidish, G. H. Michler, K. Knoll, "*Correlation between morphology and mechanical properties of different styrene/butadiene triblock copolymers: A scanning force microscopy study*", Journal of macromolecular science, Part B, 2001, 40:5, 833-847

[275] I.W. Hamley "*Ordering in thin films of block copolymers: Fundamentals to potential applications*", Progress in polymer science, 2009

[276] R. Scott Mclean, Bryan B. Sauer, "*Tapping-mode AFM studies using phase detection for resolution of nanophases in segmented polyurethanes and other block copolymers,* "Macromolecules, 1997, 30 (26), pp. 8314-8317

[277] D. Raghavan, X. Gu, T. Nguyen, M. VanLandingham, A. Karim, "*Mapping polymer heterogeneity using atomic force microscopy phase imaging and nanoscale indentation*", Macromolecules, 2000, 33, 2573-2583

[278] J. Mallegol, O. Dupont, J. L. Keddie, "*Morphology and elasticity of waterborne acrylic pressure-sensitive adhesives investigated with atomic force microscopy*", 2003, J. Adhesion Sci. Technol., Vol. 17 (2), pp. 243-259

[279] B. Cappella, G. Dietler, "*Force-distance curves by atomic force microscopy*", Surface Science Reports, 1999, 34, 1-104

[280] Weisenhorn A.L., Hansma P. K., Albrecht T. R., Quate C. F., "*Forces in atomic microscopy in air and water*", Applied physics letters, 1989, vol. 54, pp. 2651-2653

[281] Marco Salerno, Ivan Bykov, NNL-CNR, NT-MDT, *"Tutorial: Mapping adhesion forces and calculating elasticity in contact-mode AFM, Microscopy and analysis"*, 2006, 2, 20

[282] J. E. Sader, "J. W. M. Chon, P. Mulvaney, "*Calibration of rectangular atomic force microscope cantilevers*", Review of scientific instruments, 1999, 70, p. 3967

[283] Christopher T. Gibson, D. Alastair Smith, Clive J. Roberts, "*Calibration of silicon atomic force microscope cantilevers*", Nanotechnology, 2006, 16, 234-238

[284] Ben Ohler, "*Practical advice on the determination of cantilever spring constants*", Veeco instruments Inc., 2007

[285] L. Marton, "*Advances in electronics and electron physics*", Volume 42, 1976, Academic press INC., New York.

[286] A. Benninghoven, et al., *"Secondary ion mass spectrometry: Basic concepts, Instrumental aspects, Applications and trends"*, 1987, Chemical analysis, Vol. 86

[287] Nicholas M., Kassis CM, Menceloglu YZ, DeSimone JM, Linton RW, Friedman RM, Parker DL, Rading D, Benninghoven A., "*Surface segregation in poly(styrene-b-isoprene): correlation of TOF-SIMS with XPS and contact angle measurement". Polym Prepr 37:309-310*

[288] Luc Van Vaeck, Annemie Adriaens, Renaat Gijbels, "*Static secondary ion mass spectrometry: (S-SIMS) part 1. Methodology and structural interpretation*", Mass spectrometry reviews, 1999, 18, 1-47. Leggert GJ. 1998. "*Mechanisms of ion production and fragmentation*", The static SIMS library, Manchester, UK, Surface spectra Ltd.

[289] Leggert G.J., 1998. "*Mechanisms of ion production and fragmentation in Static SIMS*". In: Vickerman J.C., Briggs D.,Henderson A., "The static SIMS library, Manchester, UK., Surface spectra Ltd., 19-38

[290] Briggs D, Seah MP, "*Practical surface analysis, Volume 2-Ion and neutral spectroscopy. 2nd edition*", J Wiley p 367-424

[291] Vickerman JC, Reed NM, "*The application of static ion mass spectrometry (SIMS) to the surface analysis of polymer materials",* 1993

[292] Leeson AMAlexander MR, Short RD, Briggs D, Hearn MJ, *"Secondary ion mass spectrometry of polymers: TOF SIMS study of monodispersed PMMA standards"*, Surf interface anal, 1997, 25:261-274

[293] Yub Choong Leon, Larry Mook Swee Lee, Seng Neon Gan, "*The viscoelastic properties of natural rubber pressure-sensitive adhesive using acrylic resin as a tackifier"*, Journal of applied polymer science, 2003, volume 88 issue 8, 2118-2123

[294] Yoshinobu Nakamura, Manabu Adachi, Yuta Tachibana, Yu Sakai, Shiji Nakano, Syuji Fuju, *"Tack and viscoelastic properties of an acrylic block copolymer/tackifier system"*, International Journal of Adhesion and Adhesives, Volume 29, Issue 8, 2009, 806-811

[295] A. Zosel, "*Adhesion and tack of polymers: Influence of mechanical properties and surface tensions*", Polymer Science Colloid & Polymer science, 1985, 263:541-553

[296] Dimitrios A. Dimas, Paraskevas P. Dallas, Dimitrios M. Rekkas, Nikolaos H. Choulis, "*Effect of Several Factors on the Mechanical Properties of Pressure-Sensitive Adhesives Used in Transdermal Therapeutic Systems*", AAPS PHarm. Sci. Tech., 2000, 1(2), 16

[297] Gerard Kraus, K. W. Rollman, "*Dynamic viscoelastic behaviour of ABA block polymers and the nature of the domain boundary*", Journal of polymer science , polymer physics edition, 1976, Vol. 14, 1133-1148

[298] H. Henning Winter, Diane B. Scott, "*Ordering by Flow near the Disorder-Order Transition of a Triblock Copolymer Styrene-Isoprene-Styrene*", Macromolecules, 1993, 26, 7236-7244

[299] S. R. Raghavan, S. A. Khan, "*Shear-induced microstructural changes in flocculated suspensions of fumed silica*", Journal of rheology, 1995, 39, 1311

[300] J. Schwarz, "*Explanation of the real stress-strain-behaviour of elastomers*", Kolloid-Z. U. Polymere 251, 215-224, 1973

[301] Judson T. Bauman, "*Fatigue, Stress, and Strain of Rubber Components – Guide for Design Engineers*", Carl Hanser Verlag, 2008, Germany

[302] C. A. Daniels, "*Polymers: Structure and Properties*", 1989, Technomic Publishing Company, Inc, Pennsylvania, USA

[303] Ellen M. Arruda, Mary C. Boyce, "*A Three-Dimensional Constitutive Model for Large Stretch Behaviour of Rubber Elastic Materials*", Journal of Mechanics and Physics of Solids, Vol. 41, No. 2, 1993, pp.389-412

[304] Application note, "*Glass transition measurement of an adhesive film in a material pocket*", www.perkinelmer.com

[305] Application not, "*Use of material pockets for mechanical analysis of powders*", www.perkinelmer.com

[306] Thermal analysis, "*Tg and melting point of a series of polyethylene glycols using the material pocket*", www.perkinelmer.com

[307] B. K. Hong, W. H. Jo, "*Effects of molecular weight of SEBS triblock copolymer on the morphology, impact strength, and rheological property of syndiotactic polystyrene/ethylene-propylene rubber blends*", Polymer, 2000, Vol. 41, pp. 2069-2079

[308] D. J. Houston, M. Song, A. Hammiiche, H. M. Pollock, "*Modulated differential scanning calorimetry: 6. Thermal characterisation of multicomponent polymers and interfaces*", Polymer, 1997, Vol. 38, no. 1, pp. 1-7

[309] G. Kraus, F. B. Jones, O. L. Marrs, K. W. Rollman, " *Morphology and viscoelastic behaviour of styrene-diene block copolymers in pressure-sensitive adhesives*", Journal of adhesion, 1976, Vol. 8, pp. 235-258

[310] Daisuke Yamaguchi, Jeffrey Bodycomb, Satoshi Koizumi, Takej Hashimoto, "*Ordered structure in blends of block copolymers. 4. Location of short diblock*", Macromolecules, 1999, 32, 5884-5894

[311] L. H. Lee, "*Adhesive Bonding*", Plenum: New York, 1991, p. 97

[312] Richard S. Stearns, Irl. N. Duling, Robert H. Johnson, "*Relationship of The Glass Transition Temperature of the Viscosity-Temperature Characteristics of Lubricants*", I&EC Product Research and Development, Vol. 5, No. 4, December 1966, 307

[313] F Tanaka, S. F. Edwards, "*Viscoelastic properties of physically cross-linked networks. Transient network theory*", Macromolecules, 1992, 25, 1516-1523

[314] Subiman Ghosh, D. Khastgir, Anil K. Bhowmick, *"Phase modification of sebs block copolymer by different additives and its effect on morphology, mechanical and dynamic mechanical properties"*, 1998, Vol. 67, 2015-2025

[315] Costantino Creton, Edward J. Kramer, "*Failure mechanisms of polymer interfaces reinforced with block copolymers*", Macromolecules, 1992, 25, 3075-3088

[316] Seung Bum Chun, Chang Dae Han, "*Morphology of model A/B/(C-block-D) ternary blends and compatibilization of two immiscible homopolymers A and B with a C-block-D copolymer"*, Macromolecules, 2000, 33, 3409-3424

[317] P. Hedvid, *"Dielectric Spectroscopy of Polymers*," John Wiley & Sons, New York, 1977

[318] "*α and β relaxations and calculation of activation energy*", 2007, www.perkinelmer.com

[319] K. J. Laidler, "*The World of Physical Chemistry*", Oxford University Press, 1993

[320] K. C. Manikandan Nair, Sabu Thomas, G. Groeninckx, *"Thermal and dynamic analysis of polystyrene composites reinforced with short sisal fibres"*, Composites science and technology, 2001, 61, 2519-2529

[321] Hang Gao, Julie P. Harmon, "*Para-substituted polystyrenes: Stress relaxation, creep, dynamic mechanical and dielectric analyses*", Thermochimica Acta, 1996, 284, 85-102

[322] Caiyun Wu, Guozhang Wu, Chifei Wu, *"Dynamic mechanical properties in blends of poly(styrene-b-isoprene-b-styrene) with aromatic hydrocarbon resin"*, Journal of applied polymer science, 2006, Vol. 102, 4157-4164

[323] Takeji Hashimoto, Yasuhisa Tsukahara, Kazuhisa Tachi, Hiromich Kawai, "*Structure and properties of tapered block polymers. 4. "Domain-boundary mixing and "mixing-in-domain" effects on microdomain morphology and linear dynamic mechanical response*", Macromolecules, 1983, 16 (4), 648-657

[324] www.diracdelta.co.uk

[325] H.R. Thomas, J.J. Omalley, "*Surface studies on multicomponent polymer systems by X-ray photoelectron spectroscopy. Polystyrene/poly(ethylene oxide) diblock*", Macromolecules, 1979, 12:323

[326] S. N. Maganov, J. Cleveland, Elings V., Denley D., Whangbo M.-H., "*Tapping-mode atomic force microscopy study of the near-surface composition of a styrene-butadiene-styrene triblock copolymer film*", Surface science, 1997, Vol. 389 (1-3), pp. 201-211

[327] M. Jeusette, S. Peeterbroeeck, F. Simal, D. Cossement, P. Roose, Ph. Leclere, Ph. Dubois, M. Hecq, R. Lazzaroni, "*Microscopic morphology of blends between a new all-acrylate radical block copolymer and a rosin ester resin for pressure sensitive adhesives*", European Polymer Journal, *2008, 44, 3931-3940*

[328] Peter L. Drzal, Kenneth R. Shull, "*Adhesive failure of model acrylic pressure sensitive adhesives*", The journal of adhesion, 2005, 81:397-415

[329] F. Annighoffer, W. Gronski, "*Block polymers of styrene and isoprene with variable interphase: Morphology and dynamic viscoelastic behaviour*", Colloid & Polymer Science, 1983, 261, pp. 15-25

[330] Kostas Ch. Daoulas, Doros N. Theodorou, "*Experimental and self-consistent-field theoretical study of styrene block copolymer self-adhesive materials"*, Macromolecules, 2004, 37, 5093-5109

[331] R. J. Young, P. A. Lovell, "Introduction to Polymers", 2nd ed., Stanley Ltd., UK, 1991, pp. 151-164

[332] Daisuke Yamaguchi, Jeffrey Bodycomb, Satoshi Koizumi, Takeji Hashimoto, "*Ordered structure in blends of block copolymers. 4. Location of short diblock*", Macromolecules, 1999, 32, 5884-5894

[333] A. Hotta, S. M. Clarke, E. M. Terentjev, "*Stress relaxation in transient networks of symmetric triblock styrene-isoprene-styrene copolymer*", Macromolecules, 2002, 271-277

[334] Eugene Helfand, "*Diffusion in strongly segregated block copolymers*", Macromolecules, 1992, 25, 492-493

[335]Wolfang Schartl, "*Structure and diffusion of copolymer micelles in entangled homopolymer chains*", Macromol. Chem. Phys., 1999, 200, 481-500

[336] G. Heinrich, T. A. Vilgis, "*Long-time relaxation of polymer networks*", Macromolecules, 1992, 25, 404-407

[337] Hirokazu Hasegawa, Takeji Hashimoto, *"Morphology of block polymers near a free surface",* Macromolecules, 1985, 18 (3), pp. 589-590

[338] C. Y. Ryu, T. P. Lodge, Macromolecules, 32, 1999, 7190

[339] Bernard Fouchet, "*Diffusion of Mineral Oil in Styrene-Butadiene Polymer Films*", Journal of Applied Polymer Science, 2009, Vol. 111, 2886-2891

[340] Van Gilder, R. L.; Purfeerst, R. D. TAPPI J, 1994, 77, 230

[341] Alan A. Galuska, "*ToF-SIMS Determination of Molecular Weights from Polymeric surfaces and Microscopic Phases"*, Surface and Intyerface Analysis, 1997, Vol. 25, 790-798

[342] F. W. McLafferty, "*Interpretation of Mass Spectra*", University science books, 1980, Mill Valley, CA.

[343] John T. Mehl, David M. Herkules, "*Secondary ion mass spectrometry of poly(styrene-co-isoprene) diblock copolymers: Improved surface sensitivity using the high-mass region*", Macromolecules 2001, 34, 1845-1854

[344] Keyang Xu, Andrew Proctor, David M. Herkules, "*Time-of-flight ion mass spectrometry (TOF-SIMS) of polyisoprenes*", Microchimica Acta, 1996, Vol. 122, Numbers 1-2

[345] http://www.faqs.org/patents/app/20090008808

[346] Dirac Delta Consultants Limited, Science & Engineering Encyclopaedia Version 2.4©, www.diracdelta.co.uk

[347] Nicholas M., Kassis CM, Menceloglu YZ, DeSimone JM, Linton RW, Friedman RM, Parker DL, Rading D, Benninghoven A., "*Surface segregation in poly(styrene-b-isoprene):*

correlation of TOF-SIMS with XPS and contact angle measurement". Polym Prepr 37:309-310

[348] Yujie Sun, Gilbert C. Walker, "*Viscoelastic response of poly(dimethylsiloxane) in the adhesive interaction with AFM tips*", Langmuir, 2005, 21, 8694-8702

[349] Tanja Neumann, "*Determining the elastic modulus of biological samples using atomic force microscopy*", JPK Instruments Application Report,

[350] Gwo-Wen Wu, Ging-Ho Hsiue, Jin-Sheng Yang, "*Stress relaxation in poly(styrene-butadiene-styrene) and poly(styrene-isoprene-styrene) triblock copolymers and their derivatives*", Materials Chemistry and Physics, 1994, 37, 191-196

[351] Matsuoka S., "*Relaxation phenomena in polymers*", Oxford University Press, 1992, Oxford, U.K.

[352] Typical image artifacts, Training book, Veeco instruments Inc.

[353] Michiko Fujita, Mikjo Kajiyama, Akio Takemura, Hirokunj Ono, Hiroshi Mizumachi, Shunji Hayashi, "*Effects of miscibility on peel strength of natural-rubber-based pressure-sensitive adhesives*", Journal of applied polymer science, Volume 70, pp. 777-784

[354] Benedek I, Heymans LJ., "*Pressure sensitive adhesive technology*", New York: Marcel Dekker, Inc., 1996

[355] B. V. Derjaguin, V. M. Muller, Yu. P. Toporov, J. Colloid Interface Sci. 53, 314-326, 1975

[356] L. H. G. J. Segeren, B. Siebum, F. G. Karssenberg, "*Microparticle adhesion studies by the atomic force microscope*", J. Adhesion Sci., Technol. Vol. 16, No. 7, pp. 793-828, 2002

[357] C. Ortiz, G. Hadziioannou, "*Entropic elasticity of single polymer chains of poly(methacrylic acid) measured by atomic force microscopy*", Macromolecules, 1999, 32, 780-787

[358] Seung-ho Moon, Stephanie Swearingen, Mark D. Foster, "*Scanning probe microscopy study dynamic adhesion behaviour of polymer adhesive blends*", Polymers, 45, 2004, 5951-5959

[359] L. Sirghi, F. Rossi, "*Adhesion and elasticity in nanoscale*", Applied Physics Letter, 89, 243118, 2006

[360] John Comyn, "Adhesion Science", 1997, page 10.

[361] M. Giri, D.B. Bousfield, W. N. Unertl, Langmuir 17, 2973-2981, 2001

[362] Mahdi Farchi-Tabrizi, Michael Kappl, Yajun Cheng, Jochen Gutmann, Hans-Jurgen Butt, "*On the adhesion between fine particles and noncontacts: An atomic force microscopy studies*", Langmuir, 2006, 22, 2171-2184

[363] Yueh-Lin Loo, Richard A Register, "Polymer Crystallization in 25-nm Spheres, "Volume 84, Number 18, 2000

[364] M. Portigliatti, Y. Koutsos., H. Hervet, L. Leger. Langmuir , 16, 6374-6376, 2000

[365] F. Oesterhelt, M. Rief, H. Gaub, "Single molecule force spectroscopy by AFM indicates helical structure of poly(ethylene-glycol) in water,

[366] Henkel, Slough, England

[367] Hertz H., "*Uber Die Beruhrung Fester Elasticher Korper*", Journal Reine and Angewandte Mathematik, Vol. 92, pp. 156-171 (1882)

[368] Boussinesq J., "*Applications Des Potentials a L'etude De Equibre Et Du Mouvement De Solides Elastique, Gauthier-Villars*", Paris, (1885)

[369] Sneddon I. N., "*The relationship between load and penetration in the axisymmetric Boussinesq problem for a punch of arbitrary profile*", International journal of engineering science, 1965, Vol. 3, pp. 47-56

[370] Oliver W. C., Pharr G. M., "*An improved technique for determining hardness and elastic-modulus using load and displacement sensing indentation experiments*", Journal of material research, Vol. 7, pp. 1564-1583, 1992

[371] Mark R. VanLandinghan, "*Review of Instrumental Indentation*", Journal of Research of the National Institute of Standards and Technology, 2003, Volume 108, Number 4, 249-265

[372] Anja Vinckier, Giogio Semenza, "Measuring elasticity of biological materials by atomic force microscopy", FEBS Letters, 430, 1998, 12-16

[373] C. Reynaud, F. Sommer, C. Quet, N. El Bounia, Tran Minh Duc, "*Quantitative determination of Young's modulus on a biphase polymer system using atomic force microscopy*", Surf. Interface Anal., 30, 15-189, 2000

[374] Edem. Wornyo, K. Gall, F. Yang, W. King, "*Nanoindentation of shape memory polymer networks*", Polymer, 4, 3213-322,2007

[375] Bobby Russell, Richard Chartoff, "*The influence of cure conditions on morphology and phase distribution in rubber a rubber-modified epoxy resin using scanning electron microscopy and atomic force microscopy",* Polymers, 46, 2005, pp. 785-798

[376] D. M. Schaefer, A. Patil, R. P. Andres, R. Reifenberger, "*Elastic properties of individual nanometer-size supported gold clusters*", Physical Review B, vol. 51, number 8, 1995

[377] Methporn Mareanukroh, R. K. Eby, R. J. Scavuzzo, Gary R. Hamed, "*Use of atomic microscope as a nanoindenter to characterise elastomers*", Rubber and technology, 2000, Vol. 73, pp. 912-925

[378] Wensheng Xu, Paula M. Wood-Adams, Christopher G. Robertson, *"Measuring local viscoelastic properties of complex materials with tapping mode atomic force microscopy*", Polymer 47, 2006, 4798-4810

[379] D. S. Rimai, D. J. Quesnel, A.A. Busnaina, Colloid Surfaces A 165, 3-10, 2000

[380] G. Ziskind, M. Fichman, C. Gutfinger, "*Adhesion Moment for Estimating Particle Detachment from a Substrate*", J. Aerosol. Sci., Vol. 28, No. 4, pp. 623-634, 1997

[381] Alfred J. Crosby, Kenneth R. Shull "*Adhesive Failure Analysis of Pressure Sensitive Adhesives"*, Journal of Polymer Science: Part B: Polymer Physics, Vol. 37, 3455-3472, 1999.

[382] L. J. Fetters, D. J. Lohse, D. Richter, T. A. Witten, A. Zirkel, "*Connection between Polymer Moleuclar Weight, Density, Chain Dimensions, and Melt Viscoelastic Properties", Macromolecules*, Volume 27, Number 17

[383] Marat O. Gallyamov, Bernd Tartsch, Alexei R. Khoklov, Seigei S. Sheiko, "Real-time Force Microscopy of Macromolecular Conformational Transitions", Macromolecular Rapid Communications, 2004, Volume 25, Issue 19, pp. 1703-1707

[384] McEwan, A. D., G. I. Taylor, "*The peeling of a flexible strip by a viscous adhesive*", J. Fluid Mech., 1966, 26, p. 1-15

[385] A. G. Peressadsko, S. N. Gorb, "*Surface Profile and Friction Force Generated by Insects*", First International Industrial Conference, 15(249), 257-263

[386] Stanislav N. Gorb, "*Uncovering Insect Stickiness: Structure and Properties of Hairy Attachment Devices*", American Entomologist, Volume 51, No. 1